SPRINGBACK PREDICTION IN SHEET METAL FORMING: CONSTITUTIVE EQUATIONS, FINITE ELEMENT SIMULATIONS AND EXPERIMENTAL VALIDATION

JASRI BIN MOHAMAD

Thesis submitted for the degree of Doctor of Philosophy

DEPARTMENT of DESIGN, MANUFACTURE
AND ENGINEERING MANAGEMENT
FACULTY of ENGINEERING
UNIVERSITY of STRATHCLYDE

Declaration of Authenticity and Author's Rights

'This thesis is the result of the author's original research. It has been composed by the author and has not been previously submitted for examination, which has led to the award of a degree. '

Signed:

Date:

Acknowledgments

Praises be to the Almighty God. With His blessings, I managed to complete this thesis. I would like to express my sincere appreciations to my primary supervisor, Dr. Andrzej Rosochowski for his unlimited guidance throughout the duration of this project. His willingness to share his knowledge and expertise has helped me to gain deeper understanding of the subject. I would also like to thank my second supervisor, Professor Emeritus Raj Balendra for his unending supports. I would like to extend my heartiest appreciation and many thanks to my beloved family - my loving wife Khamisah Omar, my daughter Nur Syakirah and my sons Irfan and Irham for their great support, patience and continuous prayers for this success throughout the duration of this endeavour. Last but not least, my sincere appreciation goes to my mother in-law, to all my brothers, sisters and friends.

Table of Contents

Abstract

Predictive methods appear to be the most effective way to solve springback in sheet metal forming. The accuracy of the predictions depends upon the application of accurate material modelling. Experimental devices and methods are being continuously improved to incorporate increasingly accurate plastic bending characteristics. As part of these efforts, a new tool has been developed to test and record the characteristics of sheet metal deformation by investigating the Bauschinger effect factors (BEF) and the identified hardening parameters. The developed tool is believed to simulate the actual forming conditions of bending and provide more reliable information. The initial experimental investigation shows that the Bauschinger effect does occur during bending and unbending loadings in sheet metal forming. The BEF value was found to increase as the thickness increases. Therefore this justifies the need to consider the Bauschinger effect in sheet metal forming simulation through the use of relevant constitutive equations.

A direct optimization method has been successfully applied to identify material hardening parameters from the acquired experimental data of the newly developed tool. The optimisation result shows that nonlinear kinematic hardening and nonlinear mixed hardening models are capable of fitting the smooth transition curve of the experimental hardening data. Mixed hardening model performance however is considered to be much better as proven by lower residual or fitting error values. This justifies the idea that the application of a mixed hardening model is more suitable for springback simulation in sheet metal forming. Validation work was conducted in order to test the effectiveness of applying the two hardening models by

incorporating the identified parameters in predicting springback using finite element simulation. Of the two, the mixed hardening modelling has been proven to provide better simulation results in predicting springback.

Figures

Tables

Nomenclature

The following symbols have been used throughout this thesis. The units quoted are for the purpose of calculations. The SI unit system is used in the formulae or in calculations where appropriate.

f	Function
Y	Yield stress
σ	Current stress
σ_f	Flow stress
σ_o	Stress at zero plastic strain
$Y_1(\sigma_f), Y_2(\sigma_r)$	Yield stress in forward and reverse cyclic stress-strain curve
$\Delta\sigma_p$	Permanent softening
s_{ij}	Deviatoric stress
δ_{ij}	Kronecker delta, $\delta_{ij} = 1$ *if* $i = j$ *and* $\delta_{ij} = 0$ *if* $i \neq j$
$\sigma_1, \sigma_2, \sigma_3$	Principal stresses
ε	Plastic strain
α	Back stress
$d\varepsilon$	Plastic strain increment
ε	Strain
UTS	Tensile strength
E	Young's modulus
n	Strain exponential hardening
υ	Poisson ratio
ΔM	Change in moment

M	Moment
y	Distance of sheet metal layer from neutral axis
R	Normal plastic anisotropy ratio, $R = \frac{R_0 + 2R_{45} + R_{90}}{4}$
R	Radius of curvature
ρ	Curvature
ΔR	Planar anisotropy, $\Delta R = \frac{R_0 - 2R_{45} + R_{90}}{2}$
$\Delta\theta$	Springback angle
θ	Bending angle
BEF	Bauschinger effect factor
Q	Isotropic hardening parameter
C	Kinematic hardening parameters
γ	Recall term in kinematic hardening

CHAPTER 1

INTRODUCTION

1.1. Introduction

Sheet metal forming is a very important engineering discipline in manufacturing engineering. The applications cover major manufacturing industries such as aircraft, automotive, electronics and home appliances. Several methods such as blanking, piercing, shearing, stamping, deep drawing, folding and flanging are used to produce sheet metal components using different machines and tools or dies. To a large extent, the design of sheet metal forming processes and tooling have been based on experience, rules of thumb and trial-and-error experiments. These methods are very costly and time-consuming (Keeler 1977).

For many years, efforts have been made to use scientific knowledge and engineering methods to understand sheet metal forming by investigating various aspects of this technology such as identifying critical process parameters and understanding materials response under forming conditions. In the first case, the influence of process parameters on the finished products was investigated, recorded and analysed. The information was compiled as useful design guidelines for reference by product designers and tool engineers. In the second case, one tries to achieve a better understanding of material behaviour using laboratory test

experiments to simulate actual forming processes. The outcomes are translated into mathematical models, in the form of constitutive laws, for theoretical analysis and development of the forming processes. Historically, this analysis was analytical but today it is predominantly numerical, based on the use of finite element simulation.

Apart from the mentioned approaches, in-process monitoring to rectify defects in the forming process has also been used (Kerry and Robert 2001; Sun et al. 2006). This is a method of automatically identifying defective parts during the process and immediately responding to the problem by refine-tuning the machine's parameters and/or replacing the tools.

Despite achieving basic understanding of the nature and technology of sheet metal forming, there are still issues to be addressed. These are due to the demands placed on sheet metal forming processes with regard to both the increasing tolerance requirements of the finished parts and the need for elimination or reduction of important secondary processes by using near net shape forming.

1.2. Statement of the Problem

To meet tolerance and near net shape forming requirements, the use of scientific knowledge and engineering methods is paramount. Better knowledge of sheet metals' responsive behaviour during plastic deformation, in the form of theoretical models, is desired for accurate product and tool design using finite element simulation. Knowledge improvement requires focusing on the following areas (Yoon 2007):

a. Constitutive models suitable for the description of sheet metals

b. Testing procedures and analysis methods used to measure the relevant data needed to identify the material coefficients
c. Tensile and compressive instabilities in sheet forming
d. Modelling and analysis of springback
e. Finite Element (FE) formulation
f. Tool/material contact description
g. Multi-scale approaches for both continuum and crystal plasticity mechanics

The first four areas have seen the employment of various methods and techniques ranging from the well-known tensile test to the torsion test and bending test to better understand sheet metal plastic deformation. Nevertheless, the development of material characteristics is still lacking.

1.3. Aim of the Research

The aim of the research is to improve the quality of constitutive material models by experimental identification of their parameters using a testing equipment, which resembles the actual plastic deformation process of bending. The aim is also to use these parameters in the finite element simulation in order to improve springback prediction in sheet metal bending process.

1.4. Objectives of the Research

a. To develop an experimental method for understanding the plasticity phenomenon of sheet metal deformation using techniques resembling the actual sheet forming process of cyclic loading.

b. To evaluate the responsive behaviour of sheet metal materials undergoing cyclic loading through the newly developed experimental tool.
c. To identify constitutive equation parameters from the acquired data.
d. To measure the effectiveness of the identified material parameters in predicting springback by comparing finite element simulations and experimental results.

1.5. Thesis Organization

The thesis is organized as follows:

Chapter 1: Introduction

This chapter will briefly establish the need for the research work. It covers the introduction as a summary of the area of research, a statement of problem to justify the motivation for the research, aim of the research, a list of research objectives and the organization of the thesis as an overview of the whole content of the thesis.

Chapter 2: Literature Review

This chapter reviews the available relevant documentation of the previous works. The aim is to identify the existing knowledge and any gaps in the area in order to justify the rationale and importance of the current work. The chapter will be divided into several subsections, namely the introduction, overview of sheet metal bending, basics of sheet metal bending, plasticity theory for sheet metal forming, previous works and the chapter's conclusions.

Chapter 3: Material Characteristics

This chapter will describe the method used to acquire the properties of the research materials. It presents the most fair and objective way to perform and analyse the material properties according to the established accepted standards.

Chapter 4: Cyclic Loading Experiment

This chapter presents the outcome of the cyclic experiment in terms of bending stress versus strain. Bauschinger effect factors (BEFs) are also derived based on the selected formula.

Chapter 5: Identification of Material Parameters by Optimisation

This chapter will highlight the optimisation method used to acquire constitutive equation parameters using cyclic loading data described in Chapter 4. It will also analyse the capability of the hardening models to fit the cyclic data.

Chapter 6: FE Simulations and Experimental Validation of Springback

The objective of this chapter is to present validation work in testing the effectiveness of applying kinematic hardening parameters and mixed hardening parameters derived from the optimisation of bending and unbending experimental data in predicting springback using finite element simulation. To serve the objective, springback of U-bend profiles from finite element simulation and experiment are compared for degree of differences.

Chapter 7: Conclusions and Recommendations

This chapter discusses the extent to which the results close the gap identified in Chapter 2 as well as meeting the research objectives stated in Chapter 1. The chapter ends with recommendations for future works.

CHAPTER 2

LITERATURE REVIEW

2.1. Introduction

The demands on sheet metal processes are increasing with regard to both the tolerance requirements of the finished parts and the complexity of parts. The development in this area, even though it has been established for decades, is still required. The following topics have been identified for further improvements (Yoon 2007):

a. Constitutive models suitable for the description of sheet metals.
b. Testing procedures and analysis methods used to measure the relevant data needed to identify the material coefficients.
c. Tensile and compressive instabilities in sheet forming.
d. Modelling and analysis of springback.
e. Finite Element (FE) formulation.
f. Tool/material contact description.
g. Multi-scale approaches for both continuum and crystal plasticity mechanics.

For points (a) to (d), reliable theoretical and experimental methods are necessary to observe and capture material behaviour, especially when it comes to

representing actual forming processes. This chapter presents a literature review of the research progress with respect to the analytical, experimental and numerical aspects of points (a), (b) and (d). Conclusions are drawn from the knowledge gaps that could motivate the current work. To start with, the sheet metal forming processes and information on the bending process will be briefly reviewed for an understanding of the overall subject.

2.2. Overview of Sheet Metal Bending

Sheet metal forming processes are classified as plastic deformation methods to convert a given shape of the sheet metal to another shape without changing its mass or material composition. The processes are divided into 5 subgroups based on the important differences in the effective stresses (Lange 1985):

a. Compressive forming by rolling, flow forming and indenting
b. Combined tensile and compressive forming, e.g. pulling through a die, deep drawing, spinning and flange forming.
c. Tensile forming-stretching, expanding analogous to deep drawing and recessing to form a shallow depression in flat or curved sheet metal.
d. Forming by bending such as bending with linear tool motion and bending with rotary tool motion.
e. Forming by shearing

According to (Lange 1985), “forming by bending is performed by plastically deforming the material and changing its shape. The material is stressed beyond its yield strength but below its ultimate tensile strength. There is little change to the

material’s surface area. It generally refers to deformation about one axis only. It is a flexible process by which a variety of different shapes can be produced through the use of standard die sets or bend brakes.” Figure 2.1 presents a classification of bending processes. The two major groups are bending with linear tool and rotary tool motions. The branches below spread to various specific processes carried out on different machines.

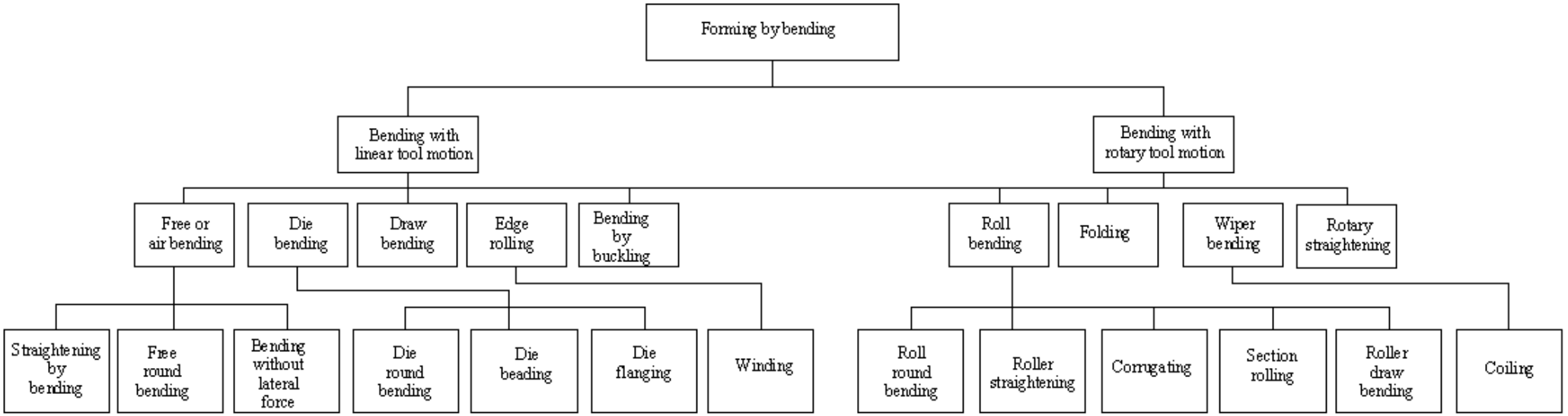

Figure 2.1 Classification of bending processes (Lange 1985)

2.3. Basics of Sheet Metal Bending

In general the bending analysis starts with an assumption of pure bending case and boundary condition as shown in Figure 2.2.

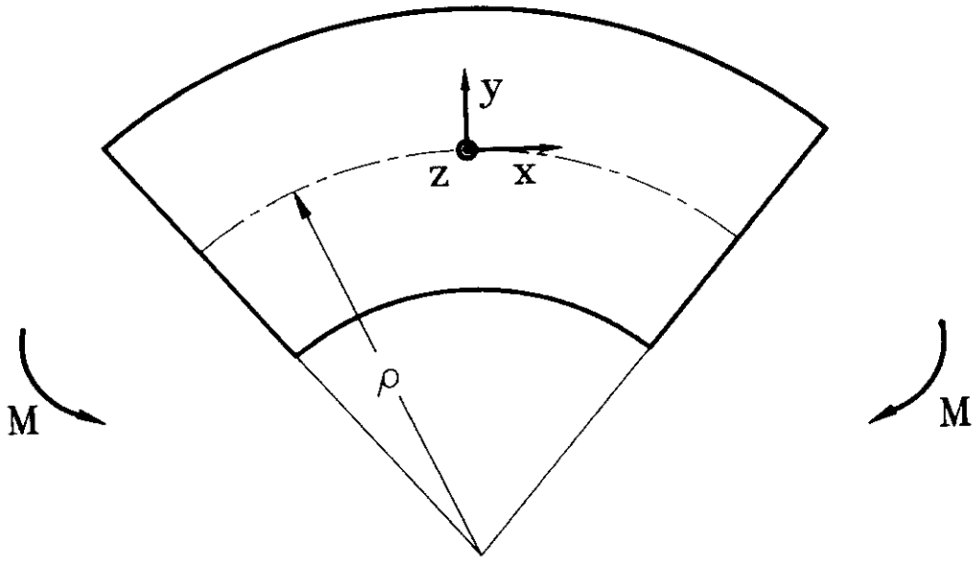

Figure 2.2 A section of sheet metal subjected to pure bending (Perduijn and Hoogenboom 1995)

The maximum tensile stress is on the outer surface of the bent component. It reduces toward the centre of the sheet thickness and becomes zero at the neutral axis. In contrast, the compressive stress increases from the neutral axis toward the inside of bent component.

By considering stress distribution on a normal section through a unit width of sheet in bending, the force acting on layers of sheet metal across the thickness

and finally bending moment can be derived. Equation 2.1 relates this moment to the stress across the sheet metal thickness (Marciniak et al. 2002).

$$M = \int_{-t/2}^{t/2} y\,\sigma\,dy$$

Equation 2.1

If a sheet metal is bent by a moment and then released (without reverse loading), springback phenomenon is observed through the change in the sheet metal bending curvature and bend angle. This phenomenon is described in Figure 2.3.

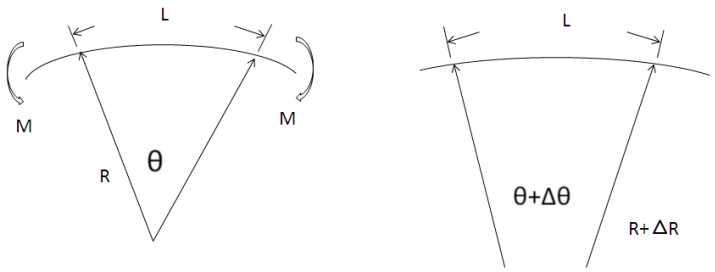

Figure 2.3 Change in bend angle and curvature in sheet metal bending during bending loading and unloading (Marciniak et al. 2002)

By assuming the length in the mid-surface (neutral axis) of the sheet thickness remains the same, Equation 2.2 has been derived to relate the bend angle and curvature of loading and unloading cases (Marciniak et al. 2002).

$$\frac{\Delta\theta}{\theta} = \frac{\Delta\left(1/R\right)}{R}$$

Equation 2.2

Plotting moment versus curvature diagram one will find that the curve is similar to the corresponding stress-strain curve. This plot is shown in Figure 2.4. For that reason suitable values of material parameters in the plasticity theories can be identified using moment-curvature based experiment as in cyclic bending test (Yoshida et al. 1998).

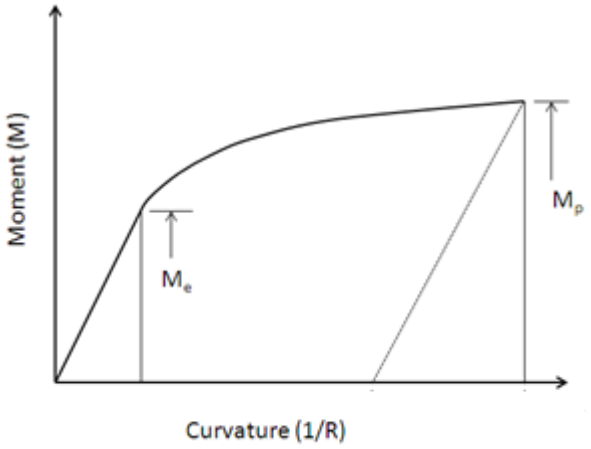

Figure 2.4 Moment versus curvature due to loading and unloading moment in sheet metal forming (Marciniak et al. 2002)

2.4. Plasticity Theory for Sheet Metal Forming

"The theory of plasticity deals with the methods of calculating stresses and strains in a deformed body, after part or all of the body has yielded. The most difficult problems to solve in plasticity are those of constrained plastic flow. These are cases where part of the body has yielded and part is still elastic, the plastic strains being of the order of the elastic strains. The compatibility equations and the stress-strain relations are difficult to handle and very few complete solutions have been obtained to such problem" (Johnson and Mellor 1973). This statement to a

large extend describes the challenge in developing a constitutive law for metal plastic deformation. This challenge, however, is worth tackling as knowing constitutive law governing sheet metal behaviour during bending helps to optimise the manufacturing process. The advantage, for example, is the ability to understand the phenomena of springback and formability limitation.

The plastic deformation of sheet metals can be modelled using two types of modelling: classical metal plasticity and cyclic plasticity (Abaqus 2000). The latter is believed to better represent actual sheet metal forming conditions due to its capability to consider the Bauschinger effect - a reduction of yield stress on load reversal when compared to forward loading. For this reason, this literature review will discuss in depth the cyclic plasticity theory, while the classical metal plasticity will only be briefly described as an overview.

2.4.1. Classical Plasticity Theory

When the inelastic flow of a metal occurs at relatively low temperatures, loading is monotonic and creep effects are not important. The deformation can be described by the classical metal plasticity model. The three main features of the plasticity model are: a yield criterion, a strain hardening rule and the plastic flow laws (Bower 2009).

A yield criterion is a condition to predict whether the solid is in elastic or plastic form. It is to determine the critical stress at which permanent deformation occurs. Some of the basic choices of the yield criteria are Von Mises and Tresca yield condition (Johnson and Mellor 1973). The following equations show the respective formulae for these criteria respectively. The symbol σ_{ij} is defined as the

stress tensor acting in a solid, σ_1, σ_2 and σ_3 are the principal values of stress tensor and σ_f is the yield (flow) stress depending on equivalent plastic strain, ε (Bower 2009).

$$f(\sigma_{ij}, \varepsilon) = \sqrt{\frac{1}{2}\left[(\sigma_1 - \sigma_2)^2 + (\sigma_1 - \sigma_3)^2 + (\sigma_2 - \sigma_3)^2\right]} - \sigma_f(\varepsilon) = 0$$

Equation 2.3

$$f(\sigma_{ij}, \varepsilon) = \max\{|\sigma_1 - \sigma_2|, |\sigma_1 - \sigma_3| |\sigma_2 - \sigma_3|\} - \sigma_f(\varepsilon) = 0$$

Equation 2.4

The materials are said to deform elastically when $f(\sigma_{ij}) < 0$ and plastically when $f(\sigma_{ij}) = 0$. A condition of $f(\sigma_{ij}) = 0$ defines a yield surface.

Instead of using principal stresses, the criteria can also be defined using stress deviator. For Von Mises, Equation 2.3 will become as below:

$$f(\sigma_{ij}, \varepsilon) = \sqrt{\frac{3}{2} s_{ij}\, s_{ij}} - \sigma_f(\varepsilon)$$

Equation 2.5

The first term in the equation represents Von Mises effective stress in deviatoric stress tensor form defined by the following equation:

$$s_{ij} = \sigma_{ij} - \frac{1}{3}\sigma_{kk}\delta_{ij}$$

Equation 2.6

In classical plasticity theory, isotropic hardening has been used as a strain-hardening rule. Isotropic hardening assumes that the yield surface is transformed by growing its size uniformly in all directions. The centre point will remain in the same

place of the stress space. Figure 2.5 shows the transformation of the yield surface due to isotropic hardening (Chaboche 2008). Equation 2.7 shows a mathematical form of the yield condition in this theory (Yu 2006). *R* denotes the yield surface size, depending on plastic strains through the hardening parameter α .

$$f(\sigma_{ij}) - R(\alpha) = 0$$

Equation 2.7

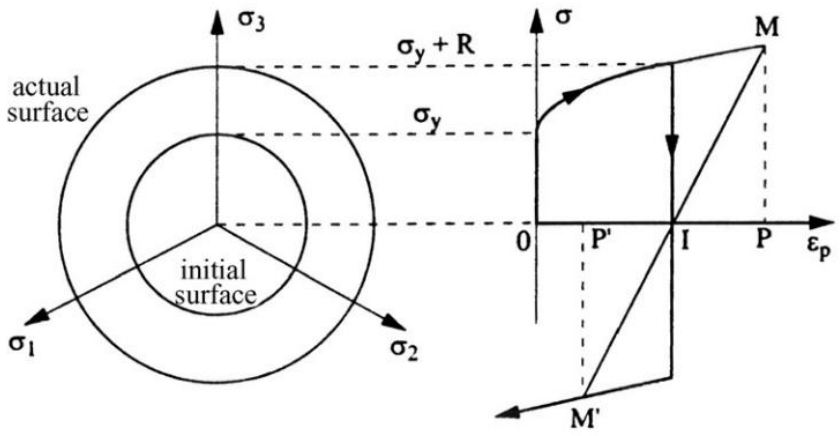

Figure 2.5 Schematics of isotropic hardening in the deviatoric stress plane and the stress versus plastic strain response (Chaboche 2008)

There are a few possible descriptions of isotropic hardening. The two equations that are commonly used are Swift law and Voce law (Butuc et al. 2011). Equation 2.8 describes the strain hardening defined by Swift law

$$\sigma_f = \sigma_o + H(\varepsilon_o + \varepsilon)^n$$

Equation 2.8

Where; σ_f is the flow stress, ε is the equivalent plastic strain, while σ_o, ε_o, H and *n* are material parameters. Equation 2.9 shows the description of isotropic hardening according to Voce law. The description is based on an exponential form of hardening.

$$\sigma_f = \sigma_Y + Q\left(1 - e^{-b\varepsilon}\right)$$

Equation 2.9

The equation assumes that the yield stress saturates at a certain point. *Q* defines the maximum change in the size of the yield surface and *b* is the rate at which that maximum is reached (Butuc et al. 2011). Other proposed isotropic hardening equations are shown below (Johnson and Mellor 1973):

Holloman

$$\sigma_f = H\varepsilon^n$$

Equation 2.10

Ludwick

$$\sigma_f = \sigma_Y + H\varepsilon^n$$

Equation 2.11

Prager

$$\sigma_f = \sigma_Y \tanh\left(E\varepsilon / \sigma_Y\right)$$

Equation 2.12

Ramberg and Osgood (Lemaitre and Chaboche 1990)

$$\sigma_f = \sigma_Y + H\varepsilon^{1/n}$$

Equation 2.13

The third element of the constitutive model is the plastic flow laws, required to predict the plastic strains components in metal deformation. The objective is to be able to determine the small change in plastic strain, $d\varepsilon_{ij}$.

For Von Mises yield criterion, the general plastic strain increment is described as in Equation 2.14 (Bower 2009).

$$d\varepsilon_{ij} = d\varepsilon \frac{\partial f}{\partial \sigma_{ij}} = d\varepsilon \frac{3}{2} \frac{s_{ij}}{\sigma_f}$$

Equation 2.14

However, the application of isotropic hardening in the classical plasticity theory is limited to monotonous and proportional deformation and it is unable to describe the Bauschinger effect of cyclic loading (Chung et al. 2005). To account for the Bauschinger effect, cyclic loading modelling has been established.

2.4.2. Cyclic Loading Model

In sheet metal forming, cyclic loading occurs due to bending and unbending of material in the die draw bead and when the sheet is drawn over a die shoulder corner (Hosford and Caddell 1993; Sanchez 2010; Yoshida et al. 2002). This is shown in Figure 2.6.

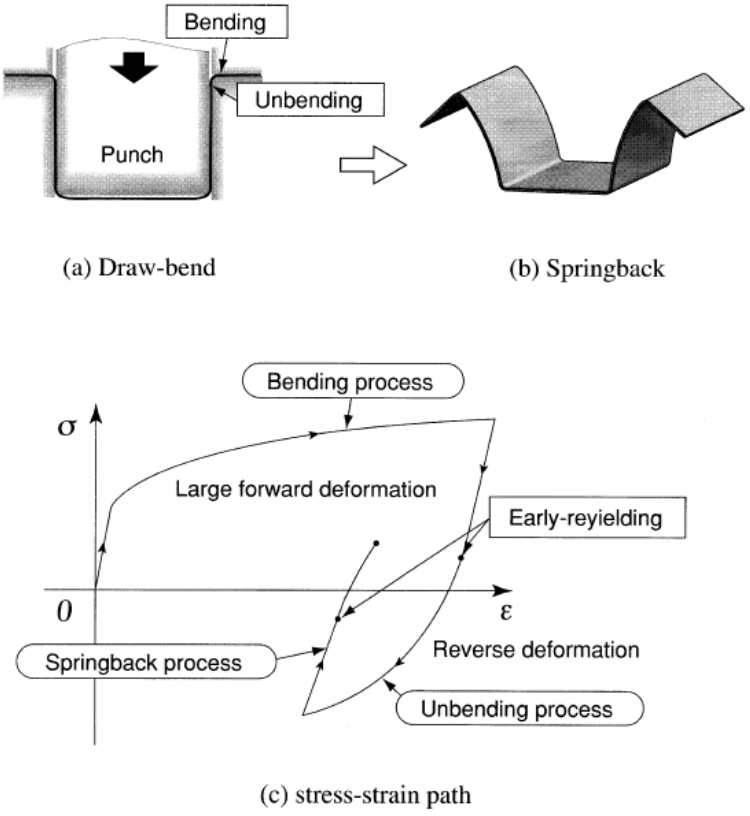

Figure 2.6 Description of cyclic loading (a) draw-bend (b) springback (c) stress-strain path (Yoshida et al. 2002)

Yoshida described this cyclic process as having four distinct features: load reversal and Bauschinger point, transient behaviour, work-hardening stagnation and permanent softening as shown in Figure 2.7 (Yoshida and Uemori 2003). The description by Yoshida indeed originated from Sowerby and Uko. To describe

cyclic loading, Sowerby and Uko used unidirectional testing, where pre-straining in tension is followed by reverse straining in compression or vice versa. Figure 2.8 shows a stress-strain curve for reverse loading using unidirectional testing (Sowerby and Uko 1979).

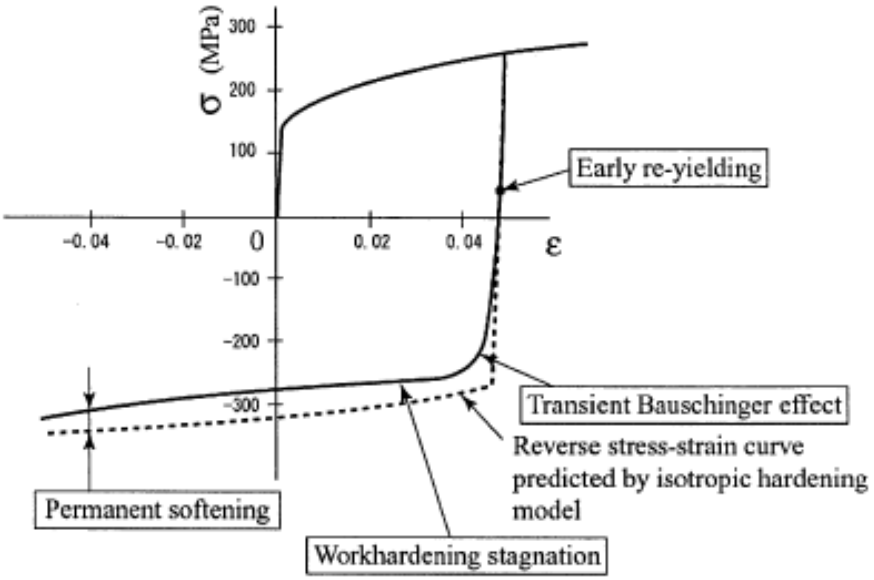

Figure 2.7 Features of cyclic loading in bending (Yoshida and Uemori 2003)

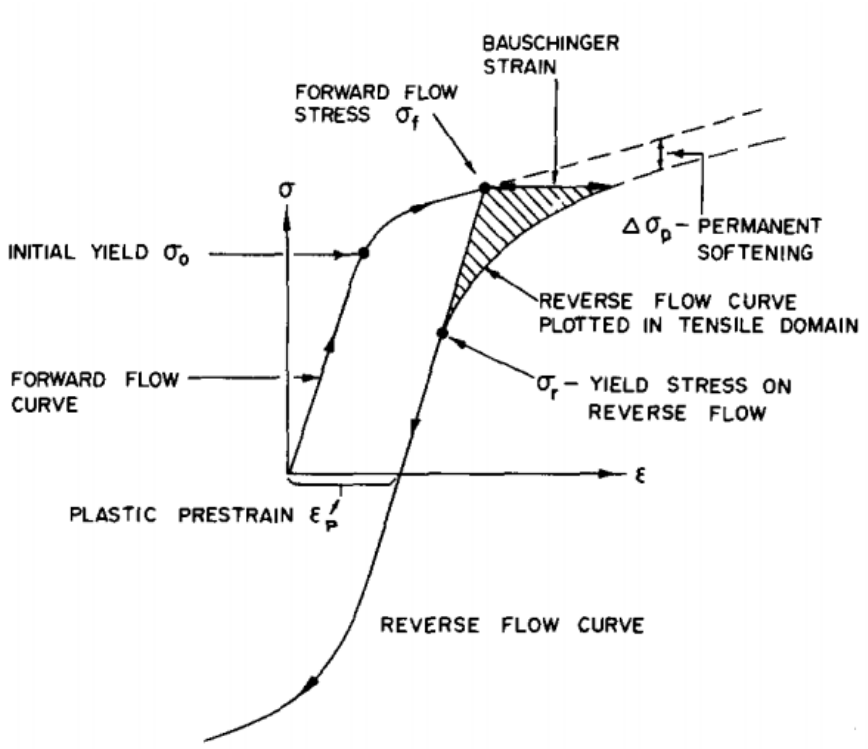

Figure 2.8 Sowerby and Uko's description of stress strain curve due to reversing loading direction (Sowerby and Uko 1979)

The Bauschinger effect, by definition, is a reduction of yield stress on the reversal of loading when compared to the forward loading. It is also known as early re-yielding. The Bauschinger effect factor, BEF, has been used to quantify the Bauschinger effect according to the following formula:

$$BEF = \frac{Y_1 - |Y_2|}{Y_1}$$

Equation 2.15

Y_1 and Y_2 are shown in Figure 2.9. A zero BEF value indicates that no Bauschinger effect is present in loading and unloading deformation (Weinmann et al. 1988).

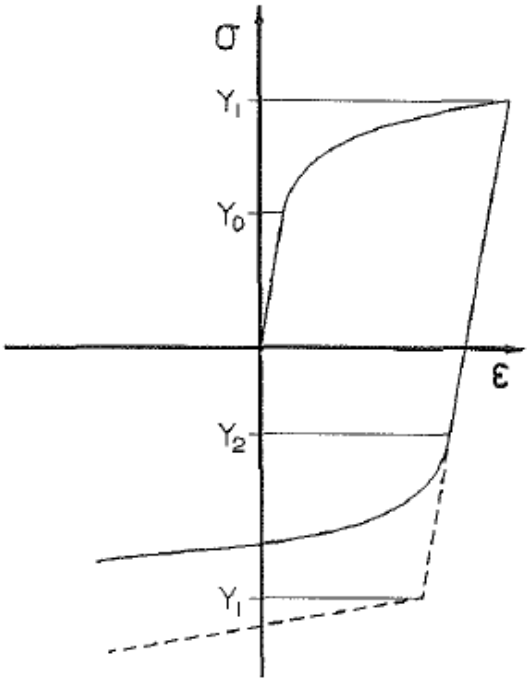

Figure 2.9 Weinmann's cyclic loading effect (Weinmann et al. 1988)

Another alternative formula is given by G.D. Moan and J.D. Embury below (Thakur et al. 1996):

$$\beta_e = \frac{\sigma_f - |\sigma_r|}{2\sigma_f}$$

Equation 2. 16

where

σ_f = maximum flow stress in forward loading

σ_r = reverse yield stress

While providing a good approach to measuring the Bauschinger effect, both formulas face a problem in determining the particular value of the reverse yield stress. Several researchers proposed the use of a 0.002 strain offset method (Thakur

et al. 1996). Figure 2.10 shows an alternative method to the 0.002 strain offset method.

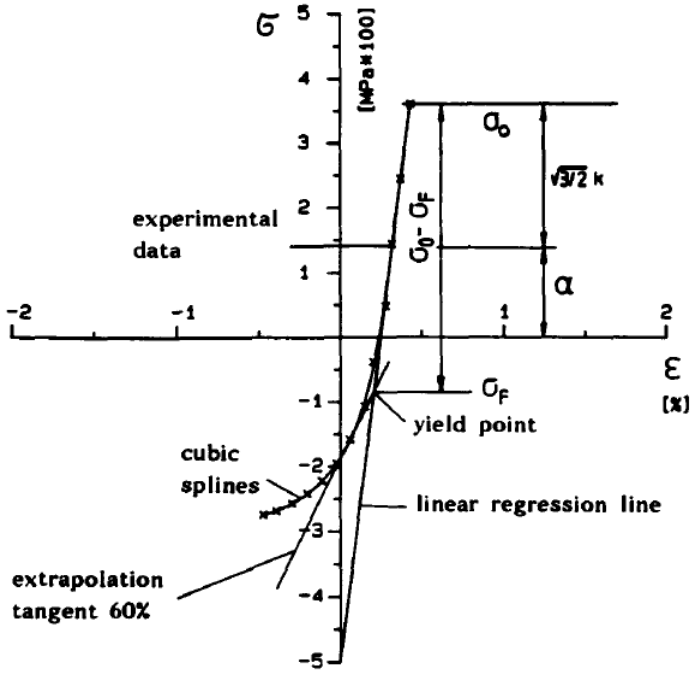

Figure 2.10 Determination of yield point by backward extrapolation method (Bruhns et al. 1992)

The method uses a straight line, whose angle is 60% offset from the elastic line (Bruhns et al. 1992).

The reverse yield point is followed by a rapid change in work hardening. Based on the position of the cyclic hardening curve relative to the monotonic hardening curve, the material is said to undergo cyclic hardening if the cyclic curve is above the monotonic curve and cyclic softening when the cyclic curve is below the monotonic hardening curve (Haupt et al. 1992; Lemaitre and Chaboche 1990). Permanent softening, $\Delta\sigma_p$ (Figure 2.8), is described by a steady difference between forward and reverse parallel stress after the transient stage. Parallelism of the

curves, however, is difficult to achieve and requires proper extrapolation (Sowerby and Uko 1979).

To improve sheet metal forming simulation, there is a need to incorporate an appropriate constitutive equation capable of describing the Bauschinger effect. Kinematic hardening has been acknowledged to provide the answer. In kinematic hardening, the yield surface is transformed by translating from one point to another point but its shape and size stay the same. Figure 2.11 illustrates the kinematic hardening case.

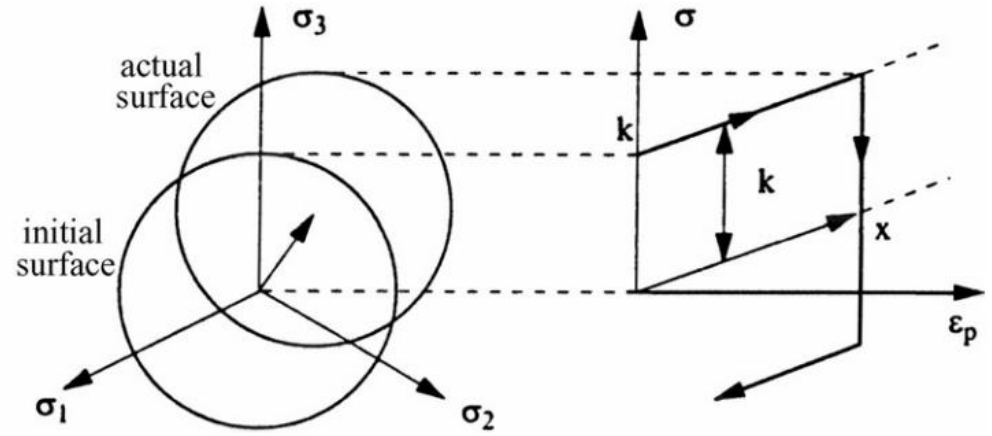

Figure 2.11 Schematics of kinematic hardening in the deviatoric stress plane and the stress versus plastic strain response (Chaboche 2008)

The translation of the yield surface for kinematic hardening model was described by (Prager 1956) as

$$f(\sigma_{ij}-\alpha_{ij})-R_o=0$$

Equation 2.17

Where α_{ij} represents the coordinates of the centre of the yield surface, which is also known as the back stress (Yu 2006). R_o is a material constant representing the size of the original yield surface. The yield criteria for this model are slightly different

from the yield criteria for isotropic hardening. Equation 2.18 shows the Von Mises yield criterion for kinematic hardening. The value for σ_f in this formula is constant.

$$f(\sigma_{ij},\varepsilon)=\sqrt{\frac{3}{2}(s_{ij}-\alpha_{ij})(s_{ij}-\alpha_{ij})}-\sigma_f=0$$

Equation 2.18

The formulation of a kinematic hardening model involves an evolution rule of the back stress, α_{ij}. The following linear kinematic hardening model was proposed by (Prager 1956)

$$d\alpha_{ij}=C\,d\varepsilon_{ij}$$

Equation 2.19

Where, *C* is a material constant. Prager's model however does not give consistent results for two and three-dimensional cases. To improve this model, Ziegler's linear hardening equation was proposed according to the following equation (Ziegler 1959)

$$d\alpha_{ij}=C\frac{1}{\sigma^o}(\sigma_{ij}-\alpha_{ij})d\varepsilon_{ij}$$

Equation 2.20

The symbol σ^o is the size of the yield surface at zero plastic strain. The linearity of Prager's hardening model and Ziegler's hardening model, however, do not represent the actual nonlinearity of plastic deformation. To account for nonlinearity condition, Armstrong-Frederick (A-F model) introduced a term γ, called dynamic recovery, into Prager's and Ziegler's linear kinematic hardening models. Equation 2.21 and

Equation 2.22 show the respective formulas for these models using nonlinear kinematic hardening (Armstrong and Frederick 1966).

$$d\alpha_{ij} = Cd\varepsilon_{ij} - \gamma\alpha_{ij}d\varepsilon$$

Equation 2.21

$$d\alpha_{ij} = C\frac{1}{\sigma^o}\left(\sigma_{ij} - \alpha_{ij}\right)d\varepsilon_{ij} - \gamma\alpha_{ij}d\varepsilon$$

Equation 2.22

C and gamma γ are material parameters to be determined from cyclic testing. *C* is a kind of hardening modulus and gamma γ defines the rate at which the kinematic hardening modulus decreases as the plastic deformation develops. The term $d\varepsilon$ is the increment of the equivalent plastic strain.

Chaboche extended the A-F model by suggesting that several kinematic hardening components (additive back stress) exist and he introduced the concept of a total back stress. The hardening laws for each back stress are given in Equation 2.23 (Chaboche 1986; Chaboche 1989).

$$\left(d\alpha_{ij}\right)_K = C\frac{1}{\sigma^o}\left(\sigma_{ij} - \alpha_{ij}\right)d\varepsilon_{ij} - \gamma\left(\alpha_{ij}\right)_K d\varepsilon$$

Equation 2.23

The overall back stress is computed from the following equation

$$\alpha_{ij} = \sum_{K=1}^{N}\left(\alpha_{ij}\right)_K$$

Equation 2.24

Where N is the number of load cycles.

Combining isotropic and nonlinear kinematic hardening has been considered to be more efficient than the application of kinematic hardening alone in sheet metal

forming simulation. This is due to the capability of isotropic hardening to improve cyclic transient of elastic to plastic in stress-strain characteristic whilst at the same time kinematic hardening continues to take care of the Bauschinger effect (Chun et al. 2002a; Chun et al. 2002b; Rauch et al. 2007; Yoshida and Uemori 2002; Yoshida and Uemori 2003). In this type of hardening model, the yield surface is subjected to both translation and expansion. The following equation describes the yield function of the model (Yu 2006)

$$f\left(\sigma_{ij}-\alpha_{ij}\right)-R(\alpha)=0$$

Equation 2.25

One of the possible combinations is between Voce isotropic hardening and Chaboche nonlinear kinematic model as shows in Equation 2.26 (Chaboche and Rousselier 1983; Chaboche 1986).

$$\sigma_f=\sigma_Y+Q\left(1-e^{-b\varepsilon}\right)+\frac{C}{\gamma}\left(1-e^{-\gamma\varepsilon}\right)$$

Equation 2.26

For the past years, several researchers have also proposed alternative cyclic models based on additional flow surfaces, called bounding surfaces. Among the latest models belonging to this group are the Geng-Wagoner hardening model (G-W) and Yoshida-Uemori hardening model (Y-U).

The G-W hardening model is a two-surface model originating from the Armstrong-Frederick hardening model. A bounding surface is introduced in the model to capture the permanent softening effect by expanding and translating yield surface. The following figure illustrates this concept (Geng and Wagoner 2000; Geng et al. 2002).

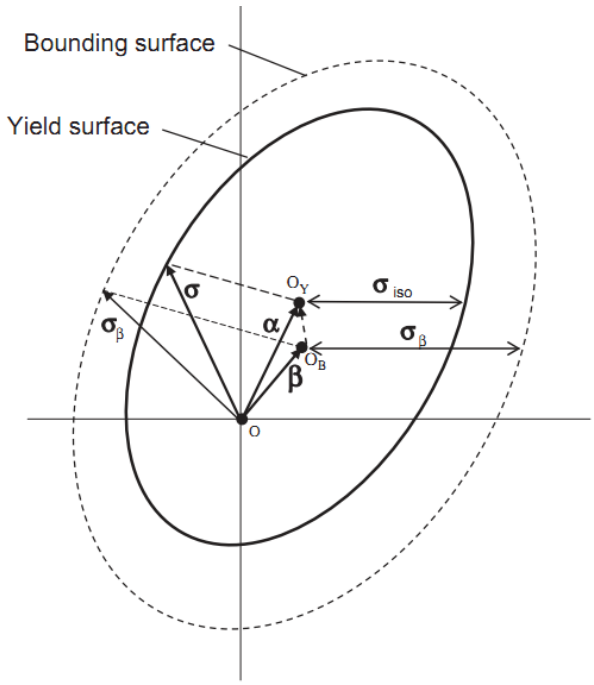

Figure 2.12 Geng-Wagoner's description of two-surface hardening model (Geng and Wagoner 2000)

The evolution of back stress α is shown below.

$$d\alpha_{ij} = C_x \left[\frac{(\alpha_{ij})_{sat}}{\sigma_{ij}} (\sigma_{ij} - \alpha_{ij}) - (\alpha_{ij} - \beta_{ij}) \right] d\varepsilon_{ij}$$

Equation 2.27

The symbol β represents the centre of the bounding surface and it is given according to the following formula

$$d\beta = \frac{h' - h'' m}{\sigma_\beta} (\sigma_B - \alpha) d\varepsilon$$

Equation 2.28

The letter *m* is the ratio between kinematic and isotropic response for the bounding surface. For *m* equal 1, hardening is purely isotropic and for *m* equal 0 hardening is purely kinematic. *h'* is plastic modulus and *h''* is another plastic modulus at a

certain distance from *h'*. The symbol σ_β is a measure of the size of the bounding surface and σ_B is the stress-mapping point on the bounding surface.

The Y-U hardening model consists of three different surfaces in the plane stress space. Apart from a yield surface and a bounding surface, an additional surface has been added to control the permanent softening and the work hardening stagnation as shown in Figure 2.7. The yield surface can only translate in stress space (kinematic hardening). So its size is constant, R_o (the initial uniaxial yield stress). The yield surface expression is given by Equation 2.17. The bounding surface on the other hand is assumed to move by translation as well as by expansion. The following equation describes the general expression for the bounding surface (Yoshida and Uemori 2003; Yoshida and Uemori 2002).

$$f\left(\sigma_{ij}-\beta_{ij}\right)-\left(B+D\right)=0$$

Equation 2.29

The symbol β here is the centre of the bounding surface, *B* is its initial size and *D* represents its isotropic hardening. Another expression for this hardening is the relative movement of the yield surface with respect to the bounding surface. The expression is as follows

$$\alpha_{ij}^{*}=\alpha_{ij}-\beta_{ij}$$

Equation 2.30

The evolution of α_{ij}^{*} and β_{ij} is given by the following equations

$$d\alpha_{ij}^{*}=C\left[\frac{B+D(\varepsilon)-R_O}{R_O}\left(\sigma_{ij}-\alpha_{ij}\right)-\alpha^{*}\right]d\varepsilon$$

Equation 2.31

$$d\beta_{ij} = k\left[\frac{b}{B + D(\varepsilon)}\left(\sigma_{ij} - \beta_{ij}\right) - \beta_{ij}\right]d\varepsilon$$

Equation 2.32

Where; *C*, *k* and *b* are material parameters.

Although the development of advanced hardening models has improved the description of cyclic loading deformation characteristics, their application in finite element software is still limited, mainly due to their computational ineffectiveness (Eggertsen and Mattiasson 2009). Isotropic hardening, kinematic hardening and mixed hardening seem to be widely accepted models applied in the finite element software. This is because of the reasonable number of material parameters required for the constitutive equation (Q, b, C, and γ) and more importantly because computation is simpler due to only one surface model (Abaqus 2000; Eggertsen and Mattiasson 2009; Eggertsen and Mattiasson 2010; Chung et al. 2005).

2.5. Previous Work on Sheet Metal Bending Research

Springback has been given major attention in sheet metal forming research with numerous studies being conducted to understand and solve the problem. They range from inventing new designs of tooling, such as flexible and warm tooling, (Bruni et al. 2006; Keum and Han 2002; Zhang and Lin 1997; Zhang et al. 1997) to improving the accuracy of springback prediction by empirical and analytical methods and computer simulation. The accuracy of the springback prediction by analytical and numerical simulation depends to a great extent on constitutive equations and material parameter identification. Thus, several studies have been performed extensively on the matter. An attempt to review previous works is

presented and their advantages and disadvantages are discussed here. Based on the review, a conclusion is drawn regarding a knowledge gap, which motivates the current research.

2.5.1. Empirical Methods of Springback Evaluation

Various experiments have been conducted to obtain empirical data on springback, which involved various bending processes such as 90-degree wiping, v-bending, air bending and deep drawing as well as actual production processes. Based on the experiments, equations or charts have been developed as a reference for product and tool design in sheet metal forming. Several factors have been considered for the empirical equations such as material properties and geometry, tool geometry and process parameters. The empirical equations have been compiled in handbooks for industrial use (Wilson et al. 1965).

Davies studied the influence of material thickness, die gap, anvil radius and prior cold work for high-strength steels subjected to 90-degree wiping bending. Several charts were produced in relation to springback angle. In general, it was concluded that springback increased proportionally to anvil radius, die gap and material strength, but decreased as thickness increased. Besides, it was found that springback can be reduced by increasing the ratio of thickness to radius of the die to a value greater than 0.4 (Davies 1981).

Using air bending and statistical methods, a study of geometric parameter interaction with the material properties was performed by Inamdar et al. The study concluded that there were interactions among the factors and the design of tools in air bending depended on material properties (Inamdar et al. 2002).

Tekiner and Tekaslan et al. found similar outcomes when performing tests on v-bending. Tekiner in addition also found that springback can be reduced by maintaining the load longer on the materials (Tekaslan et al. 2006; Tekaslan et al. 2008; Tekiner 2004).

Gau and Kinzel used a wiping tool with three different inserts, with a radius of 1/2, 3/8 and 3/16 inch, to indicate the relationship of the Bauchinger effect to springback. Figure 2.13 shows their test tool. Cyclic loading was performed on the sheet metal by the following procedure: bending (B), reverse-bending (RB), bending-reverse-bending (BRB) and bending-reverse-bending-reverse (BRBR). Except for bending (B), the next processes require the sheet metal to be turned over for bending in the opposite direction. The experimental materials were aluminium alloy, high strength steel, aluminium killed draw quality steel and bake hard steel. Figure 2.14 shows the result of springback for aluminium alloy AA6111-T4. The bending angle after springback decreases as the material is subjected to reverse loading. It was concluded that cyclic loading affects springback. In other words, Bauschinger effect should be considered in the analysis of sheet metal springback.

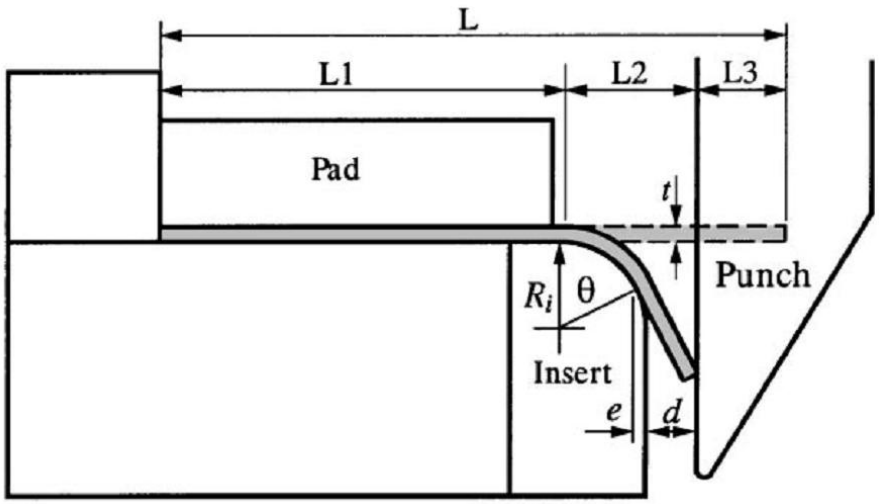

Figure 2.13 Gau and Kinzel's wiping tool

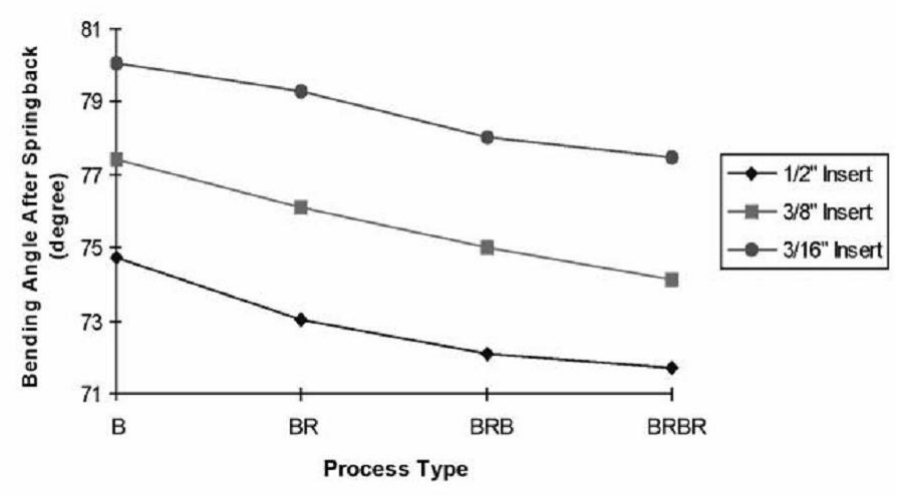

Figure 2.14 The effect of cyclic loading on springback (Gau and Kinzel 2001)

2.5.2. Analytical Methods for Springback Prediction

While providing useful information, empirical data tends to focus more on a limited set of parameters in a specific bending process. Thus, there is a need to consider an alternative more general method applicable to various bending processes with different parameters.

An approach based on the mechanics of sheet metal bending and plasticity theory has been considered as an alternative analytical method. Several model assumptions are applied. They include pure bending or tool bending of either non-hardening or hardening materials, transverse stress across the sheet, neutral axis shifting, thickness reduction, anisotropy and strain reversal effect. Rigid-perfectly plastic model was used for example by Hill in his analysis of sheet metal deformation based on plane strain bending. He assumed there was shifting of neutral surface with no thickness reduction (Hill 1998).

Based on beam elastic bending, Gardiner derived a well-known formula to define springback in bending based on bending geometry and material properties such as Young's modulus E and yield stress S (Gardiner 1957). The formula derived for the relative springback $\Delta\theta/\theta$ is

$$\Delta\theta/\theta = R/r = 4\left(RY/Et\right)^3 - 3\left(RY/Et\right) + 1$$

Equation 2.33

Where R and r are the radii of curvature of sheet metal before and after springback, E is Young's modulus, Y is yield stress and t is the sheet thickness.

Later Timoshenko and Goodier developed a formula based on elastic beam theory to account for small R/t (Sanchez et al. 1996).

$$\Delta\theta/\theta = 8M\left(1-\nu^2\right)\left(b^2-a^2\right)/\left(EN\right)$$

Equation 2.34

Where;

$N = (b^2\text{-}a^2)^2 - 4a^2b^2(\ln(b/a))^2$,

M = the bending moment applied,

v = Poisson ratio,

E=Young's modulus,

a= the inside radius of the bend,

b= the outside radius of the bend.

Sanchez et al. developed a tool, as shown on Figure 2.15 to validate Equation 2.33 and Equation 2.34. Steel F50, IF and aluminium killed draw quality steel were bent to different R/t values (1.5, 3, 3.3, 3.4, 3.7, 4.1, 4.8, 4.7 and 6.6).

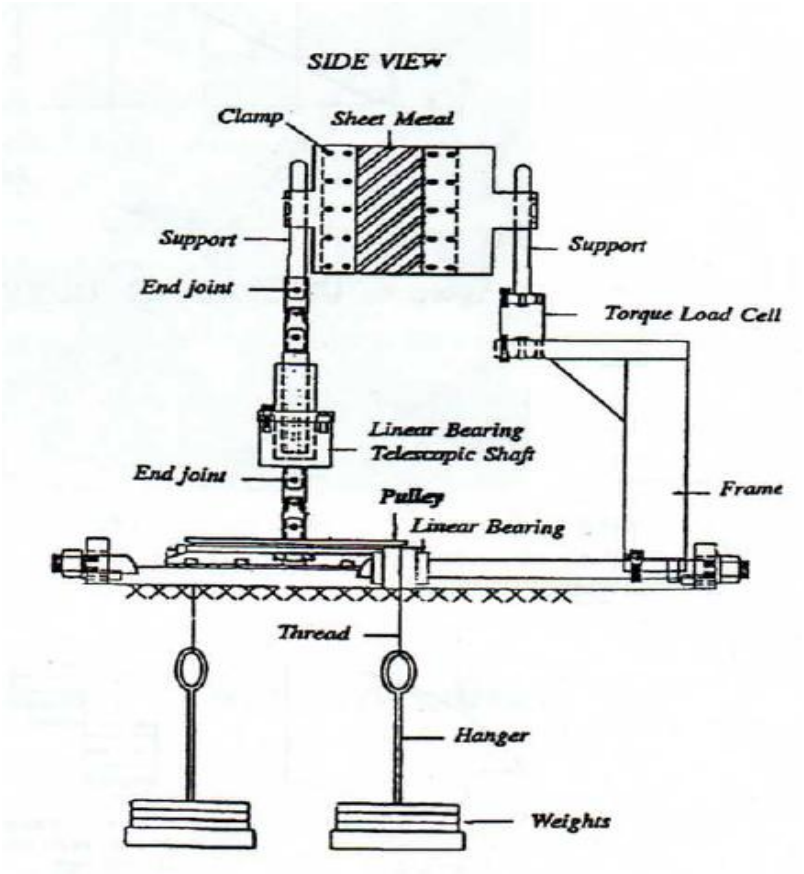

Figure 2.15 Sanchez's schematic of bend tester (Sanchez et al. 1996)

The results showed that both formulas underestimate the extent of springback mainly due to the assumption of only elastic stresses through the sheet metal thickness (Sanchez et al. 1996).

Concerning improvement of modelling reliability, the incorporation of real conditions is being considered. These include nonlinear stress strain relationship, thinning of sheet and anisotropy. Nonlinear stress-strain behaviour of bent material was taken into account by (Bower 1965); he applied Prager's isotropic hardening described by Equation 2.12. This led to the following formula:

$$\Delta\theta = 540\left(\frac{Et}{YR}\right)^{-3}\int_0^{Et/YR} x\tanh x\,dx$$

Equation 2.35

Where;

$\Delta\theta$ = springback angle,

Y = yield stress,

R = radius before springback,

t = thickness,

E = Young's modulus,

$X = Ey/RY$,

y = distance through the thickness measured from the neutral axis

To consider anisotropy, Leu used Hill's theory of plastic anisotropy and included normal anisotropy R in his formula (Leu 1997). The Bauschinger effect was neglected. The following equation was derived:

$$\frac{\Delta\theta}{\theta} = \frac{1/\rho - 1/\rho^*}{1/\rho} = \frac{UTS}{e^{-n}n^n}\left(\frac{1+R}{\sqrt{1+2R}}\right)^{1+n}\frac{3(1-\nu^2)}{2E(1+n)}\left(\frac{t}{2\rho}\right)^{n-1}$$

Equation 2.36

Where;

n = strain exponential hardening

UTS = ultimate tensile strength

ρ = radius of curvature

R = normal anisotropy

E= Young's modulus

ν= Poisson ratio

e= exponential function

2.5.3. Finite Element Simulations for Springback Prediction

Analytical methods of solving bending problems can be applied to simple shapes and idealised process conditions. Nevertheless, for complex shapes of actual products and real bending processes the analytical methods have a limited use. With advances in computing technology, finite element simulation provides an alternative solution. Yet, reliability and accuracy of the finite element approach is still a challenge. Therefore, further developments of the methods are required. Among them are the improvements in the finite element formulation (new type of elements), the robustness of the numerical methods used and the quality of the constitutive models describing the deformation behaviour of the sheet metal (Oliveira et al. 2007).

This thesis is only concerned with the last aspect of these improvements and, in particular, the hardening rules used in material models, such as isotropic hardening, linear kinematic hardening, nonlinear kinematic hardening and combination of isotropic and kinematic hardening.

Isotropic hardening for example was used by several researchers to determine geometrical effects of die gap, sheet thickness and die radius on the springback angle and to show that computer simulation can provide a better prediction of the final sheet metal shape.

Nilsson et al. conducted a v-bending test to prove that finite element simulation is a better method of predicting springback. The simulation applied simple elastic plastic isotropic hardening data from a tensile test. Materials tested were aluminium, stainless steel and low carbon steel of various grades and thicknesses. Although the simulation results underestimated the springback angle when compared with experimental data, the study concluded that the simulation could be used to predict springback (Nilsson et al. 1997).

Bakhshi-Jooybari et al. performed an experimental and simulation study using v-bend and u-bend on a CK67 steel sheet. The simulation used a similar material model as that used by Nilsson. However, the simulated springback angles were greater than the experimental ones (Bakhshi-Jooybari et al. 2009).

Using Hollomon's isotropic hardening model, Samuel focused on understanding the stress strain distribution for sheet deformation due to a draw bead with 5 mm radius. The author claimed that the drawing force and the blank holding force obtained by the simulation were accurately predicted (Samuel 2002).

Finite element simulation using complex hardening models has been considered to improve simulation of sheet metal forming. This, in particular, refers to the case when accounting for a reversal loading in which Bauschinger and the hardening transient effects are present. A study by Li et al., for example, found that including Bauschinger effect can improve springback prediction (Li et al. 2002). Thus, several studies were attempted using kinematic hardening or more complex hardening models, to improve the accuracy of the simulation. Some of the studies are presented here for reference.

Song et. al. studied straight flanging and found that using kinematic hardening produced better results in terms of springback prediction compared to isotropic hardening (Song et al. 2001). Simulations of hemispherical punch stretching, cup drawing and bending drawing tests were performed by Moreira and Ferron to investigate the impact of various types of hardening modelling in sheet metal forming. The isotropic hardening model was found to provide good simulation for the first two tests but not for the bending drawing test. They concluded that the kinematic hardening model should be considered to simulate stress reversals in the process of bending-unbending (Moreira and Ferron 2004).

Firat did a similar study and found that the kinematic hardening model provided fourfold improvement in springback prediction compared to the isotropic hardening model. Isotropic hardening produced up to one hundred percent relative errors while the kinematic hardening model showed seventeen to twenty percent relative error in terms of overall dimensional accuracy(Firat 2007; Firat et al. 2008).

Ragai et al. emphasised the importance of including the Bauschinger effect in springback prediction but found that anisotropic effect was quite small, with only

1 degree difference between the experimental results and the simulation results for different material orientations; the study was conducted using a draw-bend test for stainless steel 410 (Ragai et al. 2005). On the other hand, a study on high strength steel performed by Gomes et al. indicated that orientation has a significant influence on springback. Average simulation errors were 25% for 0 degree, 32% for 45 degree and 23% for 90 degree orientations (Gomes et al. 2005). However, the study was based on an isotropic hardening model, which meant the Bauschinger effect was neglected. It is believed that this could contribute to a bigger discrepancy between simulation and experimental results.

The influence of the hardening model has also been investigated in (Eggertsen and Mattiasson 2009; Eggertsen and Mattiasson 2010; Oliveira et al. 2007). Oliveira et al. compared the influence of the material model on springback prediction of a u-shape profile. The hardening laws used for the study were the isotropic hardening Swift law and the Voce law, a combination of Swift hardening with nonlinear kinematic hardening and a combination of Voce hardening with nonlinear kinematic hardening. The nonlinear kinematic hardening was represented by the Lemaitre-Chaboche law. The study concluded that each of the constitutive laws provides different results due to different predicted through-thickness stress gradients. The authors further concluded that the strain-path changes identified in the u-shape are very important and should be considered in the springback investigation. For that, the use of a bending-unbending test to characterize material data is required.

Eggertsen and Mattiasson studied and compared 5 hardening laws: Holloman isotropic hardening law, a combination of Holloman isotropic hardening

and Ziegler kinematic hardening law, Armstrong and Frederich hardening law (A-F), Geng and Wagoner hardening law (G-H) and Yoshida and Uemori hardening law (Y-U). Parameters of the hardening laws were determined using the inverse method based on a three-point bending proposed by (Zhao and Lee 2002). The quality of hardening rules was evaluated based on two bending processes. The first process was a three-point bending experiment, in which the performance was measured by trying to get the best fit with the experimental force-displacement curve. The findings indicated that the isotropic hardening produced the worst result. The A-F hardening model fitted well the lower part of the curve but was unable to produce a good fit for the upper part, , which is the permanent softening region. The Y-U hardening law provided the best results, but due to its mathematical complexity the preferred hardening law was that slightly less perfect one proposed by Geng and Wagoner (G-W). The second process was a Numisheet'93 standard benchmark test as in Figure 2.16. Table 2.1 shows the detailed results. Simulations of u-bending showed that all the hardening laws underestimated the springback angle, θ_1. The best prediction of the springback angles was obtained for the A-F hardening law.

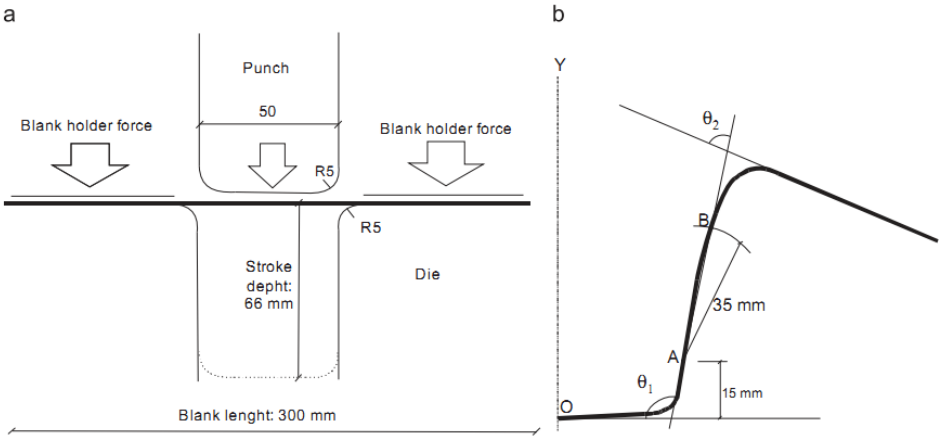

Figure 2.16 Numisheet'93 benchmark (a) experimental set-up (b) definition of the angles θ_1 and θ_2 (Eggertsen and Mattiasson 2009)

Table 2.1 Comparison between springback angles predicted by using various hardening rules and the experimental angles for material TKS-DP600 (Eggertsen and Mattiasson 2009)

Hardening law	θ_1	θ_2
Experiment	105.15 ± 0.3	82.6 ± 0.5
Isotropic hardening	100.585	81.959
Mixed hardening	100.00	84.60
Armstrong–Frederick	101.17	82.56
Geng–Wagoner	98.321	84.966
Yoshida–Uemori	97.964	85.246

Based on these results, we are able to say that the spring predictive ability of multiple-surface based hardening rules (G-W and Y-U) is not as good as in the case of the one-surface based hardening rules.

Lee, Chung and others conducted experimental validations to evaluate springback simulation based on the isotropic hardening law, kinematic hardening law and combination of the two laws. Additionally they used a new non-quadratic

anisotropic yield function. Materials tested were aluminium AA5754-O and AA6111-T4 grades and a DP-steel. Material parameters were determined using a cyclic tension and compression test. They used three bending processes, u-bending, unconstrained cylindrical bending and double-s rail bending; the last two processes are shown in Figure 2.17.

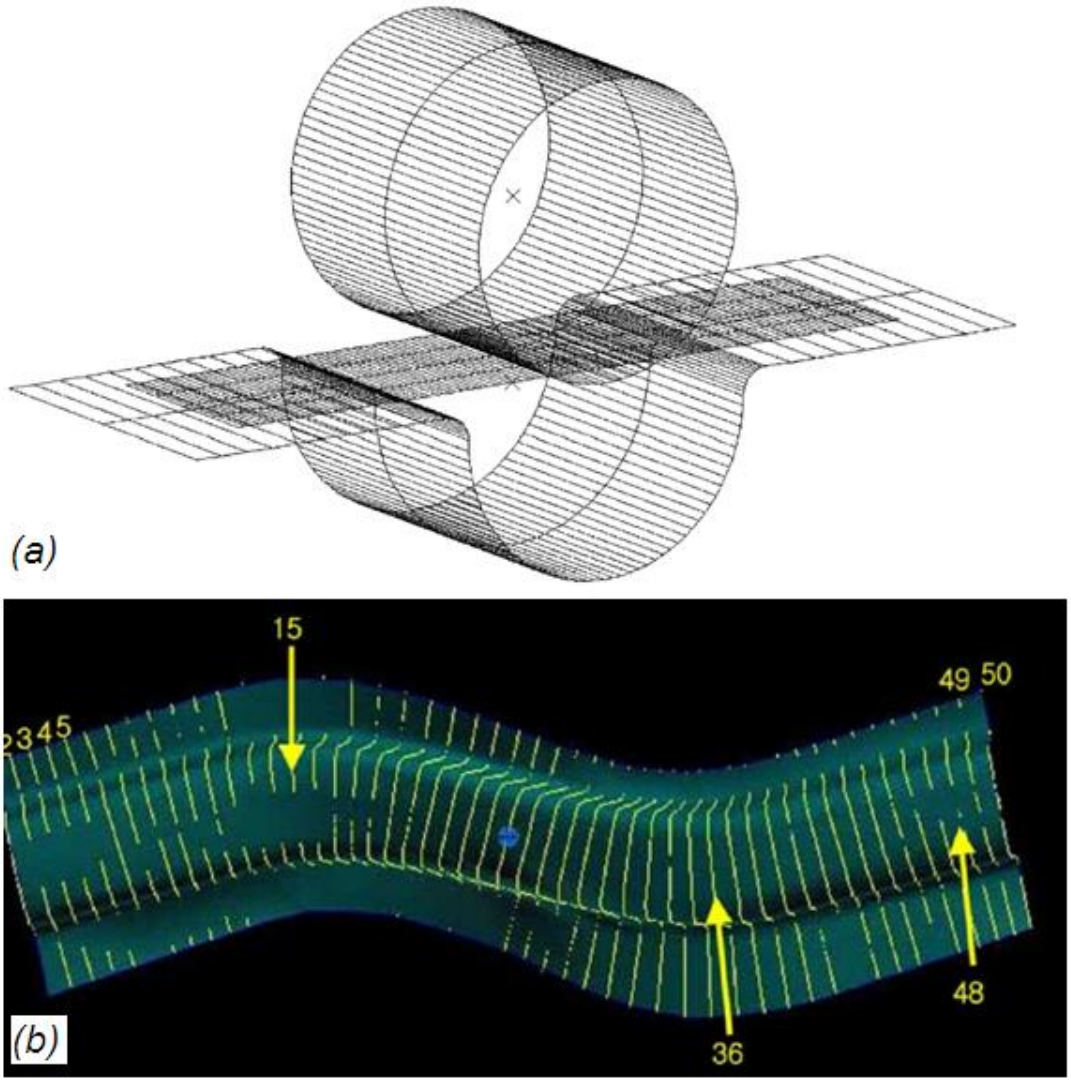

Figure 2.17 (a) Unconstrained cylindrical bending (b) double-s rail (Lee et al. 2005a)

For unconstraint cylindrical bending the overall simulation results overestimated springback. For u-bending and double-s rail, the combined hardening provided the best results compared to isotropic or kinematic hardening (Chung et al. 2005; Lee et al. 2005a; Lee et al. 2005b).

2.5.4. Cyclic Loading Experiments

The simple and efficient monotonic tensile test has been utilised extensively in early research on hardening. The need to describe the actual forming process, which involves bending-unbending requires the tensile test to perform cyclic or reverse loading, which is very difficult to perform for sheet materials. Several special design specimens and devices have been developed in an attempt to include the reversal effect in tensile tests for sheet metal. The device developed by Yoshida et al. (Yoshida and Uemori 2002; Yoshida et al. 2002; Yoshida and Uemori 2003) is shown in Figure 2.18, while the devices proposed by Boger et al. (2005), Kuwabara et al. (2009) and Cao et al. (2009) are shown in Figure 2.19, Figure 2.20 and Figure 2.21.

Yoshida and Boger's devices are almost similar. The sheets are packed together and supported by lateral plates to prevent buckling. Up to 0.25 and 0.13 compressive strains were recorded for low carbon steel and strength steel respectively. Kuwabara on the other hand used two comb-shaped dies to prevent buckling. Using a servo-controlled hydraulic cylinder A, the lower die-2 moves right and left so that a continuous tensile and compression reverse load can be applied to the sheet metal specimen. Compressive strains of 0.15-0.2 were recorded.

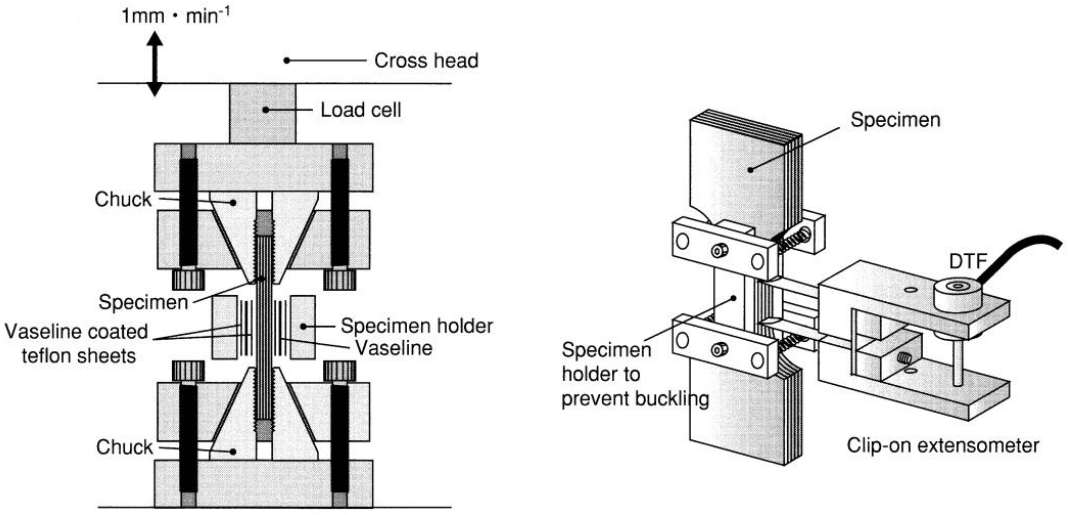

Figure 2.18 Yoshida's specimen holder to prevent buckling in compression (Yoshida et al. 2002)

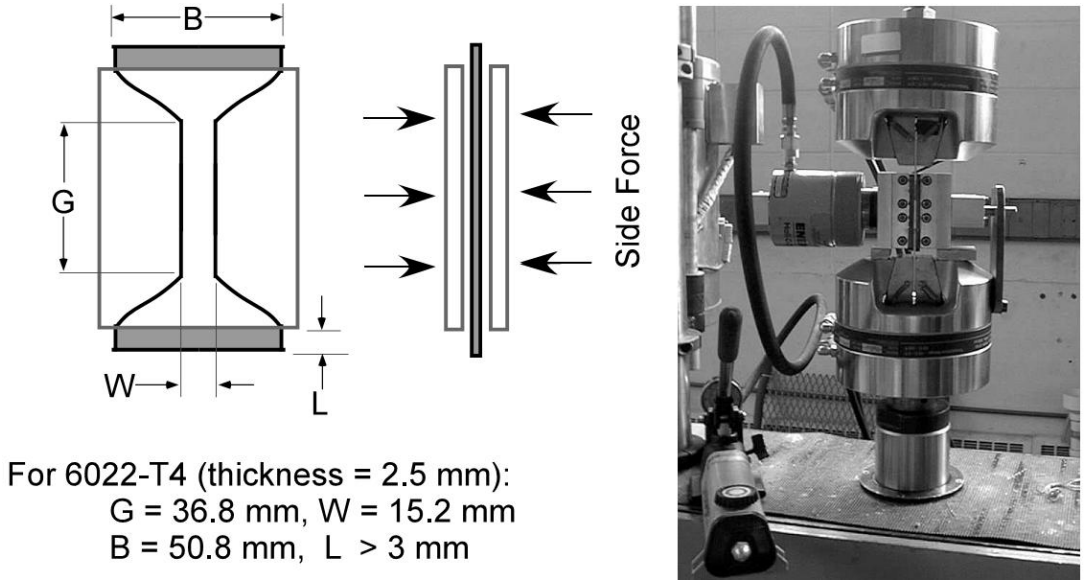

Figure 2.19 Boger's schematic representation of the sheet metal specimen and uniaxial tension/compression tool (Boger et al. 2005)

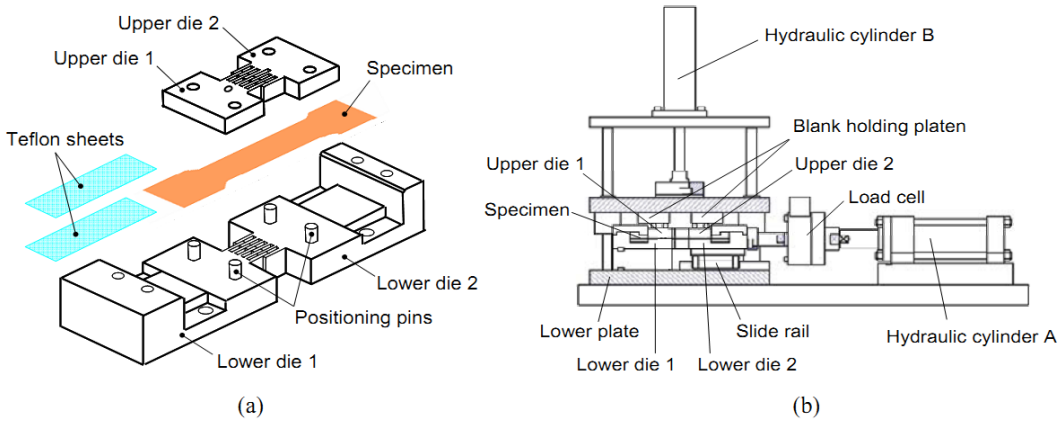

Figure 2.20 Kuwabara's comb-shaped device to prevent compression buckling (a) comb shape dies and (b) testing machine (Kuwabara et al. 2009)

Because of the need to constrain the sample in the thickness direction to prevent buckling, all raw stress-strain results require corrections for frictional and biaxial effects arising from this supporting force. Cao et al. (2009) claimed that none of the methods were capable of suppressing buckling completely due to unavoidable exposed area of the specimen. In the first two methods, the exposed areas were identified between the dies and clamps of the tensile machine; and in the latter method, between each pair of the 'fingers' of the die.

To improve the normal support on the entire specimen area during cyclic loading, they developed a four-block wedge with pre-loaded spring. Despite solving the buckling problem, the biaxial effect and the frictional effect between the die and specimen still exist. An additional frictional effect was also acknowledged between wedge plates and spring (Cao et al. 2009).

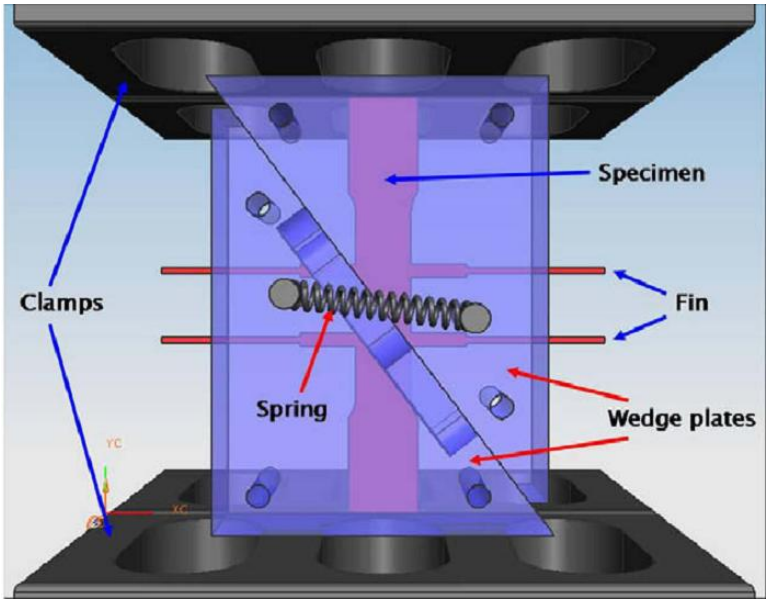

Figure 2.21 Cao's tension and compression tool (Cao et al. 2009)

In conclusion, setting up a tensile test for reversal loading is quite difficult. Cyclic torsion of sheet metal tubes and cyclic simple shear of sheet metal strips are proposed to overcome the buckling problem. One of the advantages of cyclic torsion is its capability to extend to large strain deformation. The tool, however, totally deviates from the actual sheet forming process and the sheet has to be welded, which would affect the material properties (Boger et al. 2005). The sliding effect on the other hand is the main problem in the cyclic simple shear test. Furthermore, the measurement of the local strain is quite difficult due to the limited area of the shear zone. The test however is very easy to setup and use (Thuillier and Manach 2009).

Using a cyclic bending test has been considered as another preferred alternative, considering its capability and flexibility to perform reverse loading to study the Bauschinger effect and its resemblance to industrial bending processes.

Moment and curvature relationship in association with the springback phenomenon observed in the process can be used to derive a fundamental understanding of the stress-strain behaviour during elastic-plastic deformation. Motivated by this relationship, substantial experimental research has been conducted to develop and validate stress-strain modelling in terms of moment-curvature relationship.

In Carbonniere et al. (2009), a comparison study of kinematic hardening parameters, derived from the bending-unbending test and from the shear test was conducted on 1mm thick trip steel and aluminium alloy. The bending test and a specimen used are shown in Figure 2.22.

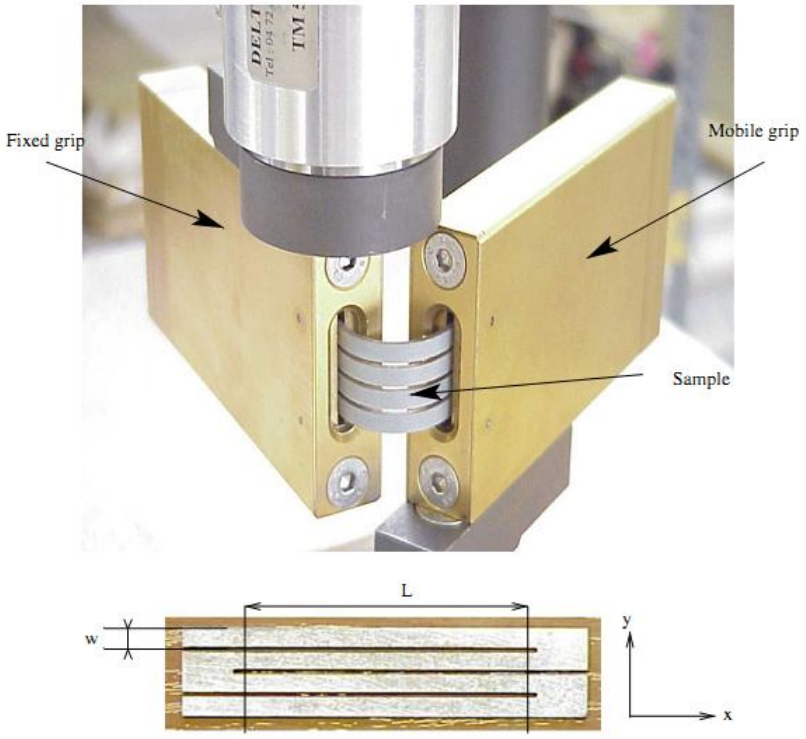

Figure 2.22 The bending device and a four-piece specimen (Carbonniere et al. 2009)

The aim was to evaluate the performance of the parameters identified in one test in finite element simulation of the results obtained in another test. The material

parameters established from the bending-unbending test, when used in the shear test simulation, provided very good description of the experimental shear data. This result is shown in Figure 2.23. When shear derived material parameters were used, the ability to describe the experimental bending-unbending data was worse. This result is shown in Figure 2.24.

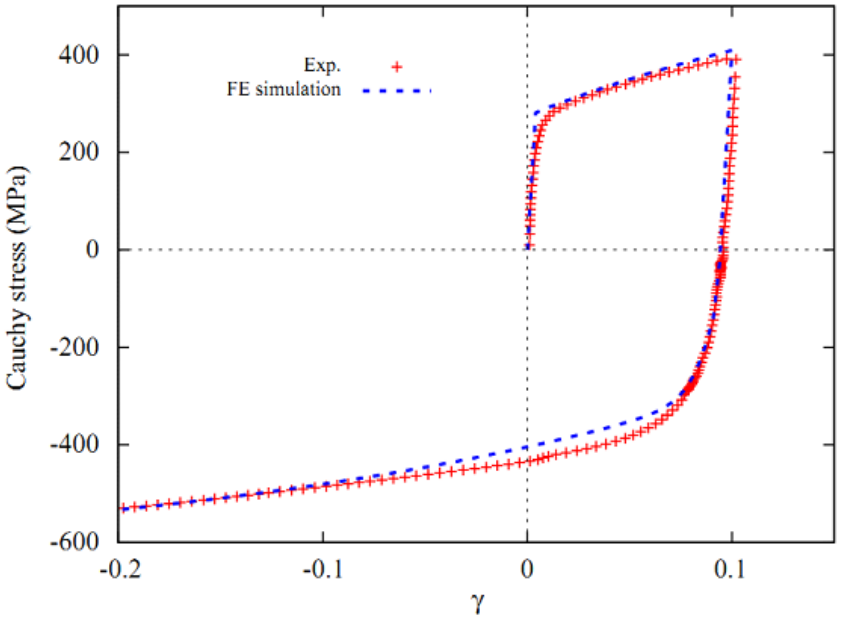

(a)

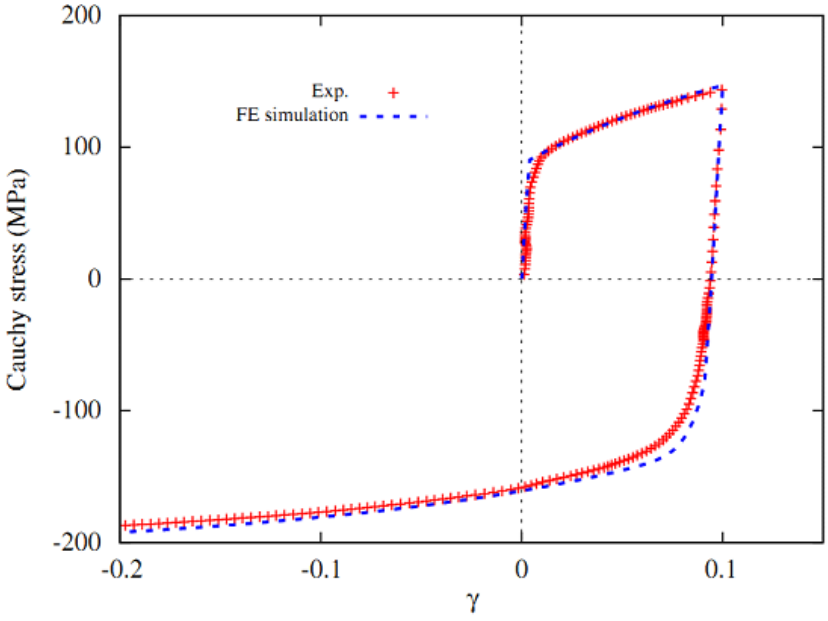

(b)

Figure 2.23 Shear test and finite element results for material parameters identified from the bending test of 1 mm thick (a) trip steel b) aluminium alloy (Carbonniere et al. 2009)

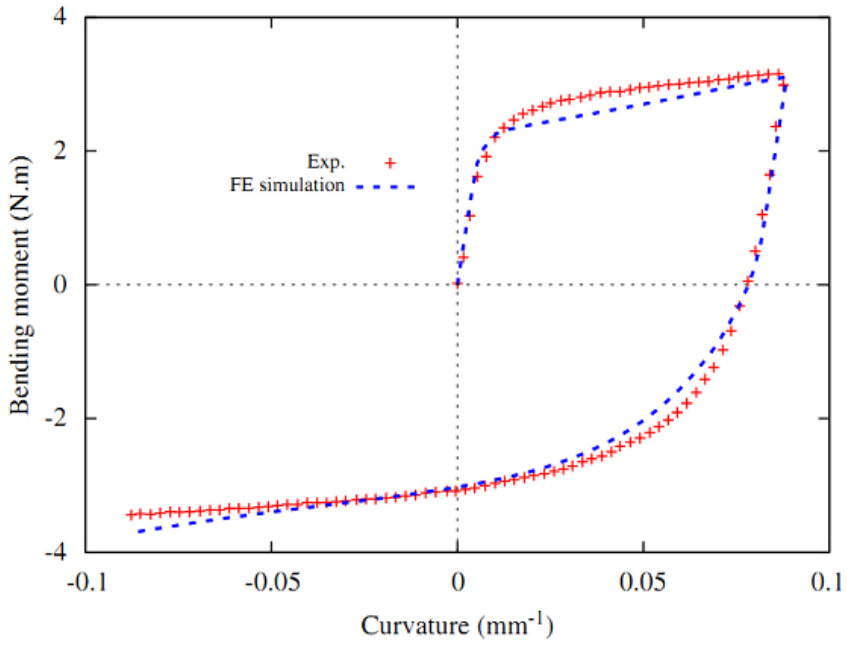

(a)

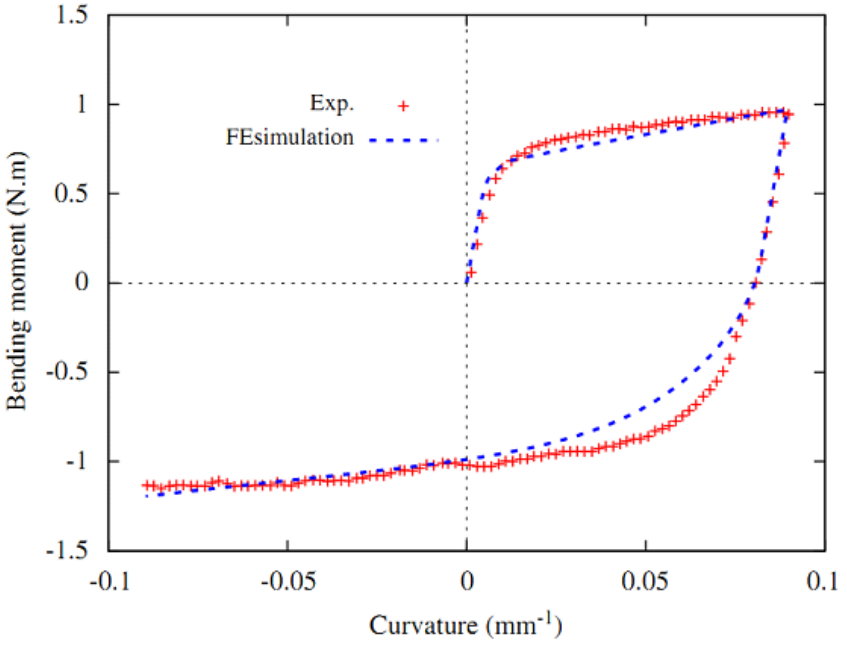

Figure 2.24 Bending test and finite element results for material parameters identified from the shear test of 1 mm thick a) trip steel b) aluminium alloy (Carbonniere et al. 2009)

In Weinmann et al. (1988), the authors conducted an experiment to capture deformation behaviour of steel and aluminium sheet in a forming operation, focused particularly on the draw beads. The authors intended to show the Baushinger effect as a function of strain amplitude, pre-strain and sheet thickness. They found that Bauschinger effect decreased as strain amplitude increased and there were no significant changes due to thickness reduction; hence the moment across the sheet thickness was carried by an individual layer in a similar manner. However, the conclusion is limited to thin sheets with 3 mm thickness and less. Pre-strain on the other hand showed a significant influence on the Bauschinger effect and quickened the development of a steady-state hysteresis loop. It was found that pre-strain increased the first cycle Bauschinger effect factor. The device used by the authors is shown in Figure 2.25.

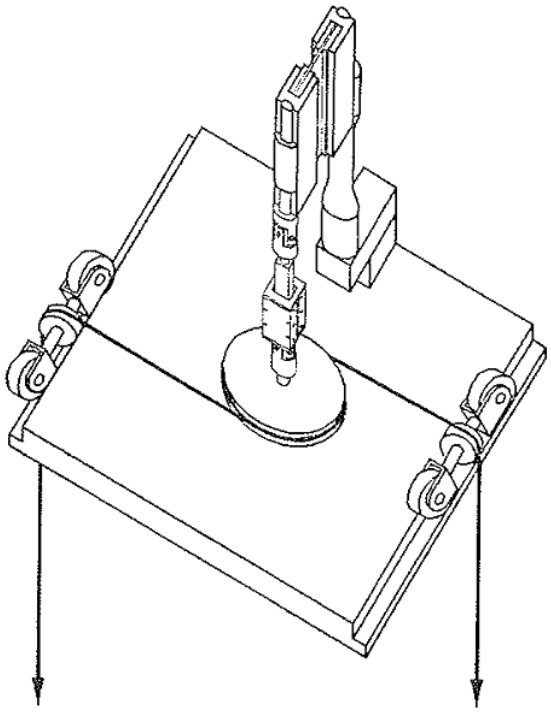

Figure 2.25 Weinmann's bending-unbending test equipment (Weinmann et al. 1988)

A similar experimental tool was developed by Yoshida (Yoshida et al. 1998), as shown in Figure 2.26, to study cyclic strain hardening and the Bauschinger effect of 0.42 mm thick stainless steel 304, 0.50 mm thick stainless steel 430 and 0.98 mm thick low carbon steel (SPCC). The authors used an optimization technique based on iterative multipoint approximation to identify material parameters for isotropic and nonlinear kinematic hardening which would give satisfactory agreement between the experimental and analytical moment-curvature results for a number of cycles. Verification was performed by comparing the stress-strain curves derived from the cyclic tests with the experimental curves obtained by tensile testing. They found a good match provided the material parameters for bending-unbending were based on experimental results for more than one cycle.

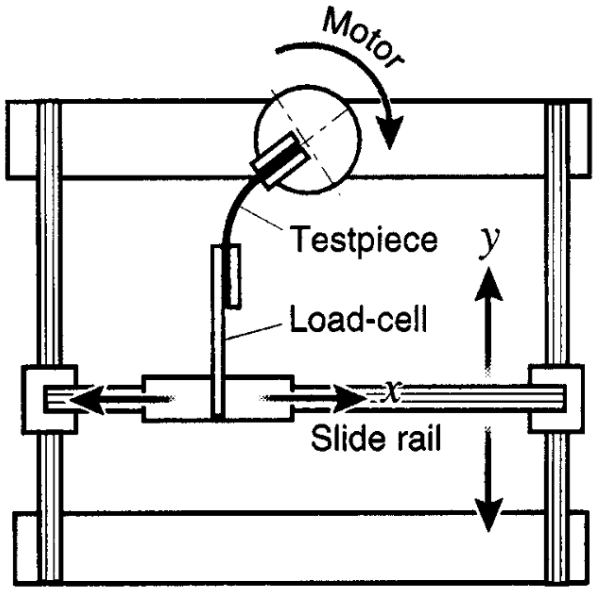

Figure 2.26 Yoshida's schematic experimental set up for cyclic bending (Yoshida et al. 1998)

In Brunet et al. (2001), the authors used a four-point bending test to study cyclic loading and the least-square optimization to identify parameters for isotropic-nonlinear kinematic hardening of the Lemaitre-Chaboche equation. Materials used were 0.8 mm thick of aluminium alloy and low carbon steel. They suggested that it was sufficient to consider the first cycle and monotonic loading for the material parameters of the constitutive equation to be established. Verification was conducted similarly to (Yoshida et al. 1998).

Figure 2.27 shows the three-point bending test used by Geng et al. (2002), Zhao and Lee (2002) and Omerspahic et al. (2006). Instead of using the moment-curvature relationship, the tool provided a force-displacement graph for the cyclic study. Geng et al. used the tool to compare hardening laws for cyclic loading with the one derived from tension-compression test. Materials for the study were aluminium alloy 6022-T4, high-strength low-alloy steel (HSLA) and drawing-quality silicon-killed steel (DQSK). They found that the constitutive models obtained by fitting the reverse-bend test and tension-compression test show significant differences when evaluated in terms of their stress-strain responses following a stress reversal and the nonlinear kinematic hardening law that was unable to match the Bauschinger effect at strains larger than 0.02.

Zhao and Lee conducted finite element analysis of the cyclic bending using isotropic, nonlinear kinematic and combined hardening for low carbon steel (SPCEN) and high strength steel (SPRC). Isotropic hardening overestimated the hardening component, while kinematic hardening underestimated it. Combined hardening was capable of showing the predictable Bauschinger effect accurately. They used a genetic algorithm to identify parameters for the combined hardening.

Omerspahic et al. continued with that work using a redesigned three-point bending tool for high strength steels ZSte340 and DP600 and aluminium alloy AA5182. Two parameters for each of the isotropic hardening and nonlinear kinematic hardening were identified by minimizing the sum of square differences between experimental and finite element results using the response surface method of an optimization code.

Chun et al. used the three-point bending and the results of Zhao and Lee to identify material parameters for their proposed hardening equation based on a modification of the Chaboche constitutive equation. The modification accounted for a permanent offset in the flow stress. It was found that the parameters describing bending were similar to parameters derived from tension-compression and fitted well the permanent offset of the experimental curve. In general, they concluded that both the three-point bending and tension-compression can be used to identify material parameters for the proposed equation (Chun et al. 2002a; Chun et al. 2002b).

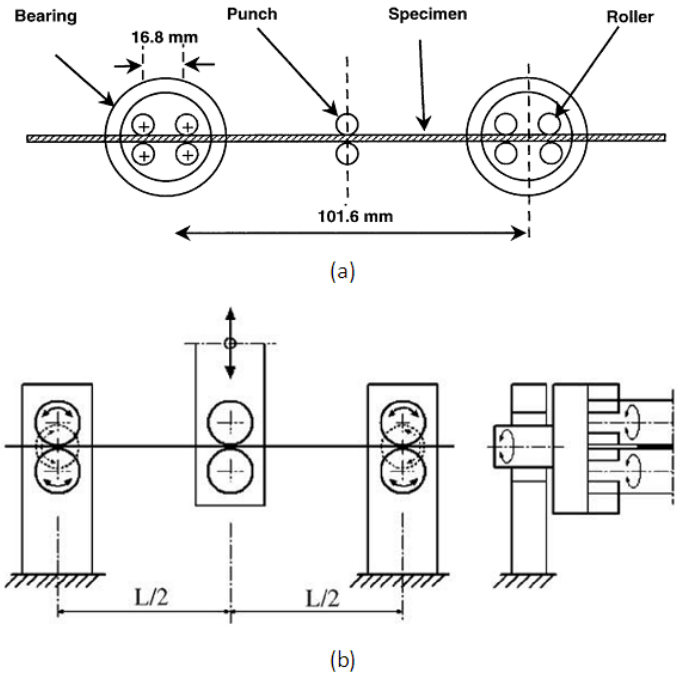

Figure 2.27 Schematic drawings of three-point bending used by (a) (Geng et al. 2002) and (Zhao and Lee 2002) and (b) (Omerspahic et al. 2006)

Boers et al. developed a bending test as in Figure 2.28, not only for studying material parameters, but also to study hardening stagnation after reverse loading.

1. left linear guide
2. right linear guide
3. left hydraulic clamp
4. right hydraulic clamp
5. sample
6. elastic joint
7. base
8. left cylinder
9. right cylinder

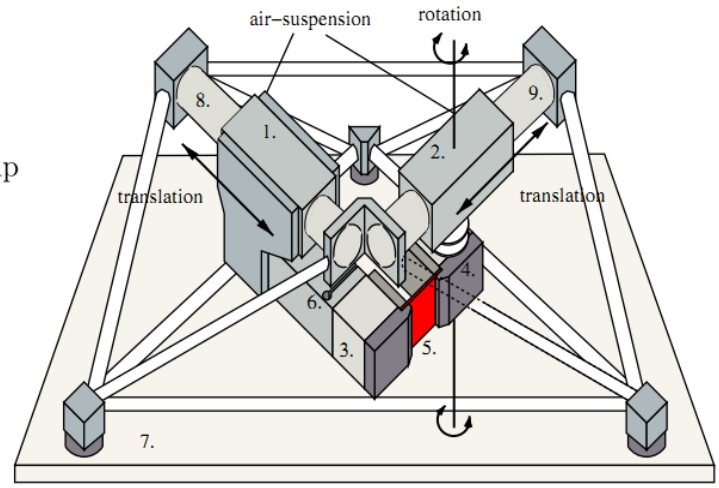

Figure 2.28 Tool for cyclic loading investigation proposed by (Boers et al. 2010)

As shown in the figure, the tool consists of eight components and one sheet metal sample (label 1 to 9). During experiment, the sides of a rectangular sample (5) are firmly clamped by a pair of hydraulically actuated clamps (3 and 4). The clamps are mounted on two air-suspended linear guides (1 and 2) that can move frictionless along and around the axes of two cylinders (8 and 9). Clamp 4 provides rotation whereas clamp 3 measures the applied bending moment by using an elastic joint (6). The authors claimed that the tool was capable of providing better results compared to cyclic shear, tension-shear and three-point bending methods (Boers et al. 2010).

2.5.5. Material Parameters Identification

Part of the crucial task of improving the constitutive models is to identify their parameters. The inverse identification method shown in Figure 2.29 has been adopted as one of the solutions (Yoshida et al. 2003). The idea is to adjust material parameters in the finite element code to produce a particular response such as geometry, force or moment that match the experimental data. The identification processes is done by minimising the difference between the finite element simulation results and the experimental results by using optimisation methods.

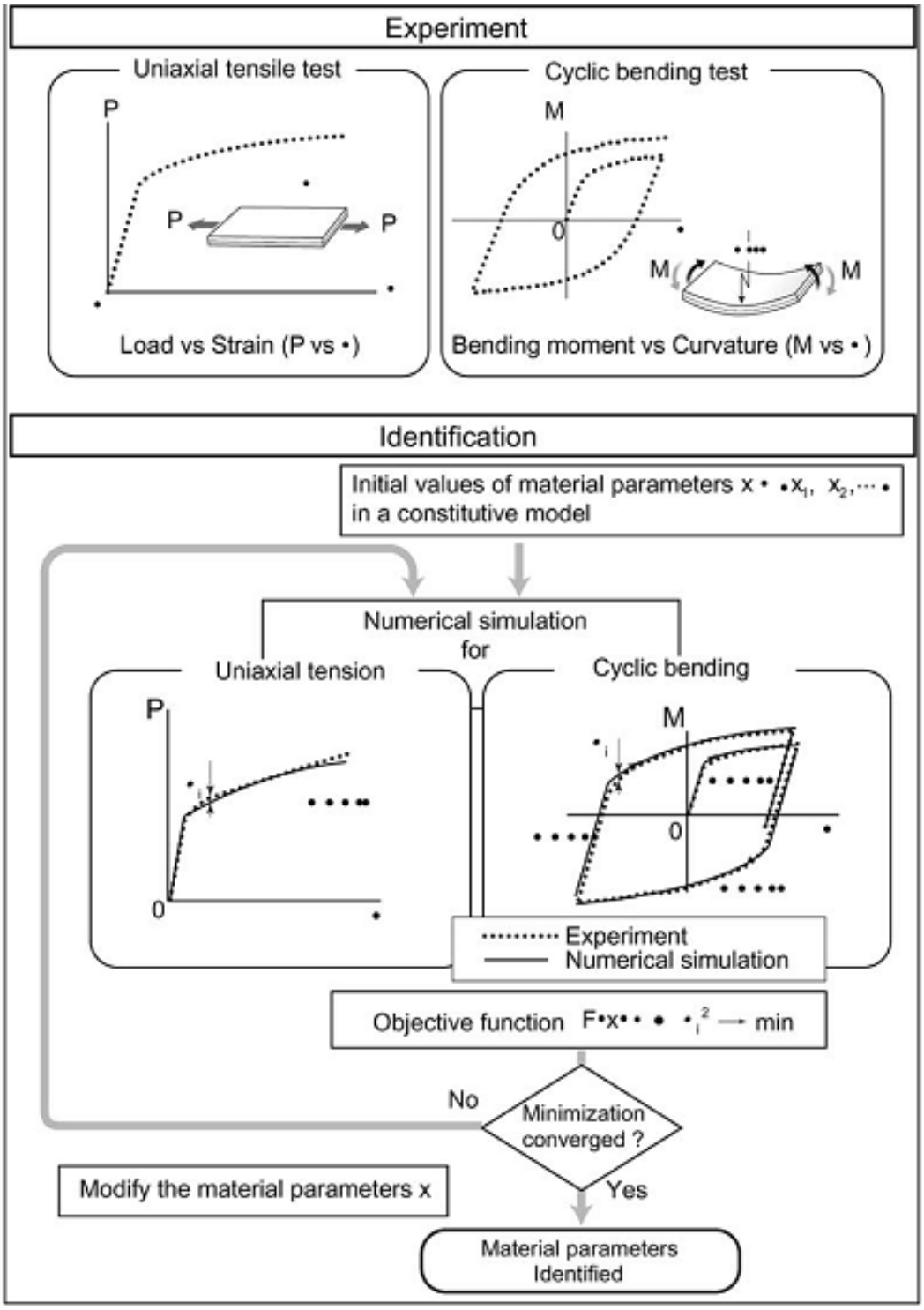

Figure 2.29 An inverse identification method to identify material parameters using finite element simulation (Yoshida et al. 2003)

This optimisation method works by finding a set of design parameters, $x = [x_1, x_2, x_3 .... x_n]$ that can in some way be defined as optimal. These parameters are obtained by minimizing or maximizing an objective function f(x), which is the difference between experimental results and numerical results. The optimisation variables are the material parameters that appear in the constitutive model (Chaparro et al. 2008). The most common optimisation methods are based on the evolutionary algorithms, derivative-free (direct search) algorithms and derivative (gradient based) algorithms. Evolutionary algorithms are judged to be very robust with the capability to tackle initial solution requirements as well as local minimum problems. However, they depend on sub-optimal algorithms to guarantee the optimisation of the global minimum of the objective function. Derivative-free (direct search) algorithms use simple strategies by eliminating derivative calculation, which leads to less Programming. However, they are time-consuming due to the need to perform many iterative calculations. The derivative algorithms on the other hand require less iterative calculation, which gives an advantage in terms of quick converging to the solution. Their limitation is due to difficulty in selecting an initial trial solution (Chaparro et al. 2008; De-Carvalho et al. 2011).

Several researchers used the inverse identification method together with a selected optimisation method to determine cyclic hardening parameters. Yoshida et al. applied inverse identification method to experimental results obtained in a bending-unbending process (Figure 2.26). The authors used an optimisation technique based on iterative multipoint approximation to identify material parameters for isotropic and nonlinear kinematic hardening, which would give satisfactory agreement between the experimental and simulation moment-curvature

results for a number of cycles. Verification was performed by comparing the stress-strain curves derived from the cyclic tests with the experimental curves obtained by tensile testing. They found a good match provided the material parameters for bending-unbending were based on experimental results for more than one cycle (Yoshida et al. 1998).

Zhao and Lee (2002) used inverse identification for three-point bending as shown in Figure 2.27(a) and a genetic algorithm optimization method to identify parameters for a combined isotropic-kinematic hardening equation. However, their tool has two distinct drawbacks. First, finite element simulation faces a contact problem at the punch rollers. To solve this problem, an equivalent non-contact model had to be built by Zhao and Lee. Second, instead of using moment-curvature, the measurement was in the form of force and displacement. As a consequence, the measurement of Bauschinger effect was not satisfactory (Geng et al. 2002).

Chun et al. used the same three-point bending test and the genetic algorithm optimisation to determine material parameters for their newly proposed anisotropic kinematic hardening and modified isotropic hardening equations. It was found that the identified parameters were comparable to parameters derived from tension-compression and fitted well the permanent offset of the experimental curve (Chun et al. 2002a). A similar type of bending but with a different type of optimisation technique was used by Omerspahic et al. Two parameters for each of the models of isotropic hardening, nonlinear kinematic hardening and viscoplastic hardening were identified by minimizing the sum of squared differences between experimental and finite element results using a response surface method of LS-OPT optimization software (Omerspahic et al. 2006).

A comparison study of kinematic hardening parameters, derived from a three point bending test and from a shear test was conducted by (Carbonniere et al. 2009). Gradient-based algorithm has been used in minimizing the difference between experimental results and numerical results. They concluded that bending-unbending testing is able to provide acceptable material parameters.

Zhang et al. used four-point bending and a gradient-based optimisation method (Guess-Newton algorithm) to determine isotropic hardening parameters, Young's modulus and initial yield stress for a stainless steel clad with copper sheet (bimetallic). They concluded the inverse identification method is applicable to bimetallic sheet metal (Zhang et al. 2010).

Some researchers did not use finite element simulation as part of the inverse method. Instead, they applied optimisation directly to match a constitutive equation and experimental results. The application of this approach to bending-unbending, however, is very limited. One such particular work was by Brunet et al. (2001). They used a three-point bending tool, an analytical formula describing bending-unbending results and a sequential quadratic Programming optimisation algorithm to identify parameters in a combined isotropic-kinematic hardening model. Verification of the material parameters application to springback prediction was not performed but it was strongly suggested by the authors (Brunet et al. 2001).

Direct application of optimisation to other types of testing is noticeable through several papers. Some of the works focused on material parameters identification and quite a number focused on evaluating optimisation performance for different algorithms. Andrade-Campos et al. sought to determine 16 parameters of a thermo-elastic viscoplastic constitutive model using a gradient based algorithm

method and a continuous evolutionary algorithm method for an aluminium alloy grade AA1050-O. The experimental data came from a tensile test and a shear test. The study found that the evolutionary algorithm results were only slightly better than the gradient based results. Thus, it was fair to conclude that both methods were applicable to determine material parameters for the constitutive model (Andrade-Campos et al. 2007).

Mahmoudi et al. used a multi-objective genetic algorithm to derive parameters for the Chaboche kinematic hardening model. The experimental data came from a tension-compression test. They claimed that the derived parameters were capable of improving prediction of cyclic ratcheting and the hysteresis loop model (Mahmoudi et al. 2011).

Several researchers proposed a combination of two or more optimisation methods as a strategy to combine the advantages of individual optimisation methods. Chaparro et al., for instance, proposed a combination of two gradient-based algorithms and an evolutionary-based algorithm. The two gradient-based algorithms were the steepest descent method and the Lavenberg-Marquardt (LM) method, while the genetic algorithm was represented by the evolutionary-based algorithm (EA). The strategy was used to identify parameters for the Barlat'91 yield criterion, an isotropic Voce type law and a kinematic Lemaitre and Chaboche law for 1 mm EN AW-5754 of aluminium alloy subjected to uniaxial tensile test and a simple shear test. Performances of the combined algorithm strategies were compared with performances of single algorithm strategies. The combined strategies (EA, the steepest descent method and LM) recorded 25 minutes of CPU calculation time, as compared to 30 minutes and 60 minutes recorded for Lavenberg-Marquardt

and the evolutionary algorithm, respectively. The results, however, did not show any significant differences, which meant that optimisation is relatively well performed by all algorithms (Chaparro et al. 2008).

De-Carvalho et al. compared the performance of various strategies (cascade, parallel and hybrid) for combining Laverbert-Marquardt (LM) and evolutionary algorithm (EA) in material parameter identification. The performance was measured by taking into account the value of the objective function, the number of iterations as well as the material parameters identified. Several constitutive models were used including a nonlinear isotropic hardening model and an elasto-viscoplastic model of isotropic and kinematic hardening. The first model used data from uniaxial tension of stainless steel AISI 304 and the latter used data from monotonous tensile and shear tests of low carbon steel E220BH. For cascade strategies applied to elastic-plastic hardening, it was concluded that all the strategies led to satisfactory results and similar final parameters. Performing LM followed by EA slightly improved the objective function but with a considerably larger number of iterations. Similar results were observed for the parallel strategy in terms of material parameter identification. However, the objective function was better than for single algorithm strategies. As for hybrid methods, the performance was evaluated based on elasto-viscoplastic model. Again material parameter identification produced insignificant differences among the strategies, with hybrid strategies showing considerable improvement only in terms of objective function values. In certain cases, LM performed better than hybrid strategies. Model parameters established by all strategies produced acceptable fit of experimental results (De-Carvalho et al. 2011).

2.6. Conclusions

Despite various efforts to improve sheet metal forming through accurate springback prediction and material modelling, there remains room for improvement of knowledge in this subject. One area of improvement is the adequacy and quality of experimental tests used to identify material parameters in constitutive equations. More accurate constitutive laws describing material behaviour are required to improve the quality of the analytical and finite element simulation results so that they can better represent the real deformation process.

Property data obtained from the uniaxial tensile-compression test is no longer sufficient. An attempt to account for the Baushinger effect in cyclic testing of sheet faces a buckling issue and suffers from friction due to the side support. Cyclic bending test managed to produce better results but they often refer to an ideal three-point bending rather than real industrial bending processes. This gap in the knowledge of plastic deformation requires further works.

Experimental identification of material parameters using inverse method requires an efficient optimisation strategy. The potential of using direct optimisation should be further explored; this method has an advantage of avoiding complex boundary conditions in the finite element model of a bending process.

To address the above issues in the current research, a plain-strain pure bending tool has been developed to perform experiments on a selection of materials, with a view to identifying material parameters for constitutive equations for a range of thicknesses. It is expected that this research will improve the predictive capability of sheet-metal forming practitioners so the throughput times can be reduced.

CHAPTER 3

MATERIAL CHARACTERISTICS

3.1. Introduction

Stress-strain relations describing the work hardening, strength and formability of the material are among the material properties of significant importance and are obtained by using tensile testing. In this work, tensile testing was used to evaluate the fundamental material properties of cold rolled low carbon steel and stainless steel of various thicknesses. The objective is to apply the properties as input data for finite element simulation in Chapter 6. The mechanical properties of the materials stated from some of literatures are shown in Table 3.1 and 3.2 (Groover 2002; Budynas and Nisbett 2008).

Table 3.1 Cold rolled low carbon steel

Standard and grade	EN10130:1999: DC01 BS1449:1991: CR4 JIS G3141: SPCC SAE: 1010
Chemical composition, %	C = 0.120, P = 0.045, S = 0.045, MN = 0.6
Mechanical properties	Yield strength : 140–280 MPa Tensile strength: 270–410 MPa Young's modulus: 207 GPa Total elongation: 30% Strength coefficient: 500 MPa Strain hardening exponent: 0.25

Table 3.2 Stainless steel

Standard and grade	ASTM: 304 2B 2B denotes cold rolled, heat treated, pickled, skin passed.
Chemical composition, %	C = 0.055, Cr = 18.2, Ni = 8.1, Mn = 1.8, P = 0.31, S = 0.001, Si = 0.357
Mechanical properties	Yield strength: 275 MPa Tensile strength: 650 MPa Young's modulus: 190-200 GPa Total Elongation: 55 Strength coefficient: 1200 MPa Strain hardening exponent: 0.40

3.2. Material Preparation and Procedure

3.2.1. Specimen Preparation

The tensile test specimens were manufactured in the form of bundles from rough blanks using a CNC milling machine. Prior to machining, the specimen blanks were cut in the direction of 0º from the direction of sheet metal rolling. In order to avoid buckling of the thin and high strength material, a pin-loaded type specimen with 50 mm gage length was used as suggested by the ASTM E8M. Detailed dimensions of this standard are shown in Figure 3.1.

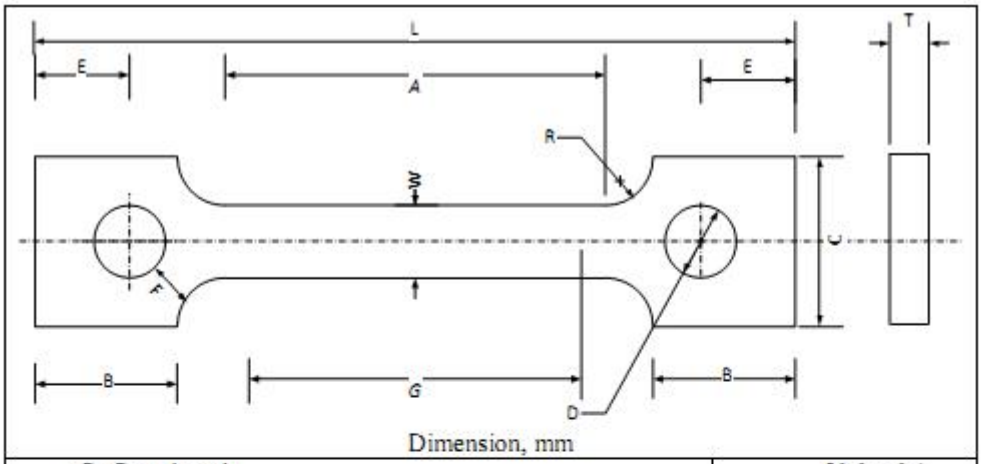

Dimension, mm

G: Gage length	50.0 ± 0.1
W: Width	12.5 ± 0.2
T: Thickness, max.	13
R: Radius of fillet, min.	13
L: Overall length, min.	200
A: Length of reduced section, min.	57
B: Length of grip section, min.	50
C: Width of grip section, approximate	50
D: Diameter of hole for pin, min.	13
E: Edge distance from pin, approximate	40
F: Distance from hole to fillet, min.	15

Figure 3.1Standard tensile specimen geometry and the prepared specimens (ASTM E8M 2004)

3.2.2. Test Procedure and Set-up

The tensile test standard used was ASTM E8M: "Standard test methods for tension testing of metallic materials (metric)". All tests were performed at room temperature. From the experimental data, true stress-strain graphs were derived and the Young's modulus and yield strength of the material were recorded. The test procedure is described below:

i. The machine was warmed up to normal operating temperature to minimize errors that may result from transient conditions.

ii. The specimen was held in vertical grips.

iii. The specimen was stretched until fracture at a crosshead speed of 5.0 mm /minute.

iv. Force and extension data were recorded.

v. Engineering stress (s) and strain (e) were calculated from these data with reference to the initial cross-sectional area of the specimen before test.

vi. These values of engineering stress and engineering strain were used to calculate the true stress and true strain for each specimen by using the following relationships:

$$\sigma = s(e+1)$$

$$\varepsilon = \ln(e+1)$$

vii. A similar procedure was applied to all specimens.

Figure 3.2 shows the experimental set-up of the test. 50 kN tensile machine, an extension meter model 7609V and Rubicon 825 data acquisition system from Denison Mayes Group were used for this experiment. Figure 3.3 shows the method used to establish the Young's modulus and yield strength from the true stress-strain graph of the data.

Figure 3.2 Tensile test experimental set-up

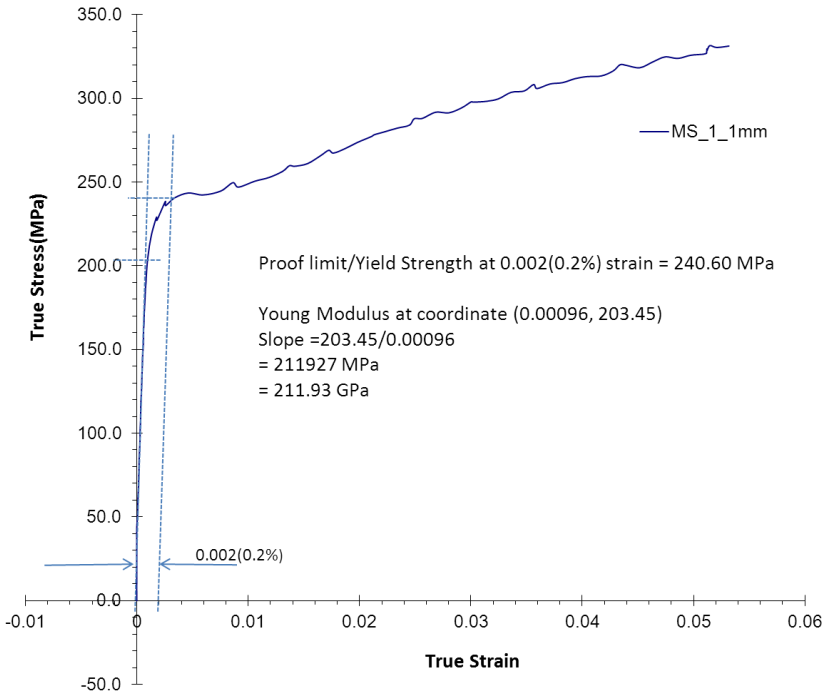

Figure 3.3 Identification of material properties by using true stress-strain graph

3.3. Results and Discussions

Figure 3.4 shows the force versus extension for low carbon steel and stainless steel obtained for different specimen thicknesses. A comparison based on the same thickness shows that plastic deformation of stainless steels requires higher force than plastic deformation of low carbon steel. Forces recorded for 1.5 mm and 1 mm thick low carbon steel specimens show a short plateau at the onset of plastic deformation (confirmed in stress-strain graphs later on in this chapter), which may indicate the occurrence of Luders bands, but no attempt was made to actually observe them during the test. All curves showed a typical smooth transition from elastic to elastic-plastic deformation.

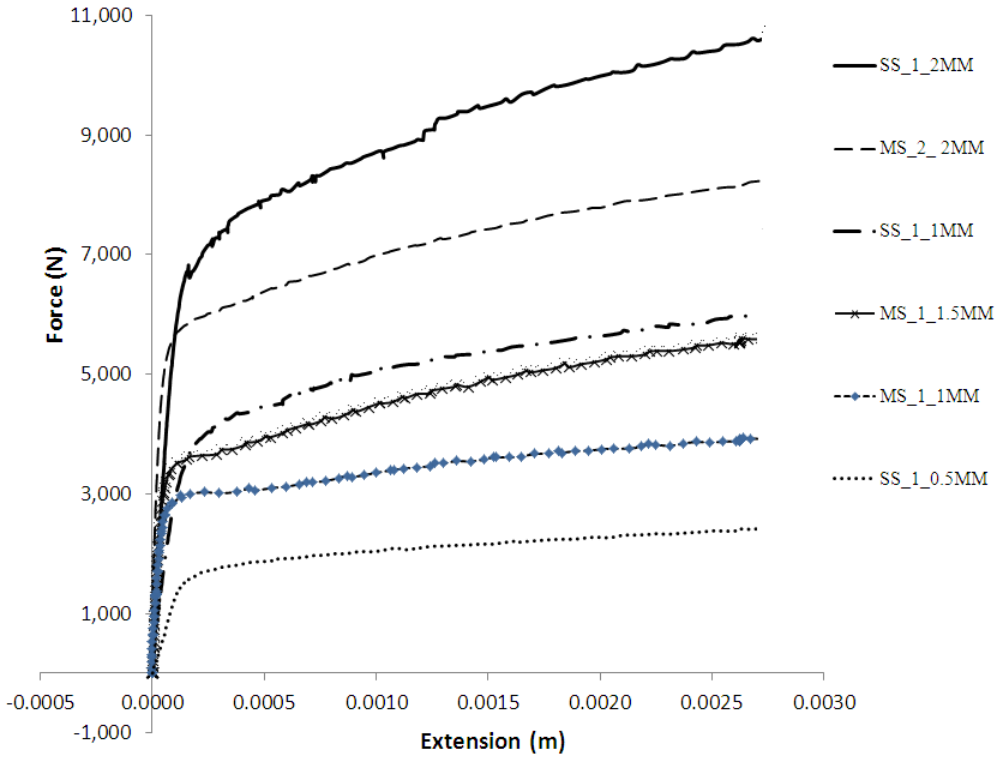

Figure 3.4 Force versus extension for cold rolled low carbon steel (MS) and stainless steel (SS) subjected to tensile test

3.3.1. True Stress-Strain Characteristics for Cold Rolled Low Carbon Steel

Figure 3.5 shows the true stress-strain relationship for cold rolled low carbon steel of 1 mm thick.

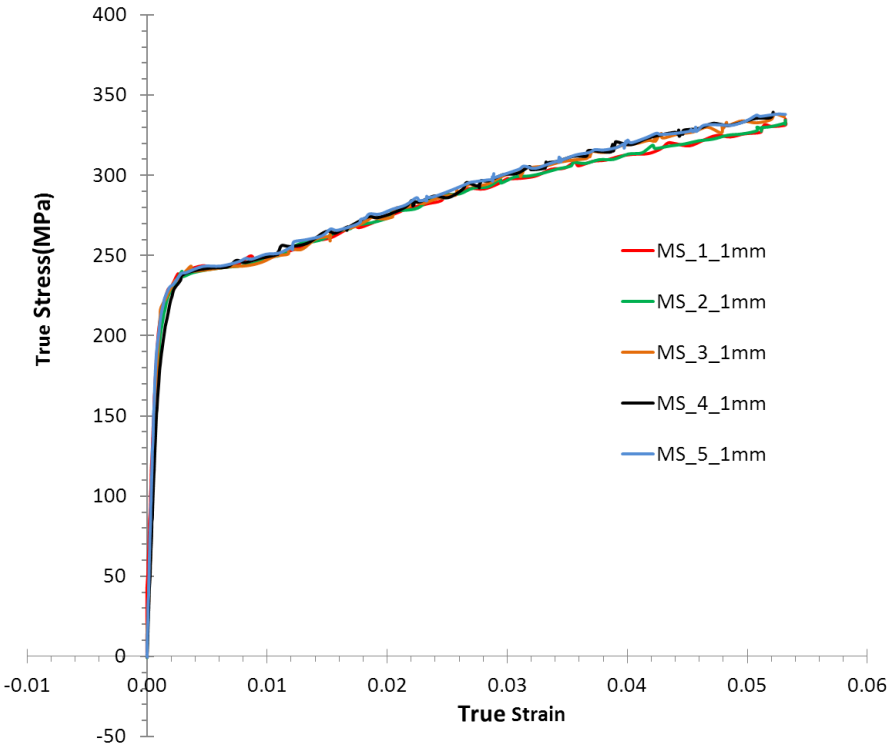

Figure 3.5 True stress versus true strain for 1 mm cold rolled low carbon steel

As mentioned before, the 1 mm thickness curve shows the Luders band effect explicitly. Although the overall stress-strain curves for the specimens were similar, the calculated Young's moduli were found to be scattered, as indicated in Table 3.3.

Table 3.3 Material properties of 1 mm cold rolled low carbon steel

Sample	1	2	3	4	5	Average
Young's modulus (GPa)	211.93	168.70	195.10	138.40	185.07	179.84
Difference (value minus average)	32.09	–11.14	15.26	–41.44	5.23	
Yield strength (MPa)	240.60	239.83	234.58	240.16	239.17	238.87
Difference (value minus average)	1.73	0.96	–4.29	1.29	0.30	

Sample	2	3	5	Average
Young's modulus (GPa)	168.70	195.10	185.07	182.96
Yield strength (MPa)	239.83	234.58	239.17	237.86

Therefore, only the best three specimens were considered for an average value, which was useful for application in the finite element simulation. The best three specimens were selected from among the lower values of the absolute difference between the Young's modulus of the specimen and the average Young's modulus of five specimens. The results show that the values of yield strength were almost similar, with differences ranging from 0.3 to 4.29 MPa. Young's moduli on the other hand were slightly scattered. The absolute differences ranged from 5.23 to 41.44. The best three samples selected were samples 2, 3 and 5.

Figure 3.6 shows the stress-strain curve for 1.5 mm cold rolled carbon steel. The Luders bands were slightly noticeable and the stress beyond the yield point was consistent for all specimens.

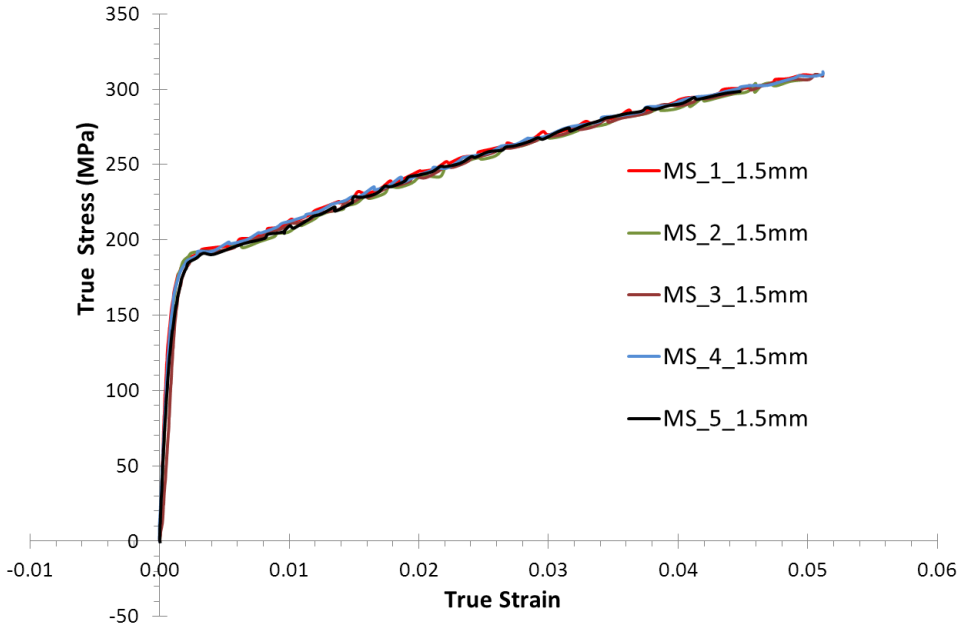

Figure 3.6 True stress versus true strain for 1.5 mm cold rolled low carbon steel

Table 3.4 shows the mechanical properties for 1.5 mm cold rolled low carbon steel.

Table 3.4 Material properties of 1.5 mm cold rolled low carbon steel

Sample	1	2	3	4	5	Average
Young's modulus (GPa)	172.57	157.19	118.22	175.83	150.55	154.87
Difference (value minus average)	17.70	2.32	–36.65	20.95	–4.32	
Yield strength (MPa)	191.34	191.48	191.18	189.55	187.83	190.28
Difference (value minus average)	1.06	1.20	0.90	–0.73	–2.45	

Sample	1	2	5	Average
Young's modulus (GPa)	172.57	157.19	150.55	160.10
Yield strength (MPa)	191.34	191.48	187.83	190.22

The results show that the values of yield strength were almost the same, with differences ranging from 0.73 to 2.45 MPa. The Young's moduli on the other hand were slightly scattered. The absolute differences ranged from 2.32 to 36.65. The best three samples were samples 1, 2 and 5.

Figure 3.7 and Table 3.5 show the true stress–true strain graph and mechanical properties for 2 mm cold rolled low carbon steel specimens.

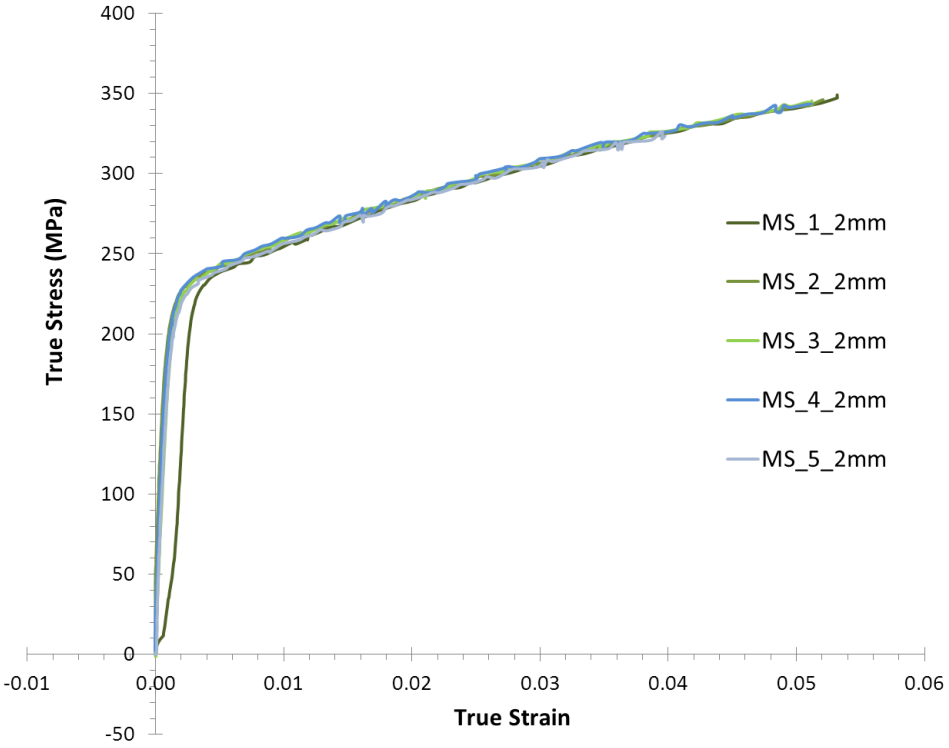

Figure 3.7 True stress versus true strain for 2 mm cold rolled low carbon steel

From the graph, sample 1 was out of range and considered disqualified for further analysis. Overall, the stress beyond the yield point was very consistent for all the samples.

Table 3.5 Material properties of 2 mm cold rolled low carbon steel

Sample	1	2	3	4	5	Average
Young's modulus (GPa)	91.35	199.24	163.35	234.95	153.28	168.43
Difference (value minus average)	–77.08	30.80	–5.08	66.52	–15.15	
Yield strength (MPa)	238.02	232.98	234.38	222.71	223.85	230.39
Difference (value minus average)	7.63	2.59	3.99	–7.68	–6.53	

Sample	2	3	5	Average
Young's modulus (GPa)	199.24	163.35	153.28	171.96
Yield strength (MPa)	232.98	234.38	223.85	230.40

The yield strength value of 2 mm cold rolled low carbon steel (230.40 MPa) in Table 3.5 was almost equal to the yield strength value of 1 mm low carbon steel (237.86 MPa) in Table 3.3. The yield strength values for all specimens were almost similar, with differences ranging from 2.59 to 7.68 MPa. The Young's moduli on the other hand were quite scattered. The absolute differences ranged from 5.08 to 77.08. The best three samples, with the smallest absolute differences were samples 2, 3 and 5.

3.3.2. True Stress-Strain Characteristics for Stainless Steel

The same approach as that used for low carbon steel was applied to determine the best values of the mechanical properties of stainless steel. Figure 3.8 and Table 3.6 show the graph and mechanical properties of stainless steel of 0.5 mm thickness.

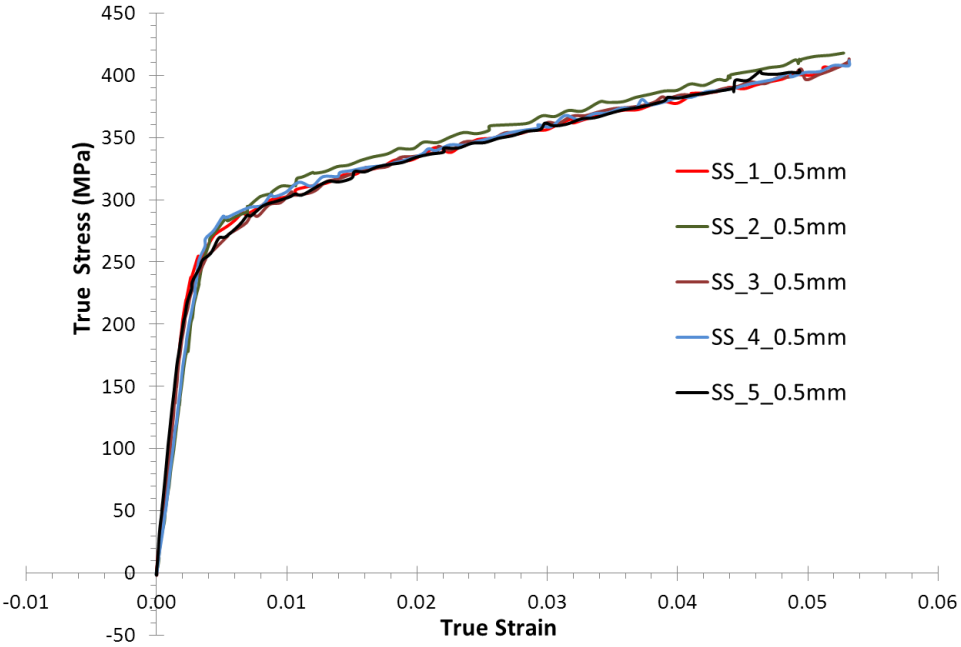

Figure 3.8 True stress versus true strain for 0.5 mm stainless steel

Table 3.6 Material properties of 0.5 mm stainless steel

Sample	1	2	3	4	5	Average
Young's modulus (GPa)	101.24	74.87	93.20	77.25	106.73	90.66
Difference (value minus average)	10.58	–15.79	2.54	–13.41	16.07	
Yield strength (MPa)	272.38	286.07	270.92	285.52	269.17	276.81
Difference (value minus average)	–4.43	9.26	–5.89	8.71	–7.64	

Sample	1	3	4	Average
Young's modulus (GPa)	101.24	93.20	77.25	90.56
Yield strength (MPa)	272.38	270.92	285.52	276.27

The results in Table 3.6 show that the values of yield strength were similar, with differences ranging from 4.43 to 9.26 MPa. The Young's moduli were scattered. The absolute differences ranged from 2.54 to 16.07. The best three samples having Young's modulus values with the smallest absolute differences were samples 1, 3 and 4.

Figure 3.9 and Table 3.7 show the true stress-strain and mechanical properties of 1 mm stainless steel. From the figure, the flow stress for specimen 5 was lower than the stresses of the rest of the specimens at a strain value of more than 0.02.

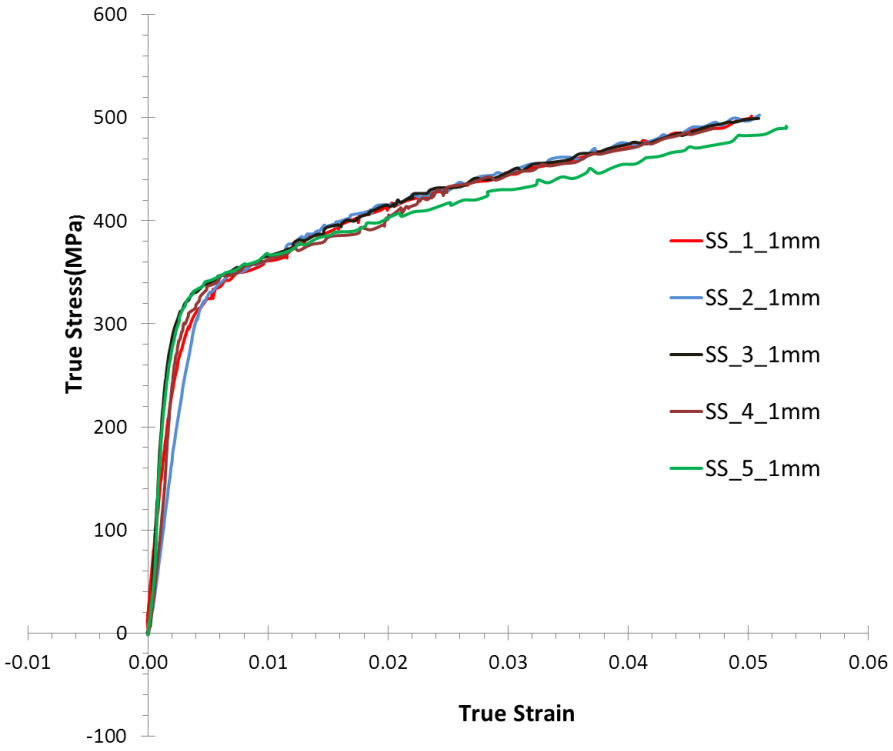

Figure 3.9 True stress versus true strain for 1 mm stainless steel

Table 3.7 Material properties of 1 mm stainless steel

Sample	1	2	3	4	5	Average
Young's modulus (GPa)	106.48	80.09	175.75	116.88	147.74	125.39
Difference (value minus average)	–18.91	–45.30	50.36	–8.51	22.35	
Yield strength (MPa)	315.20	341.03	302.51	322.57	329.18	322.10
Difference (value minus average)	–6.90	18.93	–19.59	0.47	7.08	

Sample	1	4	5	Average
Young's modulus (GPa)	106.48	116.88	147.74	123.70
Yield strength (MPa)	315.20	322.57	329.18	322.32

The difference in yield strength and Young's modulus of the specimen were very low and considered very acceptable. Overall, the values of yield strength were almost similar, with differences ranging from 0.47 to 19.59 MPa. The Young's moduli on the other hand were scattered. The absolute differences ranged from 8.51 to 50.36. The best three samples having Young's modulus values with the smallest absolute differences were samples 1, 4 and 5.

Figure 3.10 and Table 3.8 show the true stress-strain and mechanical properties of 2 mm stainless steel.

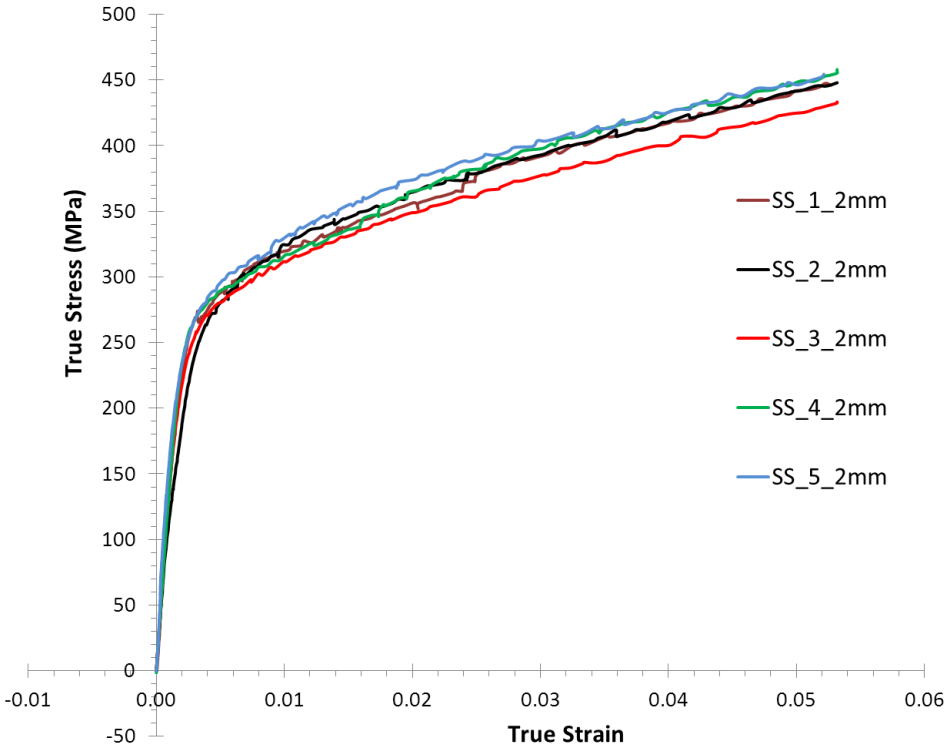

Figure 3.10 True stress versus true strain for 2 mm stainless steel

Table 3.8 Material properties of 2 mm stainless steel

Sample	1	2	3	4	5	Average
Young's modulus (GPa)	127.32	95.84	123.41	122.88	140.06	121.90
Difference (value minus average)	5.42	–26.06	1.51	0.98	18.16	
Yield strength (MPa)	274.08	271.97	266.49	274.42	278.54	273.10
Difference (value minus average)	0.98	–1.13	–6.61	1.32	5.44	

Sample	1	3	4	Average
Young's modulus (GPa)	127.32	123.41	122.88	124.54
Yield strength (MPa)	274.08	266.49	274.42	271.66

The flow stress of specimen no. 3 was lower than that of the other samples. The differences in the yield point and Young's modulus however were among the lowest and are considered acceptable. Overall, the values of yield strength were similar, with differences ranging from 0.98 to 6.61 MPa. The Young's moduli for samples 2 and 5 were quite different. The absolute differences range from 0.98 to 26.06. The best three samples having the smallest absolute differences in Young's modulus values were samples 1, 3 and 4.

3.4. Conclusions

i. The tensile test graphs explicitly show the nonlinear and linear hardening of material behaviour in sheet metal deformation, which will be included in the material model used in this research.

ii. Except for 1 mm and 1.5 mm cold rolled low carbon steels, in which Luders bands were observed, the transitions between the elastic and plastic deformation for other materials were very smooth. With the effect of the Luders bands, the yield strength of 1 mm low carbon steel was slightly greater than the yield strength for 2 mm cold rolled low carbon steel.

iii. The yield points for stainless steel were distinctly observed, with 1 mm thick samples showing the largest yield point followed by 2 mm and then 0.5 mm samples. The elastic-plastic transition was very smooth and the Luders bands did not occur.

iv. The Young's modulus values deviated from the normally acceptable values of 200 GPa to 210 GPa, values for steels. For this reason the Young's modulus values of 207 GPa and 190 GPa for low carbon steel and stainless steel respectively were applied in this research. These values were adopted from Budynas and Nisbett (2008). The yield strength values however are within acceptable ranges.

CHAPTER 4

CYCLIC LOADING EXPERIMENT

4.1. Introduction

In sheet metal forming, cyclic loading occurs due to bending and unbending of material as in the die draw bead and when the sheet is drawn over a die shoulder corner (Hosford and Caddell 1993; Sanchez 2010; Yoshida et al. 2002). This has been illustrated in Figure 2.6 in Chapter 2 but it is also shown in Figure 4.1 below for convenience.

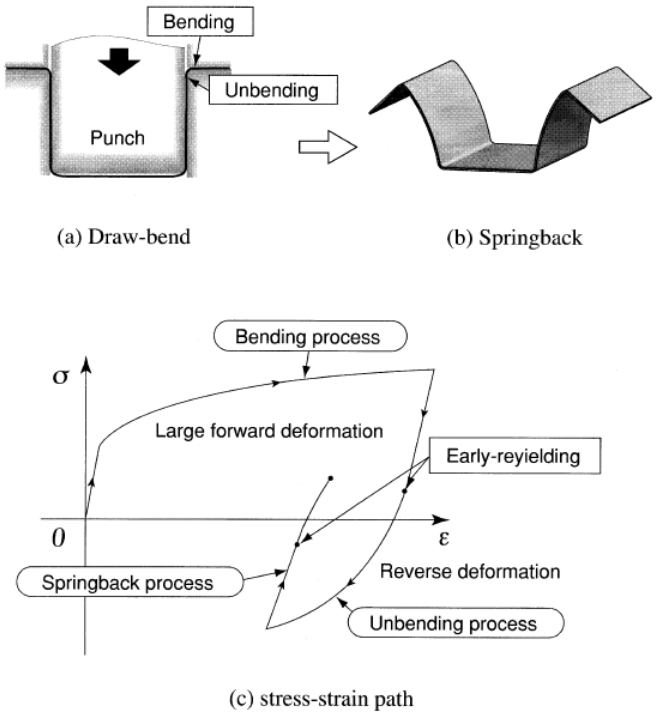

Figure 4.1 Description of cyclic loading (a) draw-bend (b) springback (c) stress-strain path (Yoshida et al. 2002)

The bending-unbending deformation causes an effect where the yield stress during reversal loading is lower than the yield stress during forward loading. This effect is known as Bauschinger effect. To improve sheet metal forming simulation, there is a need to incorporate an appropriate constitutive equation capable of describing the Bauschinger effect and so-called cyclic transient, which describes transition between the elastic and elastic-plastic state during repeated loading. A combination of isotropic and nonlinear kinematic hardening has been considered as one of the best material models proposed for this purpose, as the former has been associated with the capability to improve cyclic transient and the latter with the capability to take care of the Bauschinger effect (Chun et al. 2002a; Chun et al. 2002b; Yoshida and Uemori 2002; Yoshida and Uemori 2003). Identification of material parameters in this and other models requires a proper cyclic bending experiment to be developed and carried out.

4.2. Objectives

i. To develop a new bending unbending tool as a way to enhance the existing knowledge of the sheet metal plasticity with regard to cyclic load bending resembling to what is happening in the sheet metal forming(in the die draw bead and when the sheet is drawn over a die shoulder corner).

ii. To evaluate the responsive behaviour of sheet metal materials undergoing cyclic loading for any Bauschinger effect, transient

behaviour and work-hardening stagnation characteristics by using the newly developed experimental tool.

iii. To acquire stress-strain data useful for identifying parameters in kinematic and mixed hardening model (the identification work however will be covered in the next chapter, Chapter 5).

4.3. Tool and Specimen Preparation

4.3.1. The Cyclic Loading Tool

Figure 4.2 shows the newly developed bending and unbending testing tool for sheet metal. It is based on the concept of symmetrical crank-slider mechanism, and consists of three main components; slider (part 1), cranks/holders (part 2) and connecting rods (part 3). Also see Appendix C. List of the parts weight is shown in Table 4.1.

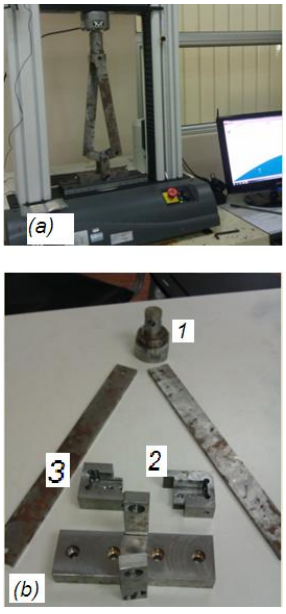

Figure 4.2 (a) The tool attached to the tensile machine (b) components of the tool: slider (1), cranks/holders (2) and connecting rod (3)

Table 4.1 List of parts' weight

Part No.	Part Name	Weight (gram)
1	Slider	1300
2	Crank/Holder	500
3	Connecting Rod	900

To operate the tool, the slider was attached to the moving part of the tensile test machine. When the tensile machine was operated, the slider would move downward or upward based on the machine stroke direction. The movement would cause the left and right cranks to rotate and subsequently bend (downward movement) or reverse bend (upward movement) the sheet metal that was being attached to it. These movements are shown in Figure 4.3. By doing this the tool realised a pure sheet bending process. The bending or downward movement result is shown in Figure 4.4.

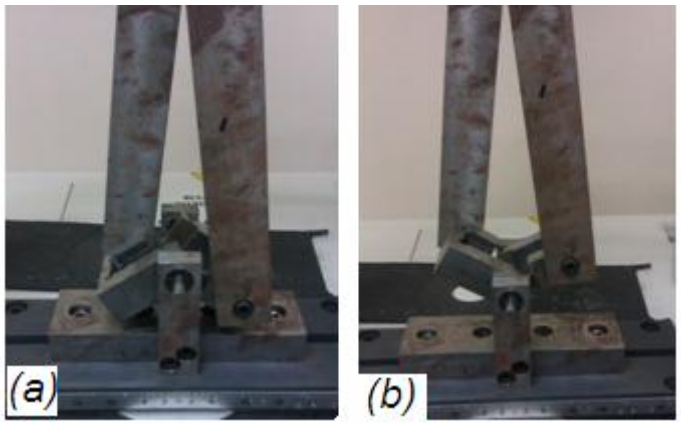

Figure 4.3 The sheet metal specimen attached to the tool is subjected to bending or reverse bending depending on the holder rotating direction, (a) moving in downward direction and (b) moving in upward direction

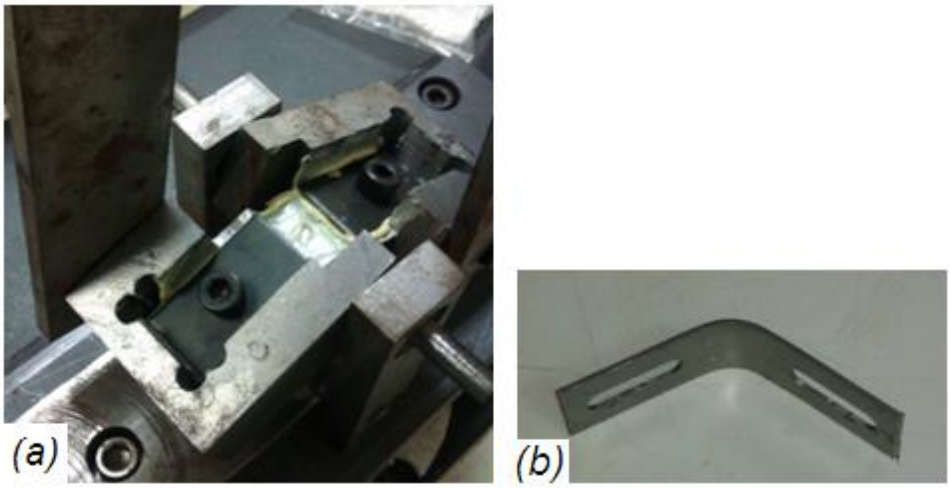

Figure 4.4 Sheet metal in bent position (a) and the produced part after the process(b)

Figure 4. 5 shows the initial, the bending and the reverse bending position of the tool's crank/holder and the forces acting on it. By knowing the forces, the bending moment can be calculated. A detail analysis to configure the bending and reverse bending moment is described in section 4.3.4. During downward movement, the bending force and the part weight (G2) will contribute to the bending moment of sheet metal. During upward movement, the weight of the components however, will resist the reverse bending force. This condition however is believed to have insignificant effect on the real physical of the sheet metal bending. Meaning the Bauchinger effect can still be investigated. In fact for the work of identifying hardening parameters, only the downward movement data or the bending operation data will be used.

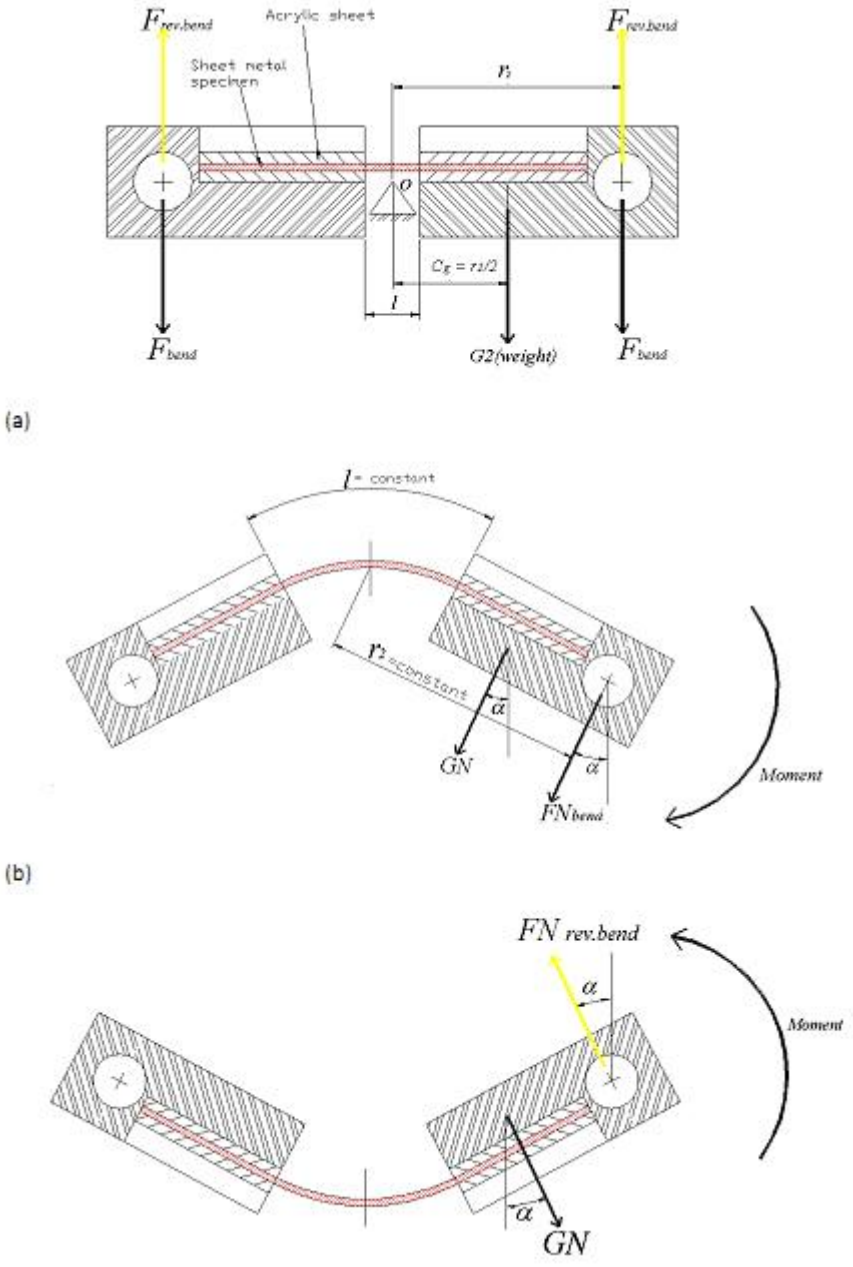

Figure 4. 5 The positions and the forces acting on the crank/holder (a) initial position, (b) bending position and (c) reverse bending position.

4.3.2. The Cyclic Loading Specimen

The cyclic loading specimen size was 105 mm long and 24.5 mm wide. It was clamped between a pair of acrylic sheets in the tool holders. Figure 4.6 shows the schematic drawing of the specimen.

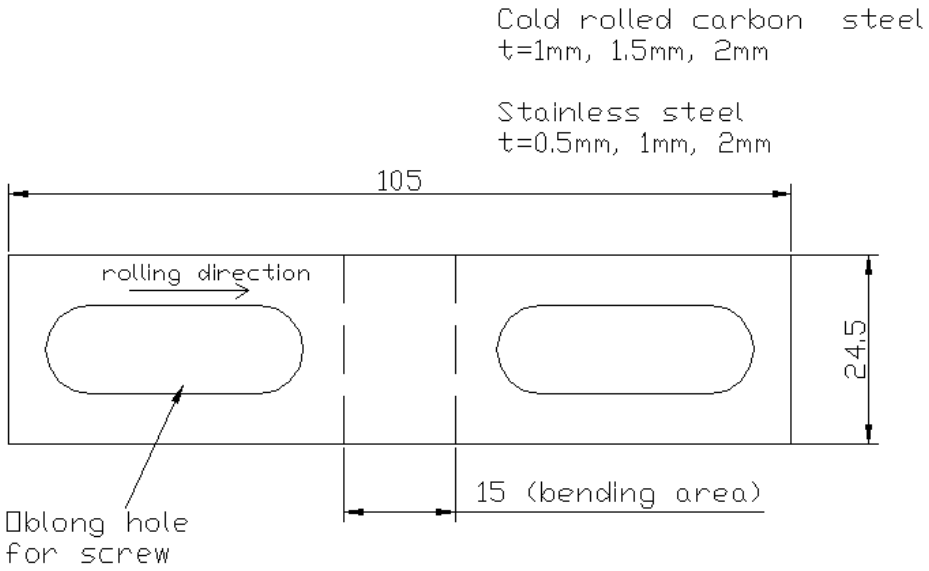

Figure 4.6 The description of specimen for newly cyclic loading tool

Figure 4.7 (a) shows the specimen together with 2 pairs of acrylic sheets used to minimise friction during the bending and unbending processes. Sheet metal plates were placed on the top of the acrylic sheets to prevent them from being tilted during the bending and unbending processes.

Fasterners were used to clamp the sheet metal plates, the acrylic sheets and the sheet metal specimen. The fasterners however were manually tightened to give a light compression force so as to allow the sheet metal specimen to slide between the acrylic sheets during the bending and unbending processes. This sliding movement

would cause the specimen to undergo axial stretching due to restriction from the fastener body (the fasteners' body penetrating through the specimen thickness). To avoid this, oblong shape holes were cut on the specimen, as shown in Figure 4.6, to allow it to slide freely without restriction. Indeed, these holes indirectly also reduced the contact area between the test specimen and the acrylic sheets and subsequently minimising the friction effect. Lubrication was applied to further reduce friction effect. The lubricant being used for this work was 1200-2 from Lubriplate as shown in Figure 4.8.

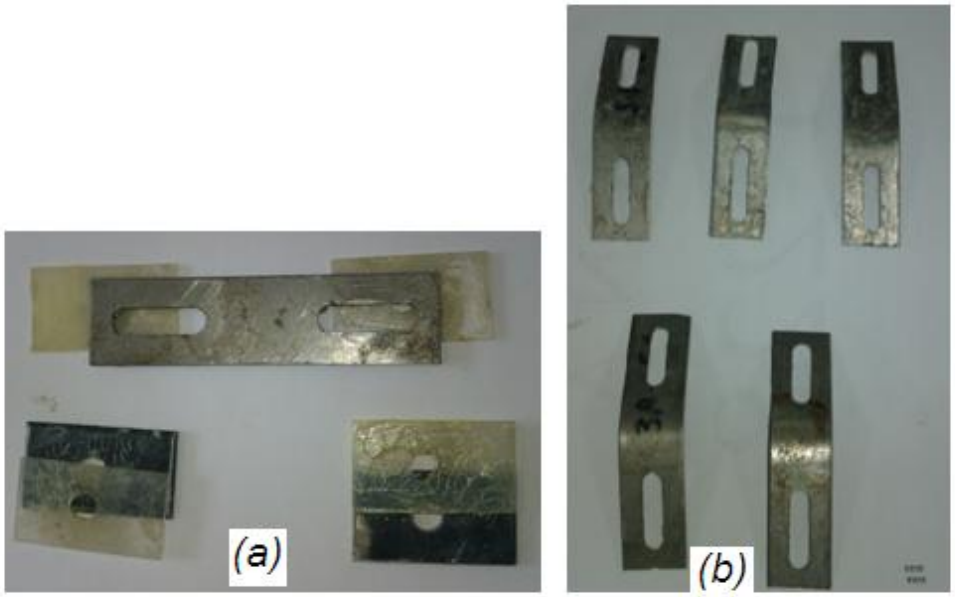

Figure 4.7 (a) Acrylic sheets used to minimise friction effect during bending and unbending processes (b) parts after bending and unbending processes

Figure 4.8 1200-2 super lubrication from Lubriplate to minimise friction effects on the specimen in bending and unbending experiments

4.3.3. Curvature and Strain Calculation

For the tool to be useful, it was necessary to convert the acquired raw data in the form of displacement into curvature and then into bending strain. For this purpose, the tool and the specimen geometrical relationship during bending condition were analysed. Figure 4.9 shows the relationship between the tool angles (θ_2) and the sheet metal bending angle (α) which was then related to curvature (ρ) by an equation, ρ=1/radius of curvature (R).

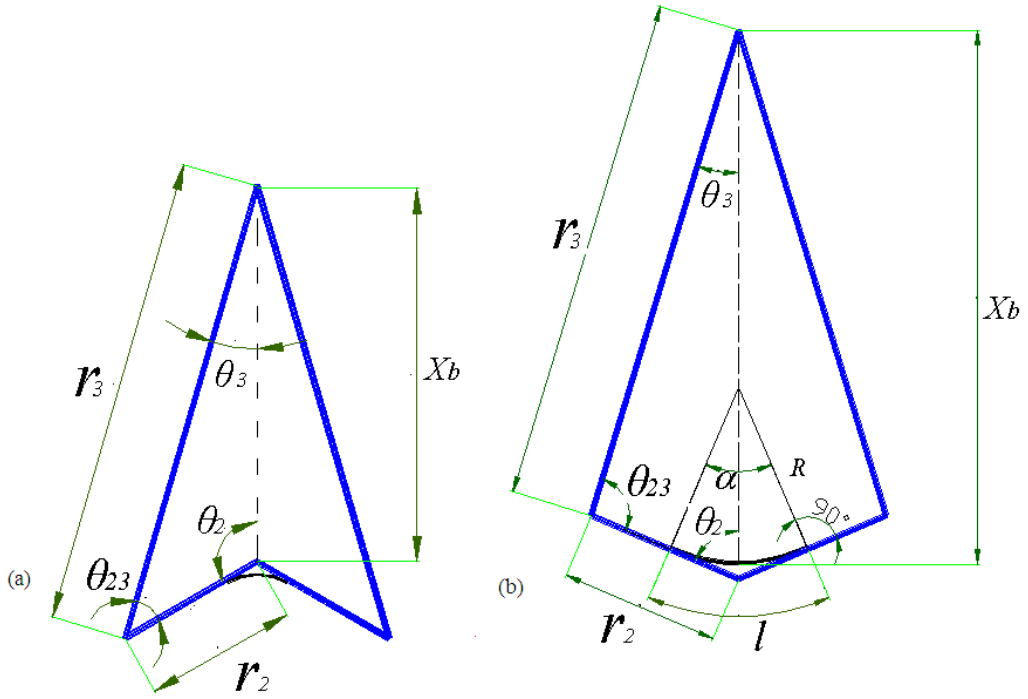

Figure 4.9 Geometrical parameters of the tool and sheet metal specimen (a) bending direction and (b) reverse bending direction

The symbol *l* and α shown only in Figure 4.9(b) are the length of sheet metal that was being subjected to reverse bending operation and its bending angle. The length was equal to the gap between the rights and left tool holder or the cranks. The bending angle, α depended directly on the crank angle, θ_2 and indirectly to the connecting rod angle θ_3. The first angle was a function of the slider displacement in the form of X_b distance and the tool length, r_2 and r_3 whilst the connecting rod angle was a function of the crank angle and the tool length. The relationship is shown in Equation 4.1 and Equation 4.2 and is applicable for bending and reverse bending (Shigley and Uicker 1995).

$$\theta_2 = cos^{-1} \frac{X_b^{\,2} + r_2^{\,2} - r_3^{\,2}}{2X_b r_2}$$

Equation 4.1

$$\theta_3 = Sin^{-1}\left[\frac{r_2 Sin\theta_2}{r_3}\right]$$

Equation 4.2

$\theta_2 = crank\ angle$
$\theta_3 = connecting\ rod\ angle$
$X_b = distance\ from\ centre\ of\ slider\ to\ rotating\ centre\ of\ crank$
$r_2 = crank\ length$
$r_3 = connecting\ rod\ length$

The curvature of sheet metal bending was calculated using Equation 4.3 (Marciniak et al. 2002).

$$\rho = 1/R$$

Equation 4.3

The following procedure shows how this curvature was being derived based on the tool's geometrical configuration, during downward and upward operations (Figure 4.10 and Figure 4.11). Only half of the tooling was considered for the derivation.

a) Downward movement (bending operation)

The crank angle in a downward movement is always in the range of $90 < \theta_2 < 180$.

To calculate curvature, triangle $\angle ABC$ as in Figure 4.10 was used to find relationship between the crank angle and the bending angle.

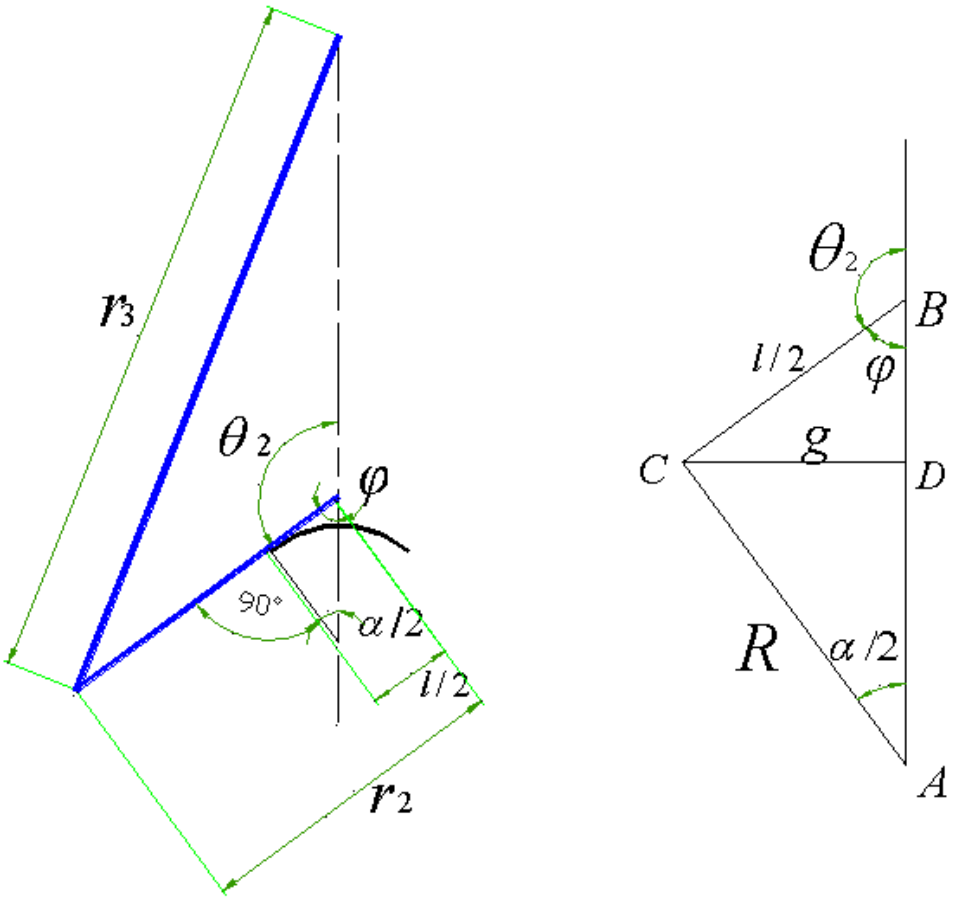

Figure 4.10 Tool's geometrical configuration for curvature derivation during downward movement/bending operation

$$180 = 90 + \frac{\alpha}{2} + \varphi$$

$$\frac{\alpha}{2} = 180 - 90 - \varphi$$

$$\varphi = 180 - \theta_2$$

$$\frac{\alpha}{2} = 180 - 90 - (180 - \theta_2)$$

$$\frac{\alpha}{2} = \theta_2 - 90$$

Equation 4. 4

Since $90 < \theta_2 < 180$, so $\alpha/2$ is always positive

Using the following equation from (Marciniak et al. 2002)

$$l = R\alpha$$

Equation 4. 5

The curvature formula is derived as described below

$$R = l / \alpha \ \ or$$

$$R = \frac{l/2}{\alpha/2}$$

$$R = \frac{l/2}{\theta_2 - 90}$$

$$\rho = \frac{1}{R}$$

$$\rho = \frac{\theta_2 - 90}{l/2}$$

Equation 4. 6

Angles in this formula should be converted into radian.

b) Upward movement (reverse bending)

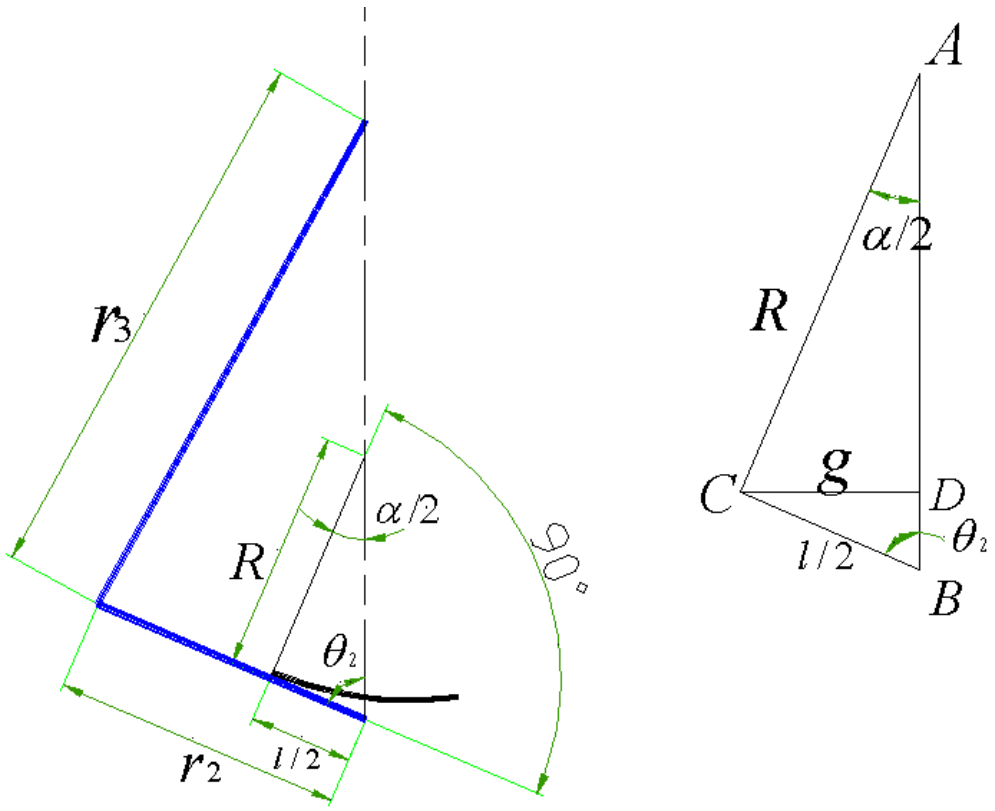

Figure 4.11 Tool's geometrical configuration for curvature derivation during upward operation/reverse bending operation

The crank angle in an upward movement is always in the range of $0 < \theta_2 < 90$.

From Triangle $\angle ABC$

$$180 = 90 + \frac{\alpha}{2} + \theta_2$$

$$\frac{\alpha}{2} = 180 - 90 - \theta_2$$

$$\frac{\alpha}{2} = 90 - \theta_2$$

$$\frac{\alpha}{2} = -(\theta_2 - 90)$$

Equation 4.7

Since $0 < \theta_2 < 90$, $\alpha/2$ is always positive.

Since Equation 4.7 is similar to Equation 4.4, Equation 4.6 is applicable to find curvature for reverse bending movement.

To change the curvature value into strain the following formula is used (Marciniak et al. 2002):

$$\varepsilon = \ln\left[1 + \frac{y}{R}\right]$$

$$\varepsilon = \ln[1 + y\rho]$$

Equation 4. 8

where *y* is a distance from the middle surface of the sheet metal. For y equal to half of the sheet metal thickness, the strain calculated is for the outer surface.

4.3.4. Moment Calculation

To calculate bending moment, we need to know the forces acting on the bending tool. For this purpose, the crank-slider static force analysis was performed with an assumption that the inertial force could be neglected due to a nearly constant or uniform motion so the value of such force would be relatively small compared to other forces such as gravity force and reaction forces from the sheet metal specimen. Friction forces were also assumed to be negligible. An analysis to derive the moment equation was performed based on a downward movement and an upward movement of the slider.

a) Downward movement (bending operation)

The analysis began by configuring reaction forces acting on the tool and its components by using free body diagram as shown in Figure 4.12.

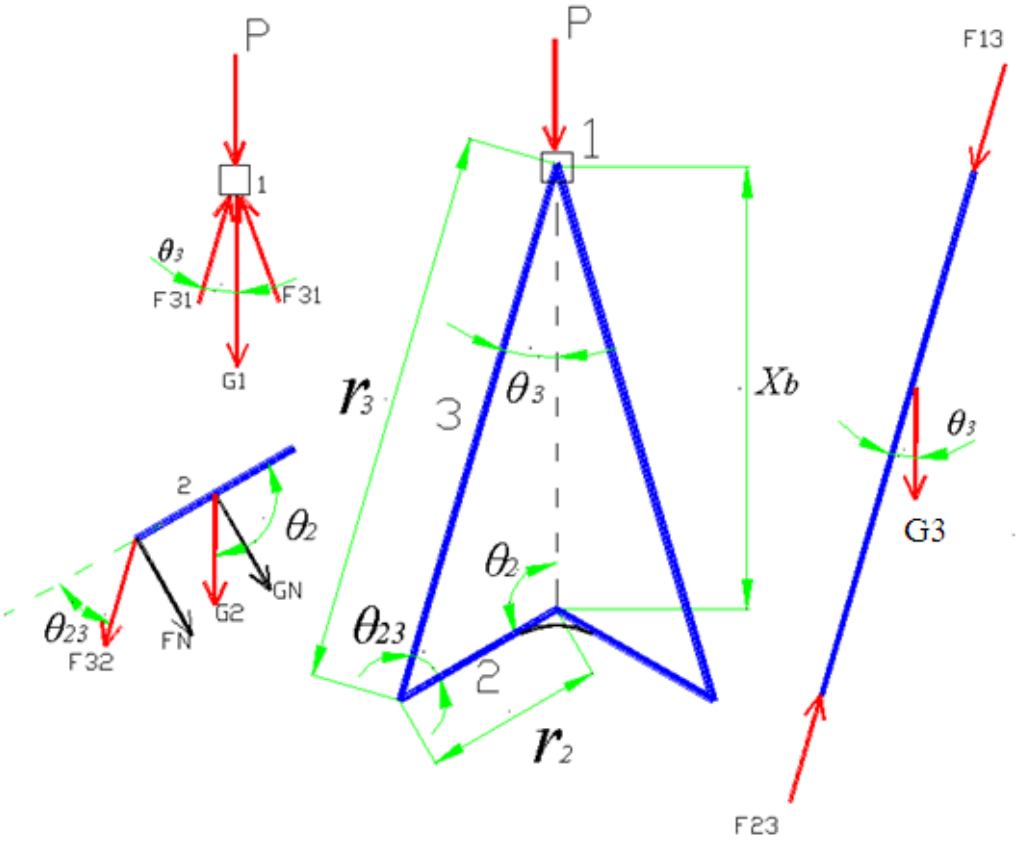

Figure 4.12 Free body diagrams for a downward movement of the bending tool and its components

This free body diagram was analysed part by part beginning from part 1, part 3 and then part 2.

For slider (part 1)

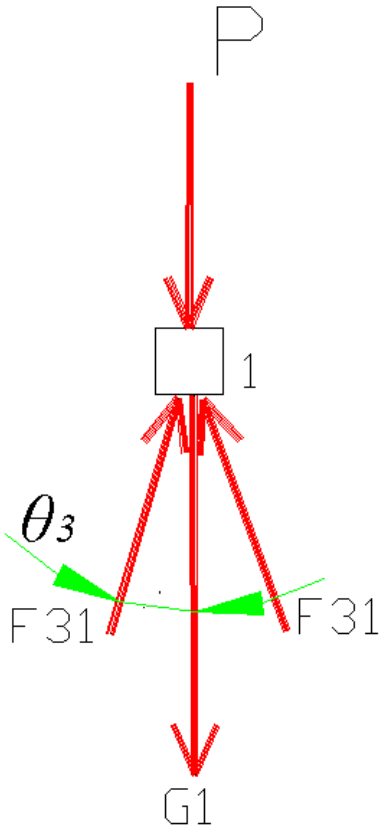

$$+\uparrow \sum F = 0$$

$$-P - G_1 + F_{31}\cos\theta_3 + F_{31}\cos\theta_3 = 0$$

$$F_{31} = \frac{P + G_1}{2\cos\theta_3}$$

For connecting rod (part 3)

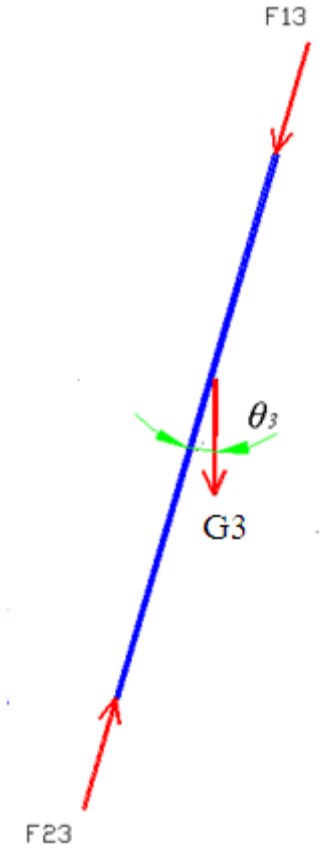

$$+\uparrow \sum F = 0$$

$$-G_3 + F_{23}\cos\theta_3 - F_{13}\cos\theta_3 = 0$$

$$F_{23} = \frac{F_{13}\cos\theta_3 + G_3}{\cos\theta_3}$$

$$F_{23} = F_{13} + \frac{G_3}{\cos\theta_3}$$

$$F_{13} = |F_{31}|$$

$$F_{23} = \frac{P + G_1}{2\cos\theta_3} + \frac{G_3}{\cos\theta_3}$$

$$F_{23} = \frac{P + G_1 + 2G_3}{2\cos\theta_3}$$

$$F_{23} = |F_{32}|$$

Using equations derived from part 1 and part 3, moment acting on part 2 was calculated as follows:

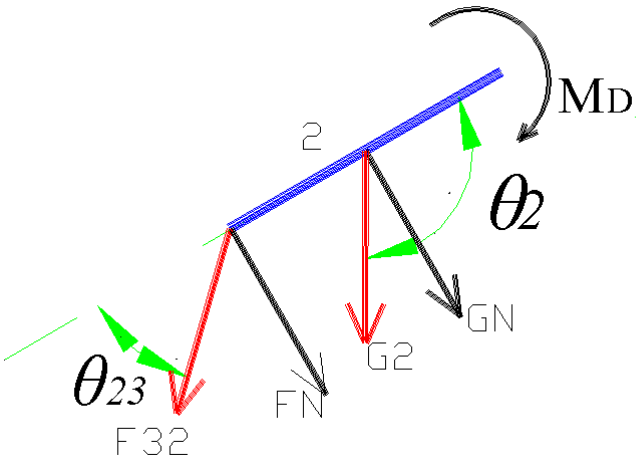

$$+CW\sum M = 0$$

$$M_D - FN(r_2) - GN(r_2/2) = 0$$

$$FN = F_{32}\sin\theta_{23}$$

$$F_{32} = |F_{23}|$$

$$FN = \left[\frac{P + G_1 + 2G_3}{2\cos\theta_3}\right]\sin\theta_{23}$$

$$GN = G_2\cos(\theta_2 - 90) = G_2\sin\theta_2$$

$$M_D - (r_2)\left[\frac{P + G_1 + 2G_3}{2\cos\theta_3}\right]\sin\theta_{23} - (r_2/2)G_2\sin\theta_2 = 0$$

$$M_D = (r_2)\left[\frac{P + G_1 + 2G_3}{2\cos\theta_3}\right]Sin\theta_{23} + (r_2/2)G_2\sin\theta_2$$

$$\theta_{23} = 180 - \theta_3 - \theta_2$$

So

$$\sin\theta_{23} = \sin(180 - \theta_3 - \theta_2) = \sin(\theta_3 + \theta_2)$$

$$M_D = (r_2)\left[\frac{P + G_1 + 2G_3}{2\cos\theta_3}\right]\sin(\theta_3 + \theta_2) + (r_2/2)G_2\sin\theta_2$$

$$M_D = \frac{r_2}{2}\left[(P + G_1 + 2G_3)\frac{\sin(\theta_2 + \theta_3)}{\cos\theta_3} + G_2\sin\theta_2\right]$$

Equation 4.9

b) Upward movement (reverse bending)

The free body diagram for upward movement is shown in Figure 4.13. The analysis was performed as in the case for downward movement.

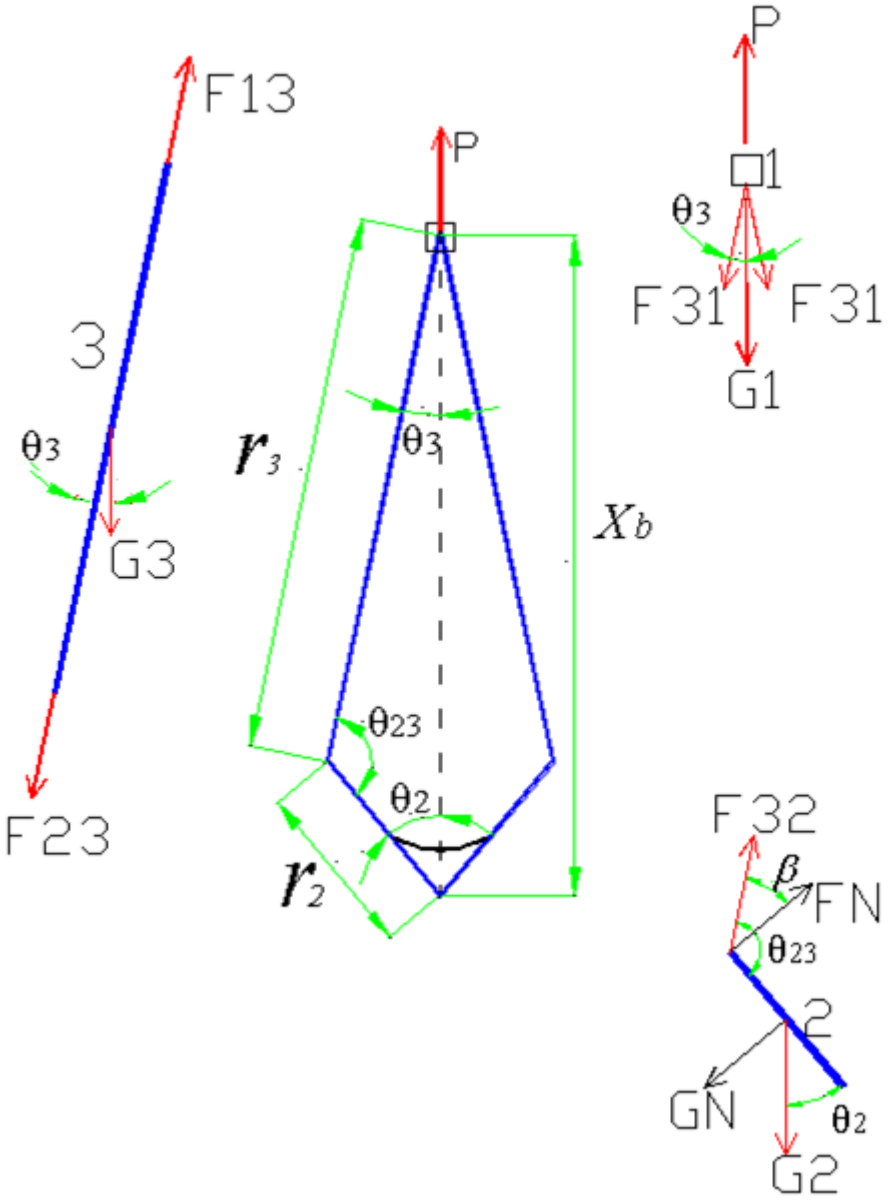

Figure 4.13 Free body diagrams for an upward movement of the bending tool and its components

For slider (part 1)

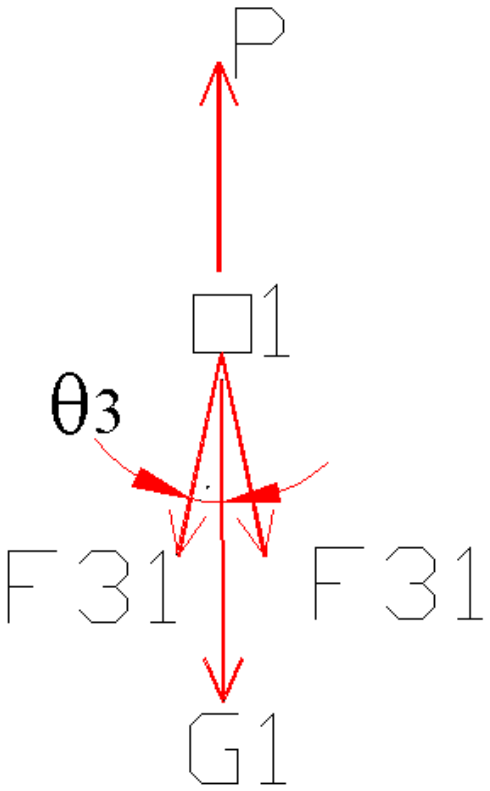

$$+\uparrow \sum F = 0$$

$$P - G_1 - F_{31}\cos\theta_3 - F_{31}\cos\theta_3 = 0$$

$$F_{31} = \frac{P - G_1}{2\cos\theta_3}$$

For connecting rod (part 3)

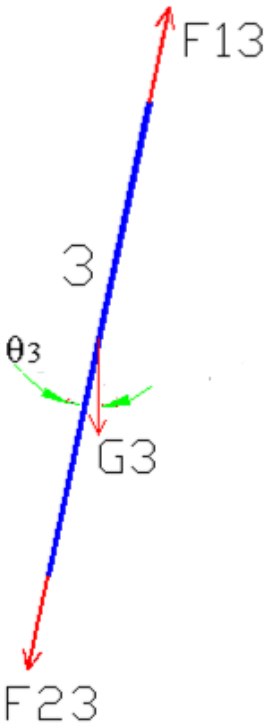

$$+\uparrow \sum F = 0$$

$$-G_3 - F_{23}\cos\theta_3 + F_{13}\cos\theta_3 = 0$$

$$F_{23} = \frac{F_{13}\cos\theta_3 - G_3}{\cos\theta_3}$$

$$F_{23} = F_{13} - \frac{G_3}{\cos\theta_3}$$

$$F_{13} = F_{31}$$

$$F_{23} = \frac{P - G_1}{2\cos\theta_3} - \frac{G_3}{\cos\theta_3}$$

$$F_{23} = \frac{P - G_1 - 2G_3}{2\cos\theta_3}$$

$$F_{23} = F_{32}$$

From the information from part 1 and part 3, moment acting on part 2 was calculated based on the following free body diagram:

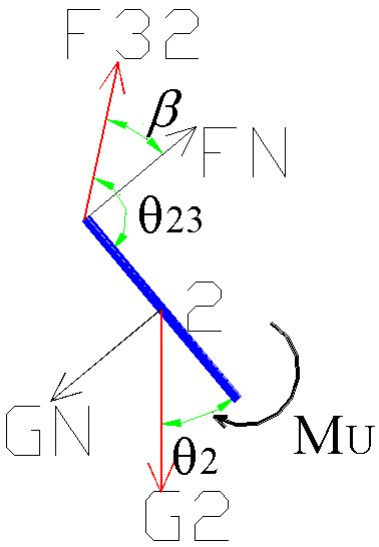

$$+CW\sum M = 0$$

$$M_U + FN(r_2) - GN(r_2/2) = 0$$

$$FN = F_{32}\cos\beta$$

$$F_{32} = F_{23}$$

$$FN = \left[\frac{P - G_1 - 2G_3}{2\cos\theta_3}\right]\cos\beta$$

$$\beta = \theta_{23} - 90$$

$$\theta_{23} = 180 - \theta_3 - \theta_2$$

$$\beta = 90 - \theta_3 - \theta_2$$

$$FN = \left[\frac{P - G_1 - 2G_3}{2\cos\theta_3}\right]\cos\left(90 - \theta_3 - \theta_2\right)$$

but

$$\cos\left(90 - \theta_3 - \theta_2\right) = \sin\left(\theta_3 + \theta_2\right)$$

$$FN = \left[\frac{P - G_1 - 2G_3}{2\cos\theta_3}\right]\sin\left(\theta_3 + \theta_2\right)$$

$$GN = G_2 \sin\theta_2$$

$$M_U + (r_2)\left[\frac{P - G_1 - 2G_3}{2Cos\,\theta_3}\right]\sin(\theta_3 + \theta_2). - (r_2/2)G_2\cos(\theta_2 - 90) = 0$$

$$M_U = (r_2)\left[\frac{-P + G_1 + 2G_3}{2\cos\theta_3}\right]\sin(\theta_3 + \theta_2) + (r_2/2)G_2\sin\theta_2$$

$$M_U = \frac{r_2}{2}\left[(-P + G_1 + 2G_3)\frac{\sin(\theta_2 + \theta_3)}{\cos\theta_3} + G_2\sin\theta_2\right]$$

Equation 4. 10

Except for the force P sign, the two equations (Equation 4.9 and Equation 4. 10) were the same. The acquired data needed to be analysed in the form of stress. To convert bending moment, M into stress, the following formula was applied (Marciniak et al. 2002).

$$M = \int_{-t/2}^{t/2} \sigma\, W y dy$$

$$M = 2\int_{0}^{t/2} \sigma W\, y dy$$

$$M = 2\sigma W \int_{0}^{t/2} y dy$$

$$\sigma = \frac{4M}{Wt^2}$$

Equation 4.11

W and *t* are the width and thickness of the material.

4.4. Results and Discussions

Results in the form of stress versus strain graphs are shown in Appendix A. Significant observations can be derived from the graphs. Data from the second bending cycle (label B2) and third bending cycle (label B3) were used for optimisation work described in Chapter 5. Reversed bending data (label RB1 and RB2), though similar in trend, were not considered for this purpose since the acquired data at second and third bending cycle were sufficient. Reverse bending data were used only for quantifying the Bauschinger effect.

From the graphs, the bending and reverse bending showed a distinct elastic behaviour before the yield point. The cyclic loading reached a steady state condition or stabilized immediately after the first cycle. Except for specimen (a) of 1 mm thickness, the curves for low carbon steels (Figure 4.14 and Figure 4.16) showed a nonlinear stress-strain relationship after the yield point. A smooth elastic-plastic transient curve was followed by rapid work- hardening curve. Work hardening stagnation as mentioned by Yoshida and Uemori (2003), however, was not visible. Thus the existence of this stagnation behaviour in cyclic loading was not further studied in this work. From the onset of plastic region to near the middle of the plastic region the hardening curves for each specimen seemed to be consistent in path. The curves however were slightly deviated from each other towards the end of the plastic region. This deviation was believed to be caused by friction between specimen's and the tool holders' surfaces.

Figure 4.17, 4.18 and 4.19 show results for stainless steel of 2 mm, 1 mm and 0.5 mm thickness. The results were similar in trends for all the graphs. The curves showed rapid work hardening after the yield point. There was a sign of stress drop at strain around 0.01, 0.007 and 0.002 for 2 mm, 1 mm and 0.5 mm thickness, respectively. The stress then continued to increase more or less in linear relation to strain. There was a sign of deviation of the hardening curves at the end of plastic region.

This characteristic and stress drop was believed to be caused by friction. Two sources of the friction were suspected to contribute to this observation. The first was the specimen-tool contact and the second was the tool fitting used in all joints. This includes tolerances, allowed clearances, roughness in the working surfaces and lubrication. Although, attempt had been made to minimize friction effect from the specimen-tool contact by placing the layer of acrylic sheets above and below the sheet metal material specimen plus with sufficient lubricant, it was still unavoidable due to the tool fitting. The effects, however, were considered small and the data acquired especially at the beginning of the work on hardening region were sufficient for identifying hardening parameters. Thus the data were acceptable and the capability of the tools to provide information on cyclic loading was proven.

In contrast to Thakur's statement (Thakur et al. 1996) the reverse re-yielding from the results of the current work was quite obvious to trace and there was a distinct indicator for the particular point. This led to a simple 0.002 offset way in identifying the reversal yield stress point useful for calculating Baushinger Effect Factors (BEF). Based on the method, BEF for low carbon steel and stainless steel

were calculated using the formula (Equation 2.15) proposed by Weinmann (Weinmann et al. 1988) as shown below:

$$BEF = \frac{Y_1 - |Y_2|}{Y_1} \qquad \text{Equation 2.37}$$

Y_1 and Y_2 are shown in Figure 2.9. A zero BEF value indicates that no Bauschinger effect is present in loading and unloading deformations. The results are shown in Table 4.2 and 4.3. The values for Y_1 were taken from average of B2 and B3 cyclic data and Y_2 were taken from average of RB1 and RB2 cyclic data.

Table 4.2 Summary of BEF data for cold rolled low carbon steel

2 mm thick							
no	Y_1-B2	Y_1-B3	Average	$\|Y_2$-RB1$\|$	$\|Y_2$-RB2$\|$	Average	BEF
1	987.971	990.637	989.304	144.414	138.192	141.303	0.857
2	1061.245	1029.037	1045.141	178.515	178.515	178.515	0.829
3	1014.546	1017.451	1015.998	191.017	186.420	188.719	0.814
						Average	0.834
1.5 mm thick							
no	Y_1-B2	Y_1-B3	Average	$\|Y_2$-RB1$\|$	$\|Y_2$-RB2$\|$	Average	BEF
1	937.421	938.102	937.762	168.923	161.782	165.353	0.824
2	936.890	922.366	929.628	165.516	173.485	169.501	0.818
3	837.108	846.571	841.839	203.075	202.641	202.858	0.759
						Average	0.800
1 mm thick							
no	Y_1-B2	Y_1-B3	Average	$\|Y_2$-RB1$\|$	$\|Y_2$-RB2$\|$	Average	BEF
1	1206.976	1201.468	1204.222	482.512	478.348	403.785	0.665
2	1242.286	1202.057	1222.172	572.366	557.959	474.150	0.612
3	1144.893	1126.840	1135.867	350.313	409.653	380.734	0.665
						Average	0.647

Table 4.3 Summary of BEF data for stainless steel

2 mm thick							
no	Y_1-B2	Y_1-B3	Average	$\lvert Y_2$-RB1$\rvert$	$\lvert Y_2$-RB2$\rvert$	Average	BEF
1	922.399	926.486	924.443	146.725	139.290	143.008	0.845
2	980.960	939.876	960.418	154.348	149.167	151.758	0.842
3	914.360	987.514	950.937	158.904	155.694	157.299	0.835
						Average	0.841
1 mm thick							
no	Y_1-B2	Y_1-B3	Average	$\lvert Y_2$-RB1$\rvert$	$\lvert Y_2$-RB2$\rvert$	Average	BEF
1	1099.429	1086.720	1093.075	296.007	293.242	294.625	0.730
2	1037.715	1086.720	1062.218	305.542	291.994	298.768	0.719
3	1099.429	977.849	1038.639	248.382	243.161	245.772	0.763
						Average	0.738
0.5 mm thick							
no	Y_1-B2	Y_1-B3	Average	$\lvert Y_2$-RB1$\rvert$	$\lvert Y_2$-RB2$\rvert$	Average	BEF
1	1208.418	1116.225	1162.322	739.792	738.368	739.080	0.364
2	1242.168	1166.875	1204.522	769.019	793.935	781.477	0.351
3	1342.295	1166.875	1254.585	767.667	789.071	778.369	0.380
						Average	0.365

The values in the tables proved that the Baushinger effect exists when sheet metal was subjected to bending and unbending loadings. It was very interesting to note that the thickness of the material seemed to have influence on the Bauschinger effect as indicated by the increase of BEF values when the thickness increased. This was contrary to the finding by Weinmann who stated that the material thickness had insignificant relationship with the Bauschinger effect. This finding however should not over rule Weinmann's statement completely as the materials used for experiments may undergo different rolling processes during production. Further investigation perhaps is necessary.

4.5. Conclusions

The following conclusions were derived based on the experimental results. The outcomes were believed to have enhanced knowledge in the field of plasticity of sheet metal forming.

i. The developed experimental tool was capable of providing significant data for analysis of the Bauschinger effect and understanding behaviour of sheet metal materials undergoing cyclic loading.

ii. The yield point for stress-strain curve from bending unbending loading was traceable. This point was followed by a smooth elastic-plastic transient curve and steady work hardening curve.

iii. The existence of work hardening stagnation in the cyclic stress-strain curves was not observed. This likely due to small bending angle of about 20 degree (first bending) to 40 degree (subsequent bending) which produced insufficient accumulated strain for work hardening stagnation to be observed.

iv. The Bauschinger effect did occur during bending unbending loading in sheet metal forming as indicated by BEF values in Tables 4.1 and 4.2. Thus the Bauschinger effect should be considered in sheet metal forming simulation through the use of related constitutive equations.

CHAPTER 5

IDENTIFICATION OF MATERIAL PARAMETERS BY OPTIMISATION

5.1. Introduction

Part of the crucial task in improving the constitutive models is determining the most accurate method to identify their parameters. The inverse identification method, as shown in Figure 2.29 and updated here in Figure 5.1, has been adopted to provide the solution. This identification processes was done by minimising the difference between the finite element simulation result and the experimental result by updating material parameters. The method however faced several limitations, such as a lengthy computing time, nonlinearity of geometrical boundary conditions, convergent issues due to contact and friction of the tools' nodes and material's nodes and sensitivity of numerical elements.

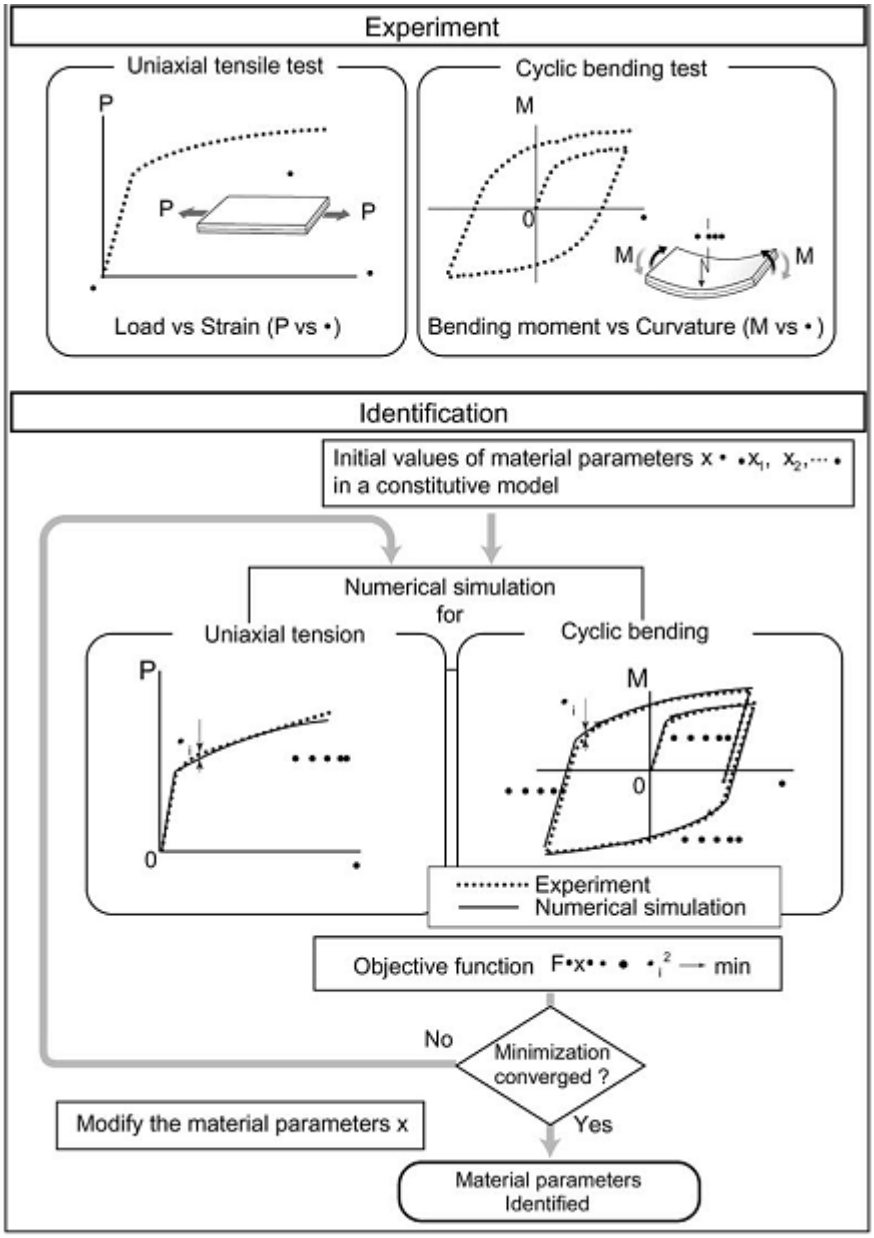

Figure 5.1 An inverse identification method to identify material parameters using finite element simulation (Yoshida et al. 2003)

To avoid these limitations, direct application of optimisation algorithms has been applied on the cyclic experimental data by several researchers. The most common optimisation methods are the derivative (gradient based) algorithm, derivative-free (direct search) algorithm and evolutionary algorithm.

Evolutionary algorithms are judged to be very robust methods with the capability to tackle initial solution requirements as well as local minimum problems. However, these methods still depend on sub-optimal algorithms to guarantee identification of the global minimum of the objective function. Direct search algorithms, also known as derivative-free algorithms, use simple strategies by eliminating derivative calculation. This approach is more favourable due to its simplicity, flexibility and reliability. The methods, however, are time-consuming, user-dependent and faced with a convergence problem for local minimums. The gradient-based algorithms have limitations due to being strongly dependent on user skills and the requirement for initial trial solutions, as well as the convergence problem.

Even though most of the methods show significant differences in computation time, the parameters' identified values are insignificantly different. Thus it is acceptable to use any of the optimisation methods as long as the computing time is acceptable. For that reason, the simplified Nelder–Mead method was selected to perform the minimisation optimisation for the current work.

This particular chapter thus deals with the optimisation works being conducted to identify the constitutive parameters. It begins with an introduction to the Nelder–Mead direct search method and proceeds with a discussion on the Programming algorithms of the identification methods.

5.2. Objectives

Three objectives have been set for this chapter, namely:

i. To determine material parameters for nonlinear kinematic hardening and mixed hardening equations.

ii. To identify the best material model capable of fitting the bending-unbending data.

iii. To evaluate the applicability of using direct search optimization method in materials parameters identification.

The Chaboche nonlinear kinematic hardening model as described by Equation 5.1 was chosen for kinematic hardening in this work. A combination of this hardening model and Voce isotropic hardening models in Equation 5.2 was selected to represent the mixed hardening model as shown by Equation 5.3

$$\sigma = \sigma_0 + \frac{C}{\gamma}(1 - e^{-\lambda\bar{\varepsilon}})$$

Equation 5.1

$$\sigma = \sigma_0 + Q(1 - e^{-b\bar{\varepsilon}})$$

Equation 5.2

$$\sigma = \sigma_0 + Q(1 - e^{-b\bar{\varepsilon}}) + \frac{C}{\gamma}(1 - e^{-\lambda\bar{\varepsilon}})$$

Equation 5.3

The parameters involved are: Q, b, C and γ. Q defines the maximum change in the size of the yield surface and b is the rate at which that change occurs.

C is a kind of kinematic hardening modulus and γ defines the rate at which the kinematic hardening modulus decreases as the plastic deformation develops. This is a widely accepted model in sheet metal forming (Chun et al. 2002a) and has been applied in finite element software, such as Abaqus (Abaqus 2000).

5.3. Overview of Nelder–Mead Simplex-Direct Search

Nelder-Mead Simplex is a derivative free optimisation method and is widely used by researchers in the fields of chemistry, engineering and medicine. It is available in several forms of optimisation software such as Matlab (Lagarias et al. 1998). The main disadvantage of the algorithms is its difficulty in convergence. While the advantages of the algorithm are its robustness, simplicity in Programming as well as its low consumption of storage space and computing time. The robustness is judged based on its capability to tolerate noise in the function values. The simplicity in Programming is evident from its simple algebraic manipulation using only function values. When the number of variables is small, the algorithms are acceptably equal to much more complex algorithms that require a great deal of storage overhead and algebraic manipulation (Dennis Jr and Woods 1985). Taking these advantages into consideration, this method has been favourable in certain cases.

Briefly, the algorithm works by forming a simplex, a geometrical figure, which is formed by n+1 vertices, to converge to minima. The symbol “n” is assigned as number of variables of a function. For every iteration, the algorithm starts calculating a reflected point of the worst point through the centroid. According to this value, the algorithm will carry out a reflection or extension,

contraction or shrink to form a new simplex. In other words, the function values at each vertex will be evaluated in every iteration, and the worst vertex with the highest value will be replaced by another vertex, which has just been found. Otherwise, a simplex will be shrunk around the best vertex. This process will be repeated iteratively until a desired error value is satisfied.

The convergence speed of the simplex method may be affected by three parameters, α, β, γ (reflection coefficient, contraction coefficient and expansion coefficient). Depending on these coefficients, the volume of the simplex will be changed by the operations of reflection, contraction or expansion respectively. The steps can be summarised as follows (Pham and Wilamowski 2011):

Step 1: obtain α, β, γ, select an initial simplex with random vertices *x0, x1,..., xn* and calculate their function values.

Step 2: sort the vertices *x0.,x1,..., xn* of the current simplex so that *f0, f1,..., fn* are in an ascending order.

Step 3: calculate the reflected point *xr, fr*

Step 4: if *fr* < *f0*:

(a) calculate the extended point *xe, fe*

(b) if *fe* < *f0* , replace the worst point by the extended point *xn* = *xe, fn* = *fe*

(c) if *fe* > *f0* , replace the worst point by the reflected point *xn* = *xr, fn* = *fr*

Step 5: if *fr* > *f0*:

(a) if *fr* < *fi*, replace the worst point by the reflected point *xn* = *xr, fn* = *fr*

(b) if $fr > fi$:

(b1) if $fr > fn$: calculate the contracted point xc, fc

(c1) if $fc > fn$ then shrink the simplex

(c2) if $fc < fn$ then replace the worst point by the contracted point $xn = xc$, $fn = fc$

(b2) if $fr < fn$: replace the worst point by the reflected point $xn = xr$, $fn = fr$

Step 6: if the stopping conditions are not satisfied, the algorithm will continue at step 2

5.4. Programming for Material Parameter Identification

A computer program using Mathlab software by The MathWorks Inc. was developed, incorporating commands to perform least square optimisation of nonlinear kinematic hardening and mixed hardening. The *fiminsearch* subroutine from the Nelder–Mead Simplex optimisation method was used. The algorithm of the Programming was (The MathWorks Inc. 2008):

Step 1: Writing M-code for importing input data from Microsoft Excel.

Step 2: Writing objective functions for constitutive model

Step 3: Initial guess

Step 4: Minimisation using *fminsearch* command to call for the Nelder–Mead algorithm.

Step 5: Return the results

There were two parts for the Programming code, the main body and the subroutine. Step 1 and step 5 were structured in the main body of the code, while steps 2, 3 and 4 were structured in the subroutine Programming. The main body of the program included tasks such as importing input data of bending-unbending from Microsoft Excel, calculation of adjusted R-square and residuals. Adjusted R-square is an indication of goodness of fit for hardening models on the experimental data. A value closer to 1 indicates a better fit. Residuals are defined as the difference between the data values and the values that are predicted by the model. A residual plot with lower random errors indicates a good fit of the hardening models to the experimental data.

To simplify the Programming code and to satisfy the requirement of only real number calculation for Nelder–Mead for this work, the x values of the imported data were repositioned to start from 0-value. The subroutine of the program included tasks for initial guess input and declaring the constitutive formula as an objective function. The steps and the coding for the optimisation program are shown below.

Step 1: Writing M-code for importing input data from Microsoft Excel and a command to call the objective function. The code requires the file name, the sheet and the column and the row number of the data in the Microsoft Excel file.

The code to import low carbon steel data is:

```
nydata=xlsread('MS2mm.xls','b2_a','v17:v3000');
nxdata=xlsread('MS2mm.xls','b2_a','u17:u3000');
```

The code to import stainless steel data is:

```
nydata=xlsread('SS2mm.xls','b2_a','v17:v3000');
nxdata=xlsread('SS2mm.xls','b2_a','u17:u3000');
```

A command to call the objective function for nonlinear kinematic hardening equation and mixed hardening equation are K2 and MIXED respectively. The calling coding for K2 is shown below.

```
[estimates, model,C,gamma,ErrorVector]=K2(nxdata,nydata);
[sse,FittedCurve] = model(estimates);
```

Step 2, Step 3 and Step 4: Writing the objective function for the constitutive model, initial guess and optimisation

The objective function formula was abbreviated as *FittedCurve*. Another subroutine named *model* was created to calculate the sum square error (sse) and to fit it to the calculated curve of the constitutive model. The outputs of this calculation were used to calculate adjusted R-square and the residuals in the main program. The program for nonlinear kinematic hardening equation is shown below. To identify the four mixed hardening parameters, the formula and the start points were replaced with mixed hardening formula and additional two values, Q and b, of initial guess from isotropic hardening equation.

```
function [estimates,model,C,gamma,ErrorVector] = K2(nxdata,nydata)

    start_point =[1000 1];
    model = @expfun;
    options=optimset('MaxFunEvals',10e9,'MaxIter',10e9)

    estimates = fminsearch(model, start_point,options);
    function [sse,FittedCurve] = expfun(params)
C = params(1);
     gamma = params(2);

FittedCurve =200+(C/gamma)*(1-exp(-gamma*nxdata));
     ErrorVector= (FittedCurve-nydata);
     sse =sum((ErrorVector .^ 2));
```

```
end
 end
```

Step 5: Return the function results and plot the graph with parameters.

The function results include calculating adjusted R-square (Adj_Rq) and residuals.

```
  %MSE=SSE/v, v=n-m, n=#of data, m=# of parameters
    n=3000-17;
    m=2;
    v=n-m;
    MSE=sse/(v-3)% MSE: the mean square error or the
residual mean square.m is number parameter
    RMSE=sqrt(MSE)% STANDARD DEVIATION
    nyA=(sum(nydata))/(n); %denumerator depends on
initial and final data
    Residual=ErrorVector
    G=(nydata-nyA);
    SSE=sse
    SST=sum((G.^2))
    Rq=1-(sse/SST)
    Adj_Rq=1-(SSE*(n-1))/(SST*(v))
```

Coding for plotting the graphs and results

```
plot(x, y, 'c')
    hold on
 plot(nxdata, nydata, 'b')
    hold on
 plot(nxdata, FittedCurve, '--r');

 xlabel('nxdata')
  ylabel('f(estimates,nydata)')
title(sprintf('C=%1.3f,gamma=%1.3f, Adj_R=%1.4f,',...
      C,gamma,Adj_Rq));
legend('data','data','fit using N-Kinematic Equation ')
    hold off
```

The Programming codes are attached in Appendix B for reference.

5.5. Results and Discussions

Average data from the second cyclic loading (label B2) and third cyclic loading (label B3) were used for optimisation. The aims are to identify the best material model capable of fitting the experimental data, to evaluate the applicability of using direct search optimisation method and to determine the material hardening parameters. The discussion begins by looking at kinematic hardening performance and later at mixed hardening performance.

Figure 5.2, 5.3 and 5.4 illustrate how well the nonlinear kinematic hardening model fitted the experimental data for 2 mm, 1.5 mm and 1 mm low carbon steel. The adjusted R square values were above 0.9976. Hence, the optimisation technique and the capability of the nonlinear kinematic hardening equation to fit the data were accepted.

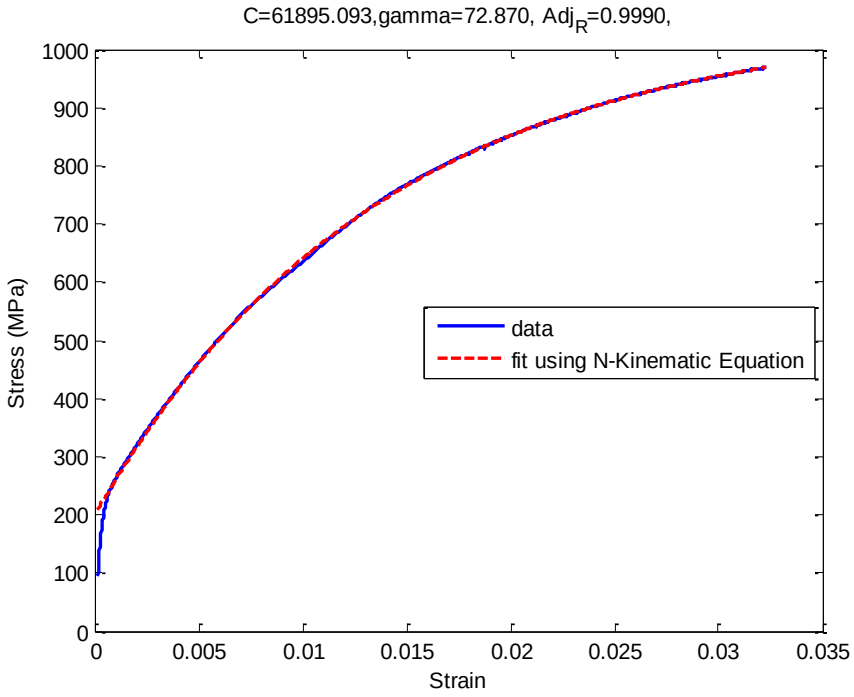

(a)

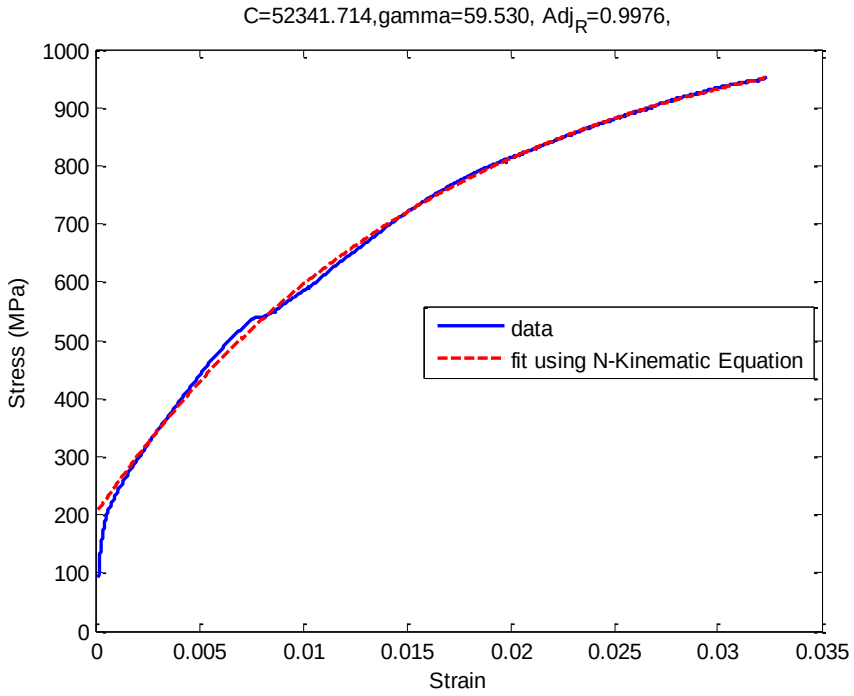

(b)

Figure 5.2 Optimisation of cold rolled low carbon steel data using nonlinear kinematic equation for t= 2 mm (a) B2 (b) B3

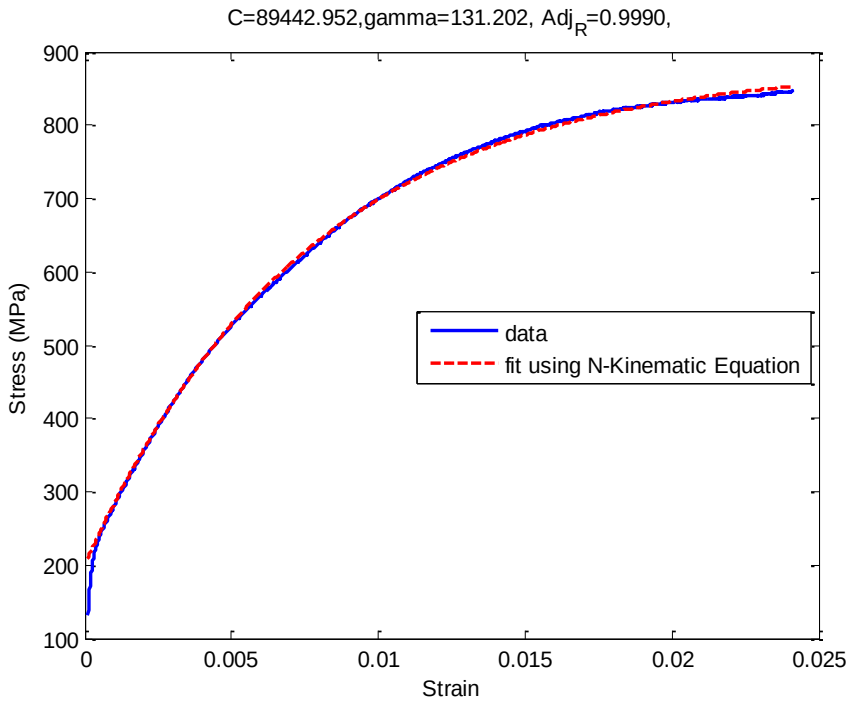

(a)

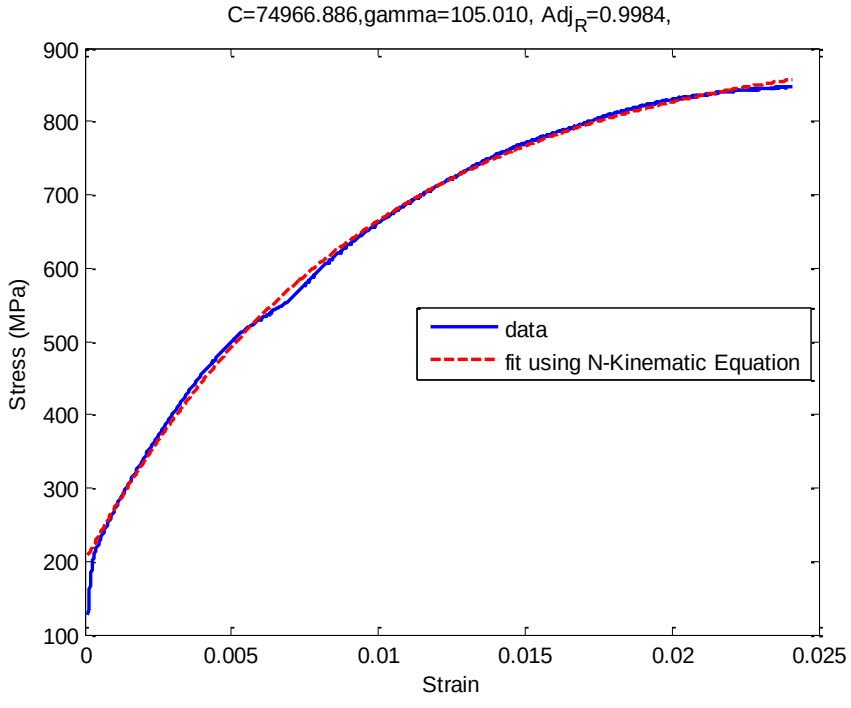

(b)

Figure 5.3 Optimisation of cold rolled low carbon steel data using nonlinear kinematic equation for t= 1.5 mm (a) B2 (b) B3

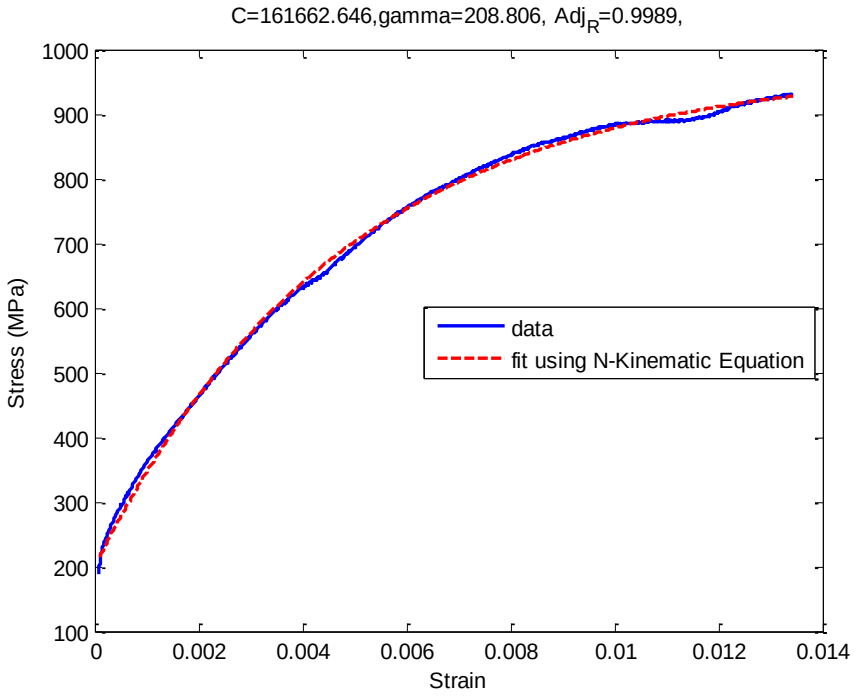

(a)

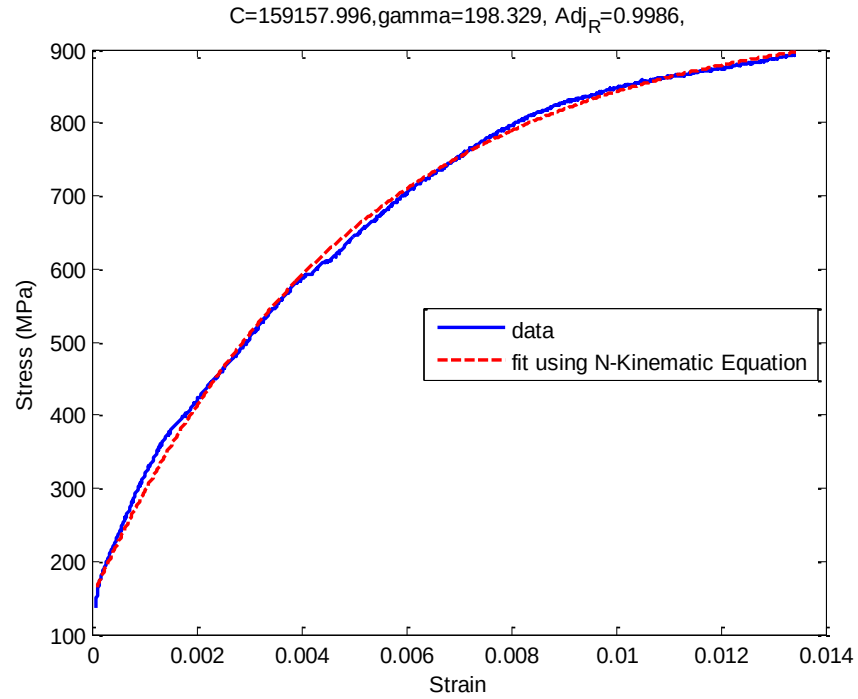

(b)

Figure 5.4 Optimisation of cold rolled low carbon steel data using nonlinear kinematic equation for t= 1 mm (a) B2 (b) B3

Figure 5.5 shows fitting results of nonlinear kinematic hardening equation on 2 mm thickness stainless steel data. The adjusted R-square values recorded were around 0.9791which was lower than the values recorded for 2 mm thick low carbon steel (0.9976). This result was believed to be due to the equation inability to properly fit the decreasing stress curve at strain around 0.01. The cause of the condition was explained in Chapter 4. Figure 5.6 show residual graphs for fitting the hardening equation for stainless steel. The calculated data were well distributed with the highest error occurring at the decreasing stress curve with residual value about 50 MPa for B2.

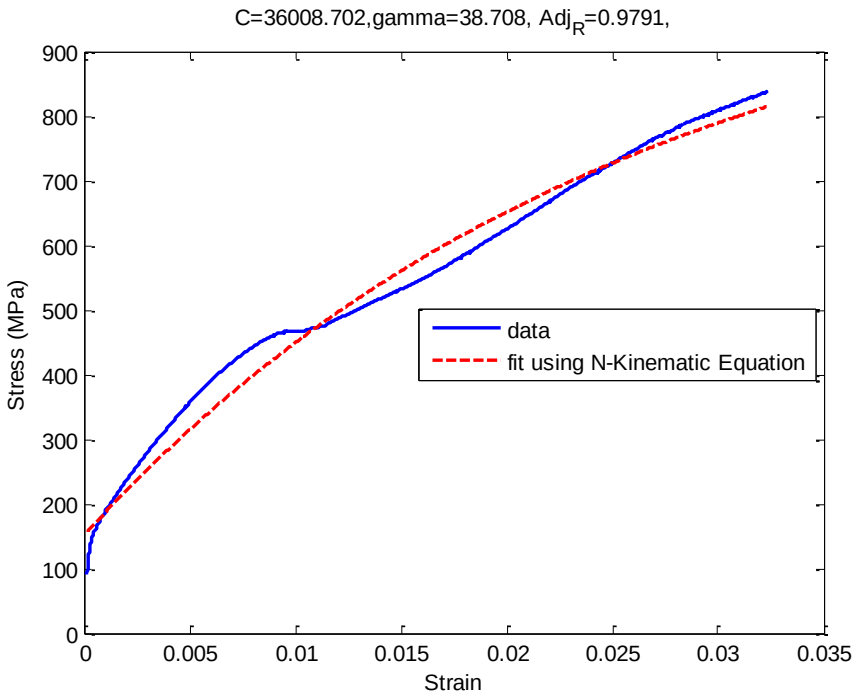

(a)

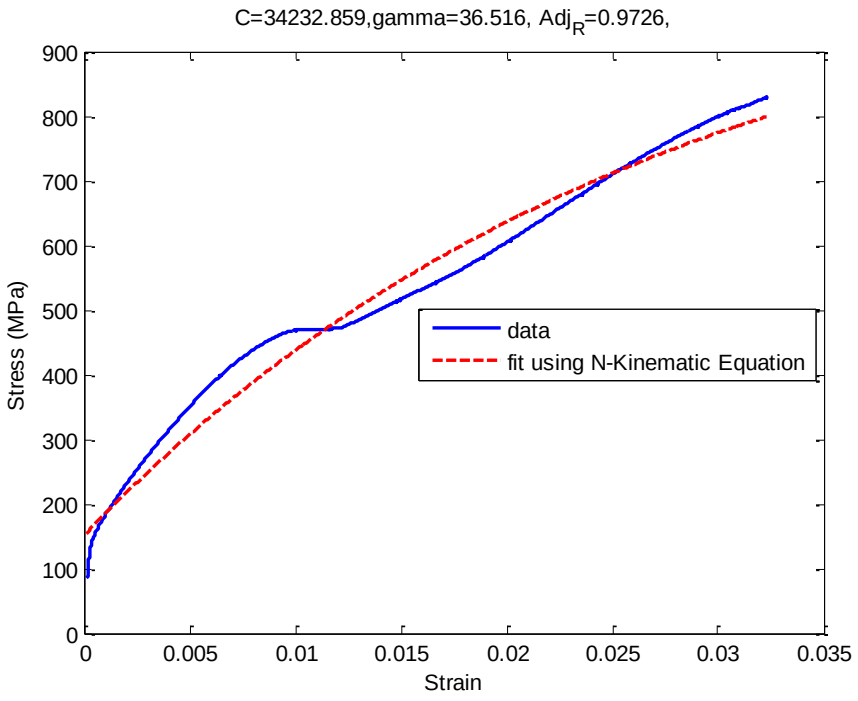

(b)

Figure 5.5 Optimisation of stainless steel data using nonlinear kinematic equation for t= 2 mm (a) B2 (b) B3

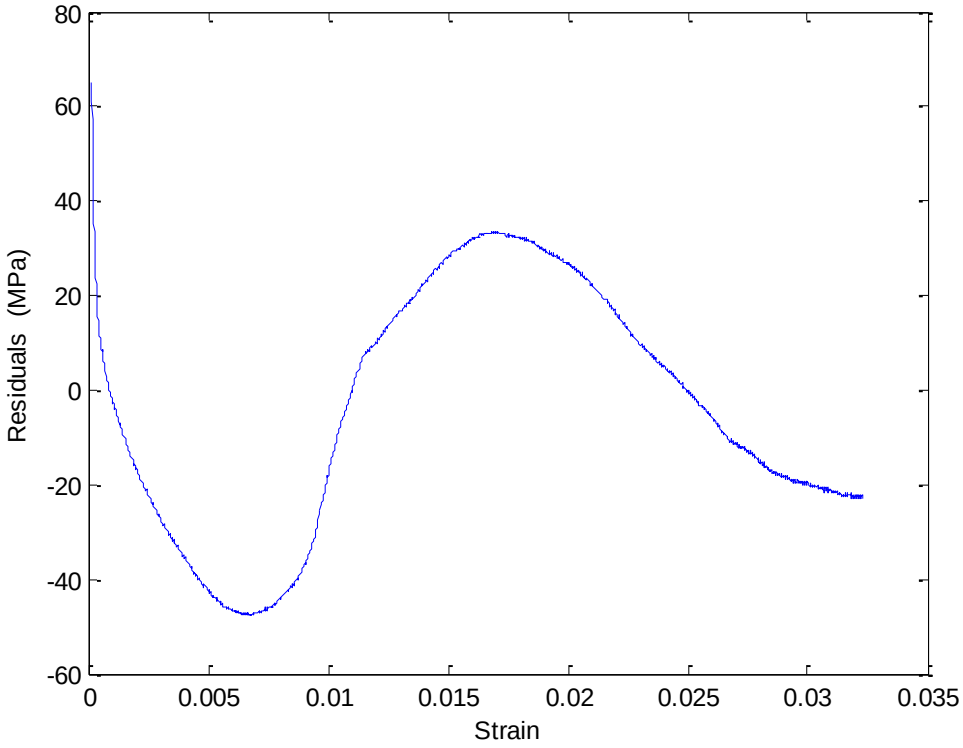

Figure 5.6 Residuals for fitting nonlinear kinematic hardening on B2 stainless steel data of 2 mm thickness

Figures 5.7 and 5.8 show fitting results of nonlinear kinematic hardening equation on 1 mm and 0.5 mm thickness stainless steel data. The adjusted R-square values about 0.9584 for 1 mm and above 0.9715 for 0.5 mm thickness. Figure 5.9 shows the residual graph for 1 mm thickness stainless. The calculated data were well distributed and the highest residual recorded was nearly 60 MPa at strain 0.009.

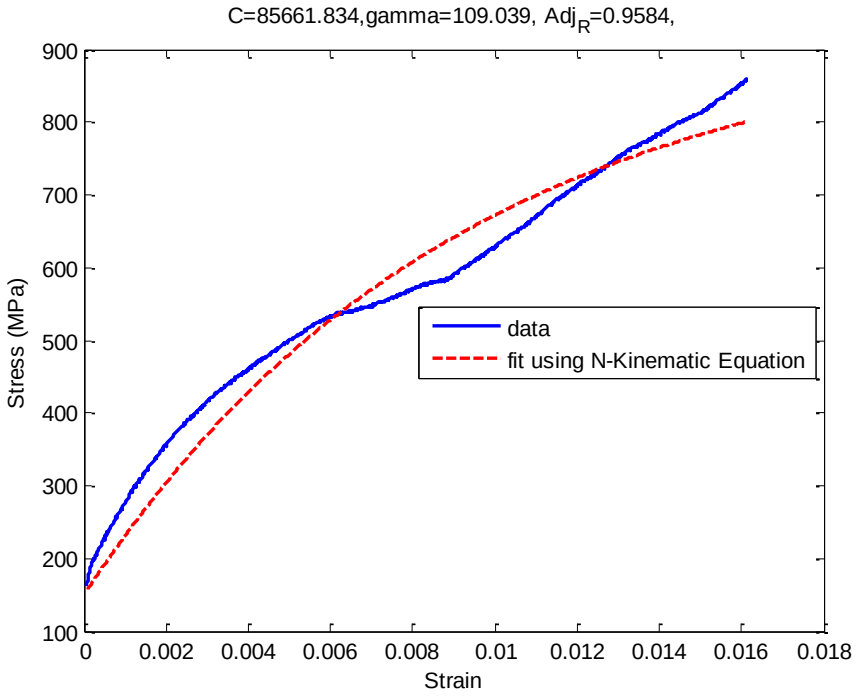

(a)

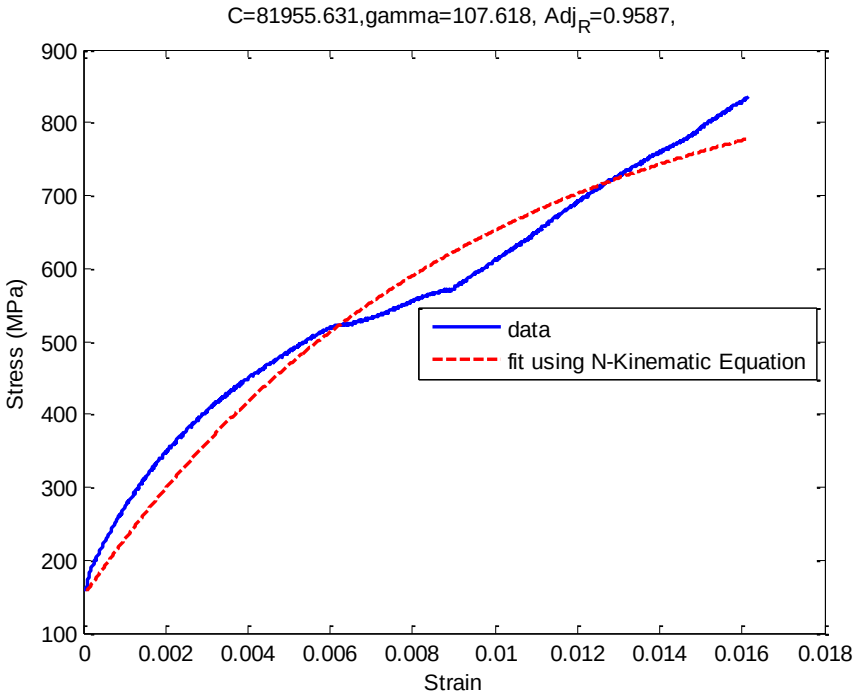

(b)

Figure 5.7 Optimisation of stainless steel data using nonlinear kinematic equation for t= 1mm (a) B2 (b) B3

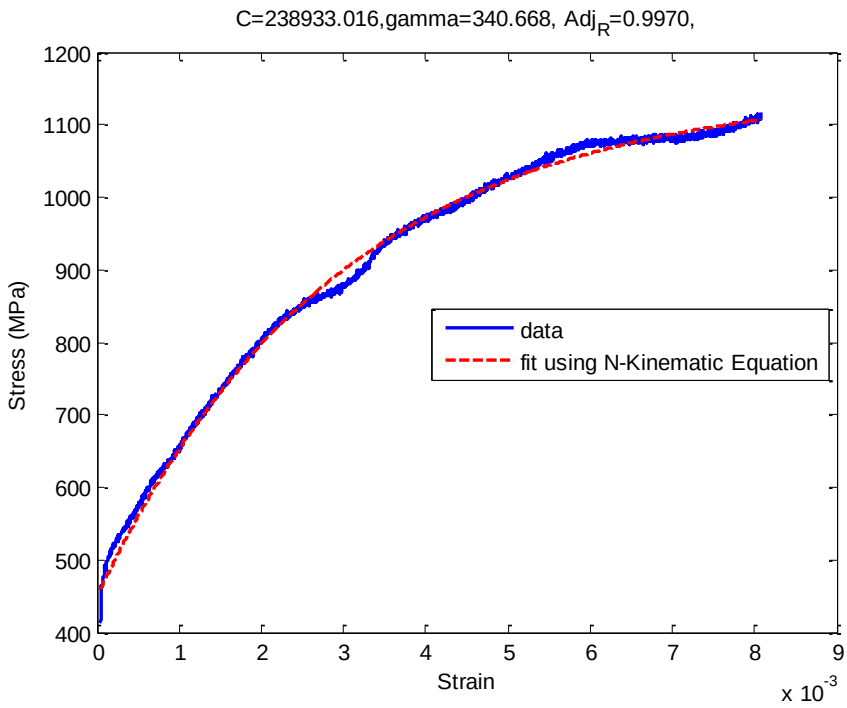

(a)

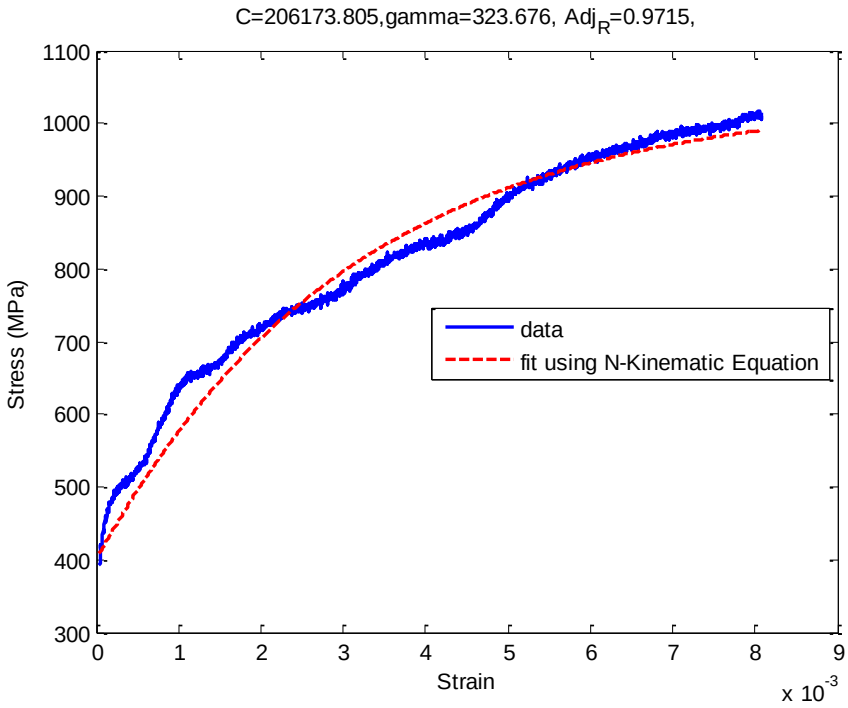

(b)

Figure 5.8 Optimisation of stainless steel data using nonlinear kinematic equation for t= 0.5mm (a) B2 (b) B3

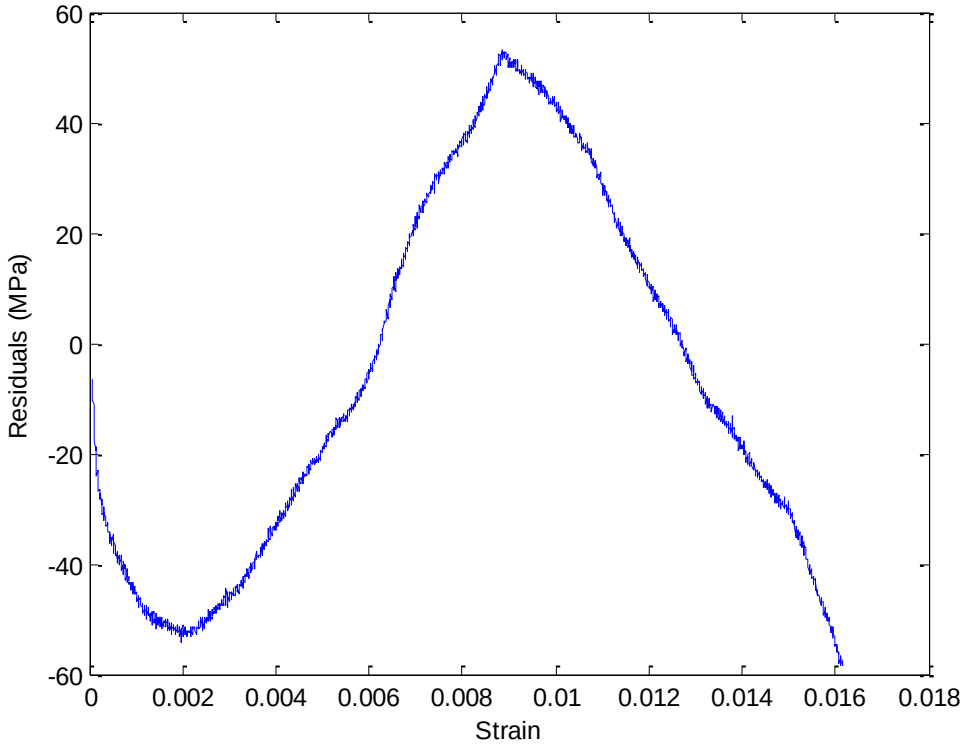

Figure 5.9 Residuals for fitting nonlinear kinematic hardening on B2 stainless steel data of 1 mm thickness.

Table 5.1 shows values for C and gamma of kinematic hardening equation derived from the optimisation result of cold rolled low carbon steel and stainless steel.

Table 5.1 Nonlinear kinematic parameters for cold rolled low carbon steel and stainless steel

	Bending cycle	Low carbon steel		Stainless steel	
		C(MPa)	γ	C(MPa)	γ
2 mm	B2	61895.093	72.87	36008.702	38.708
	B3	52341.714	59.53	34232.859	36.516
*1.5 / 1 mm	B2	89442.952	131.202	85661.834	109.039
	B3	74966.886	105.01	81955.631	107.618
*1/ 0.5 mm	B2	161662.646	208.806	238933.016	340.668
	B3	159157.996	198.329	206173.805	323.676
Note:	*Low carbon steel / Stainless steel				

Figure 5.10, illustrates how well the nonlinear mixed hardening model fits the experimental results for 2 mm thickness low carbon steel. The adjusted R-square value was about 0.999. Similar result was also observed for 1.5 mm and 1 mm thickness as shown in Figure 5.11 and Figure 5.12. The fitting performance of mixed hardening equation thus was marginally better than that of kinematic hardening for low carbon steel.

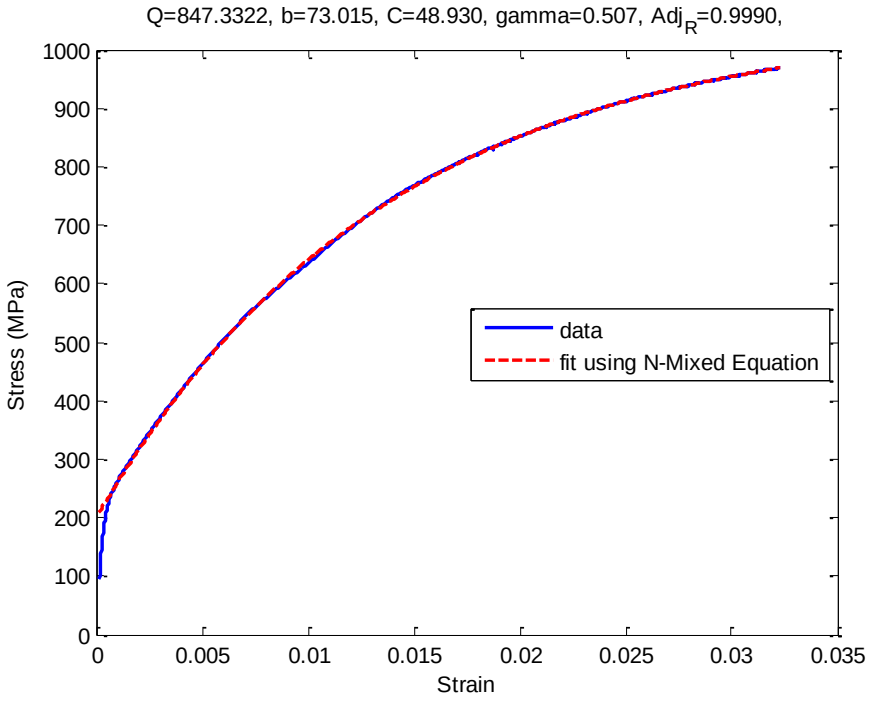

(a)

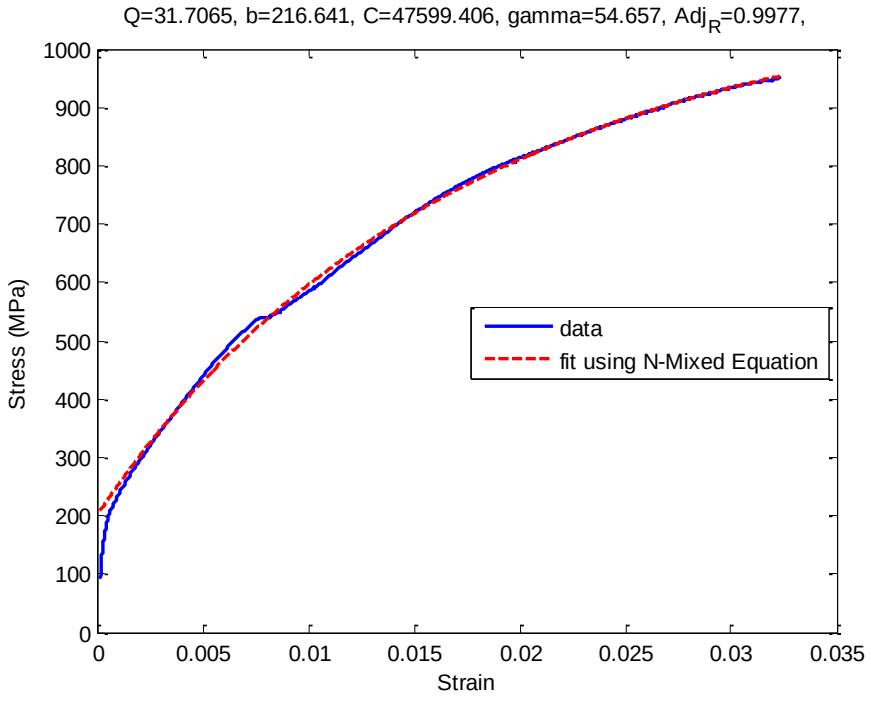

(b)

Figure 5.10 Optimisation of cold rolled low carbon steel data using nonlinear mixed hardening for t= 2 mm (a) B2 (b) B3

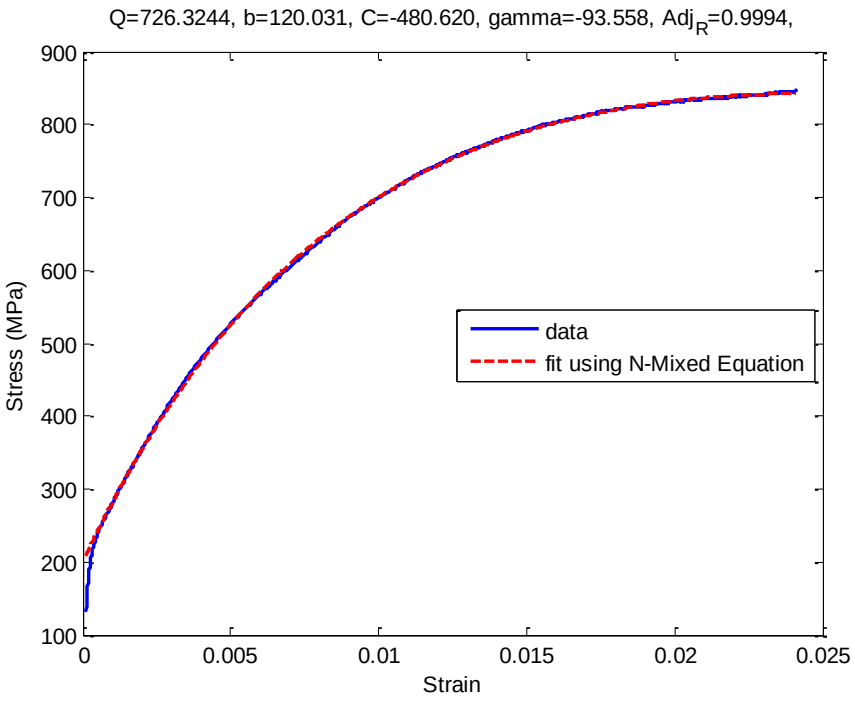

(a)

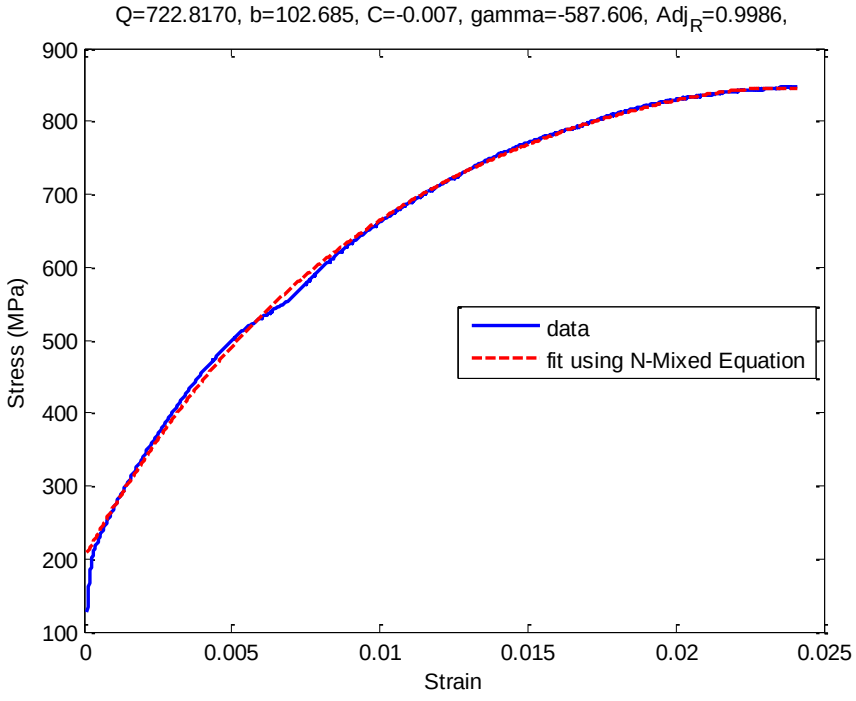

(b)

Figure 5.11 Optimisation of cold rolled low carbon steel data using nonlinear mixed hardening for t= 1.5 mm (a) B2 (b) B3

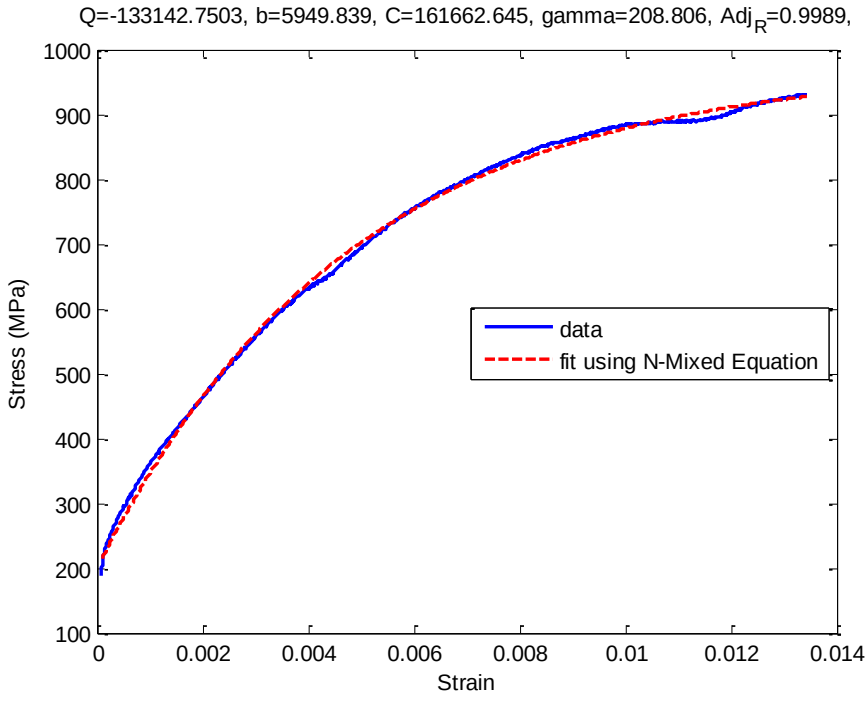

(a)

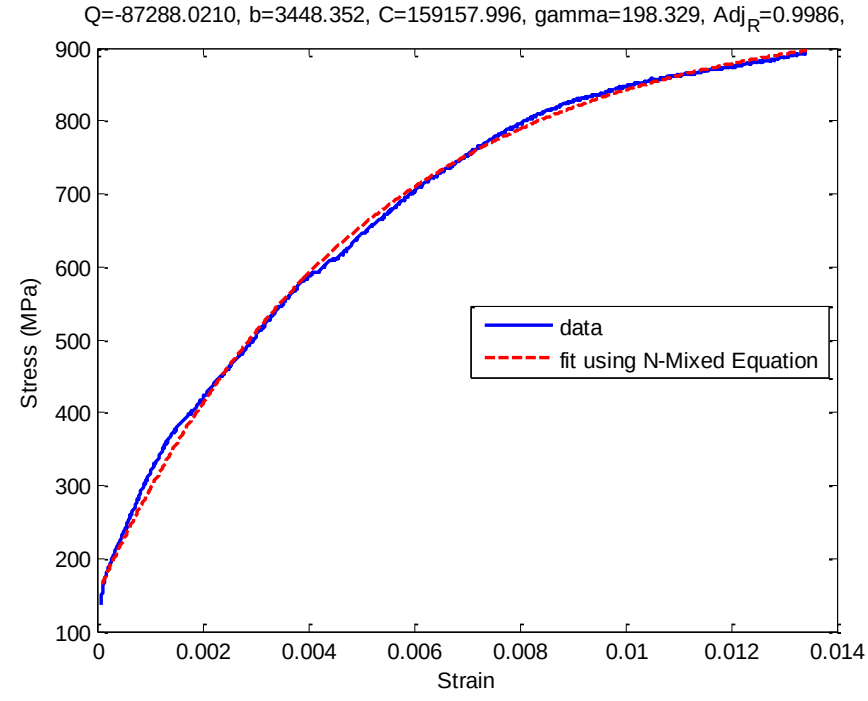

(b)

Figure 5.12 Optimisation of cold rolled low carbon steel data using nonlinear mixed hardening for t= 1 mm (a) B2 (b) B3

In contrast to the results on low carbon steels, one will notice that the mixed hardening equation performance is better than the kinematic hardening equation for fitting stainless steels data. Most of the adjusted R-square values were above 0.99 for all thicknesses as indicated in Figure 5.13, 5.14 and 5.15 as compare to the adjusted R-square values that are shown in Figure 5.5, 5.7 and 5.8.

.

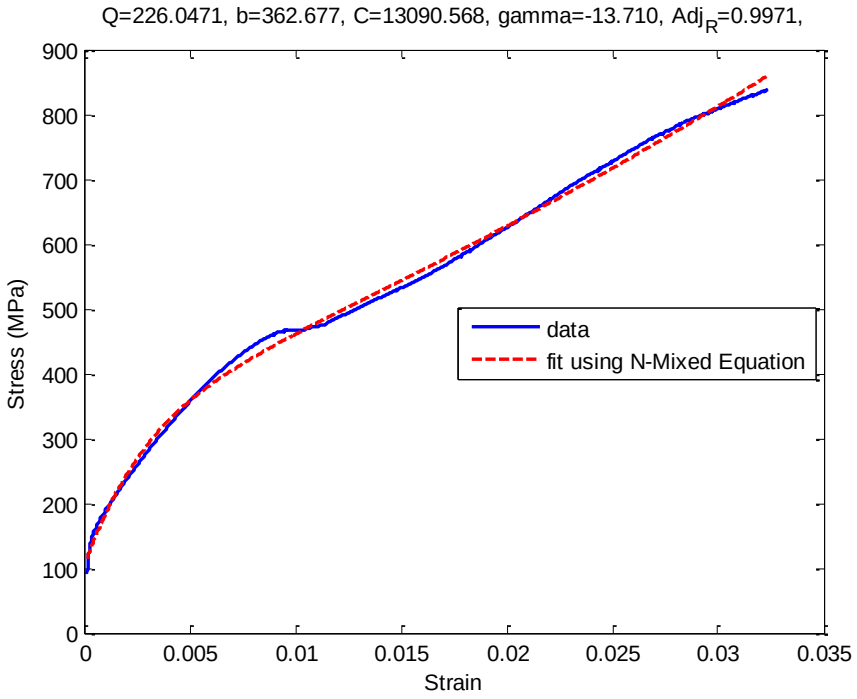

(a)

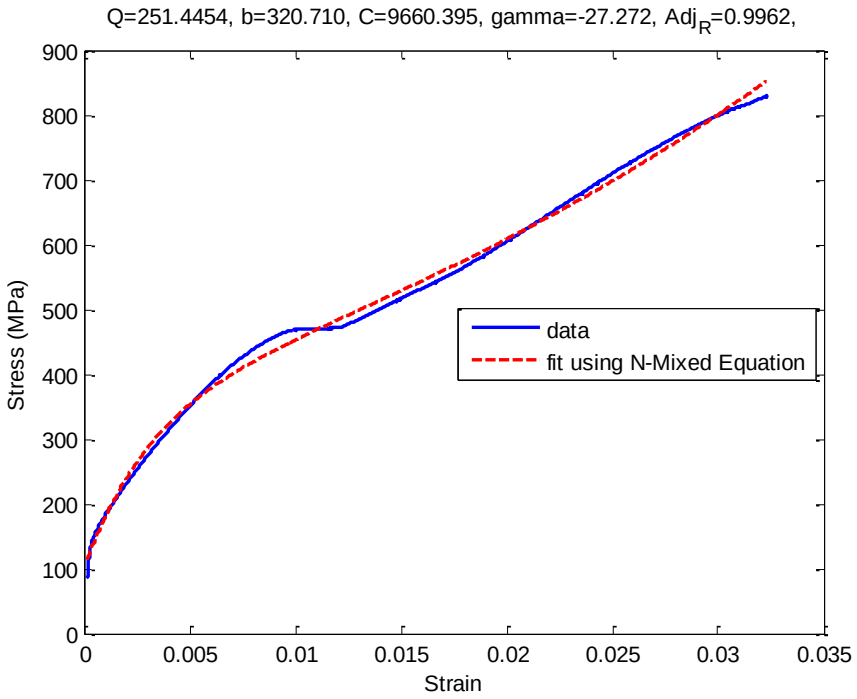

(b)

Figure 5.13 Optimisation of stainless steel data using nonlinear mixed hardening for 2 mm (a) B2 (b) B3

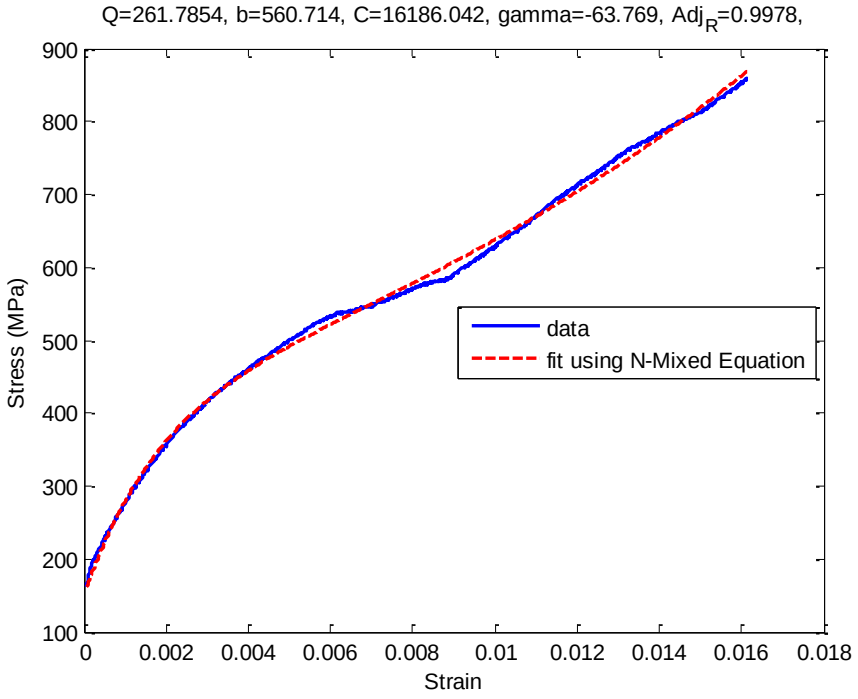

(a)

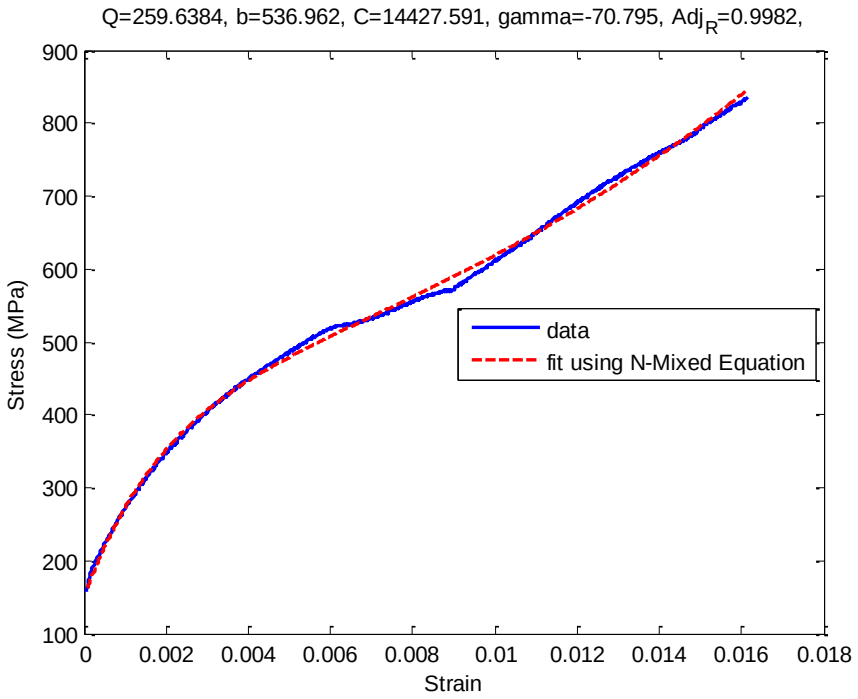

(b)

Figure 5.14 Optimisation of stainless steel data using nonlinear mixed hardening equation for t= 1 mm (a) B2 (b) B3

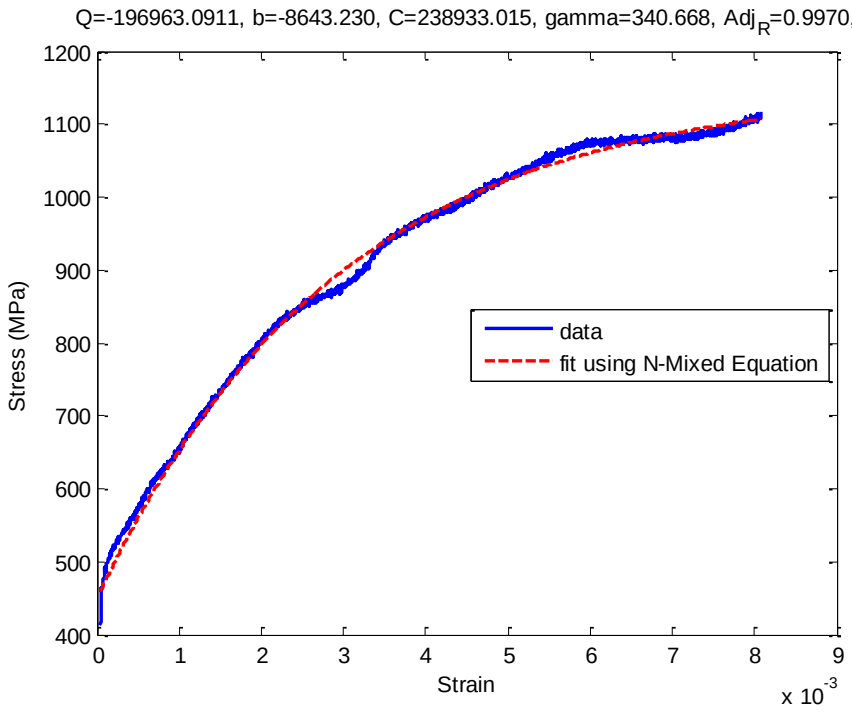

(a)

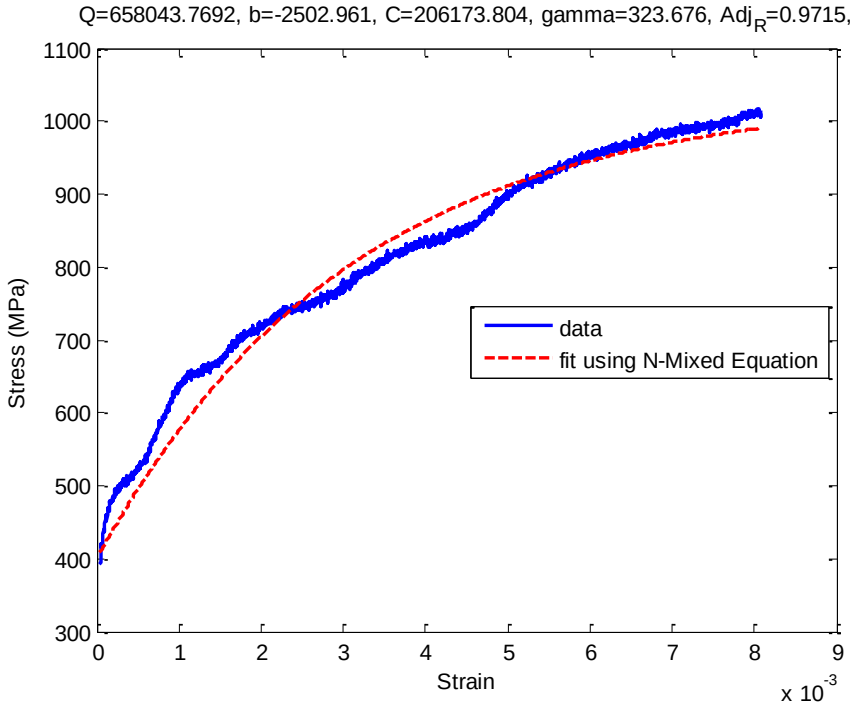

(b)

Figure 5.15 Optimisation of stainless steel data using nonlinear mixed hardening equation for t= 0.5 mm (a) B2 (b) B3

It was noted that the residual values recorded for 2 mm and 1 mm thicknesses were about 20 MPa as shown in Figure 5.16, Figure 5.17 and Figure 5.18. This value was less than the values recorded by fitting using kinematic hardening equations shown in Figure 5.6 and Figure 5.9 (about 60 MPa).This finding justified the capability of the mixed equation to model the hardening deformation curve better than the kinematic hardening equation.

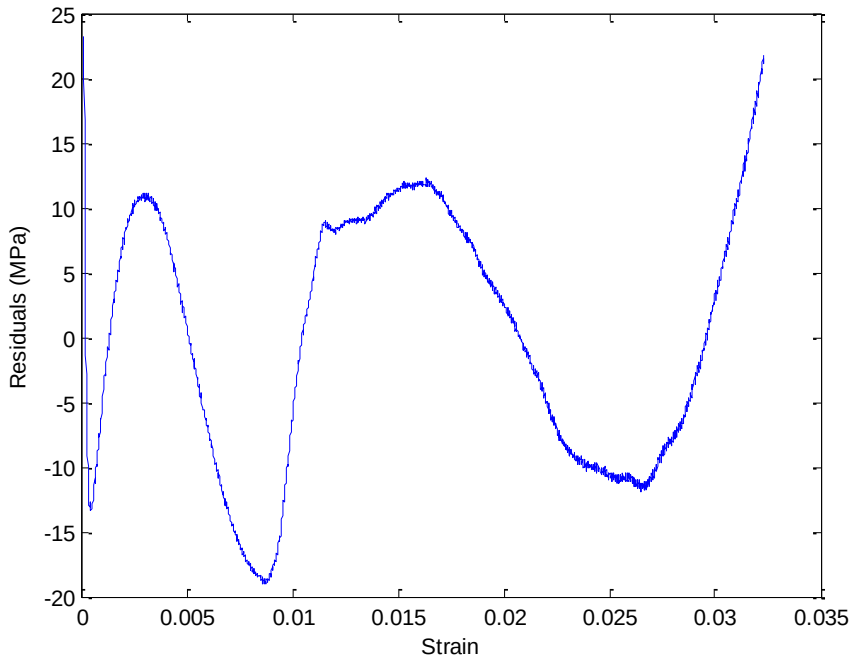

Figure 5.16 Residuals for fitting mixed hardening on B2 stainless steel data of 2 mm thickness

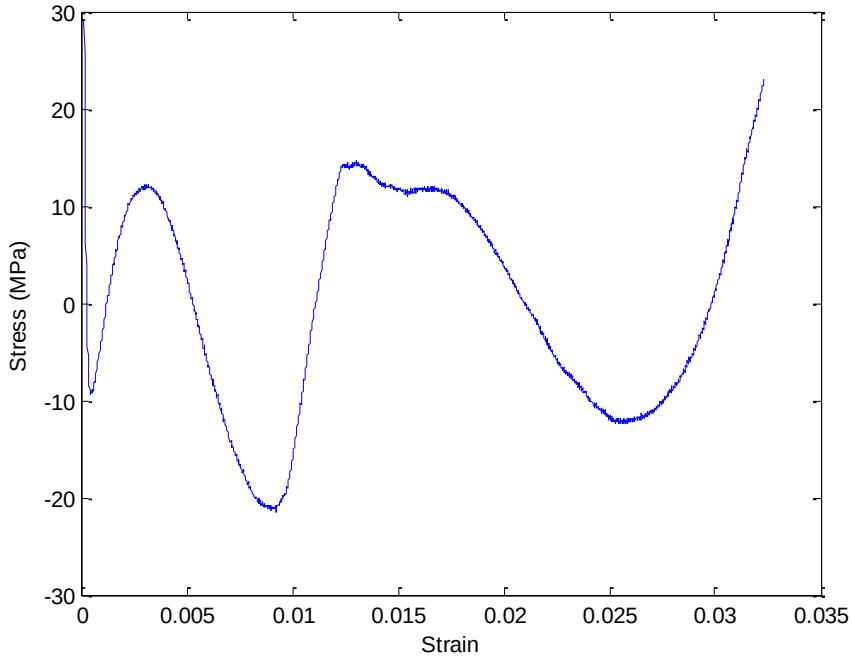

Figure 5.17 Residuals for fitting mixed hardening on B3 stainless steel data of 2 mm thickness

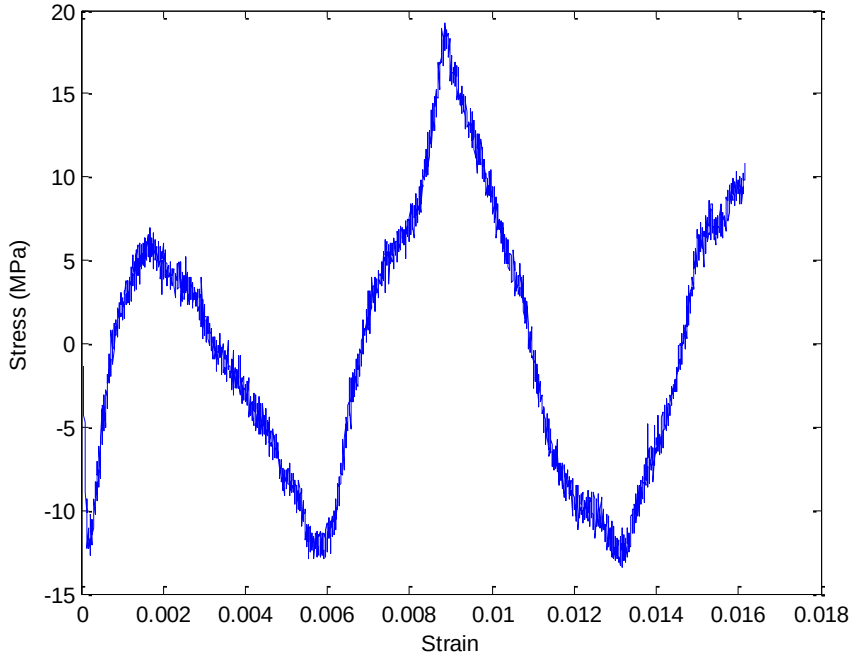

Figure 5.18 Residuals for fitting mixed hardening on B2 stainless steel data of 1 mm thickness

Table 5.2 indicates the mixed hardening parameters derived from the optimisation. Part of the data from this table and Table 5.1 were utilized to validate the effectiveness of kinematic and mixed hardening parameters in predicting springback using finite element simulation (Chapter 6).

Table 5.2 Mixed hardening parameters for cold rolled low carbon steel and stainless steel

	Bending cycle	Low carbon steel				Stainless steel			
		Q(MPa)	b	C(MPa)	γ	Q(MPa)	b	C(MPa)	γ
2 mm	B2	847.332	73.015	48.93	0.507	226.047	362.677	13090.568	13.71
	B3	31.7065	216.641	47599.406	54.657	251.445	320.71	9660.395	27.272
*1.5 / 1 mm	B2	726.324	120.031	480.62	93.558	261.785	560.714	16186.042	63.769
	B3	722.817	102.685	0.007	587.606	259.638	536.962	14427.591	70.795
*1/ 0.5 mm	B2	133142.75	5949.839	161662.645	208.806	196963.091	8643.23	238933.015	340.668
	B3	87288.021	3448.352	159157.996	198.329	658043.769	2502.961	206173.804	323.676
Note:	*Low carbon steel / Stainless steel								

5.6. Conclusions

i. A combination of the developed tool for cyclic bending data acquisition and a robust Programming optimisation technique provides a way to reduce time and problems in material parameter identification for constitutive equations compared to the inverse and iterative method by finite element simulation.

ii. Though the overall fitting using nonlinear kinematic model was relatively smooth and considered acceptable, its capability however was still less than the performance shown by mixed hardening model. This justifies the idea that the application of mixed hardening model is welcome for springback simulation in sheet metal forming.

iii. Optimisation technique using the Nelder–Mead Simplex direct search method was capable of providing an accurate and fast solution for material parameters identification for constitutive equation.

CHAPTER 6

FE SIMULATIONS AND EXPERIMENTAL VALIDATION OF SPRINGBACK

6.1. Introduction

Using a complex hardening model has been considered to improve finite element simulation of sheet metal forming. This, in particular, refers to the effect of reversal loading or the Bauschinger and hardening transient effects. A study by Li et al. found that including the Bauschinger effect can improve the quality of springback prediction (Li et al. 2002). Several other studies were conducted using various hardening models to investigate the accuracy of the simulation. Some of these works were presented in Chapter 2.

To improve sheet metal forming simulation there is a need to incorporate an appropriate constitutive equation capable of describing the Bauschinger and the cyclic transient effect. Combining isotropic and nonlinear kinematic hardening has been considered as one of the best choices; as the former has been associated with the capability to improve cyclic transient and the latter with the capability to accommodate the Bauschinger effect (Chun et al. 2002a; Chun et al. 2002b; Rauch et al. 2007; Yoshida and Uemori 2002; Yoshida and Uemori 2003).

6.2. Objectives

The objective of this chapter is to present validation work in testing the effectiveness of applying kinematic hardening model and mixed hardening model in predicting springback using finite element simulation. The Chaboche nonlinear kinematic hardening model was chosen for kinematic hardening, whilst a combination of the kinematic hardening model and isotropic hardening model was selected to represent the mixed hardening model. The mixed modelling equation is shown in Equation 6. 1. The first part of the equation represents the isotropic hardening model while the second part represents the Chaboche nonlinear kinematic hardening model.

$$\sigma = \sigma_0 + Q(1 - e^{-b\bar{\varepsilon}}) + \frac{C}{\gamma}(1 - e^{-\lambda\bar{\varepsilon}})$$

Equation 6. 1

To meet the validation criteria, a U-shaped bending tool was developed and an experiment was conducted to produce U-shaped parts. The parts' profile was compared with the finite element result of U-shape part. The results were analysed in term of springback angle for the degree of difference between the experiments and the simulations.

6.3. Springback Measurement

The Numisheet'93 method has been widely used to define springback measurement in a U bending profile. It is shown in Figure 6.1 (Lee and Yang 1998).

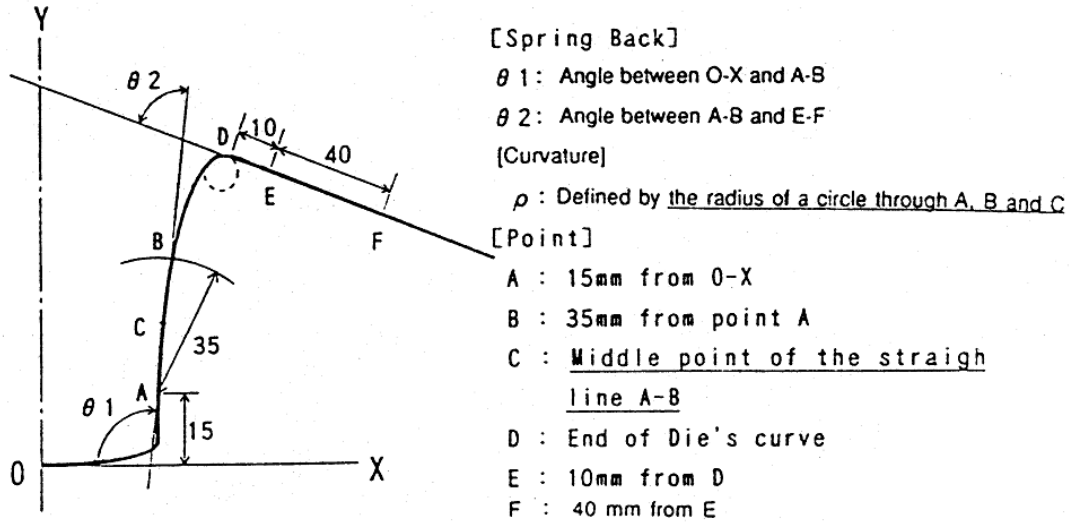

Figure 6.1 Numisheet'93 method to measure springback (Lee and Yang 1998)

In certain cases, the dimension for point A is changed to suit the depth of die drawing, such as the one shown in Figure 6.2.

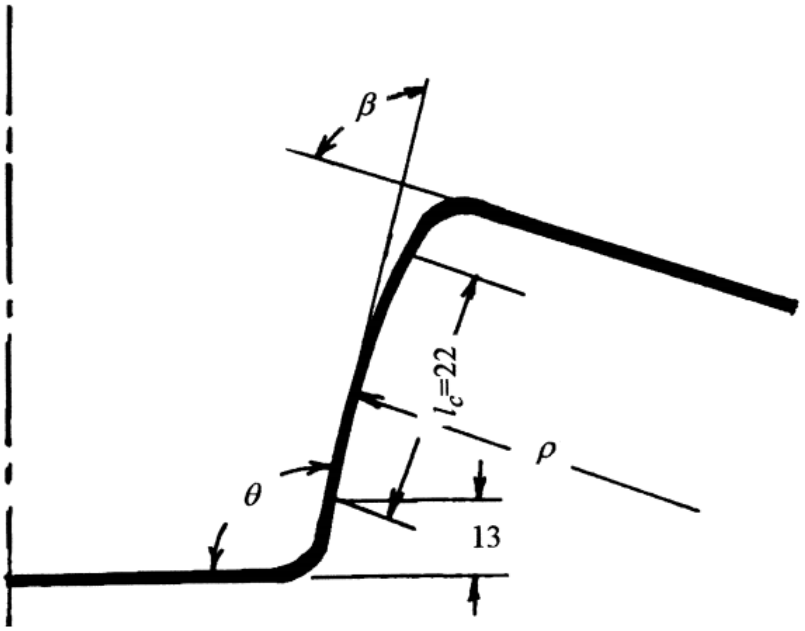

Figure 6.2 Modified Numisheet'93 method to measure springback (Samuel 2000)

In general, the springback measurement is based on two angles, θ1 and θ2 (θ and β in Figure 6.2). By definition, θ1 is characterised as the angle between the bottom surface of the punch and the sheet metal wall, whilst θ2 is the angle between the wall and the flange. Another measurement is the curvature radius of sidewall, ρ. For the current work, the springback measurement was calculated based on 17 mm depth of the drawing die and the reference point A in Figure 6.1 was set at 8.5 mm.

6.4. U-bending Experiment

The Numisheet'93 experimental setup was used for experimental validation of the finite element simulation. Figures 6.3 and 6.4 show the experimental setup and the developed die. The detail drawings are shown in Appendix D for reference. The die is very similar to the die design used by Oliveira (2007) and Taherizadeh (2009) for studying the draw bead effect in material springback.

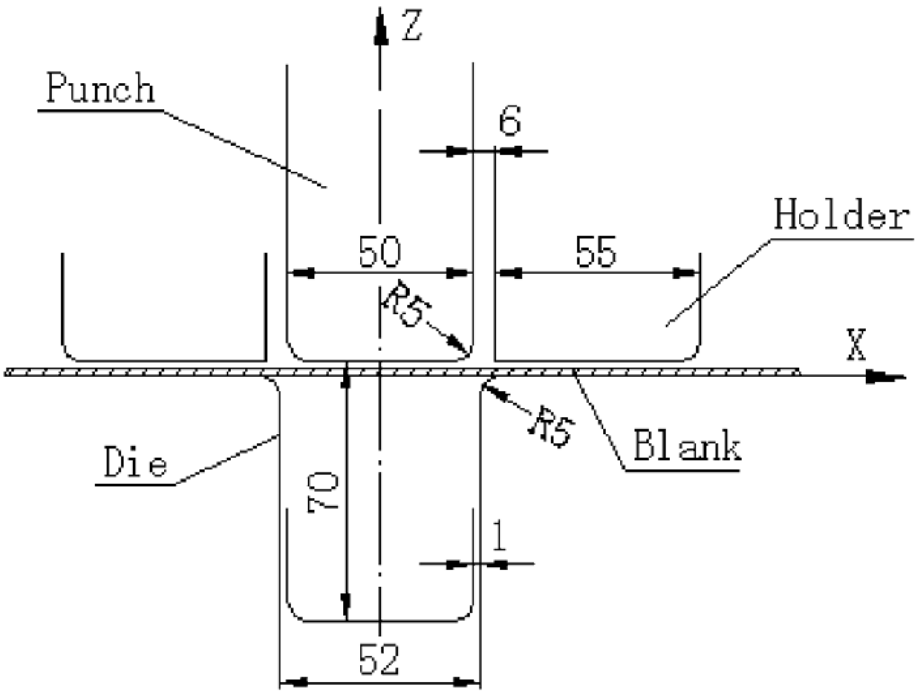

Figure 6.3 Numisheet'93 geometry for U-die bending (Liu et al. 2002)

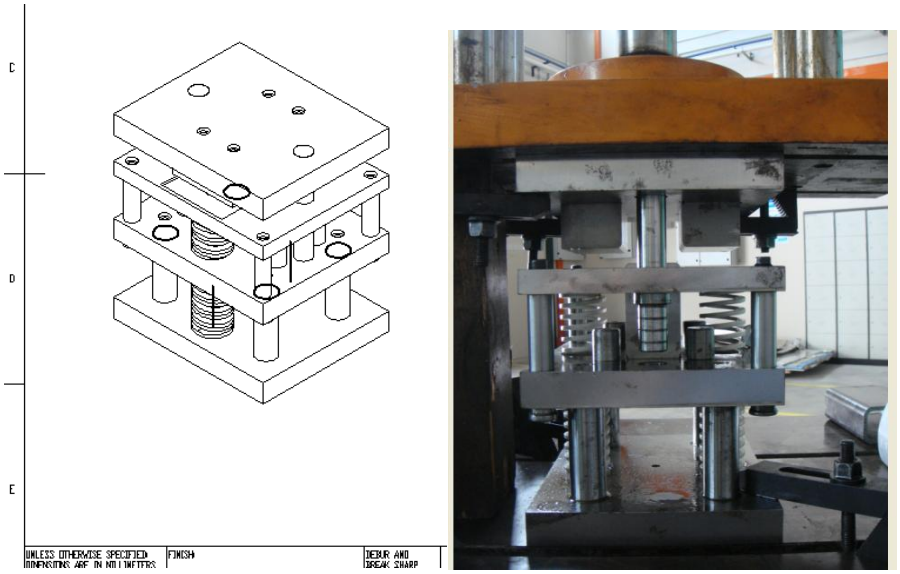

Figure 6.4 U-bending die developed for the validation work

Materials used in the experiment were 1 mm stainless steel and 1.5 mm cold rolled low carbon steel. The blank size for the material was 150 mm long and 25 mm wide. The outcome of the bending experiment is shown in Figure 6.5.

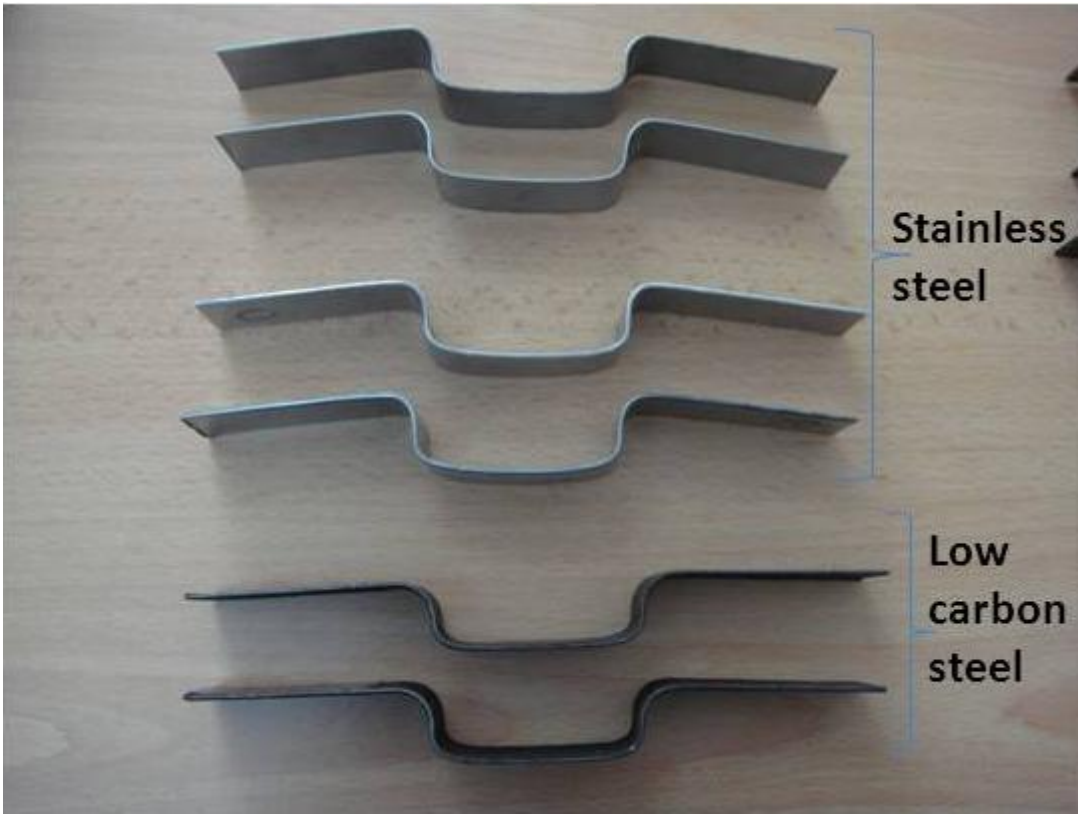

Figure 6.5 Experimental U-bending parts of stainless steel and cold rolled low carbon steel

To measure the θ1 and θ2 angles, x-y coordinates of five control points in the parts were acquired using a profile projector as shown in Figure 6.6 and Figure 6.7(a).

Figure 6.6 Acquiring x-y data using profile projector for five points of the U-bending parts.

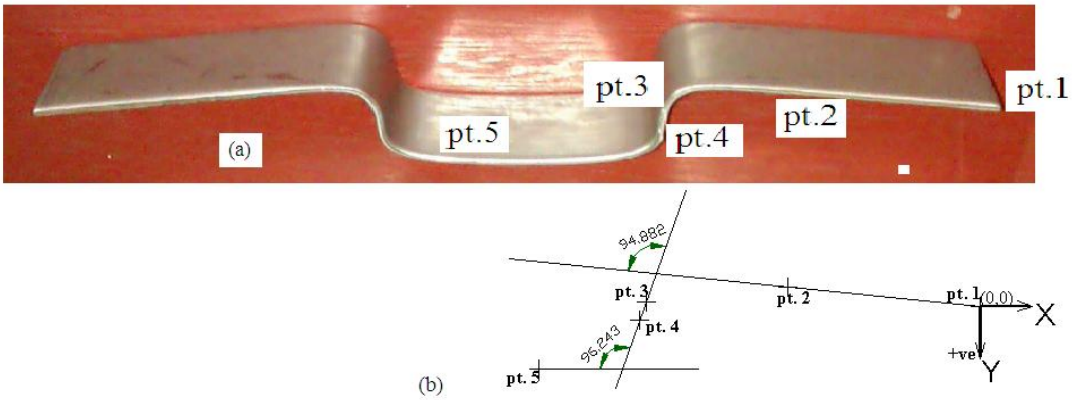

Figure 6.7 Measuring springback angle for 1 mm thick stainless steel from U-bending part (a) the control points location used for acquiring the x-y coordinates (b) determining the angles using AutoCad.

The coordinates were used to draw lines representing the part's profile. For this purpose, AutoCad software was used. To draw line, point 1 was connected to point 2, while point 3 to point 4. As for point 5, it was a straight line parallel to x-axis. Using command "lengthen" from AutoCad, the lines were lengthened to cross each other as required to obtain springback angles. The springback angles were

determined by using the angular dimensioning feature. This approach is shown in Figure 6.7(b).

Table 6.1 and 6.2 show the x-y coordinates acquired using the mentioned approach for stainless steel and low carbon steel. The identified springback angles based on the drawings generated from these coordinates are shown in Table 6.3 and Table 6.4. Three samples were used for each of the materials.

Table 6.1 X-Y coordinates acquired from 1mm thick stainless steel part (mm)

Stainless steel						
	Sample 1		Sample 2		Sample 3	
Point	X	Y	X	Y	X	Y
1	0	0	0	0	0	0
2	-28.37	-1.488	-37.901	-0.122	-31.527	-0.492
3	-55.763	5.549	-59.568	8.464	-56.783	7.212
4	-55.957	7.132	-59.681	9.836	-56.962	8.663
5	-82.18	14.936	-84.966	16.669	-81.191	16.76

Table 6.2 X-Y coordinates acquired from 1.5 mm thick cold rolled low carbon steel part (mm)

Low carbon steel						
	Sample 1		Sample 2		Sample 3	
Point	X	Y	X	Y	X	Y
1	0	0	0	0	0	0
2	-24.475	-1.52	-24.759	-2.832	-30.06	-1.633
3	-55.566	5.183	-55.975	3.027	-57.701	5.356
4	-55.707	6.858	-56.151	4.083	-57.863	6.741
5	-86.576	18.414	-82.071	14.5	-83.851	17.096

Table 6.3 Springback angles for stainless steel (degree)

Stainless steel				
angle\sample	1	2	3	Average
θ1	96.987	94.708	97.033	96.243
θ2	93.984	94.524	96.139	94.882

Table 6.4 Springback angles for cold rolled low carbon steel (degree)

Low carbon steel				
angle\sample	1	2	3	Average
θ1	94.812	99.462	96.671	96.982
θ2	91.258	92.937	93.562	92.586

The average springback values measured from low carbon steel were 96.982 and 92.586 for θ1 and θ2, respectively. As for stainless steel, the values measured were 96.243 for θ1 and 94.882 for θ2. These experimental results were required to validate the reliability of the kinematic and mixed hardening parameters derived from the bending-unbending experimental data in predicting springback of the same part profile using finite element simulation.

6.5. Finite Element Simulation

The finite element simulation was performed using Abaqus software. The simulation used a 2-dimensional model and an incremental implicit approach. The model and approach have been widely used in U-bending, especially because of its unconditional stability with large time steps and the capability to ensure the convergence to a globally self-equilibrated stress-state (Firat 2007). Three major stages were involved: loading, unloading and springback deformation. In the loading stage, the punch moved downward to a specified distance step by step. During this procedure the punch established contact with the sheet metal blank and deformed it into the desired shape. In the unloading stage, the punch moved upwards and lost contact with the sheet metal. While in the final step, the blank holder was released and the workpiece was rejected from the die. As a result of these steps the part underwent springback, primarily due to the unbalance in through-thickness stresses.

Due to the symmetry of the tooling, only half of the geometry was generated. Three rigid body parts and one deformable body were drawn for the tooling model. The rigid bodies were punch, die and blank holder, whilst the deformable part was the 75 mm long blank material. 1 mm and 1.5 mm thick blanks were used to represent stainless steel and low carbon steel material respectively. The gap between the die and the punch is equal to two times thickness of the respective blank. For 1 mm thick stainless steel, the gap was 2 mm and for 1.5 mm thick cold rolled carbon steel the gap was 3 mm.

The blanks were meshed using a continuum, plane strain, 4 nodes- reduced-integration element (CPE4R) for its capability to handle simulation involving large mesh distortion or large strain analysis. For better simulation result as well as for reasonable computing time, the element length should be smaller than the die and punch radii (Abaqus 2002). For that reason the element length should be smaller than 5 mm of die and punch radii. The element size for stainless steel is 0.75 mm in length and 0.25 mm in height. As for cold rolled carbon steel, the size is 1 mm time 0.375 mm.

Friction coefficient was assumed to be 0.17 for both stainless steel and low carbon steel (Samuel 2000; Firat 2007). The blank holding forces were 118 kN and 45 kN for low carbon steel and stainless steel respectively. The values were reasonable to avoid profound deformation on the blank due to holding pressure (Bouvier et al. 2005). Figure 6.8 shows the tooling model and the simulation stages involved.

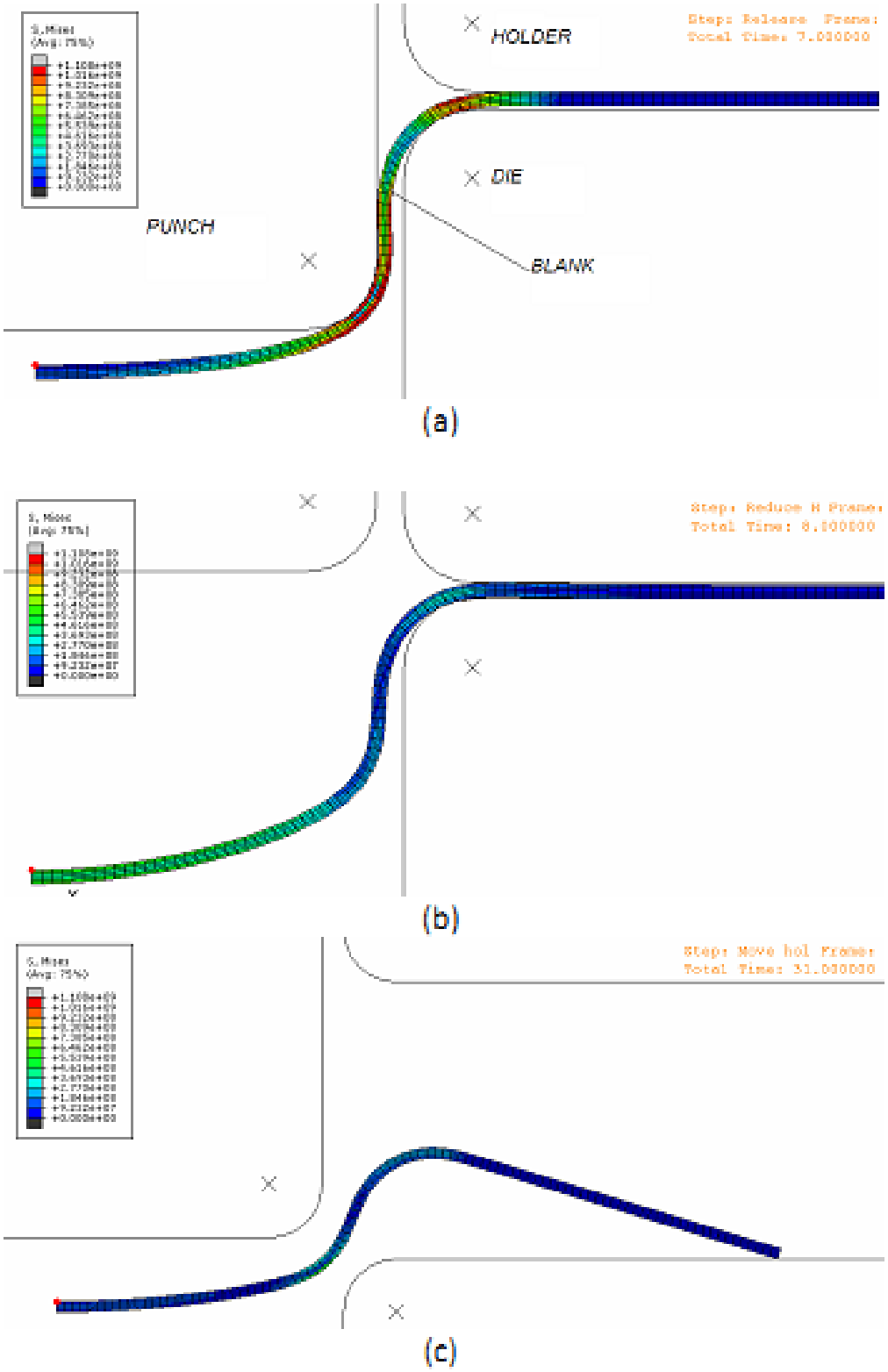

Figure 6.8 2-dimension model of finite element simulation for U-bending (a) loading stage, (b) unloading stage and (c) springback stage

Table 6.5 shows the mechanical properties of 1 mm stainless steel and 1.5 mm low carbon steel used in the simulation. The kinematic hardening parameters and mixed hardening parameters are shown in Table 6.6 and 6.7. The values were derived from cycle B2 of cyclic loading test as described in Chapters 4 and Chapter 5.

Table 6.5 Mechanical properties of cold rolled low carbon steel and stainless steel

Low Carbon Steel		Stainless Steel	
Young Modulus(GPa)	Yield Strength(MPa)	Young Modulus(GPa)	Yield Strength(MPa)
207.00	190.22	190.00	322.32

Table 6.6 Kinematic hardening parameters for cold rolled low carbon steel and stainless steel

Low carbon steel (1.5 mm)		Stainless steel(1 mm)	
C(MPa)	γ	C(MPa)	γ
89442.952	131.202	85661.834	109.039

Table 6.7 Mixed hardening parameters for cold rolled low carbon steel and stainless steel

Low carbon steel (1.5 mm)			
Q(MPa)	b	C(MPa)	γ
726.324	120.031	480.62	93.558
Stainless steel (1 mm)			
Q(MPa)	b	C(MPa)	γ
261.785	560.714	16186.042	63.769

Four simulations were performed based on the type of cyclic hardening properties being used. To measure springback angles, x-y coordinates from five control points or element nodes were recorded from the top surface of the blank

model. Figure 6.9 shows the simulation result for 1 mm thick stainless steel using non-linear kinematic hardening parameters. All recorded x-y values are shown in Table 6.8 and Table 6.9.

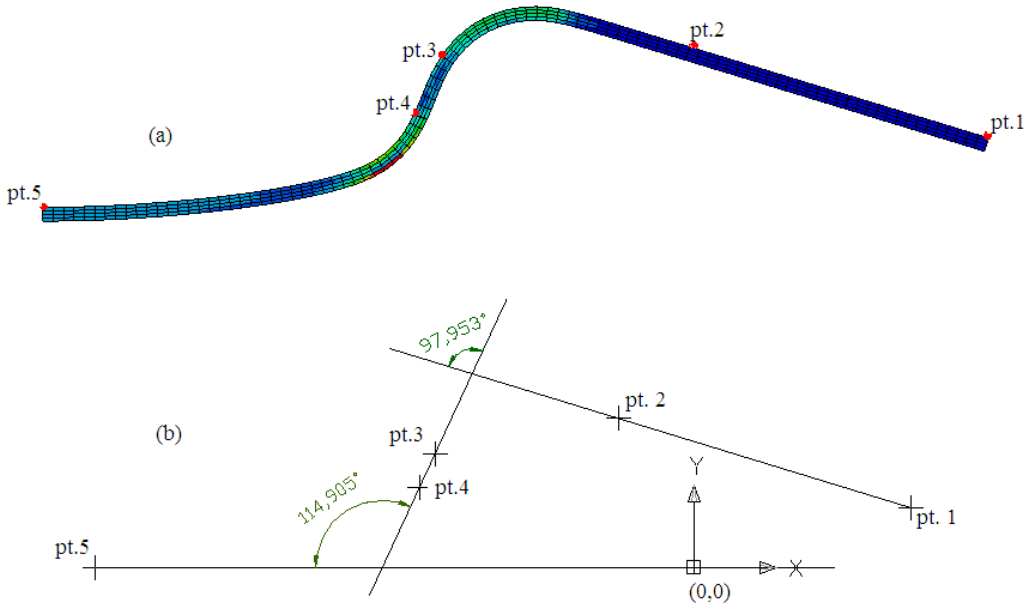

Figure 6.9 Measuring springback angle for 1 mm thick stainless steel from FE result (a) the control points location used for acquiring the x-y coordinates (b) determining the angles using AutoCad.

Table 6.8 X-Y coordinates acquired from simulation using kinematic and mixed hardening parameters for 1 mm thick stainless steel (mm)

Stainless Steel					
		Kinematic Hardening		Mixed Hardening	
point	node	x	y	x	y
1	501	1.81E+01	4.98E+00	1.70E+01	1.02E+01
2	331	-6.30E+00	1.24E+01	-7.61E+00	1.68E+01
3	216	-2.21E+01	9.50E+00	-2.26E+01	1.25E+01
4	196	-2.33E+01	6.73E+00	-2.35E+01	9.63E+00
5	1	-5.00E+01	-3.16E-03	-5.00E+01	3.21E+00

Table 6.9 X-Y coordinates acquired from simulation using kinematic and mixed hardening parameters for 1.5 mm thick cold rolled low carbon steel (mm)

Low Carbon Steel					
		Kinematic Hardening		Mixed Hardening	
point	node	x	y	x	y
1	501	4.00E+01	5.50E+00	4.03E+01	5.50E+00
2	331	6.01E+00	6.26E+00	6.33E+00	5.76E+00
3	161	-2.45E+01	-1.40E+00	-2.45E+01	-1.39E+00
4	151	-2.48E+01	-3.40E+00	-2.47E+01	-3.38E+00
5	1	-5.00E+01	-1.32E+01	-5.00E+01	-1.30E+01

These coordinates were used as control points to draw lines representing parts of U-bending top surface profile in AutoCad software. Using angular measurement feature from the software, the springback angles were determined. This approach is similar to the method used to measure springback angles from the experimental part as shown in Figure 6.7.

6.6. Results and Discussions

Table 6.10 shows a summary of the springback angles from the experiment and simulation for stainless steel. The per cent difference of the simulation results and the experimental results is used to indicate the performance of the particular hardening model. The smaller the difference, the better is the performance of the particular hardening model.

Table 6.10 Springback angle measured from experiments and simulations of 1 mm thick stainless steel material

Stainless steel			
	Experiment	Kinematic	Mixed
θ1	96.243	114.905	107.552
	%DIFF	19.391	11.750
θ2	94.882	97.953	92.573
	%DIFF	3.237	-2.434
%DIFF. = [Simulation-Experiment/Experiment]*100			

From Table 6.10, it is very obvious that the springback angles which were predicted by using mixed hardening model were better than the angles predicted by using kinematic hardening model. The difference between the experimental results and the simulation results by using mixed hardening model was less than 12 per cent. The best predicted value was for angle θ2 where only about 2.4 per cent differences were recorded. The worst predicted springback angle was for θ1 which was produced by using kinematic hardening model. The per cent difference

recorded was around 19. The per cent recorded by using mixed hardening however was not very good also; though the value recorded (11.75 per cent) was less than 19 per cent. For angle θ2, both models performance was within acceptable value that is about 3 per cent.

Further investigation of the results for low carbon steel proved that using mixed hardening model did provide better solutions in predicting springback. These results are summarised in Table 6.11.

Table 6.11 Springback angle measured from experiments and simulations of 1.5 mm thick cold rolled low carbon steel material

Low carbon steel			
	Experiment	Kinematic	Mixed
θ1	96.982	101.239	96.583
	%DIFF	4.389	-0.411
θ2	92.586	99.956	96.136
	%DIFF	7.960	3.834
%DIFF. = [Simulation-Experiment/Experiment]*100			

The performance of the simulation using mixed hardening model is far better than the results produced by kinematic hardening model. The per cent difference recorded for the model was less than 4. The best predicted angle was for angle θ1. The worst predicted springback angle was for θ2 by using kinematic hardening model. The per cent difference recorded was around 8. For angle θ1, the model performance was better with value less than 5 per cent.

The simulation results obtained using kinematic hardening model over predicted all the springback angles, both for stainless steel and low carbon steel.

Simulations results using mixed hardening model on the other hand seemed to show both over and under predicted springback angles. These predicted angles however were very close to the experimental results. In conclusion, this indicated a significant improvement of springback predicting capability when using mixed hardening model.

6.7. Conclusions

i. Comparing kinematic hardening model with mixed hardening model, the mixed hardening model provided better simulation results in predicting springback. This was due to the capability of isotropic hardening to represent cyclic transient better, whilst the nonlinear kinematic hardening had the capability to improve description of the Bauschinger effect.

ii. Kinematic hardening however, on its own was capable of providing relatively good springback simulation illustrated by errors of less than 8 per cent, except for angle θ1 of low carbon steel.

iii. Overall, the data provided by the bending-unbending experiments was considered valuable and reliable for simulating springback prediction. Although the highest percentage error recorded was 19% (kinematic hardening), the rest of the percentage errors recorded were between 12% and 0.411% (mixed hardening). Thus, the percentage errors were acceptable.

CHAPTER 7

CONCLUSIONS AND RECOMMENDATIONS

7.1. Conclusions

The following conclusions are drawn based on the results of the current work. Some of the conclusions are repeated from the chapters' conclusions, specifically from Chapter 4, 5 and 6. The outcomes are believed to enhance knowledge in the field of plasticity of sheet metal forming.

i. Although further improvements are still required, the developed experimental tool and the method are capable of providing an insight into behaviour of sheet metal subjected to cyclic loading, thus enhancing our knowledge of sheet metal forming with regard to the Bauschinger effect. Using the tool and the established formula, the Bauschinger effect factor (BEF) was found.

ii. The sheet material tested using the developed tool showed a typical stress response with a distinct elastic region, a low value yield point followed by work hardening. The existence of work hardening stagnation in cyclic stress-strain curves was not observed. This is likely due to small bending angle of about 20 degree (first bending) to 40 degree (subsequent bending) which produced insufficient accumulated strain for work hardening stagnation to be observed.

iii. The bending data obtained in cycle two and cycle three of bending unbending experiments was successfully approximated using an efficient direct optimisation method (Nelder-Mead Simplex), which enabled identification of material parameters for two constitutive equations used.

iv. Of the two hardening models – kinematic hardening and mixed hardening, the mixed hardening model provided better simulation results in predicting springback. This was due to the capability of the isotropic hardening part of this model to describe cyclic transient and the kinematic hardening part to improve description of the Bauschinger effect. Overall, data provided by bending-unbending experiments proved to be valuable for supporting the job of simulating springback.

7.2. Recommended Future Work

i. It is recommended that more validation test is performed to test the effectiveness of the material parameters identified by the current method and tool. It is suggested that an established standard for U-bending part, such as the NUMISHEET standard, continues to be used for the validation test and should be conducted with careful selection of thickness and blank holding pressure combinations. It is also recommended that the materials hardening parameters, identified using the developed tool, are systematically tested with various numerical parameters of simulation for more comprehensive investigation and validation.

ii. Further improvement on the cyclic bending tool is necessary. Reason for discrepancy between experimental data (not smooth strain-stress behaviour) and numerical prediction should be identified. Construction of the bending tool should be investigated thoroughly in terms of fittings used in all joints. This includes tolerances, allowed clearances, roughness on the working surfaces, lubrications and other that are necessary.

iii. It is recommended that an inverse identification method is applied based on the developed tool to further investigate the reliability of constitutive equations and the materials parameters being identified. Although it has certain limitations, the inverse identification method is worth exploring.

iv. It is suggested that the work in (iii) is also used to investigate and improve the finite element simulation limitations such as a lengthy computing time, nonlinearity of geometrical boundary conditions, convergent issues due to contact and friction description of tools nodes and material nodes and sensitivity of numerical element.

v. In this work, the effects of microstructure changes and Young's modulus changes due to deformation were not considered. To further improve the reliability of the springback prediction, it is recommended that these effects on reversal stress flows are investigated and described into constitutive equations.

REFERENCE LIST

Abaqus (2000). "ABAQUS Analysis User's Manual:Models for metals subjected to cyclic loading." Hibbitt, Karlsson and Sorensen, Inc, RI, U.S.A.

Abaqus (2002). "Getting Started with Abaqus/Standard (Interactive Version)." Hibbit, Karlsson and Sorensen, Inc, RI, U.S.A.

Andrade-Campos, A., Thuillier, S., Pilvin, P., and Teixeira-Dias, F. (2007). "On the determination of material parameters for internal variable thermoelastic-viscoplastic constitutive models." *International Journal of Plasticity*, 23, 1349-1379.

Armstrong, P. J., and Frederick, C. O. (1966). "A mathematical representation of the multiaxial Bauschinger effect." *Rep. No. CEGB Report : RD/B/N731*, Berkeley Nuclear Laboratories.

ASTM E8M (2004). "Annual Book of ASTM Standard: Standard test methods for tension testing of metallic materials." ASTM International, U.S.A.

Bakhshi-Jooybari, M., Rahmani, B., Daeezadeh, V., and Gorji, A. (2009). "The study of spring-back of CK67 steel sheet in V-die and U-die bending processes." *Materials and Design*, 30, 2410-2419.

Boers, S. H. A., Schreurs, P. J. G., Geers, M. G. D., Levkovitch, V., Wang, J., and Svendsen, B. (2010). "Experimental characterization and model identification of directional hardening effects in metals for complex strain path changes." *International Journal of Solids and Structures*, 47, 1361-1374.

Boger, R. K., Wagoner, R. H., Barlat, F., Lee, M. G., and Chung, K. (2005). "Continuous, large strain, tension/compression testing of sheet material." *International Journal of Plasticity*, 21, 2319-2343.

Bouvier, S., Alves, J. L., Oliveira, M. C., and Menezes, L. F. (2005). "Modelling of anisotropic work-hardening behaviour of metallic materials subjected to strain-path changes." *Computational Materials Science*, 32, 301-315.

Bower, A. F. (2009). "Applied Mechanics of Solids." CRC Press, Boca Raton Florida, U.S.A.

Bower, J. E. (1965). "Use of Springback Tester with Steel Having Nonlinear Stress-Strain Curves." *Material Research and Standards*, 5, 607-610.

Bruhns, O. T., Lehmann, T., and Pape, A. (1992). "On the description of transient cyclic hardening behaviour of mild steel CK15." *International Journal of Plasticity*, 8, 331-359.

Brunet, M., Morestin, F., and Godereaux, S. (2001). "Nonlinear kinematic hardening identification for anisotropic sheet metals with bending-unbending tests." *Journal of Engineering Materials and Technology*, 123(October), 378-383.

Bruni, C., Forcellese, A., Gabrielli, F., S, and oncini, M. (2006). "Air bending of AZ31 Magnesium Alloy in warm and hot forming conditions." *Journal of Materials Processing Technology*, 177, 373-376.

Budynas, R. G., and Nisbett, J. K. (2008). "Shigley's Mechanical Engineering Design." McGraw-Hill Education (Asia), Singapore.

Butuc, M. C., Teodosiu, C., Barlat, F., and Gracio, J. J. (2011). "Analysis of sheet metal formability through isotropic and kinematic hardening models." *European Journal of Mechanics A/Solids*, 30, 532-546.

Cao, J., Lee, W., Cheng, H. S., Seniw, M., and Wang, H.-P. (2009). "Experimental and numerical investigation of combined isotropic-kinematic hardening behaviour of sheet metals." *International Journal of Plasticity*, 25, 942-972.

Carbonniere, J., Thuillier, S., Sabourin, F., Brunet, M., and Manach, P. Y. (2009). "Comparison of the work hardening of metallic sheets in bending-unbending and simple shear." *International Journal of Mechanical Sciences*, 51, 122-130.

Chaboche, J. L. (1986). "Time-independent constitutive theories for cyclic plasticity." *International Journal of Plasticity*, 2, 149-188.

Chaboche, J. L. (1989). "Constitutive equations for cyclic plasticity and cyclic viscoplasticity." *International Journal of Plasticity*, 5, 247-302.

Chaboche, J. L. (2008). "A review of some plasticity and viscoplasticity constitutive theories." *International Journal of Plasticity*, 24, 1642-1693.

Chaboche, J. L., and Rousselier, G. (1983). "On the plastic and viscoplastic constitutive equations, part I: rules developed with internal variable concept." *Journal Pressure Vessel Technology*, 105, 153-158.

Chaparro, B. M., Thuillier, S., Menezes, L. F., Manach, P. Y., and Fernandes, J. V. (2008). "Material parameters identification: Gradient-based, genetic and hybrid optimization algorithms." *Computational Materials Science*, 44, 339-346.

Chun, B. K., Jinn, J. T., and Lee, J. K. (2002a). "Modeling the Bauschinger effect for sheet metals, part I: theory." *International Journal of Plasticity*, 18, 571-595.

Chun, B. K., Kim, H. Y., and Lee, J. K. (2002b). "Modeling the Bauschinger effect for sheet metals, part II: applications." *International Journal of Plasticity*, 18, 597-616.

Chung, K., Lee, M. G., Kim, D., Kim, C., Wenner, M. L., and Barlat, F. (2005). "Spring-back evaluation of automotive sheets based on isotropic-kinematic hardening laws and non-quadratic anisotropic yield functions, Part I: theory and formulation." *International Journal of Plasticity*, 21, 861-882.

Davies, R. G. (1981). "Springback in high-strength steels." *Journal of Applied Metalworking*, **1** (4), 45-52.

De-Carvalho, R., Valente, R. A. F., and Andrade-Campos, A. (2011). "Optimization strategies for non-linear material parameters identification in metal forming problems." *Computers & Structures*, 89, 246-255.

Dennis Jr, J. E., and Woods, D. J. (1985). "Optimization on microcomputers: the Nelder-Mead simplex algorithm." *Rep. No. Technical Report 85-9*, ARO, Delaware.

Eggertsen, P.-A., and Mattiasson, K. (2009). "On the modelling of the bending-unbending behaviour for accurate springback predictions." *International Journal of Mechanical Sciences*, 51, 547-563.

Eggertsen, P.-A., and Mattiasson, K. (2010). "On constitutive modeling for springback analysis." *International Journal of Mechanical Sciences*, 52, 804-818.

Firat, M. (2007). "U-channel forming analysis with an emphasis on springback deformation." *Material and Design*, 28, 147-154.

Firat, M., Kaftanoglu, B., and Eser, O. (2008). "Sheet metal forming analyses with an emphasis on the springback deformation." *Journal of Materials Processing Technology*, 196, 135-148.

Gardiner, F. J. (1957). "The springback of metals." *Trans. ASME*, 1-9.

Gau, J. T., and Kinzel, G. L. (2001). "An experimental investigation of the influence of the Bauschinger effect on springback predictions ." *Journal of Materials Processing Technology*, 108, 369-375.

Geng, L., Shen, Y., and Wagoner, R. H. (2002). " Anisotropic hardening equations derived from reverse-bend testing." *International Journal of Plasticity*, 18, 743-767.

Geng, L., and Wagoner, R. H. (2000). "Springback analysis with a modified hardening model." *Rep. No. Paper No. 2000-01-0768*, SAE, Inc..

Gomes, C., Onipede, O., and Lovell, M. (2005). "Investigation of springback in high strength anisotropic steels." *Journal of Materials Processing Technology*, 159, 91-98.

Groover, M.P. (2002).”Fundamental of Modern Manufacturing-materials,processes, and systems.” John Willey and Sons., New York, U.S.A.

Haupt, P., Kamlah, M., and Tsakmakis, C. H. (1992). "Continuous representation of hardening properties in cyclic plasticity." *International Journal of Plasticity*, 8, 803-817.

Hill, R. (1998). "The Mathematical Theory of Plasticity." Oxford University Press, Oxford, UK.

Hosford, W. F., and Caddell, R. M. (1993). "Metal Forming: Mechanics and Metallurgy." PTR Prentice Hall., Upper Saddle River, NJ, U.S.A.

Inamdar, M. V., Date, P. P., and Sabnis, S. V. (2002). "On the effect of geometric parameters on springback in sheets of five materials subjected to air vee bending." *Journal of Applied Metalworking*, 123, 459-463.

Johnson, W., and Mellor, P. B. (1973). "Engineering Plastcicty." Van Nostrand Reinhold Company Ltd, London, UK.

Keeler, S. P. (1977). "Proceeding of a Symposium on Mechanics of Sheet Metal Forming: Sheet Metal Stamping Technology-Need for fundamental understanding." Warren, Michigan.

Kerry, L. E., and Robert, H. S. (2001). "Design of sensor for on-line measurement of loaded bend angle for pressbrake control." *Robotics and Computer Integrated Manufacturing*, 17, 329-340.

Keum, Y. Y., and Han, B. Y. (2002). "Springback of FCC sheet in warm forming." *Journal of Ceramic Processing Research*, 3, 159-165.

Kuwabara, T., Kumano, Y., Ziegelheim, J., and Kurosaki, I. (2009). "Tension-compression asymmetry of phosphor bronze for electronic parts and its effect on bending behaviour." *International Journal of Plasticity*, 25, 1759-1776.

Lagarias, J. C., Reeds, J. A., Wright, M. H., and Wright, P. E. (1998). "Convergence properties of the Nelder-Mead simplex method in low dimensions." *SIAM Journal on Optimization*, 9(1), 112-147.

Lange, L. (1985). "Handbook of Metal Forming." Society of Manufacturing Engineers, Dearborn, Michigan, U.S.A.

Lee, M.-G., Kim, D., Kim, C., Wenner, M. L., and Chung, K. (2005a). "Spring-back evaluation of automotive sheets based on isotropic-kinematic hardening laws and non-quadratic anisotropic yield functions, Part III: application." *International Journal of Plasticity*, 21, 915-953.

Lee, M.-G., Kim, D., Kim, C., Wenner, M. L., Wagoner, R. H., and Chung, K. (2005b). "Spring-back evaluation of automotive sheets based on isotropic-kinematic hardening laws and non-quadratic anisotropic yield functions, Part II: characterization of material properties." *International Journal of Plasticity*, 21, 883-914.

Lee, S. W., and Yang, D. Y. (1998). "An assessment of numerical parameters influencing springback in explicit finite element analysis of sheet metal forming process." *Journal of Materials Processing Technology*, 80-81, 60-67.

Lemaitre, J., and Chaboche, J. L. (1990). "Mechanics of Solid Materials." Cambridge University Press, Cambridge, UK.

Leu, D. K. (1997). "A simplified approach for evaluating bendability and springback in plastic bending of anisotropic sheet metals." *Journal of Materials Processing Technology*, **66**, 9-17.

Li, K. P., Carden.W.D., and Wagoner, R. H. (2002). "Simulation of springback." *International Journal of Mechanical Sciences*, 44, 103-122.

Liu, G., Lin, Z., and Bao, Y. (2002). "Improving dimensional accuracy of a u-shaped part through an orthogonal design experiment." *Finite Elements In Analysis And Design*, 39, 107-118.

Mahmoudi, A. H., Pezeshki-Najafabadi, S. M., and Badnava, H. (2011). "Parameter determination of Chaboche kinematic hardening model using a multi objective genetic algorithm." *Computational Materials Science*, 50, 1114-1122.

Marciniak, Z., Duncan, J. L., and Hu, S. J. (2002). "Mechanics of Sheet Metal Forming." Butterworth-Heinemann, Oxford, UK.

Moreira, L. P., and Ferron, G. (2004). "Influence of plasticity model in sheet metal forming simulations." *Journal of Materials Processing Technology*, 155-156, 1596-1603.

Nilsson, A., Melin, L., and Magnusson, C. (1997). "Finite-element simulation of v-die bending: A comparison with experimental results." *Journal of Materials Processing Technology*, 65, 52-58.

Oliveira, M. C., Alves, J. L., Chaparro, B. M., and Menezes, L. F. (2007). "Study on the influence of work-hardening modeling in springback prediction." *International Journal of Plasticity*, 23, 516-543.

Omerspahic, E., Mattiasson, K., and Enquist, B. (2006). "Identification of material hardening parameters by three-point bending of metal sheets." *International Journal of Mechanical Sciences*.

Perduijn, A. B., and Hoogenboom, S. M. (1995). " The pure bending of sheet." *Journal of Materials Processing Technology*,(51), 274-295.

Pham, N., and Wilamowski, B. M. (2011). "Improved Nelder Mead's simplex method and application." *Journal of Computing*, 3(3), 55-63.

Prager, W. (1956). "A new method of analysing stresses and strains in work hardening plastic solids." *Journal of Applied Mechanics*, 23, 493-496.

Ragai, I., Lazim, D., and Nemes, J. A. (2005). "Anisotropy and springback in draw-bending of stainless steel 410: experimental and numerical study." *Journal of Materials Processing Technology*, 166, 116-127.

Rauch, E. F., Gracio, J. J., and Barlat, F. (2007). "Work-hardening model for polycrystalline metals under strain reversal at large strains." *Acta Mater.*, 55, 2939-2948.

Samuel, M. (2000). "Experimental and numerical prediction of springback and side wall curl in u-bendings of anisotropic sheet metals." *Journal of Materials Processing Technology*, 105, 382-393.

Samuel, M. (2002). "Influence of drawbead geometry in sheet metal forming." *Journal of Applied Materials Processing Technology*, 122, 94-103.

Sanchez, L. R. (2010). "Modeling of springback, strain rate and Bauschinger effects for two-dimensional steady state cyclic flow of sheet metal subjected to bending under tension." *International Journal of Mechanical Sciences*, 52, 429-439.

Sanchez, L. R., Robertson, D., and Gerdeen, J. C. (1996). "Springback of sheet metal bent to small radius/thickness ratios." *Society of Automotive Engineers*, 105(paper 960595), 650-656.

Shigley, J. E., and Uicker, J. J. (1995). "Theory of Machines and Mechanisms." McGraw-Hill, Inc., Singapore.

Song, N., Qian, D., Cao, J., Liu, W. K., and Li, S. (2001). "Effective models for prediction of springback in flanging." *Trans. ASME, Oct. 2001. 123.*.

Sowerby, R., and Uko, D. K. (1979). "A review of certain aspects of the Bauschinger effect in Metals." *Materials Science and Engineering*, 41, 43-58.

Sun, P., Gracio, J. J., and Ferreira, J. A. (2006). "Control system of a mini hydraulic press for evaluating springback in sheet metal forming." *Journal of Materials Processing Technology*, 176, 55-61.

Taherizadeh, A., Ghaei, A., Green, D. E., and Altenhof, W. J. (2009). "Finite element simulation of springback for a channel draw process with drawbead using different hardening models." *International Journal of Mechanical Sciences*, 51, 314-325.

Tekaslan, O., Gerger, N., and Seker, U. (2008). "Determination of springback of stainless steel sheet metal in v bending dies." *Materials and Design*, 29, 1043-1050.

Tekaslan, O., Seker, U., and Ozdemir, A. (2006). "Determining springback amount of steel sheet metal has 0.5 mm thickness in bending dies." *Materials and Design*, **27**, 251-258.

Tekiner, Z. (2004). " An experimental study on the examination of springback of sheet metals with several thicknesses and properties in bending dies." *Journal of Materials Processing Technology*, 145, 109-117.

Thakur, A., Nasser, N., and Vecchio, K. S. (1996). "Dynamic Bauchinger effect." *Acta Mater.*, 44(7), 2797-2807.

The MathWorks Inc. Release Notes for R2008a. www.mathworks.com . 2008.
Ref Type: Online Source

Thuillier, S., and Manach, P. Y. (2009). "Comparison of the work-hardening of metallic sheets using tensile and shear strain paths." *International Journal of Plasticity*, 25, 733-751.

Weinmann, K. J., Rosenberger, A. H., and Sanchez, L. R. (1988). "The Bauschinger effect of sheet metal under cyclic reverse pure bending." *Annals of the CIRP*, 37, 289-293.

Wilson, F. W., Harvey, P. D., and Gump, C. B. (1965). " Die Design Handbook." McGraw-Hill Publishing Company, NY, U.S.A.

Yoon, J. W. (2007). "Advances in metal forming: experiments, constitutive models and simulations." *International Journal of Plasticity*, 23(3), 343-560.

Yoshida, F., and Uemori, T. (2002). "A model of large-strain cyclic plasticity describing the Bauschinger effect and workhardening stagnation." *International Journal of Plasticity*, 18, 661-686.

Yoshida, F., and Uemori, T. (2003). "A model of large-strain cyclic plasticity and its application to springback simulation." *International Journal of Mechanical Sciences*, 45, 1687-1702.

Yoshida, F., Uemori, T., and Fujiwara, K. (2002). "Elastic–plastic behavior of steel sheets under in-plane cyclic tension–compression at large strain." *International Journal of Plasticity*, 18, 633-659.

Yoshida, F., Urabe, M., Hino, R., and Toropov, V. V. (2003). "Inverse approach to identification of material parameters of cyclic elasto-plasticity for component layers of bimetallic sheet." *International Journal of Plasticity*, 19, 2149-2170.

Yoshida, F., Urabe, M., and Toropov, V. V. (1998). "Identification of material parameters in constitutive model for sheet metals from cyclic bending tests." *International Journal of Mechanical Sciences*, 40(Nos. 2-3), 237-249.

Yu, H.-S. (2006). "Foundation of the theory of plasticity." *Plasticity and Geotechnics*, Springer, 22-39.

Zhang, H., Lin, X., Wang, Y., Zhang, Q., and Kang, Y. (2010). "Identification of elastic-plastic mechanical properties for bimetallic sheets by hybrid-inverse approach." *Acta Mechanica Solids Sinica*, 23(1), 30-35.

Zhang, L. C., and Lin, Z. (1997). "An analytical solution to springback of sheet metals stamped by a rigid punch and an elastic die." *Journal of Materials Processing Technology*, 63, 49-54.

Zhang, L. C., Lu, G., and Leong, S. C. (1997). " V-shaped sheet forming by deformable punches." *Journal of Materials Processing Technology*, 63, 134-139.

Zhao, K. M., and Lee, J. K. (2002). "Finite element analysis of the three-point bending of sheet metal." *Journal of Applied Materials Processing Technology*, 122, 6-11.

Ziegler, H. (1959). "A modification of Prager's hardening rule." *Quarterly of Applied Mechanics*, 17, 55-65.

APPENDICES

A CYCLIC LOADING RESULTS

A1: Low Carbon Steel

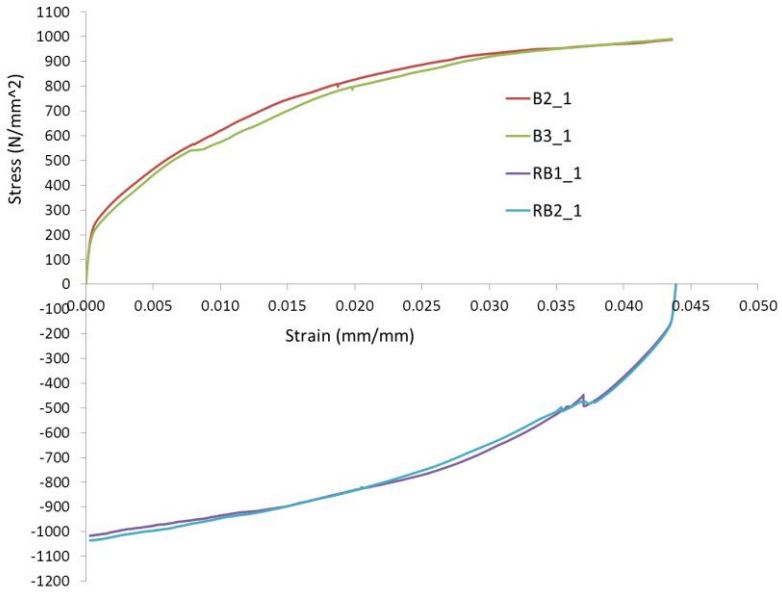

(a)

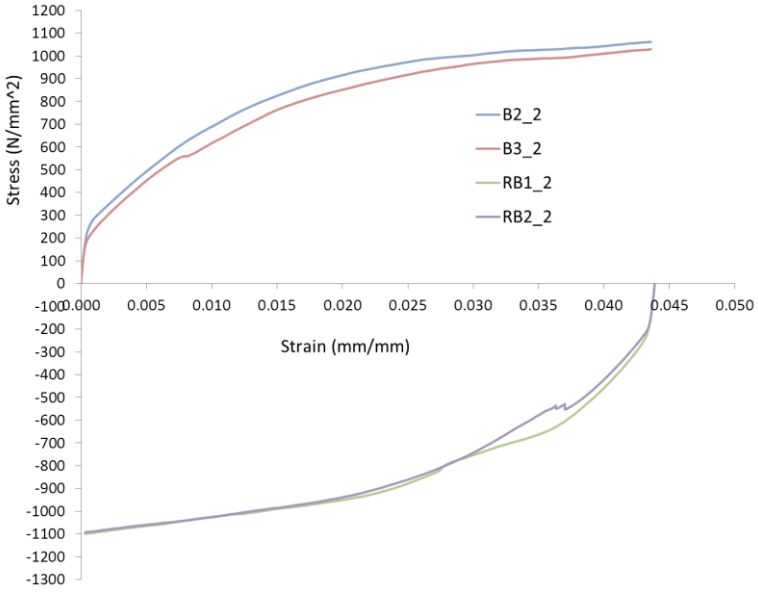

(b)

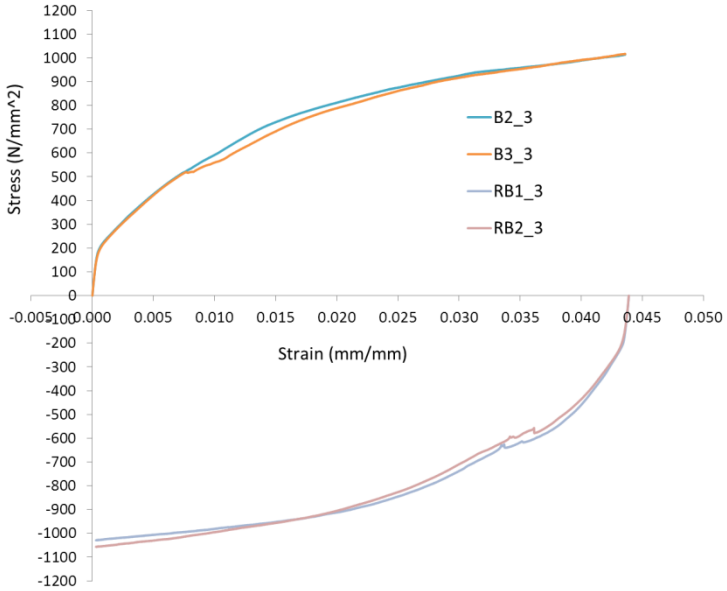

(c)

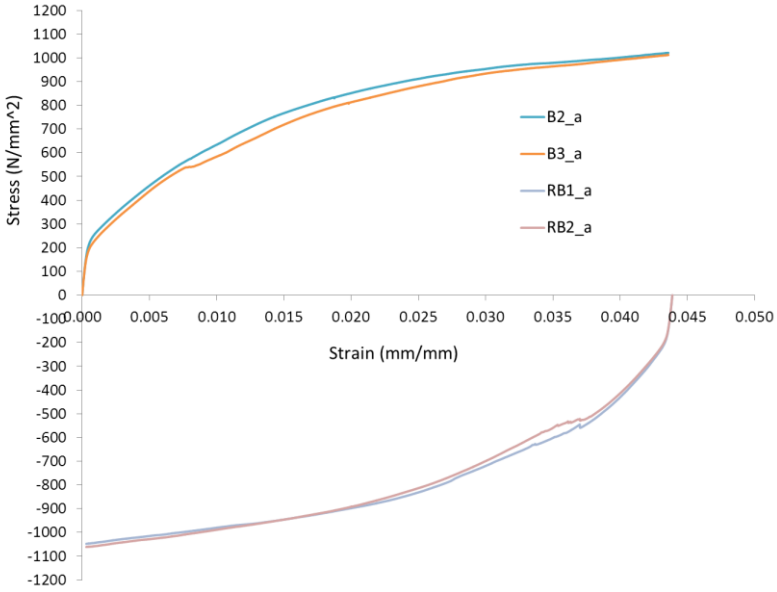

(d)

Figure 4.14 Cyclic stress-strain graphs for low carbon steel 2 mm thick (a) specimen no.1, (b) specimen no. 2, (c) specimen no. 3 and (d) average (stress)

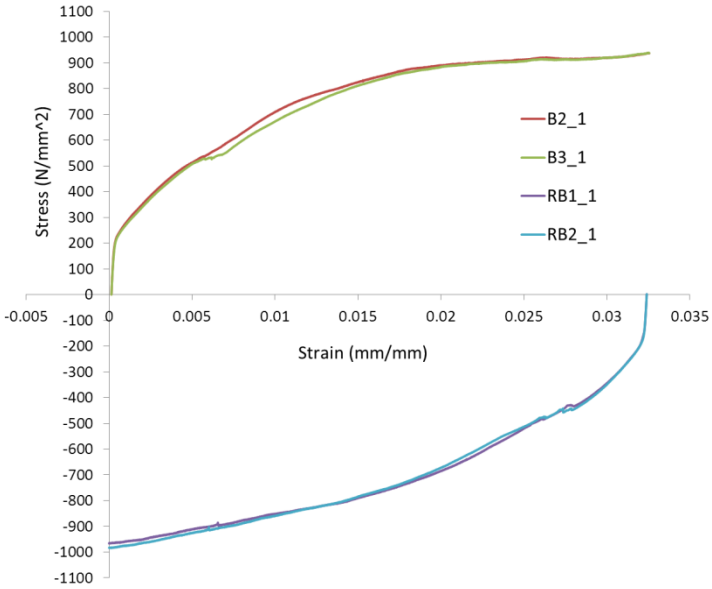
Stress (N/mm^2)
Strain (mm/mm)
B2_1
B3_1
RB1_1
RB2_1

(a)

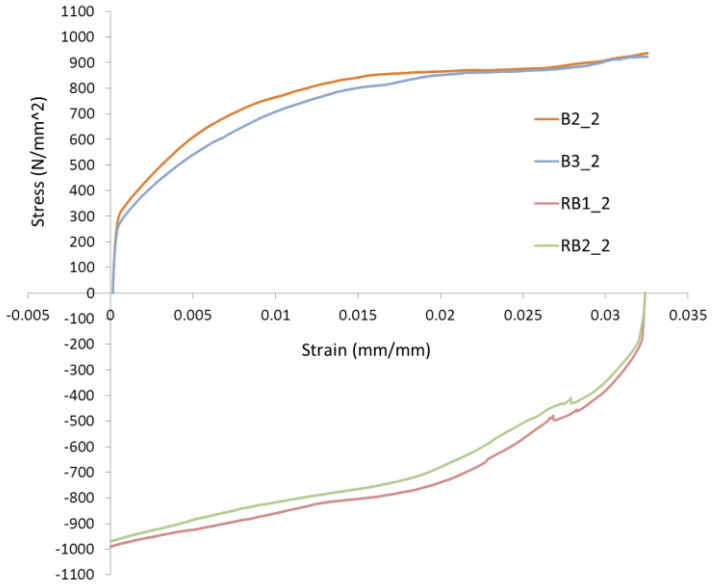
Stress (N/mm^2)
Strain (mm/mm)
B2_2
B3_2
RB1_2
RB2_2

(b)

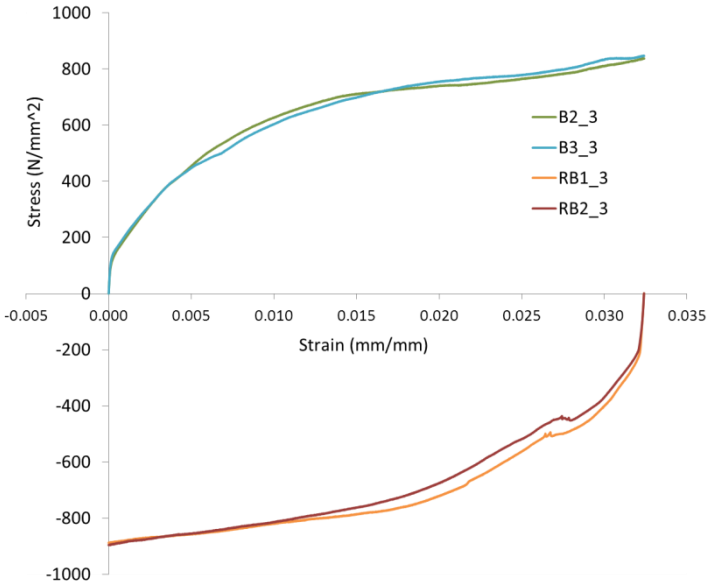

(c)

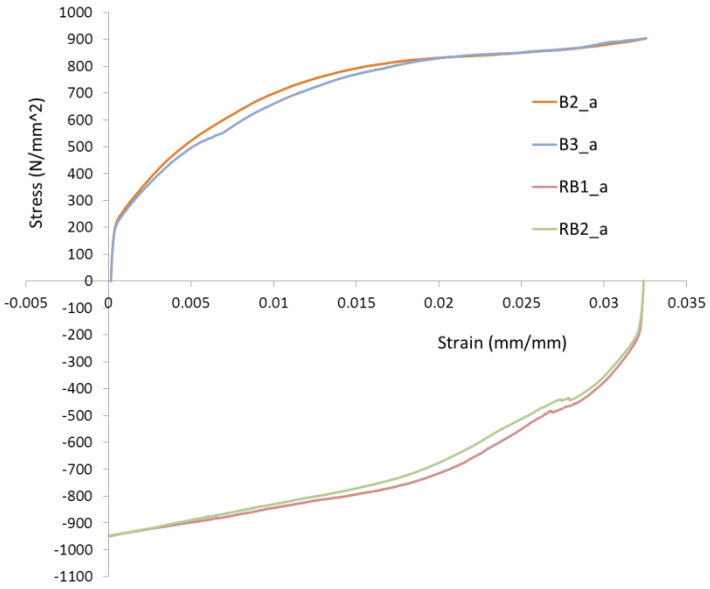

(d)

Figure 4.15 Cyclic stress-strain graphs for low carbon steel 1.5 mm thick (a) specimen no.1, (b) specimen no. 2, (c) specimen no. 3 and (d) average (stress)

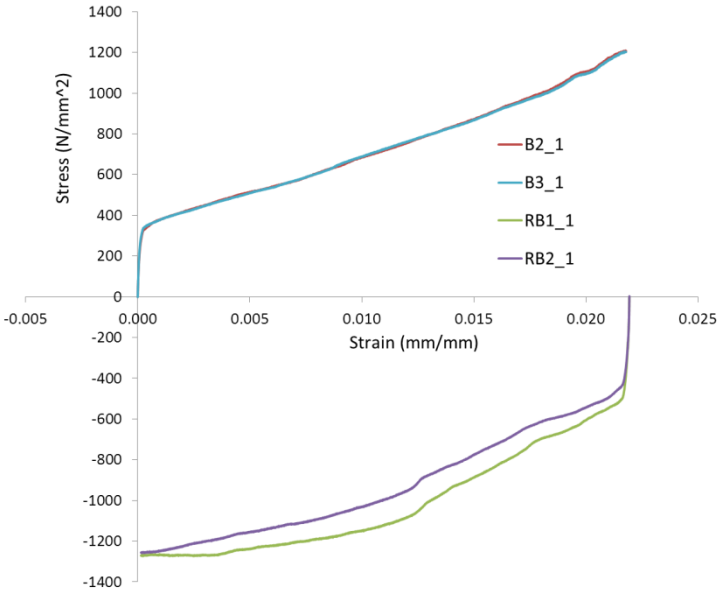
Stress (N/mm^2)
Strain (mm/mm)
B2_1
B3_1
RB1_1
RB2_1

(a)

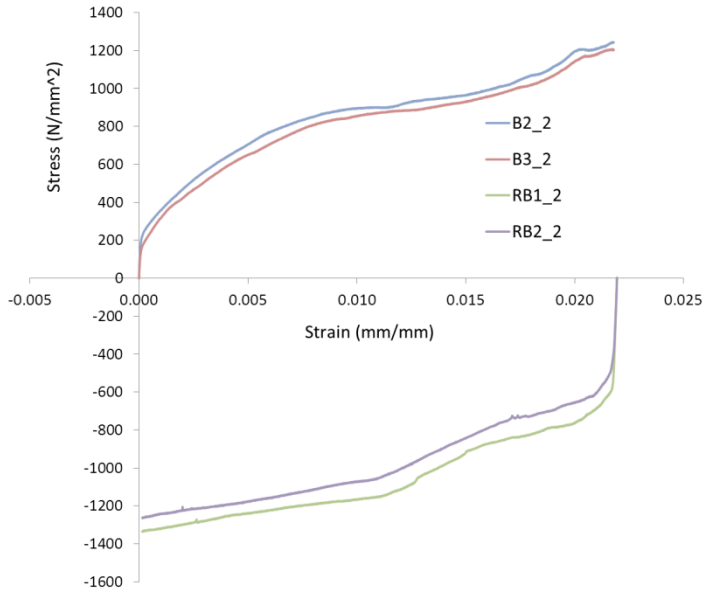
Stress (N/mm^2)
Strain (mm/mm)
B2_2
B3_2
RB1_2
RB2_2

(b)

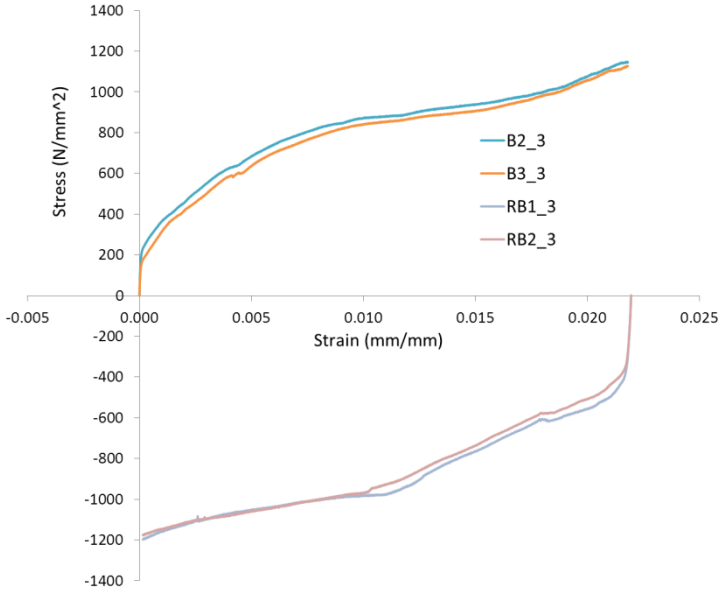

(c)

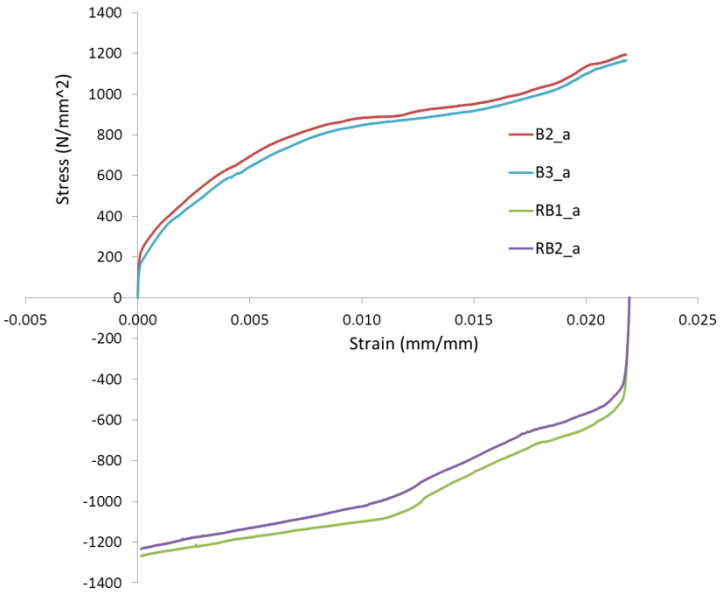

(d)

Figure 4.16 Cyclic stress-strain graphs for low carbon steel 1 mm thick (a) specimen no.1, (b) specimen no. 2, (c) specimen no. 3 and (d) average (stress)

A2: Stainless Steel

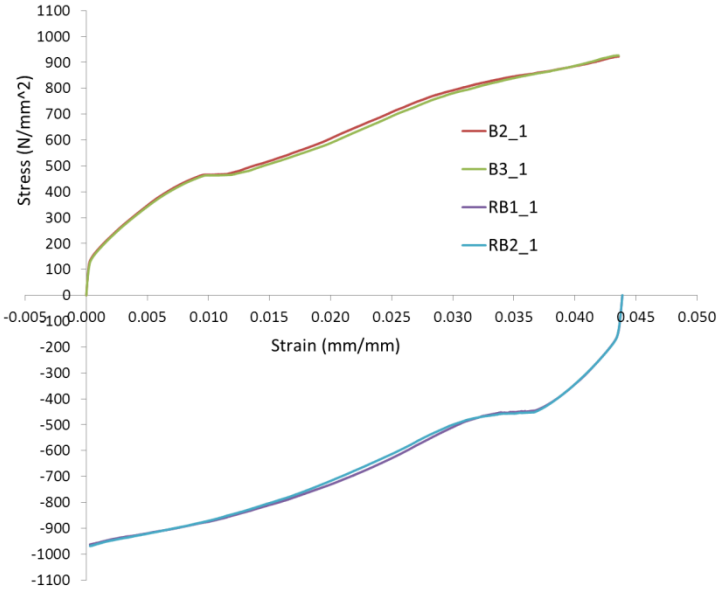

(a)

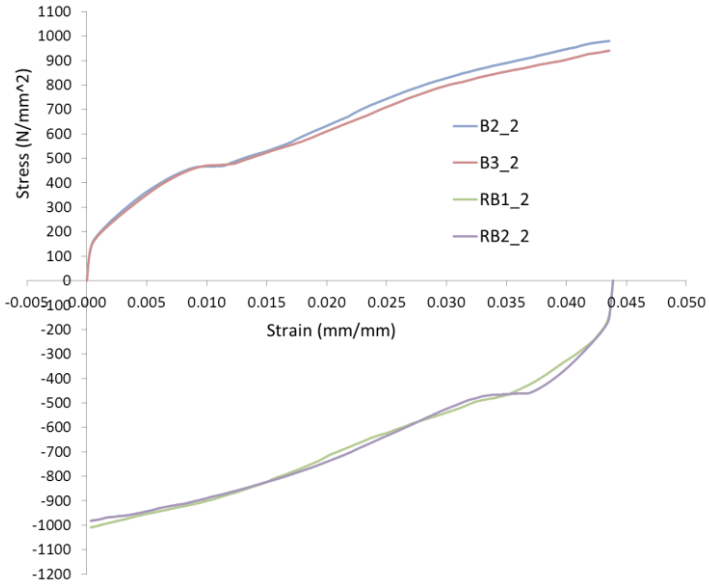

(b)

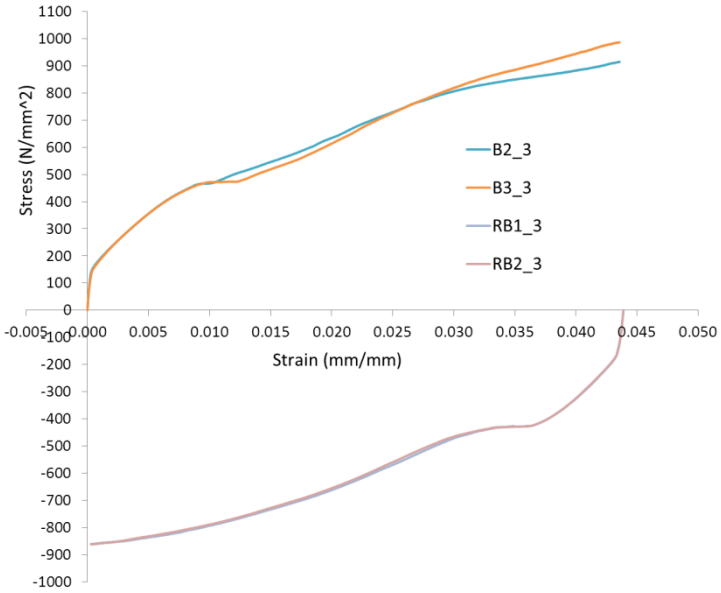

(c)

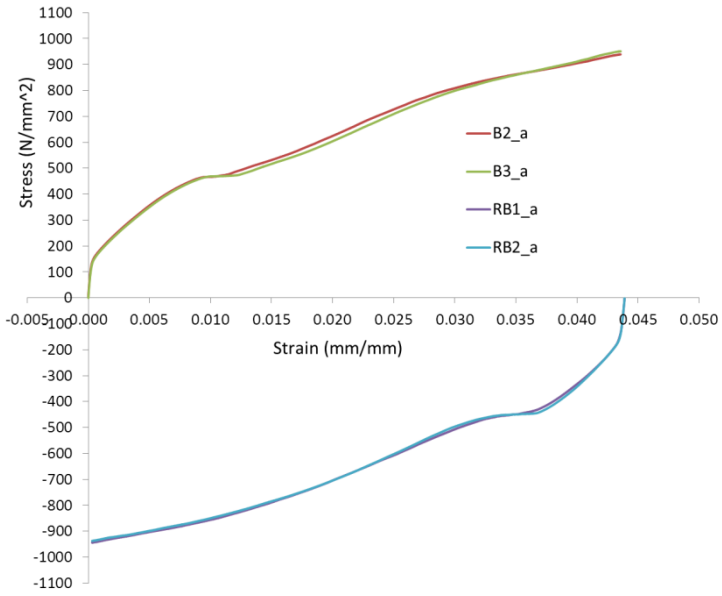

(d)

Figure 4.17 Cyclic stress-strain graphs for stainless steel 2 mm thick (a) specimen no.1, (b) specimen no. 2, (c) specimen no. 3 and (d) average (stress)

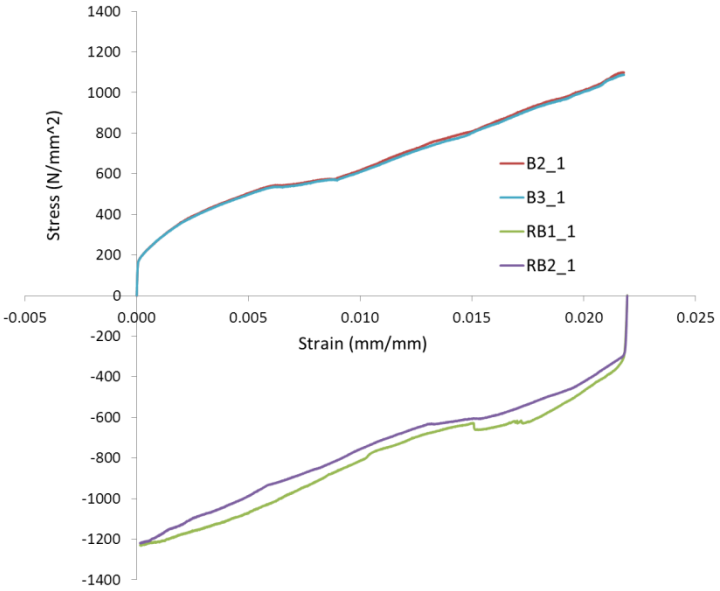
Stress (N/mm^2)
Strain (mm/mm)
B2_1
B3_1
RB1_1
RB2_1

(a)

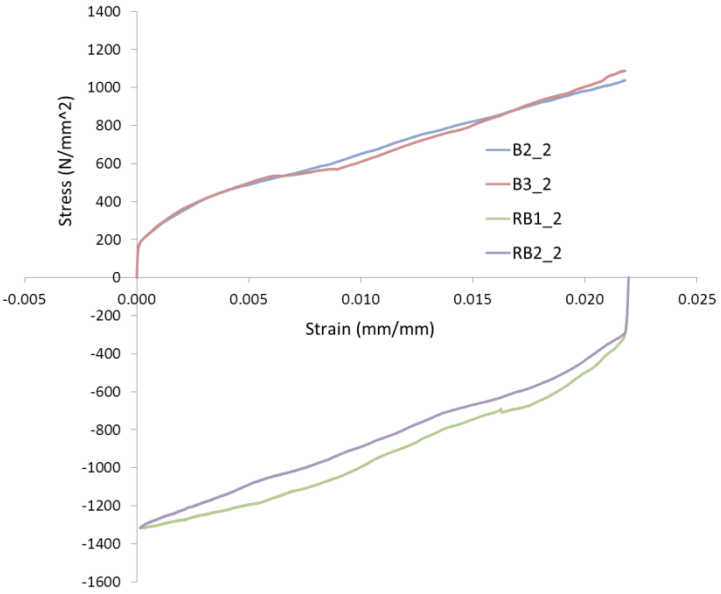
Stress (N/mm^2)
Strain (mm/mm)
B2_2
B3_2
RB1_2
RB2_2

(b)

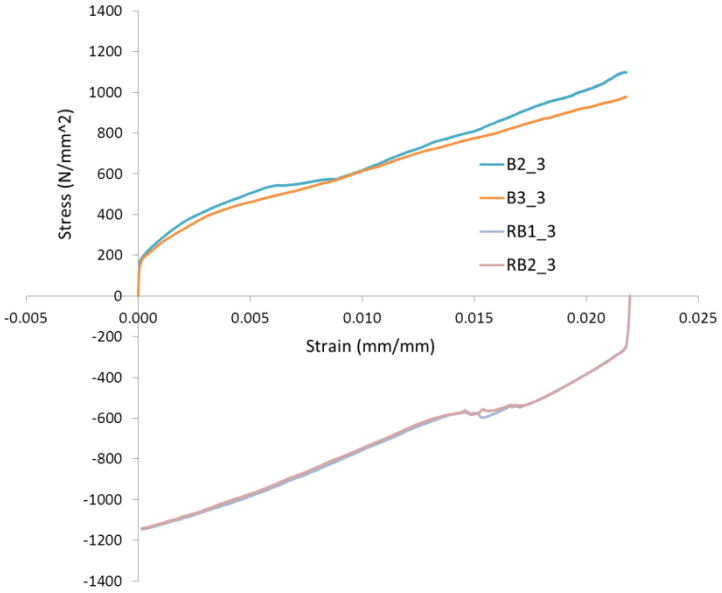

(c)

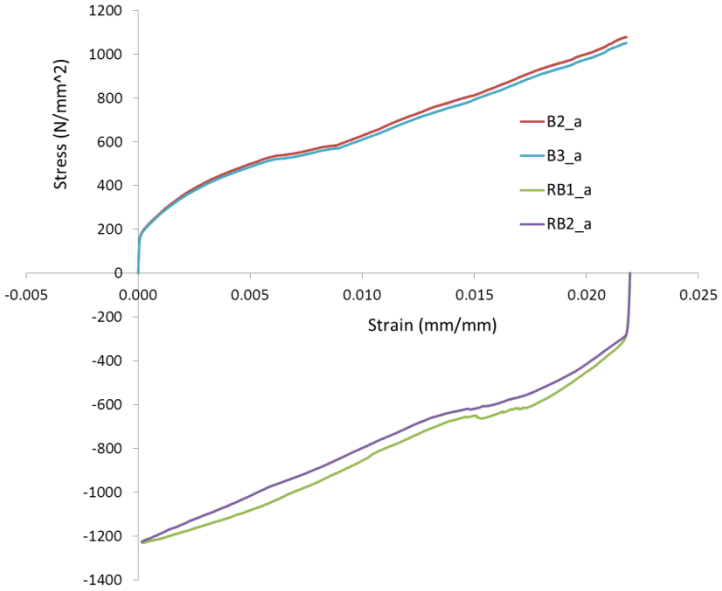

(d)

Figure 4.18 Cyclic stress-strain graphs for stainless steel 1 mm thick (a) specimen no.1 (b) specimen no. 2, (c) specimen no. 3 and (d) average (stress)

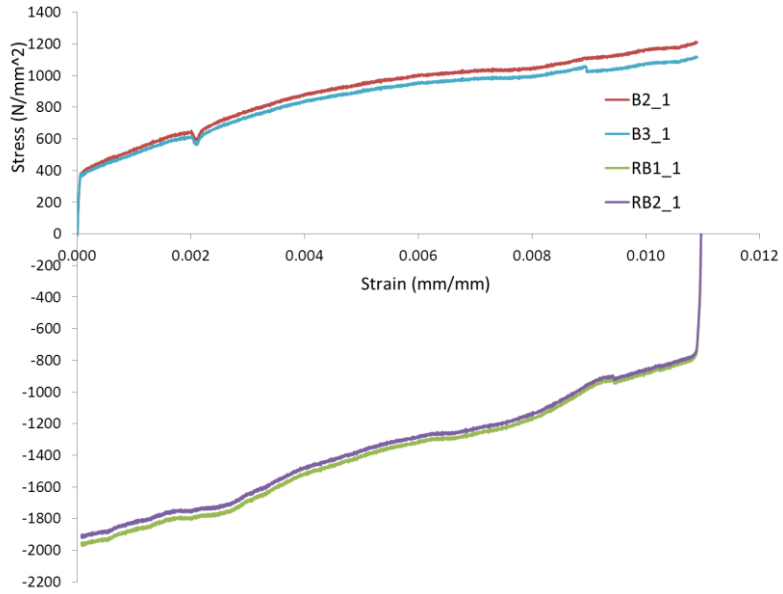
Stress (N/mm^2)
Strain (mm/mm)
B2_1
B3_1
RB1_1
RB2_1

(a)

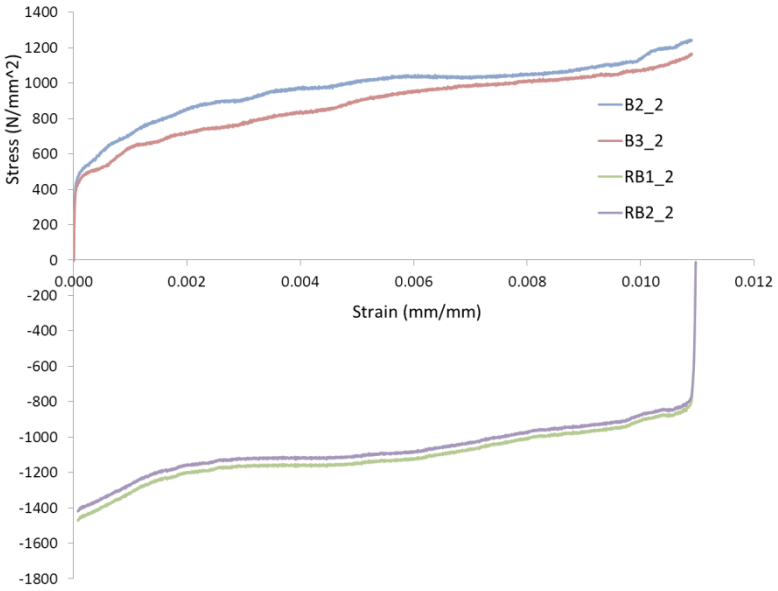
Stress (N/mm^2)
Strain (mm/mm)
B2_2
B3_2
RB1_2
RB2_2

(b)

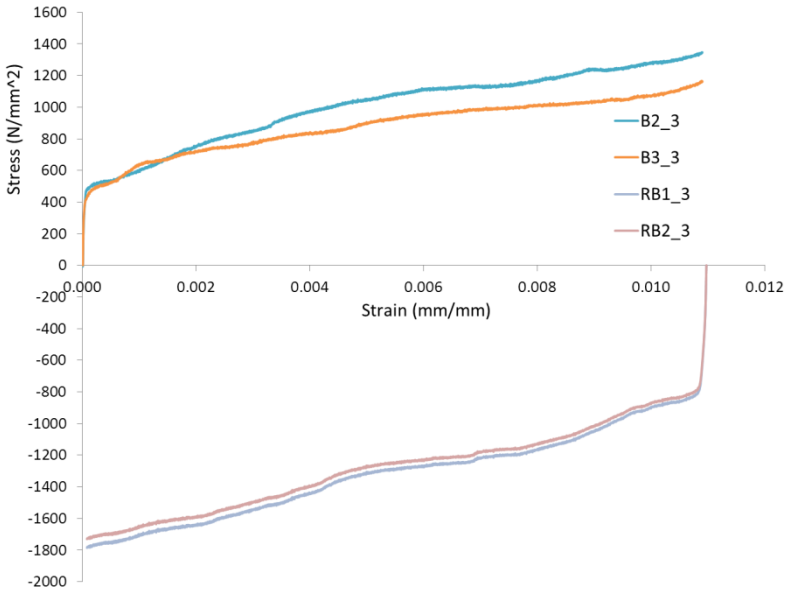

(c)

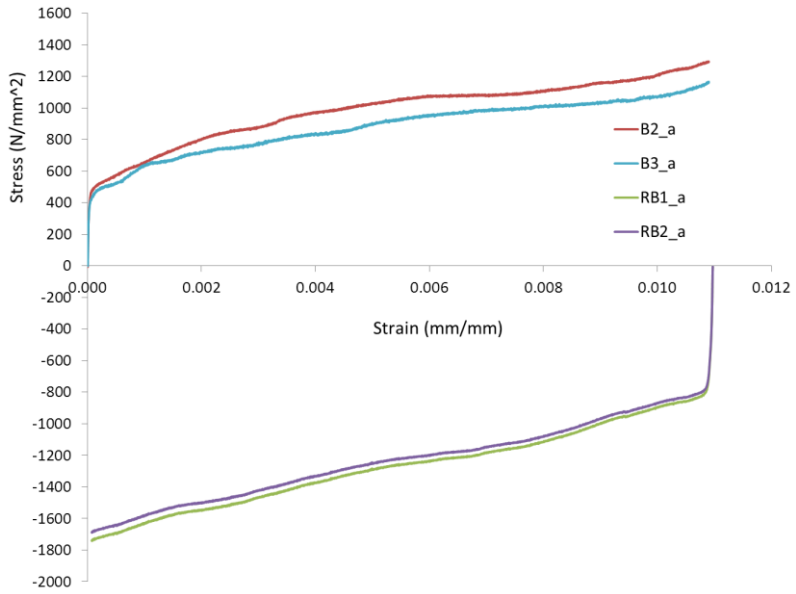

(d)

Figure 4.19 Cyclic stress-strain graphs for stainless steel 0.5 mm thick (a) specimen no.1, (b) specimen no. 2, (c) specimen no. 3 and (d) average (stress)

B OPTIMISATION

Coding for Nonlinear Kinematic Hardening

```
clc;clear all;
global nxdata nydata
% Identification of kinematic hardening material parameters for
%  Low carbon steel(2 mm, 1.5 mm and 1 mm) and stainless steel
%  (2mm, 1 mm and 0.5 mm).
%  Average Data taken from cyclic loading experiment.
% To run the optimization for the particular data, delete the %
symbol in front
% of the data line AND delete symbol in front of the Reverse
bending rb1 data line.
%_____________________________________________________________
%                          Low Carbon Steel

%                             2MM // to use Formula 1 in subroutine
K2
%     Bending B2
%            nydata=xlsread('MS2mm.xls','b2_a','v17:v3000');
%            nxdata=xlsread('MS2mm.xls','b2_a','u17:u3000');
%     Bending B3
%            nydata=xlsread('MS2mm.xls','b3_a','v17:v3000');
%            nxdata=xlsread('MS2mm.xls','b3_a','u17:u3000');
%     Reverse bending rb1
%              y=xlsread('MS2mm.xls','rb1_a','w5:w3000');
%              x=xlsread('MS2mm.xls','rb1_a','v5:v3000');

%                            1.5 mm// to use Formula 1 in subroutine
K2
%    Bending B2
%            nydata=xlsread('MS15mm.xls','b2_a','v17:v3000');
%            nxdata=xlsread('MS15mm.xls','b2_a','u17:u3000');
%    Bending B3
%            nydata=xlsread('MS15mm.xls','b3_a','v17:v3000');
%            nxdata=xlsread('MS15mm.xls','b3_a','u17:u3000');
%    Reverse bending rb1
%              y=xlsread('MS15mm.xls','rb1_a','w5:w3000');
%              x=xlsread('MS15mm.xls','rb1_a','v5:v3000');

%                             1 MM // to use Formula 2 in subroutine
K2
%    Bending B2
          nydata=xlsread('MS1mm.xls','b2_a','v17:v3000');
          nxdata=xlsread('MS1mm.xls','b2_a','u17:u3000');
%    Bending B3
%         nydata=xlsread('MS1mm.xls','b3_a','v17:v3000');
%         nxdata=xlsread('MS1mm.xls','b3_a','u17:u3000');
% %     % Reverse bending rb1
        y=xlsread('MS1mm.xls','rb1_a','w5:w3000');
        x=xlsread('MS1mm.xls','rb1_a','v5:v3000');

%_____________________________________________________________
___
```

```
%                           Stainless Steel

%                             2MM // to use Formula 3 in subroutine
K2
%    Bending B2
%            nydata=xlsread('SS2mm.xls','b2_a','v17:v3000');
%            nxdata=xlsread('SS2mm.xls','b2_a','u17:u3000');
%    Bending B3
%            nydata=xlsread('SS2mm.xls','b3_a','v17:v3000');
%            nxdata=xlsread('SS2mm.xls','b3_a','u17:u3000');
%    Reverse bending rb1
%              y=xlsread('SS2mm.xls','rb1_a','w5:w3000');
%              x=xlsread('SS2mm.xls','rb1_a','v5:v3000');

 %                           1 MM // to use Formula 3 in subroutine
K2
%    Bending B2
%            nydata=xlsread('SS1mm.xls','b2_a','v17:v3000');
%            nxdata=xlsread('SS1mm.xls','b2_a','u17:u3000');
%    Bending B3
%         nydata=xlsread('SS1mm.xls','b3_a','v17:v3000');
%         nxdata=xlsread('SS1mm.xls','b3_a','u17:u3000');
%   Reverse bending rb1
%         y=xlsread('SS1mm.xls','rb1_a','w5:w3000');
%         x=xlsread('SS1mm.xls','rb1_a','v5:v3000');

%                           0.5 MM // to use Formula 4 in
subroutine K2
%   Bending B2
%            nydata=xlsread('SS05mm.xls','b2_a','v17:v3000');
%            nxdata=xlsread('SS05mm.xls','b2_a','u17:u3000');
%   Bending B3
%            nydata=xlsread('SS05mm.xls','b3_a','v17:v3000');
%            nxdata=xlsread('SS05mm.xls','b3_a','u17:u3000');
%   Reverse bending rb1
%              y=xlsread('SS05mm.xls','rb1_a','w5:w3000');
%              x=xlsread('SS05mm.xls','rb1_a','v5:v3000');

%_____________________________________________________________________
   thedata=[nxdata nydata];
    nxdata=thedata(:,1);
    nydata=thedata(:,2);

    [estimates, model,C,gamma,ErrorVector]=K2(nxdata,nydata);
    [sse,FittedCurve] = model(estimates);
    %MSE=SSE/v, v=n-m, n=#of data, m=# of parameters
    n=3000-17;
    m=2;
    v=n-m;
    MSE=sse/(v-3)% MSE: the mean square error or the residual mean
square.m is number parameter
    RMSE=sqrt(MSE)% STANDARD DEVIATION
    nyA=(sum(nydata))/(n); %denumerator depends on initial and
final data
    Residual=ErrorVector
    G=(nydata-nyA);
    SSE=sse
```

```
    SST=sum((G.^2))
    Rq=1-(sse/SST)
    Adj_Rq=1-(SSE*(n-1))/(SST*(v))

    plot(x, y, 'c')
    hold on
    plot(nxdata, nydata, 'b')
    hold on
    plot(nxdata, FittedCurve, '--r');

    xlabel('nxdata')
    ylabel('f(estimates,nydata)')
    title(sprintf('C=%1.3f,gamma=%1.3f, Adj_R=%1.4f,',...
      C,gamma,Adj_Rq));
    legend('data','data','fit using N-Kinematic Equation ')
    hold off
```

K2 Objective Function

```
function [estimates,model,C,gamma,ErrorVector] = K2(nxdata,nydata)
   start_point =[1000 1];
model = @expfun;
options=optimset('MaxFunEvals',10e9,'MaxIter',10e9)
estimates = fminsearch(model, start_point,options);

    function [sse,FittedCurve] = expfun(params)

   C = params(1);
   gamma = params(2);

% Choose the equation from the lists. To use the formula, delete
the %
% symbol from the formula line AND place % on the other formula
line.

%   1. Formula for MS 2 mm and 1.5 mm
%       FittedCurve =200+(C/gamma)*(1-exp(-gamma*nxdata));
%   2. Formula for MS 1 mm MS
        FittedCurve =250+(C/gamma)*(1-exp(-gamma*nxdata));

%   3. Formula for SS 2 mm and 1 mm
%       FittedCurve =150+(C/gamma)*(1-exp(-gamma*nxdata));

%   4. Formula for SS 0.5 mm
%       FittedCurve =435+(C/gamma)*(1-exp(-gamma*nxdata));

 ErrorVector= (FittedCurve-nydata);
 sse =sum((ErrorVector .^ 2));

 end
end
```

Coding for Mixed Hardening

```
clc;clear all;
global nxdata nydata
% Identification of MIXED hardening material parameters for
%  Low carbon steel(2 mm, 1.5 mm and 1 mm) and stainless steel
%  2mm, 1 mm and 0.5 mm). Average Data taken from cyclic
%  loading experiment.
% To run the optimization for the particular data, delete the %
symbol in front
% of the data line AND delete symbol in front of the Reverse
bending rb1 data line.
%_____________________________________________________________
_________
%                       Low Carbon Steel

%                           2MM / to use Formula 1 in subroutine
MIXED
    % Bending B2
%            nydata=xlsread('MS2mm.xls','b2_a','v17:v3000');
%            nxdata=xlsread('MS2mm.xls','b2_a','u17:u3000');
    % Bending B3
%            nydata=xlsread('MS2mm.xls','b3_a','v17:v3000');
%            nxdata=xlsread('MS2mm.xls','b3_a','u17:u3000');
%   % Reverse bending rb1
%              y=xlsread('MS2mm.xls','rb1_a','w5:w3000');
%              x=xlsread('MS2mm.xls','rb1_a','v5:v3000');
%
%                           1.5 mm/ to use Formula 1 in subroutine
MIXED
    % Bending B2
%            nydata=xlsread('MS15mm.xls','b2_a','v17:v3000');
%            nxdata=xlsread('MS15mm.xls','b2_a','u17:u3000');
%   % Bending B3
%            nydata=xlsread('MS15mm.xls','b3_a','v17:v3000');
%            nxdata=xlsread('MS15mm.xls','b3_a','u17:u3000');
%   % Reverse bending rb1
%              y=xlsread('MS15mm.xls','rb1_a','w5:w3000');
%              x=xlsread('MS15mm.xls','rb1_a','v5:v3000');

%                           1 MM / to use Formula 2 in subroutine
MIXED
    % Bending B2
%            nydata=xlsread('MS1mm.xls','b2_a','v17:v3000');
%            nxdata=xlsread('MS1mm.xls','b2_a','u17:u3000');
    % Bending B3
        nydata=xlsread('MS1mm.xls','b3_a','v17:v3000');
        nxdata=xlsread('MS1mm.xls','b3_a','u17:u3000');
%   % Reverse bending rb1
        y=xlsread('MS1mm.xls','rb1_a','w5:w3000');
        x=xlsread('MS1mm.xls','rb1_a','v5:v3000');
```

```
%_____________________________________________________________________
%                           Stainless Steel

%                            2MM / to use Formula 3 in subroutine
MIXED
    % Bending B2
%              nydata=xlsread('SS2mm.xls','b2_a','v17:v3000');
%              nxdata=xlsread('SS2mm.xls','b2_a','u17:u3000');
    % Bending B3
%              nydata=xlsread('SS2mm.xls','b3_a','v17:v3000');
%              nxdata=xlsread('SS2mm.xls','b3_a','u17:u3000');
    % Reverse bending rb1
%              y=xlsread('SS2mm.xls','rb1_a','w5:w3000');
%              x=xlsread('SS2mm.xls','rb1_a','v5:v3000');

%                            1 MM / to use Formula 3 in subroutine
MIXED
    % Bending B2
%                nydata=xlsread('SS1mm.xls','b2_a','v17:v3000');
%                nxdata=xlsread('SS1mm.xls','b2_a','u17:u3000');
%    % Bending B3
%              nydata=xlsread('SS1mm.xls','b3_a','v17:v3000');
%              nxdata=xlsread('SS1mm.xls','b3_a','u17:u3000');
%    % Reverse bending rb1
%                y=xlsread('SS1mm.xls','rb1_a','w5:w3000');
%                x=xlsread('SS1mm.xls','rb1_a','v5:v3000');

%                           0.5 MM / to use Formula 4 in subroutine
MIXED
    % Bending B2
%             nydata=xlsread('SS05mm.xls','b2_a','v17:v3000');
%             nxdata=xlsread('SS05mm.xls','b2_a','u17:u3000');
%    % Bending B3
%             nydata=xlsread('SS05mm.xls','b3_a','v17:v3000');
%             nxdata=xlsread('SS05mm.xls','b3_a','u17:u3000');
%    % Reverse bending rb1
%              y=xlsread('SS05mm.xls','rb1_a','w5:w3000');
%              x=xlsread('SS05mm.xls','rb1_a','v5:v3000');

%*********************************************************************
*******
    thedata=[nxdata nydata];
    nxdata=thedata(:,1);
    nydata=thedata(:,2);

    [estimates,
model,Q,b,C,gamma,ErrorVector]=MIXED(nxdata,nydata);
    [sse, FittedCurve] = model(estimates);
%MSE=SSE/v, v=n-m, n=#of data, m=# of parameters
    n=3000-17;
    m=4;
       v=n-m;
% MSE: the mean square error or the residual mean square.m is
number parameter
    MSE=sse/(v-3);
% STANDARD DEVIATION
    RMSE=sqrt(MSE);
```

```
%Denumerator depends on initial and final data
    nyA=(sum(nydata))/(n);
    Residual=ErrorVector;
    G=(nydata-nyA);
    SSE=sse;
    SST=sum((G.^2));
    Rq=1-(sse/SST);
    Adj_Rq=1-(SSE*(n-1))/(SST*(v));

    plot(x, y, 'c')
    hold on
    plot(nxdata, nydata, 'b')
    hold on
    plot(nxdata, FittedCurve, '--r');

    xlabel('nxdata')
    ylabel('f(estimates,nydata)')

    title(sprintf('Q=%1.4f, b=%1.3f, C=%1.3f, gamma=%1.3f,
Adj_R=%1.4f,',...
         Q,b,C,gamma,Adj_Rq))
        legend('data','data','fit using Mixed Equation')%,
func2str(model)])
    hold off
```

MIXED Objective Function

```
function [estimates, model,Q,b,C,gamma,ErrorVector] =
MIXED(nxdata,nydata)

        start_point =[400 20 1000 1];
        model = @expfun;
        options=optimset('MaxFunEvals',10e9,'MaxIter',10e9)
        estimates = fminsearch(model, start_point,options);

    function [sse, FittedCurve] = expfun(params)
        Q = params(1)
        b = params(2);
        C= params(3);
        gamma= params(4);

% Choose the equation from the lists. To use the formula, delete
the %
% symbol from the formula line AND place % on the other formula
line.

 % formula uses mixed of isotropic and kinematic.

%       1. Formula for MS 2 mm and 1.5 mm
%               FittedCurve =(200+Q .*(1-exp(-
b*nxdata))+(C/gamma)*(1-exp(-gamma*nxdata)));
%       2. Formula for MS 1 mm
```

```
                FittedCurve =(250+Q .*(1-exp(-
b*nxdata))+(C/gamma)*(1-exp(-gamma*nxdata)));
%       3. Formula for SS 2 mm and 1 mm
%               FittedCurve =(150+Q .*(1-exp(-
b*nxdata))+(C/gamma)*(1-exp(-gamma*nxdata)));
%       4. Formula for SS 0.5 mm
%                FittedCurve =(435+Q .*(1-exp(-
b*nxdata))+(C/gamma)*(1-exp(-gamma*nxdata)));
     ErrorVector = FittedCurve - nydata;
     sse = sum(ErrorVector .^ 2)

    end
end
```

C CYCLIC BENDING TOOL DRAWINGS

RevNo	Revision note	Date	Signature	Checked

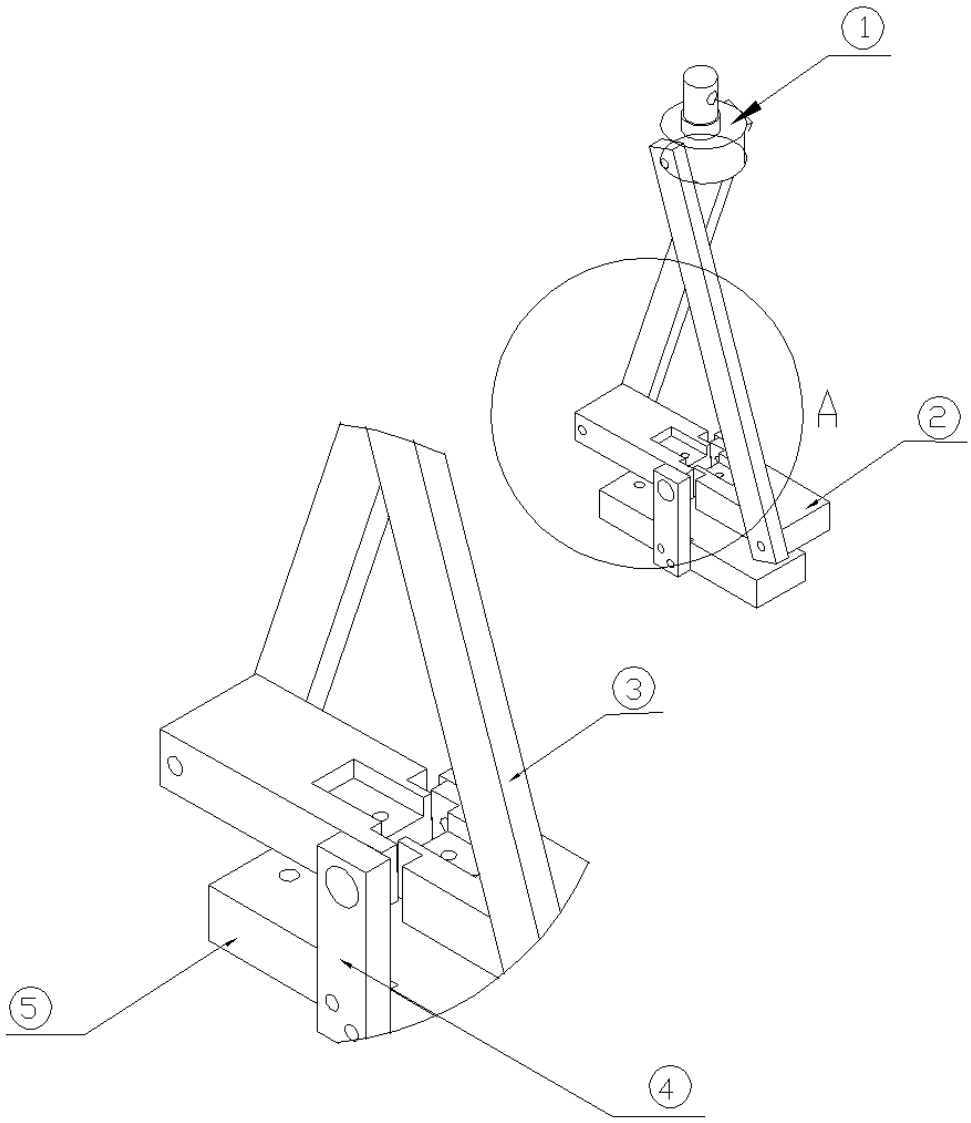

Part No.	Name	Drawing no.	Quantity	Material	Notes
5	Base	cbt_5	1	steel	
4	Column	cbt_4	2	steel	
3	Connecting rod	cbt_3	2	steel	
2	Crank	cbt_2	2	steel	
1	Slider	cbt_1	1	steel	

Drawn by	Designed by	Approved by – date	File name	Date	Scale
	J.Mohamad	J.Mohamad–00/08/12		00/08/2012	No

Cyclic bending tool

Drawing no.:	Edition	Sheet
cbt_0	0	1/6

RevNo	Revision note	Date	Signature	Checked

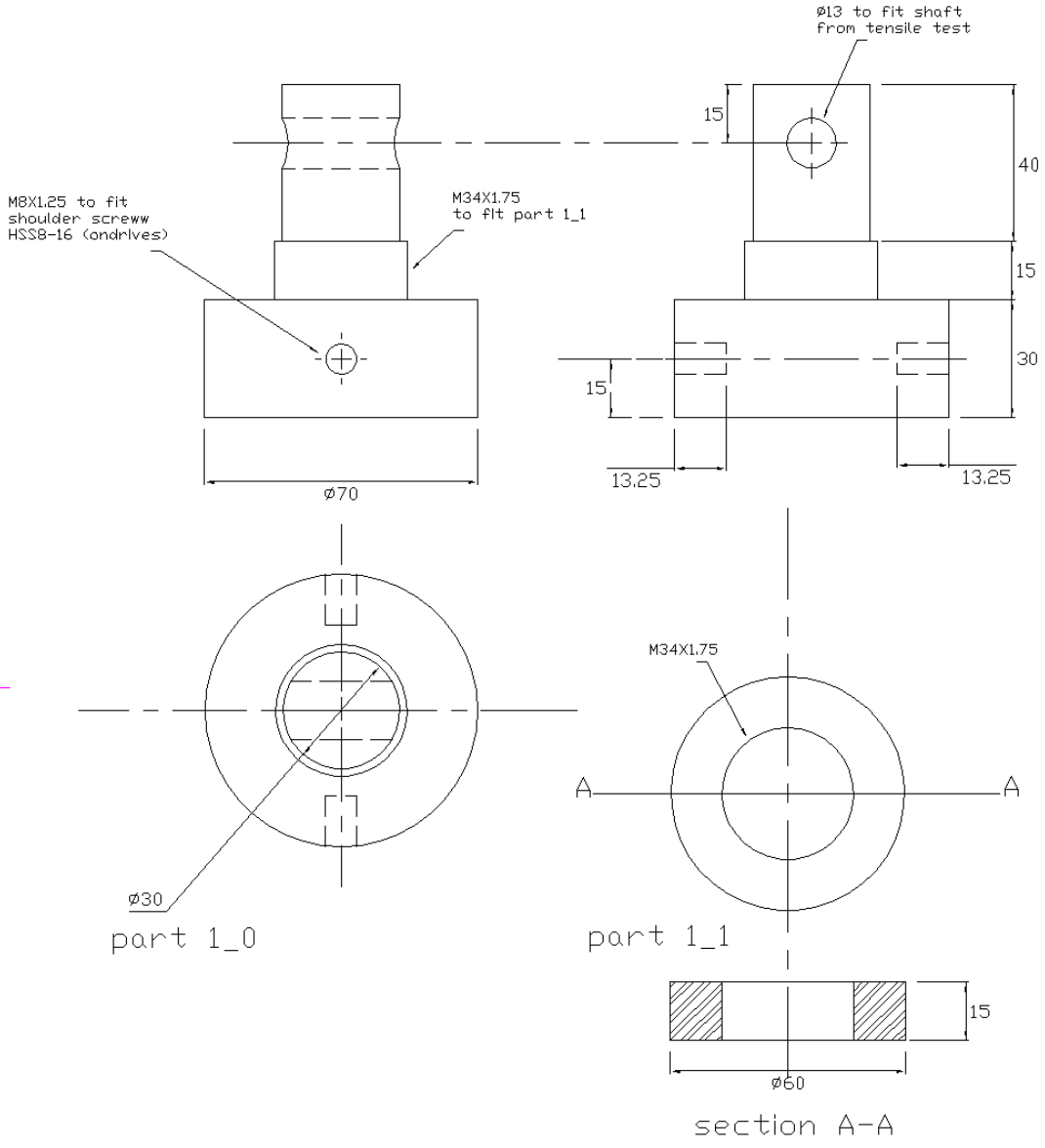

All dimensions in millimeters

1_1	Tighten	cbt_1	1	Steel	
1_0	Main slider	cbt_1	1	Steel	
Part No.	Name	Drawing no.	Quantity	Material	Notes

Drawn by	Designed by J.Mohamad	Approved by - date J.Mohamad-00/08/12	File name	Date 00/08/2012	Scale No
		Slider			
		Drawing no.: cbt_1		Edition 0	Sheet 2/6

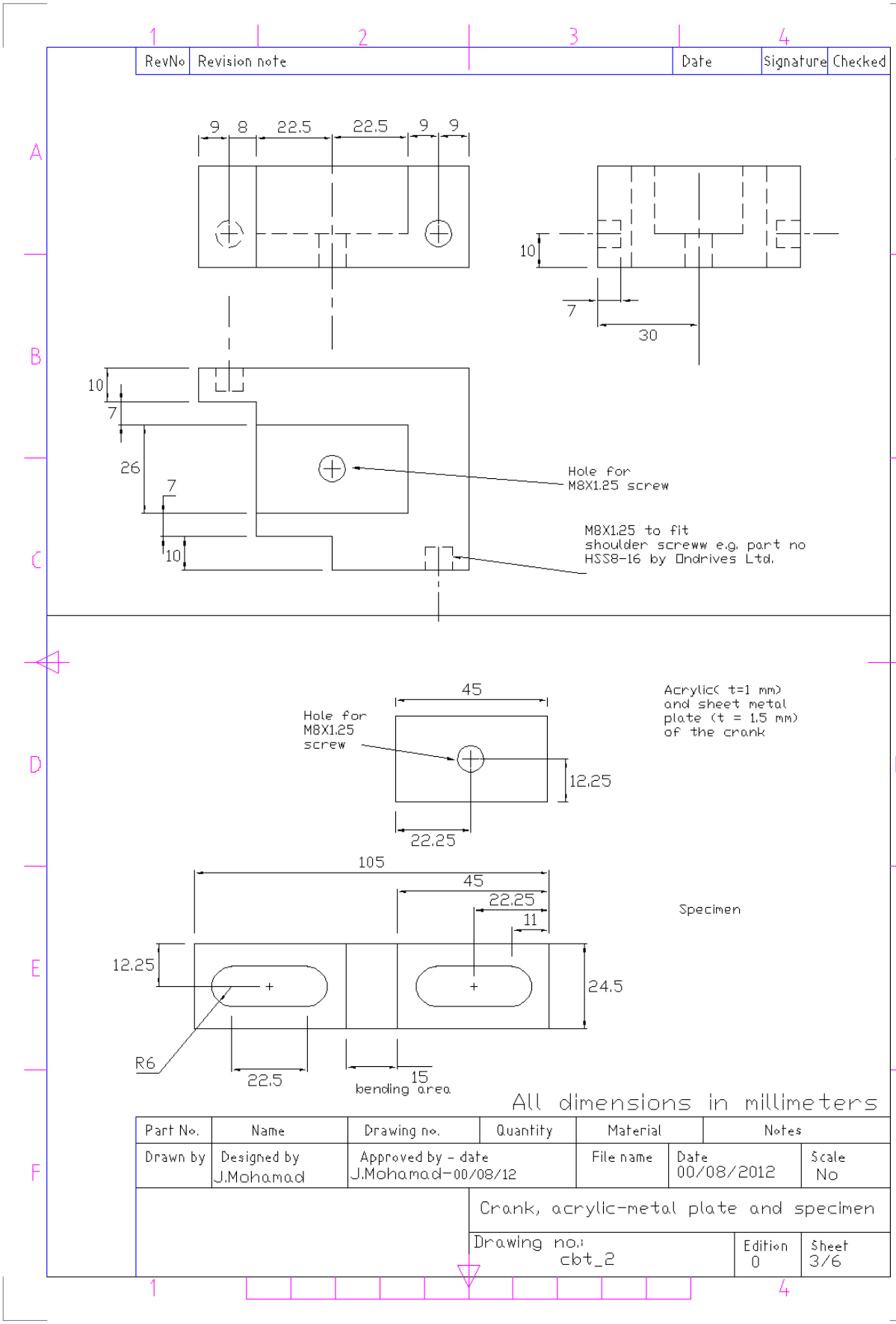
RevNo
Revision note
Date
Signature
Checked
9 8 22.5 22.5 9 9
10
7
30
10
7
26
7
10
Hole for
M8X1.25 screw
M8X1.25 to fit
shoulder screww e.g. part no
HSS8-16 by Ondrives Ltd.
45
Hole for
M8X1.25
screw
12.25
22.25
Acrylic(t=1 mm)
and sheet metal
plate (t = 1.5 mm)
of the crank
105
45
22.25
11
12.25
24.5
R6
22.5
15
bending area
Specimen
All dimensions in millimeters
Part No.
Name
Drawing no.
Quantity
Material
Notes
Drawn by
Designed by
J.Mohamad
Approved by - date
J.Mohamad-00/08/12
File name
Date
00/08/2012
Scale
No
Crank, acrylic-metal plate and specimen
Drawing no.:
cbt_2
Edition
0
Sheet
3/6

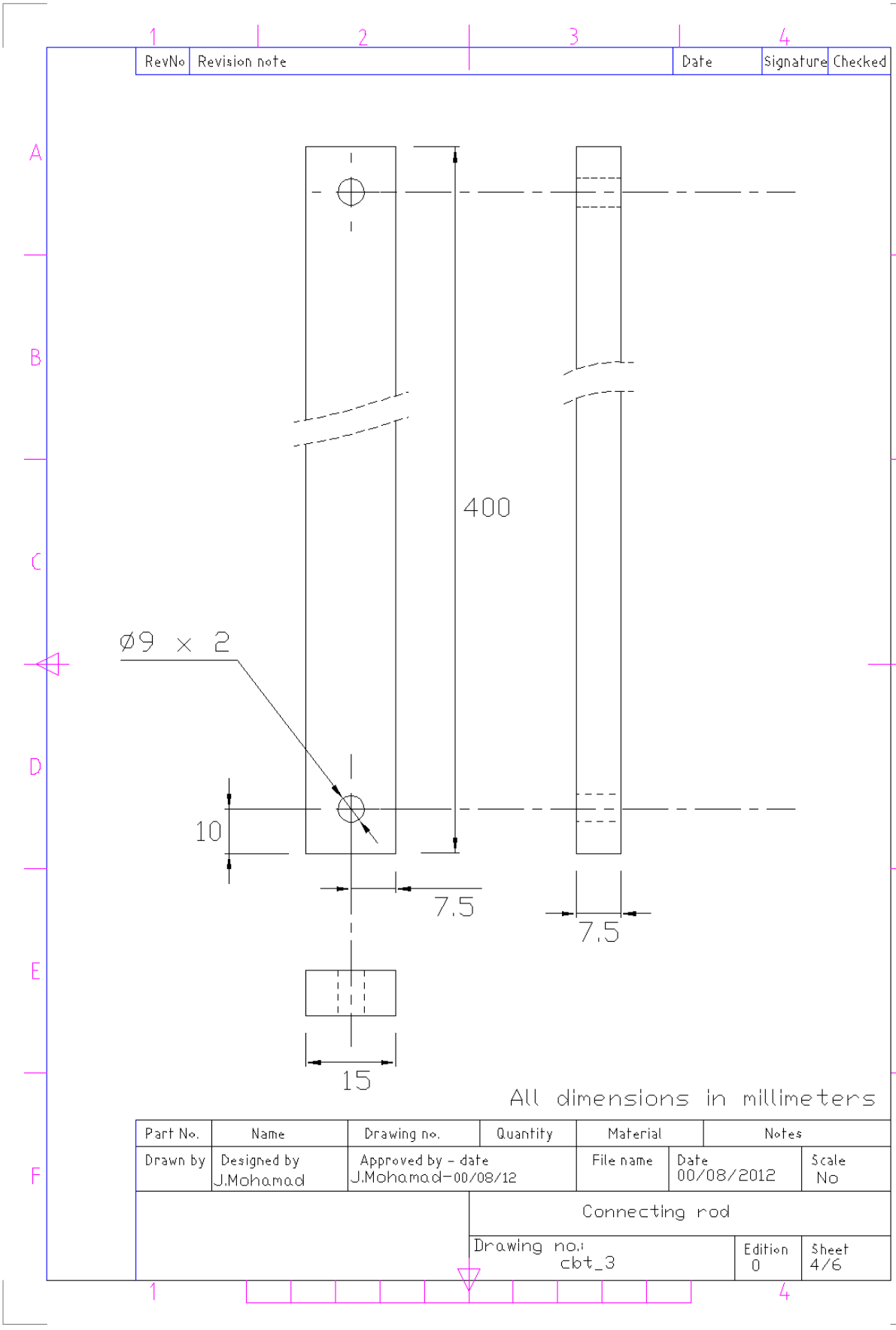
1
2
3
4
RevNo
Revision note
Date
Signature
Checked
A
B
C
D
E
F
400
Ø9 × 2
10
7.5
7.5
15
All dimensions in millimeters
Part No.
Name
Drawing no.
Quantity
Material
Notes
Drawn by
Designed by
J.Mohamad
Approved by - date
J.Mohamad-00/08/12
File name
Date
00/08/2012
Scale
No
Connecting rod
Drawing no.:
cbt_3
Edition
0
Sheet
4/6

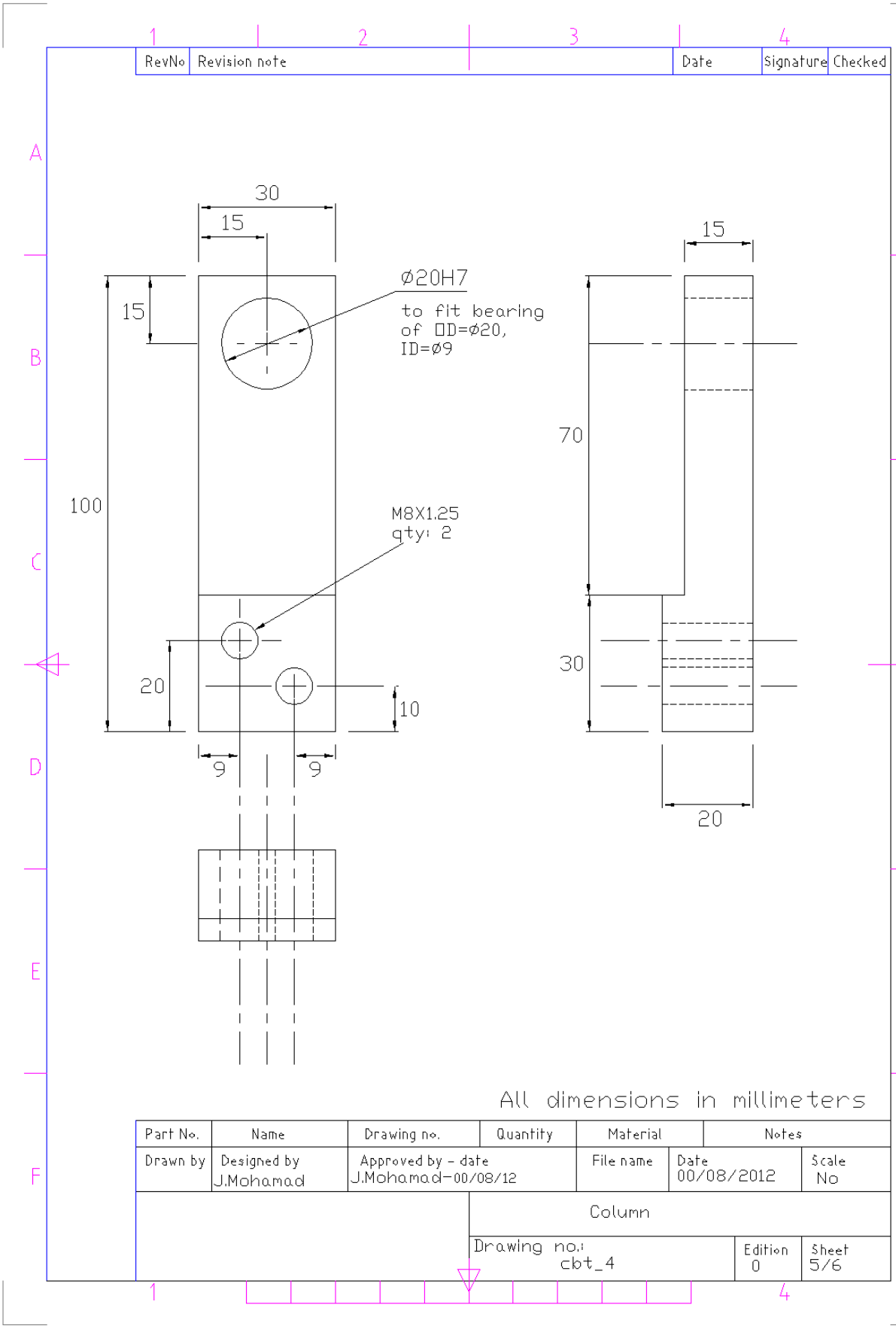
1
2
3
4
RevNo
Revision note
Date
Signature
Checked
A
B
C
D
E
F
30
15
15
Ø20H7
to fit bearing
of OD=Ø20,
ID=Ø9
100
M8X1.25
qty: 2
20
10
9
9
15
70
30
20
All dimensions in millimeters
Part No.
Name
Drawing no.
Quantity
Material
Notes
Drawn by
Designed by
J.Mohamad
Approved by - date
J.Mohamad-00/08/12
File name
Date
00/08/2012
Scale
No
Column
Drawing no.:
cbt_4
Edition
0
Sheet
5/6

RevNo	Revision note	Date	Signature	Checked

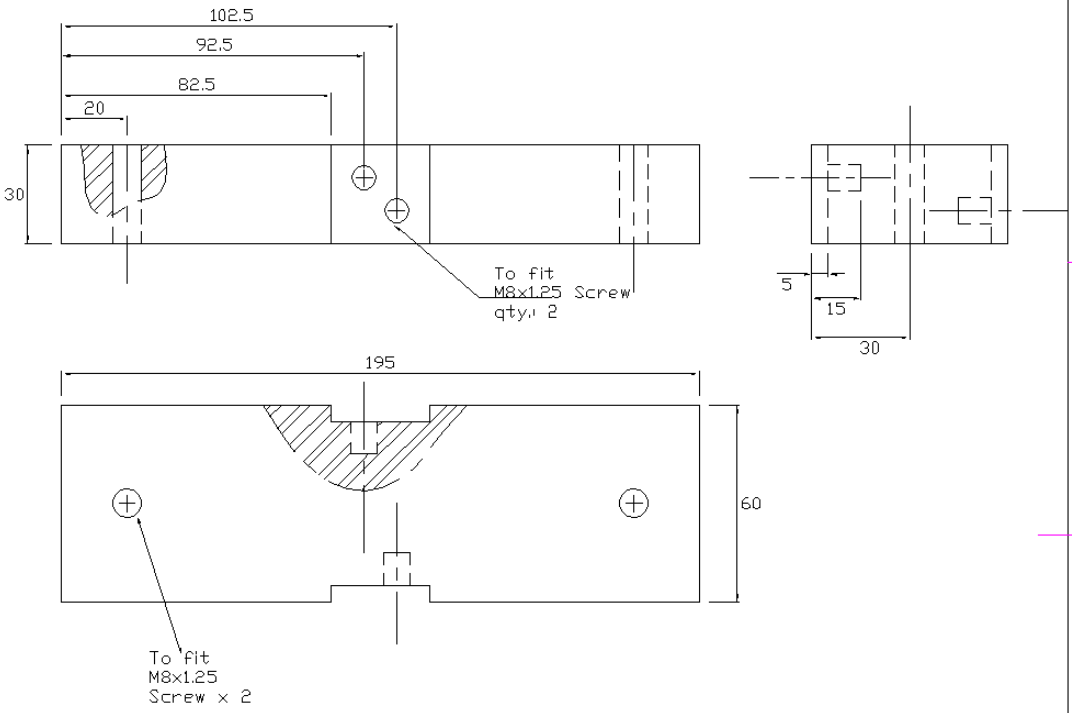

All dimensions in millimeters

Part No.	Name	Drawing no.	Quantity	Material	Notes	
Drawn by	Designed by J.Mohamad	Approved by - date J.Mohamad-00/08/12		File name	Date 00/08/2012	Scale No
		Base				
		Drawing no.: cbt_5			Edition 0	Sheet 6/6

D U-BENDING TOOL DRAWINGS

RevNo	Revision note	Date	Signature	Checked

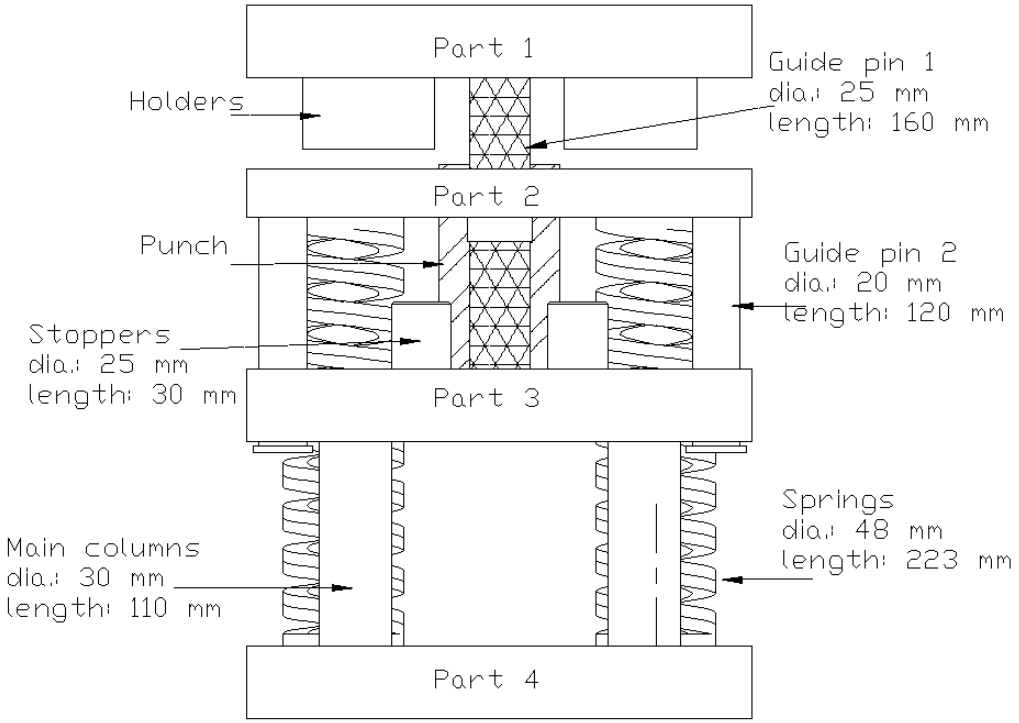

Part No.	Name	Drawing no.	Quantity	Material	Notes
11	Spring	—	2	—	
10	Main column	UBT_4_1	4	Tool steel	
9	Stopper	UBT_3_1	4	Tool steel	
8	Punch	UBT_3_1	1	Tool steel	
7	Guide pin 2	UBT_2_1	4	Tool steel	
6	Guide pin 1	UBT_1_2	2	Tool steel	
5	Blank Holders	UBT_1_1	2	Tool steel	
4	Bottom plate 2	UBT_4	1	Tool steel	
3	Bottom plate 1	UBT_3	1	Tool steel	
2	Top plate 2	UBT_2	1	Tool steel	
1	Top plate 1	UBT_1	1	Tool steel	

Drawn by	Designed by	Approved by – date	File name	Date	Scale
	J.Mohamad	J.Mohamad–00/010/12		00/10/2012	No

U BENDING TOOL

Drawing no.	Edition	Sheet
UBT_0	EDITION	SHEET

RevNo	Revision note	Date	Signature	Checked

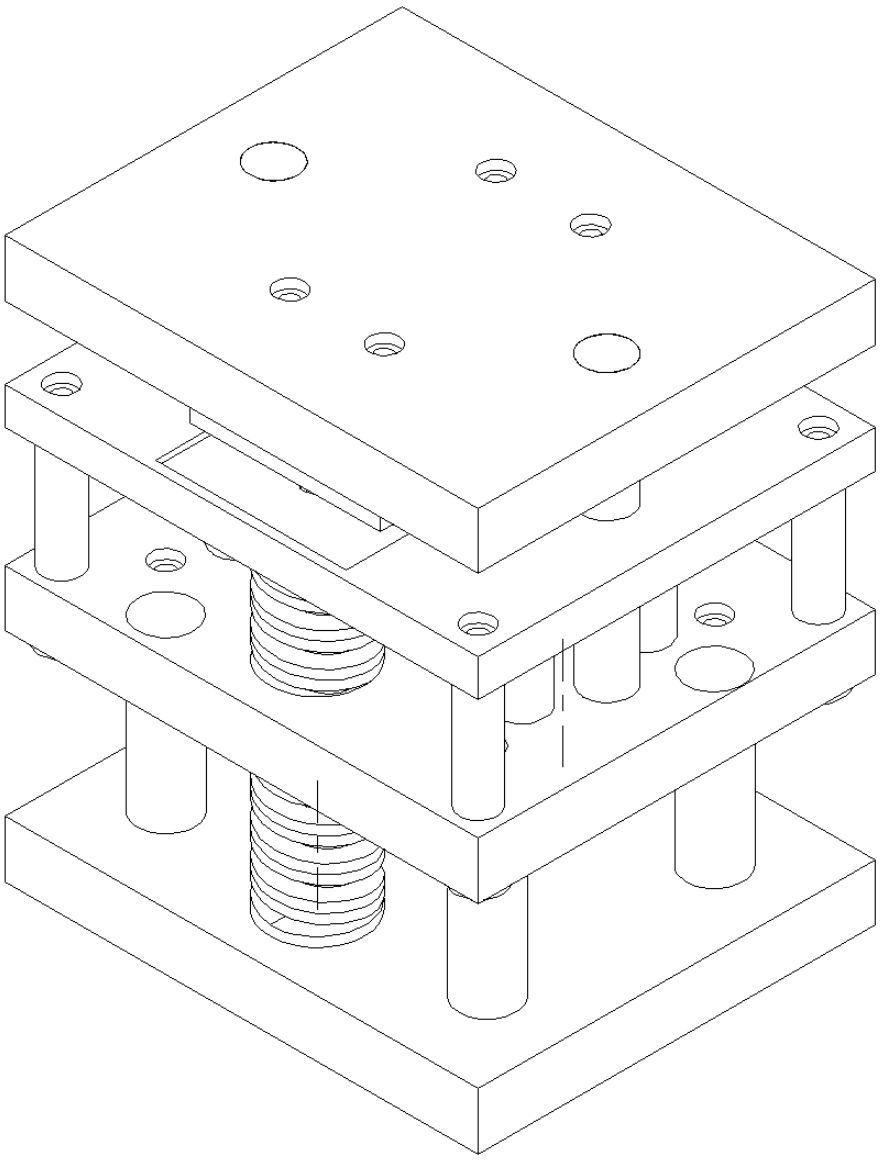

Part No.	Name	Drawing no.	Quantity	Material	Notes
Drawn by	Designed by J.Mohamad	Approved by – date J.Mohamad–00/010/12		File name	Date 00/10/2012	Scale No

U BENDING TOOL
(3D view)

Drawing no.	Edition	Sheet
UBT_0_1	EDITION	SHEET

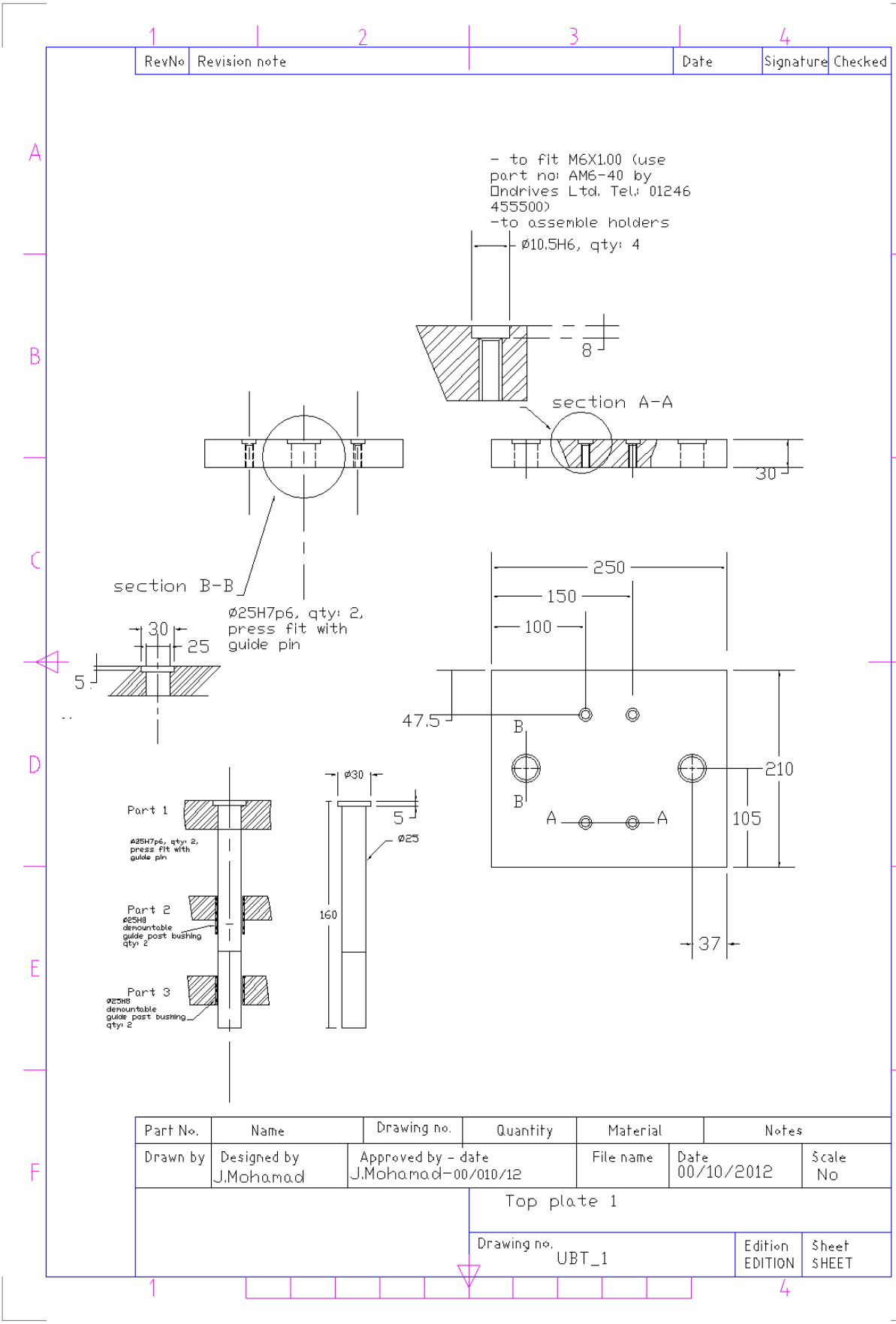
RevNo
Revision note
Date
Signature
Checked
- to fit M6X1.00 (use part no: AM6-40 by Ondrives Ltd. Tel: 01246 455500)
-to assemble holders
Ø10.5H6, qty: 4
8
section A-A
30
section B-B
Ø25H7p6, qty: 2, press fit with guide pin
30
25
5
250
150
100
47.5
B
B
A
A
210
105
37
Part 1
Ø25H7p6, qty: 2, press fit with guide pin
Part 2
Ø25H8 demountable guide post bushing qty: 2
Part 3
Ø25H8 demountable guide post bushing qty: 2
Ø30
5
Ø25
160
Part No.
Name
Drawing no.
Quantity
Material
Notes
Drawn by
Designed by J.Mohamad
Approved by - date J.Mohamad-00/010/12
File name
Date 00/10/2012
Scale No
Top plate 1
Drawing no. UBT_1
Edition EDITION
Sheet SHEET

RevNo	Revision note	Date	Signature	Checked

to be assembled on
part 1(dwg. no
UBT_1:Top plate 1)

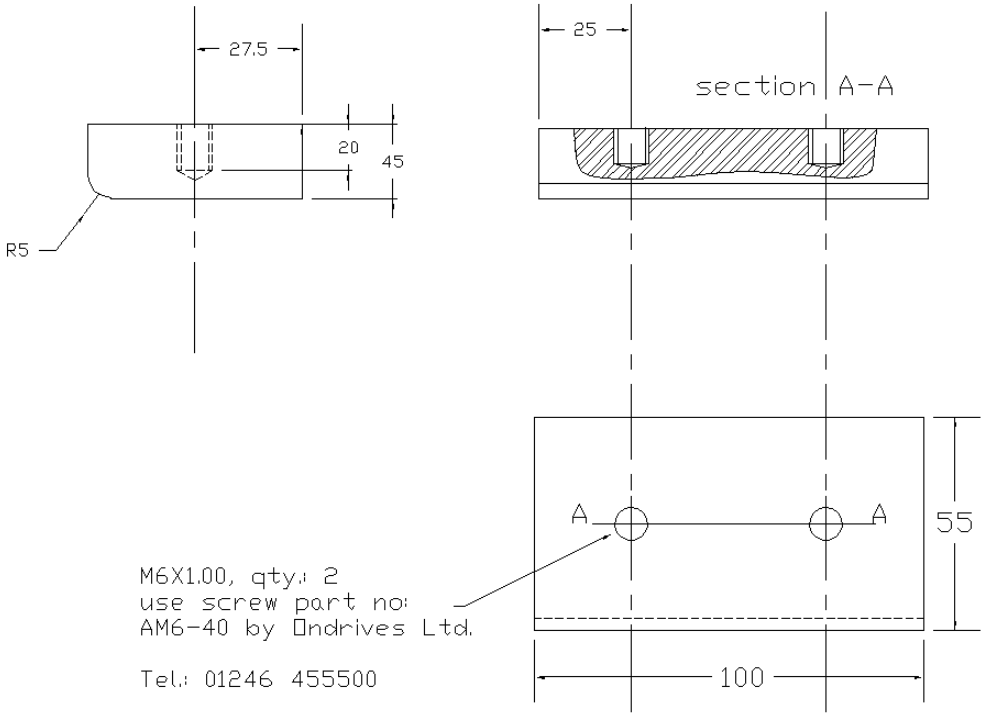

M6X1.00, qty.: 2
use screw part no:
AM6-40 by Ondrives Ltd.

Tel.: 01246 455500

Part No.	Name	Drawing no.	Quantity	Material	Notes

Drawn by	Designed by	Approved by - date	File name	Date	Scale
	J.Mohamad	J.Mohamad-00/010/12		00/10/2012	No

Blank holder

Drawing no.	Edition	Sheet
UBT_1_1	EDITION	SHEET

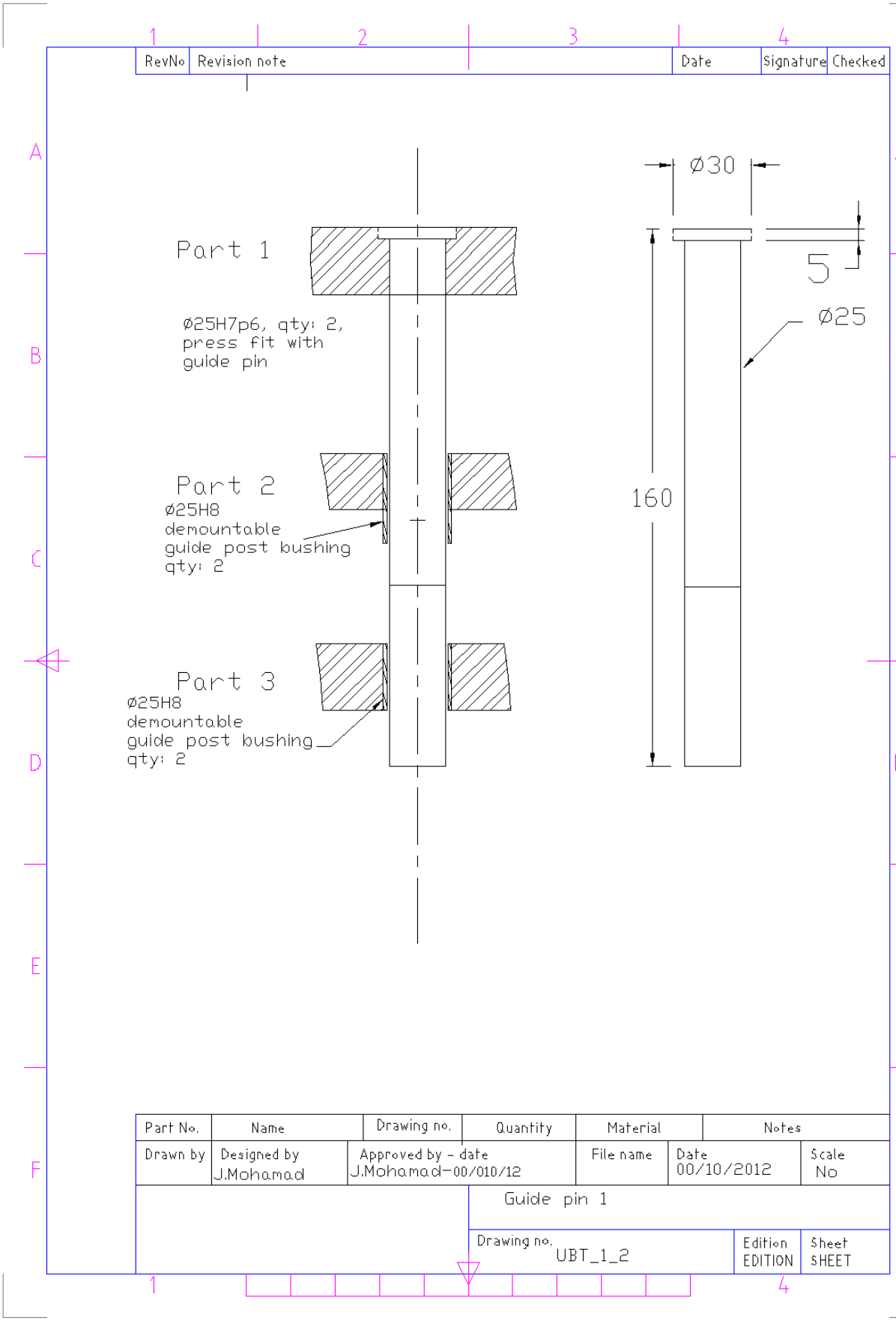
RevNo
Revision note
Date
Signature
Checked
Part 1
ø25H7p6, qty: 2,
press fit with
guide pin
Part 2
ø25H8
demountable
guide post bushing
qty: 2
Part 3
ø25H8
demountable
guide post bushing
qty: 2
ø30
5
ø25
160
Part No.
Name
Drawing no.
Quantity
Material
Notes
Drawn by
Designed by
J.Mohamad
Approved by - date
J.Mohamad-00/010/12
File name
Date
00/10/2012
Scale
No
Guide pin 1
Drawing no.
UBT_1_2
Edition
EDITION
Sheet
SHEET

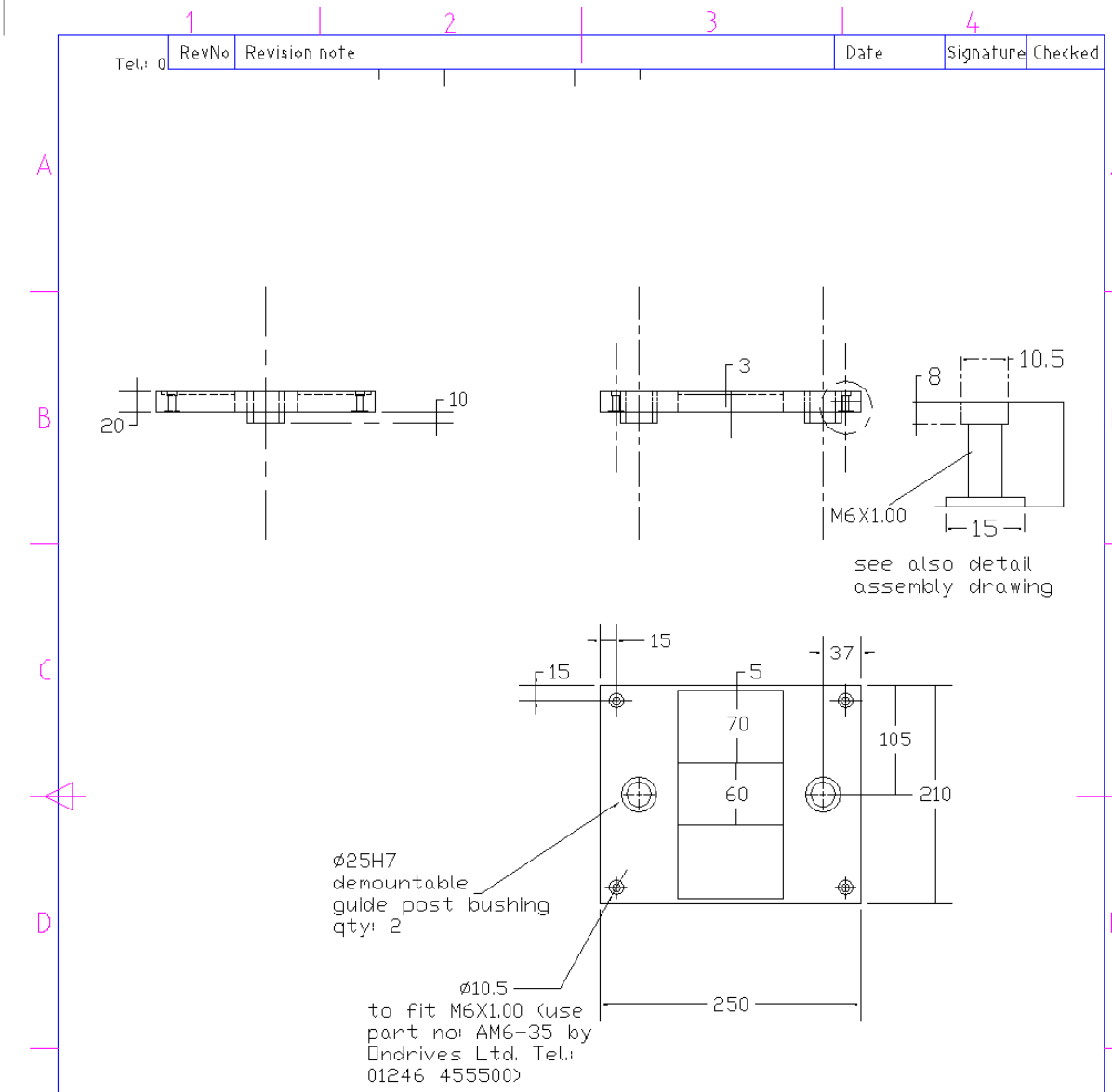
Tel.: 0
RevNo
Revision note
Date
Signature
Checked
20
10
3
8
10.5
M6X1.00
15
see also detail
assembly drawing
15
15
5
37
70
60
105
210
ø25H7
demountable
guide post bushing
qty: 2
ø10.5
to fit M6X1.00 (use
part no: AM6-35 by
Ondrives Ltd. Tel.:
01246 455500)
250
Part No.
Name
Drawing no.
Quantity
Material
Notes
Drawn by
Designed by
J.Mohamad
Approved by - date
J.Mohamad-00/010/12
File name
Date
00/10/2012
Scale
No
Top plate 2
Drawing no.
UBT_2
Edition
EDITION
Sheet
SHEET

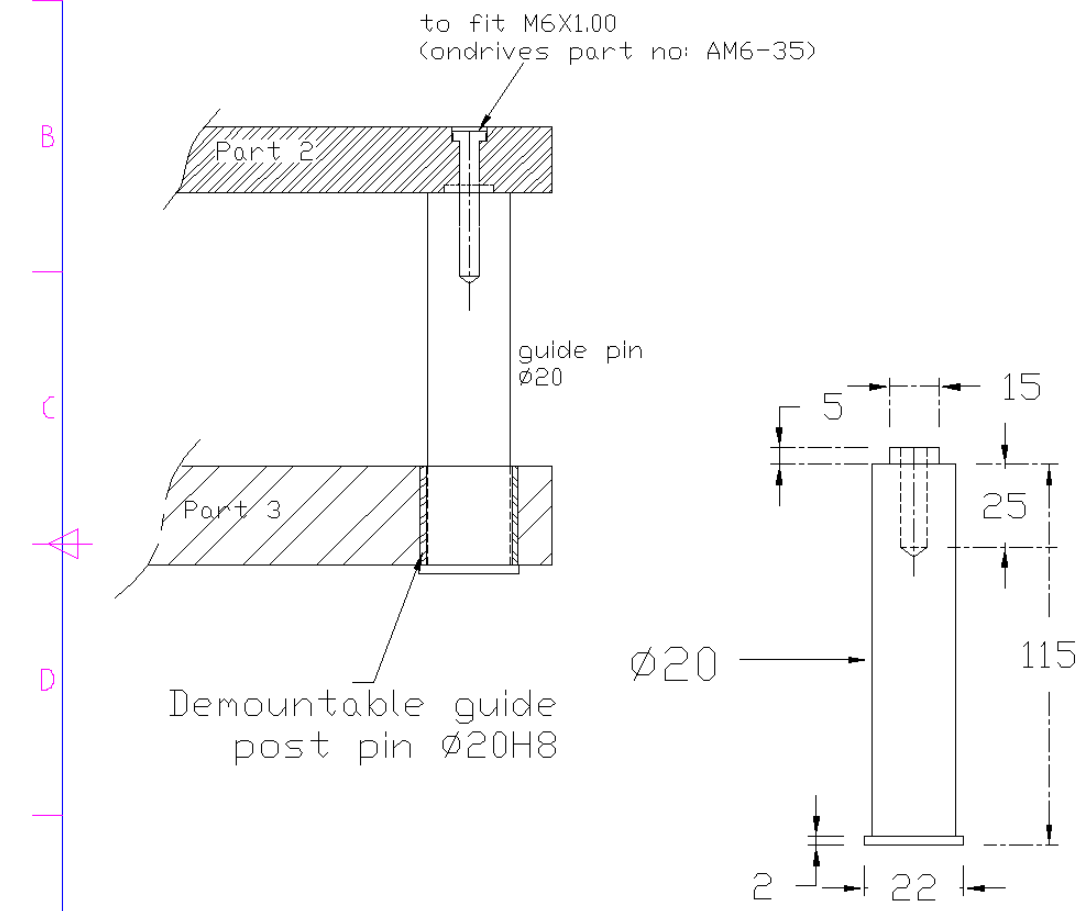

RevNo	Revision note	Date	Signature	Checked

Part No.	Name	Drawing no.	Quantity	Material	Notes

Drawn by	Designed by	Approved by - date	File name	Date	Scale
	J.Mohamad	J.Mohamad-00/010/12		00/10/2012	No

Guide pin 2

Drawing no.	Edition	Sheet
UBT_2_1	EDITION	SHEET

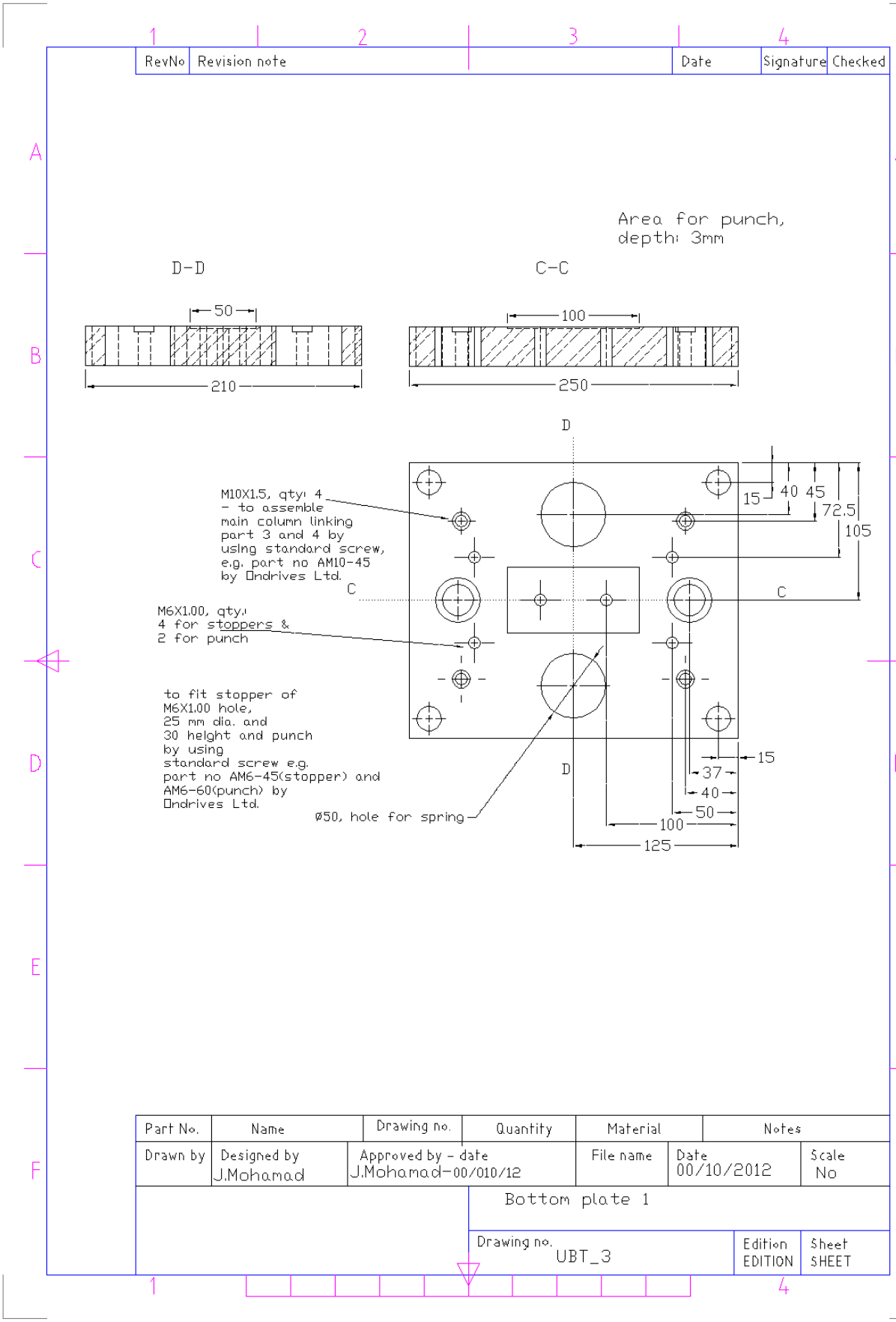
RevNo
Revision note
Date
Signature
Checked
Area for punch,
depth: 3mm
D-D
C-C
50
210
100
250
D
M10X1.5, qty: 4
- to assemble
main column linking
part 3 and 4 by
using standard screw,
e.g. part no AM10-45
by Ondrives Ltd.
C
M6X1.00, qty:
4 for stoppers &
2 for punch
to fit stopper of
M6X1.00 hole,
25 mm dia. and
30 height and punch
by using
standard screw e.g.
part no AM6-45(stopper) and
AM6-60(punch) by
Ondrives Ltd.
Ø50, hole for spring
15
40
45
72.5
105
37
50
100
125
Part No.
Name
Drawing no.
Quantity
Material
Notes
Drawn by
Designed by
J.Mohamad
Approved by - date
J.Mohamad-00/010/12
File name
Date
00/10/2012
Scale
No
Bottom plate 1
Drawing no.
UBT_3
Edition
EDITION
Sheet
SHEET

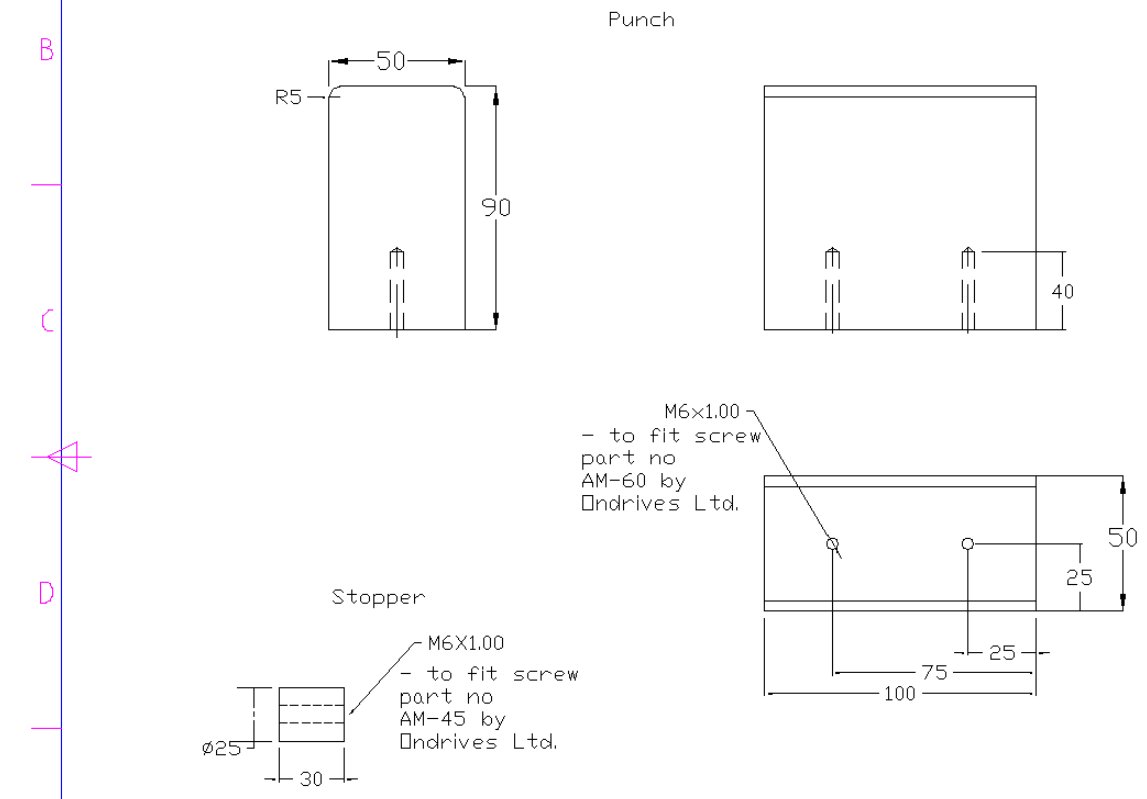

RevNo	Revision note	Date	Signature	Checked

Part No.	Name	Drawing no.	Quantity	Material	Notes

Drawn by	Designed by	Approved by - date	File name	Date	Scale
	J.Mohamad	J.Mohamad-00/010/12		00/10/2012	No

Punch and stopper

Drawing no.	Edition	Sheet
UBT_3_1	EDITION	SHEET

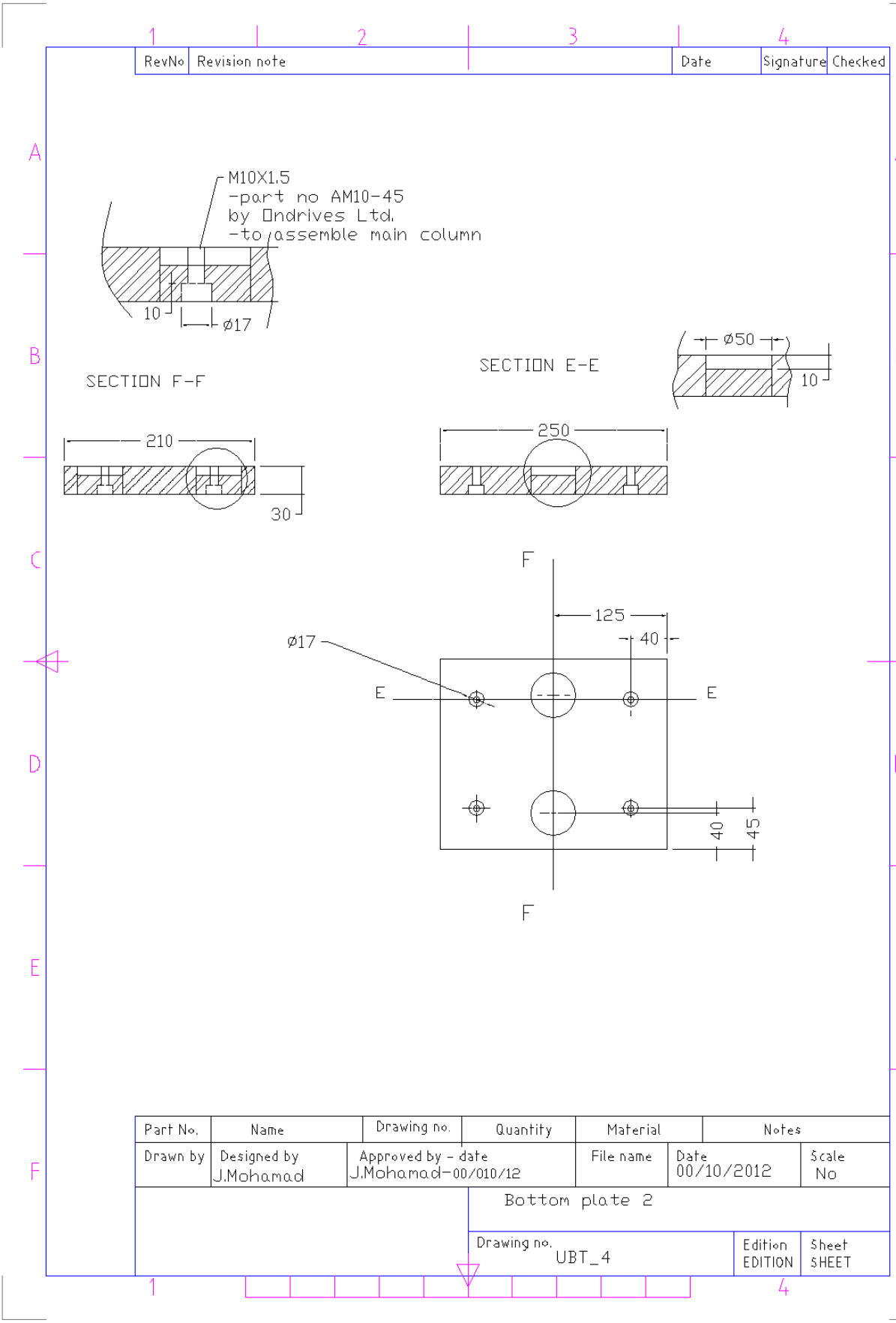
RevNo
Revision note
Date
Signature
Checked
M10X1.5
-part no AM10-45
by Ondrives Ltd.
-to assemble main column
10
ø17
SECTION F-F
210
30
SECTION E-E
ø50
10
250
F
125
40
ø17
E
E
40
45
F
Part No.
Name
Drawing no.
Quantity
Material
Notes
Drawn by
Designed by
J.Mohamad
Approved by - date
J.Mohamad-00/010/12
File name
Date
00/10/2012
Scale
No
Bottom plate 2
Drawing no.
UBT_4
Edition
EDITION
Sheet
SHEET

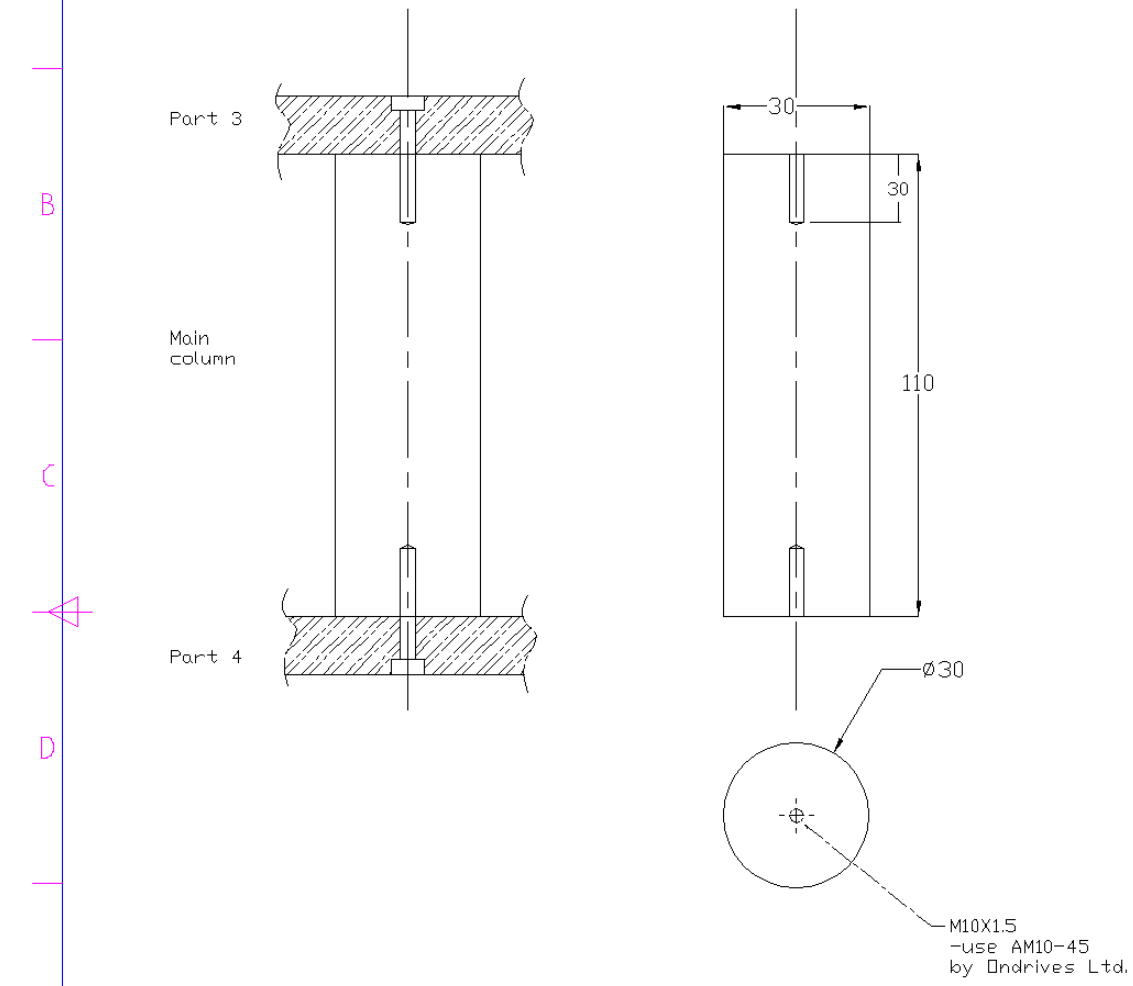

RevNo	Revision note	Date	Signature	Checked

Part No.	Name	Drawing no.	Quantity	Material	Notes

Drawn by	Designed by	Approved by – date	File name	Date	Scale
	J.Mohamad	J.Mohamad–00/010/12		00/10/2012	No

Main column

Drawing no.	Edition	Sheet
UBT_4_1	EDITION	SHEET